Expanding focal-mechanism catalogs for small earthquakes in SE Alps through automated analysis

F. Abdi[1*], A. Saraò[1], A. Magrin[1], M. Sugan[1], G. Messuti[2,3], M. Picozzi[1]

[1] National Institute of Oceanography and Applied Geophysics, OGS, Trieste, Italy

[2] Department of Physics "E.R. Caianiello", University of Salerno, Fisciano, Italy

[3] Section of Naples, National Institute for Nuclear Physics (INFN), Naples, Italy

1. Introduction

Focal mechanisms provide essential constraints on earthquake source processes, active faulting, and stress-field orientation, and are widely used in seismotectonic analyses and seismic hazard applications. However, the systematic determination of focal mechanisms for low-magnitude earthquakes remains challenging, mainly due to the limited availability and reliability of first-motion polarity observations. This issue is particularly relevant in regions where seismicity is dominated by small events but societal exposure is high.

The southeastern Alps of northeastern Italy represent a densely populated region characterized by frequent low-magnitude seismicity and significant seismic hazard. While moderate earthquakes provide important constraints on regional deformation and stress, the large number of small earthquakes potentially offers much higher spatial and temporal resolution for monitoring active structures and stress evolution. Realizing this potential requires scalable and robust methodologies for focal-mechanism determination at low magnitudes.

Recent advances in automated first-motion polarity classification, particularly based on deep-learning approaches, have substantially improved the feasibility of large-scale focal-mechanism workflows (Ross et al., 2018; Messuti et al., 2023; Zhang et al., 2025; Palo et al., 2025). In this study, we exploit these developments by integrating machine-learning–based polarity classification with probabilistic focal-mechanism inversion to systematically derive focal mechanisms for low-magnitude seismicity in the southeastern Alps.

2. Methodology and data

We implemented a fully automated workflow consisting of waveform extraction, first-motion polarity classification, probabilistic focal-mechanism inversion, and quality control. First-motion polarities are estimated using the Convolutional First Motion (CFM) deep-learning model (Messuti et al., 2023), which operates directly on raw vertical-component seismograms and outputs continuous polarity probabilities. These probabilities provide a quantitative measure of

classification confidence and are used both for event selection and to weight polarity observations.

Focal mechanisms are computed using SKHASH (Skoumal et al., 2024), which performs a stochastic grid search over strike, dip, and rake and explicitly accounts for hypocentral uncertainty through Monte Carlo perturbations. Diagnostic metrics describing polarity misfit, nodal-plane uncertainty, and station geometry are used to evaluate solution robustness and to assign quality grades to individual focal mechanisms.

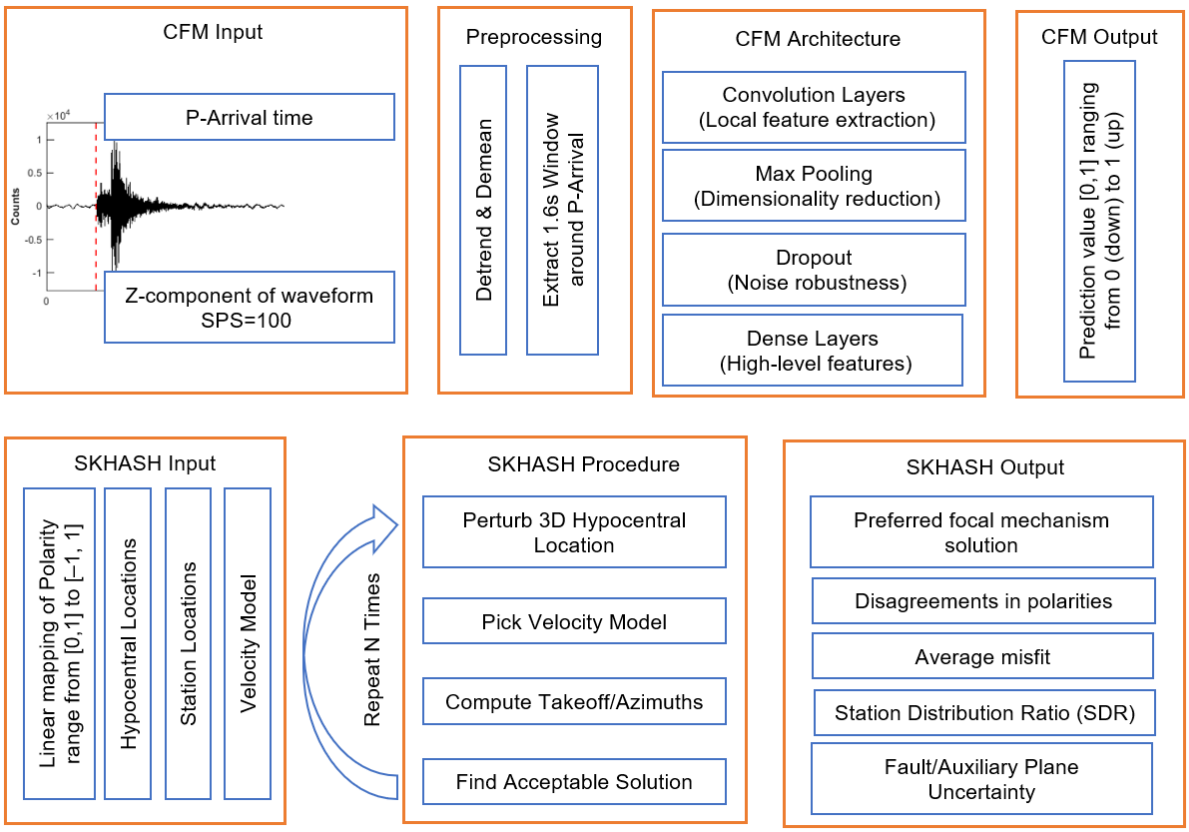

Figure 1 – Schematic representation of the automated workflow adopted in this study.

Quality control is applied at both the polarity and focal-mechanism levels, enforcing minimum requirements on the number of polarity observations, azimuthal coverage, and solution stability. The workflow is designed to minimize manual intervention and to ensure internal consistency and scalability for large regional datasets and near–real-time applications.

3. Application to the southeastern Alps

The automated workflow was first validated using a benchmark dataset of 159 earthquakes with manually reviewed polarities and reference focal mechanisms computed with FPFIT (Magrin et al., 2024). Automated polarity classification shows high consistency with manual picks (92% agreement), with polarity probabilities strongly bimodal and correlated with waveform signal-to-noise ratio, indicating that classification uncertainty is primarily controlled by data quality. Focal mechanisms derived from the automated workflow are predominantly stable, with more than 72% classified as A–B quality, and display faulting-style distributions consistent with manually derived solutions. Quantitative comparison using Kagan angles further confirms the reliability of the workflow, with 73% of events exhibiting misorientations below 30°.

Building on this validation, the workflow was applied to approximately 1,500 local earthquakes recorded between January 2024 and October 2025 (Md 1.0–4.6). Using a conservative quality-control scheme requiring a minimum of 12 high-confidence P-wave polarities, an azimuthal gap smaller than 180°, and RMS hypocentral residuals below 0.5 s, we retained 139 well-constrained focal-mechanism solutions. This subset represents the most robust portion of the automatically derived catalog and constitutes the first fully automated and systematically updated focal-mechanism dataset for the southeastern Alps.

Nearly 80% of the retained events have Md < 2.5, representing a substantial improvement in focal-mechanism completeness at low magnitudes compared to existing regional catalogs (Saraò et al., 2021; Sugan et al., 2024), with 53% of the solutions classified as A–B quality. Spatial patterns in faulting style are evident across the study area (Figure 2) are consistent with the regional tectonic framework of northeastern Italy, which lies at the transition between the eastern Southern Alps and the northwestern Dinaric domain.

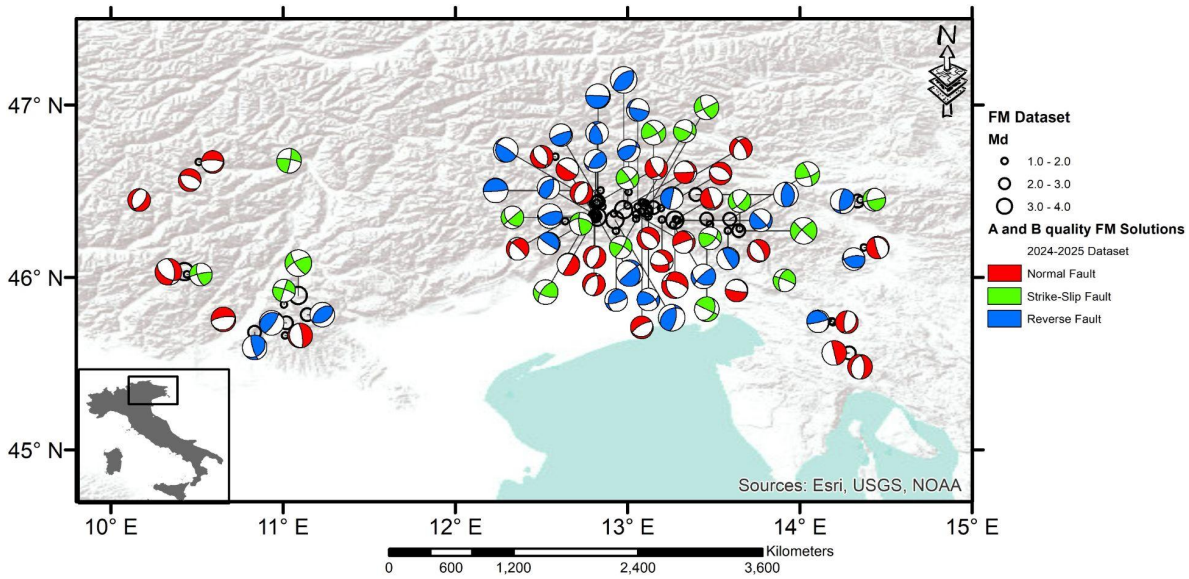

Figure 2 - Spatial distribution of A–B quality focal mechanisms, classified by faulting style

4. Conclusions

We present a fully automated workflow for focal-mechanism determination of small-to-moderate earthquakes, integrating deep-learning–based first-motion polarity classification with probabilistic focal-mechanism inversion.

Validation against 159 earthquakes with manually reviewed polarities and reference focal mechanisms shows high agreement between automated and analyst-derived solutions. Application to ~1,500 earthquakes recorded in the southeastern Alps between 2024 and 2025 yields 139 quality-controlled focal mechanisms, nearly 80% of which correspond to events with Md < 2.5, substantially increasing focal-mechanism completeness at low magnitudes.

The expanded catalog reveals variations in faulting style consistent with local stress heterogeneity in a tectonically complex compressional setting. The proposed workflow is readily transferable to other regions monitored by dense seismic networks and supports large-scale and near–real-time focal-mechanism analysis with direct implications for seismic monitoring and hazard assessment in densely populated regions.

References

Magrin, A., M. Sugan, A. Snidarcig, M. A. Romano, M. Guidarelli, M. Santulin, P. Di Bartolomeo, and A. Saraò (2024). Focal mechanism solutions of 162 earthquakes occurred between 2014 and 2023 in the Southeastern Alps, Zenodo, https://doi.org/10.5281/zenodo.10851786.

Messuti, G., S. Scarpetta, O. Amoroso, F. Napolitano, M. Falanga, and P. Capuano (2023). CFM: A convolutional neural network for first-motion polarity classification of seismic records in volcanic and tectonic areas, Front. Earth Sci. 11, https://doi.org/10.3389/feart.2023.1223686.

Ross, Z. E., M. A. Meier, and E. Hauksson (2018). P wave arrival picking and first-motion polarity determination with deep learning, J. Geophys. Res.: Solid Earth 123(6), https://doi.org/10.1029/2017JB015251.

Saraò, A., M. Sugan, G. Bressan, G. Renner, and A. Restivo (2021). A focal mechanism catalogue of earthquakes that occurred in the Southeastern Alps and surrounding areas from 1928–2019, Earth Syst. Sci. Data 13(5), https://doi.org/10.5194/essd-13-2245-2021.

Skoumal, R. J., J. L. Hardebeck, and P. M. Shearer (2024). SKHASH: A Python package for computing earthquake focal mechanisms, Seismol. Res. Lett. 95(4), 2519–2526, https://doi.org/10.1785/0220230329.

Sugan, M., A. Saraò, A. Magrin, A. Snidarcig, G. Bressan, G. Renner, M. A. Romano, M. Guidarelli, M. Santulin, P. Di Bartolomeo, and A. Restivo (2024). Focal mechanisms of the Southeastern Alps and surroundings (2.0), Zenodo, https://doi.org/10.5281/zenodo.10853582.

Corresponding author: fabdi@ogs.it

Understanding Volcano Dynamics by Unsupervised ML Clustering of Seismic Signals: A Case Study at Mount Etna

Waed Abed[1], Zahra Zali[2], Mariangela Sciotto[3], Ornella Cocina[3], Andrea Cannata[3,4], Matteo Picozzi[1], Patricia Martínez-Garzón[2,5], Alessandro Vuan[1], Angela Saraò[1], Monica Sugan[1]

[1] Istituto Nazionale di Oceanografia e di Geofisica Sperimentale – OGS, Italy
[2] Helmholtz Centre Potsdam, German Research Centre for Geosciences – GFZ, Germany
[3] Istituto Nazionale di Geofisica e Vulcanologia - Osservatorio Etneo – INGV-OE, Italy
[4] Università di Catania, Dipartimento di Scienze Biologiche, Geologiche e Ambientali, Sezione di Scienze della Terra, Catania, Italy
[5] Rheinisch-Westfälische Technische Hochschule Aachen – RWTH University of Aachen, Germany

In contrast to many volcanoes that exhibit prolonged calm intervals, Mount Etna is marked by persistent and continuous activity, with frequent Strombolian bursts, and lava fountains and effusions. This study employs an unsupervised machine learning (ML) framework, AutoencoderZ (Zali et al., 2025), that compresses high-dimensional spectrograms into small sets of extracted features that represent the data and can be used for downstream tasks such as clustering. Daily seismic spectrograms have been analyzed from two summit seismic stations (ECPN and ECNE) spanning from November 2020 to November 2021, a period that includes both quiet intervals and two major lava fountain cycles.

The aim is to automatically identify distinct patterns in seismic signals and extract clusters of signals with similar characteristics, which are data-driven sorted by spectral similarity, and to evaluate their correspondence with established volcanic activity phases. By comparing these ML-derived clusters to independent indicators, including records of lava fountaining, catalogues of volcano-tectonic earthquakes and long-period events (LP), and RMS amplitude measurements, the study assesses the capability of the unsupervised approach to reveal hidden structures in the seismic data, and to illuminate key transitions associated with processes such as magma ascent and gas pressurization. The methodology integrates both single-station and dual-station analyses to strengthen classification reliability and reduce spatial bias.

The AutoencoderZ architecture (Fig 1) includes an Encoder composed of convolutional and fully connected layers, a Bottleneck layer, and a Decoder employing transposed convolutions. Skip connections between matching Encoder and Decoder layers help retain key structural information. The optimal dimensionality of latent features was identified using the Relative Bias metric, selecting the value that minimized the discrepancy between original and reconstructed spectrograms. These latent features were then clustered using Deep Embedded Clustering (DEC), which jointly optimizes representation learning and cluster assignment to group spectrally similar seismic patterns (Jenkins et al., 2021; Mousavi et al., 2019; Snover et al., 2021). We identified four different clusters corresponding to recognised volcanic regimes: (i) quiescence or weak seismic

signals related to fluid dynamics, (ii) LP event-dominated fluid pressurisation, (iii) preparatory phase, and (iv) lava fountains episodes. These clusters closely align with expert classifications and achieve high temporal resolution, showing the ability of unsupervised ML to capture dominant spectral signatures and subtle transitions in volcanic activity (Abed et al., under review).

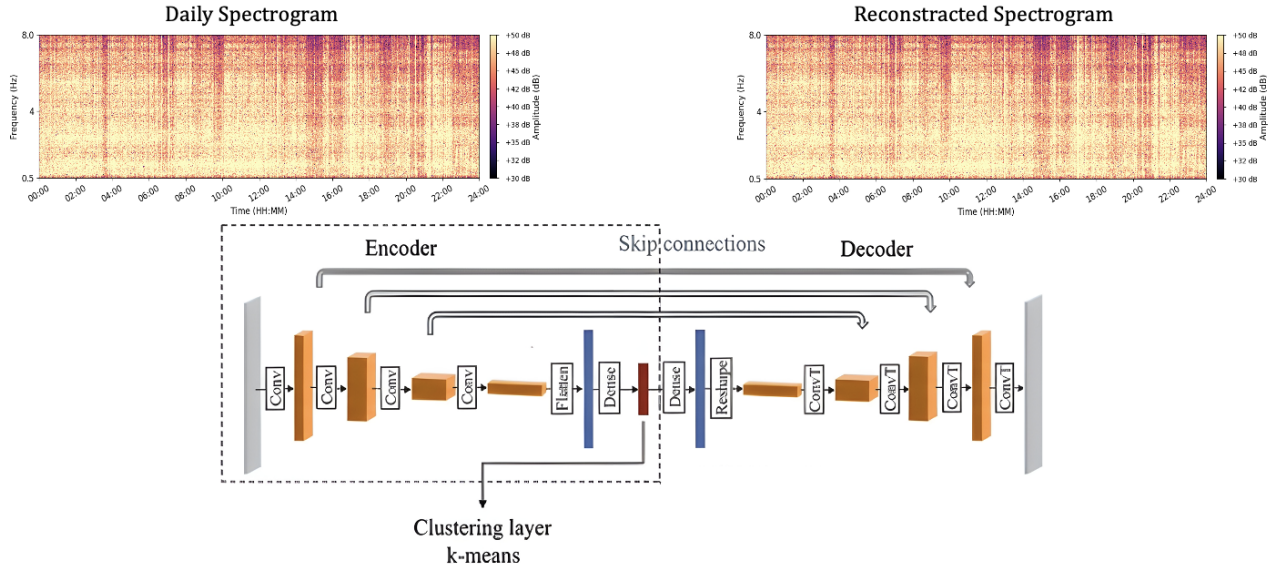

Fig 1. Overview of the workflow. The schematic diagram shows the complete analytical pipeline using data from the ECPN-HHE component. The AutoencoderZ architecture is adapted from Zali et al. (2025).

Acknowledgments

This study was carried out within the RETURN Extended Partnership and received funding from the European Union Next-GenerationEU (National Recovery and Resilience Plan – NRRP, Mission 4, Component 2, Investment 1.3 – D.D. 1243 2/8/2022, PE0000005). Computations are performed at CINECA in the framework of the HPC-TRES program agreement between OGS and CINECA.

References

Abed, W., Zali, Z., Sciotto, M., et al.; 2025: Hidden Patterns in Volcanic Seismicity: Deep Learning Insights from Mt. Etna's 2020–2021 Activity. Scientific Reports, under review.

Jenkins, W. F., Gerstoft, P., Bianco, M. J., Bromirski, P. D.; 2021: Unsupervised Deep Clustering of Seismic Data: Monitoring the Ross Ice Shelf, Antarctica. J. Geophys. Res. Solid Earth 126, e2021JB021716. https://doi.org/10.1029/2021JB021716.

Mousavi, S. M., Zhu, W., Ellsworth, W., Beroza, G.; 2019: Unsupervised Clustering of Seismic Signals Using Deep Convolutional Autoencoders. IEEE Geosci. Remote Sens. Lett. 16, 1693–1697. https://doi.org/10.1109/LGRS.2019.2909218.

Snover, D., Johnson, C. W., Bianco, M. J., Gerstoft, P.; 2021: Deep Clustering to Identify Sources of Urban Seismic Noise in Long Beach, California. Seismol. Res. Lett. 92, 1011–1022. https://doi.org/10.1785/0220200164.

Zali, Z., Martínez-Garzón, P., Kwiatek, G. et al.; 2025: Low-frequency tremor-like episodes before the 2023 MW 7.8 Türkiye earthquake linked to cement quarrying. Sci Rep 15, 6354. https://doi.org/10.1038/s41598-025-88381-x.

Corresponding author: wabed@ogs.it

Near-fault observation in a seismic gap area: the Mt. Morrone-Maiella fault system (Central Apennines, Italy)

M. Anselmi [1], P. De Gori [1], S. Bagh [1], I. Menichelli [2], R. Fonzetti [3], C.Chiarabba [1]

[1] Istituto Nazionale di Geofisica e Vulcanologia (ONT, Rome)
[2] Istituto Nazionale di Geofisica e Vulcanologia (Bologna)
[3] Istituto Nazionale di Geofisica e Vulcanologia (Sismologia e Tettonofisica, Rome)

The Apennine chain, formed by thrust and fold systems, has experienced significant tectonic activity due to the westward subduction of the Adriatic lithosphere. This has caused extensive uplifts and extensional faults, forming intermountain basins, such as those at Fucino, Sulmona, and L'Aquila, filled with Plio-Quaternary continental deposits.

The Mt. Morrone fault, situated in the Central Apennines, is known to be geologically active, as evidenced by geological and paleo-seismological studies. The Apennine sector under investigation in the southeastern part of the Abruzzo region has been affected by several significant historical earthquakes, including the 1706 (Mw = 6.6) and 1933 (Mw = 5.7) events, as well as the 1349 and 1456 seismic sequences (Mw = 6.6 and 7.0). The literature available also indicates that the 1456, 1706, and 1933 earthquakes originated in this area.

Despite this, the past 40 years have shown low seismic activity, with only a few low-magnitude events detected by the Italian Permanent Seismic Network.

This lack of correspondence between geological activity evidence and recent seismic activity raises an unanswered question: is it possible that the Morrone fault system and its surrounding faults produce low seismic events that are not detected by the permanent networks, or is it truly a low-activity fault system with slow movements and no detectable events?

The experiment presented in this work aims to answer this question. In fact, if the Morrone fault system and its surrounding faults are active and produce only microseismicity (low-magnitude earthquakes), a dense seismic network (capable of lowering the seismic detection threshold) deployed near the target area could provide a deeper understanding of their seismic behavior and the eventual microseismicity released.

Since May 2022, some INGV researchers have initiated a passive seismic experiment, which is still ongoing, as part of the PON-GRINT project in the Mt. Morrone area of the Central Apennines, Abruzzo, Italy. Between May and October 2022, twenty temporary seismic stations were deployed

across a ~250 km² area stretching from the Sulmona-Pratola Peligna basin to Mt. Morrone and the Caramanico valley (Fig. 1).

Preliminary analysis of the first 15 months of data shows sparse seismicity, mainly located beneath the Popoli-Sulmona basin. These events appear to be linked to the Mt. Morrone fault, with hypocentral depths consistent with the fault geometry. The seismicity forms two clusters: one on the northwest side of Mt. Morrone and another one between Mt. Morrone and Maiella, likely related to the Caramanico fault along the western flank of the Maiella anticline.

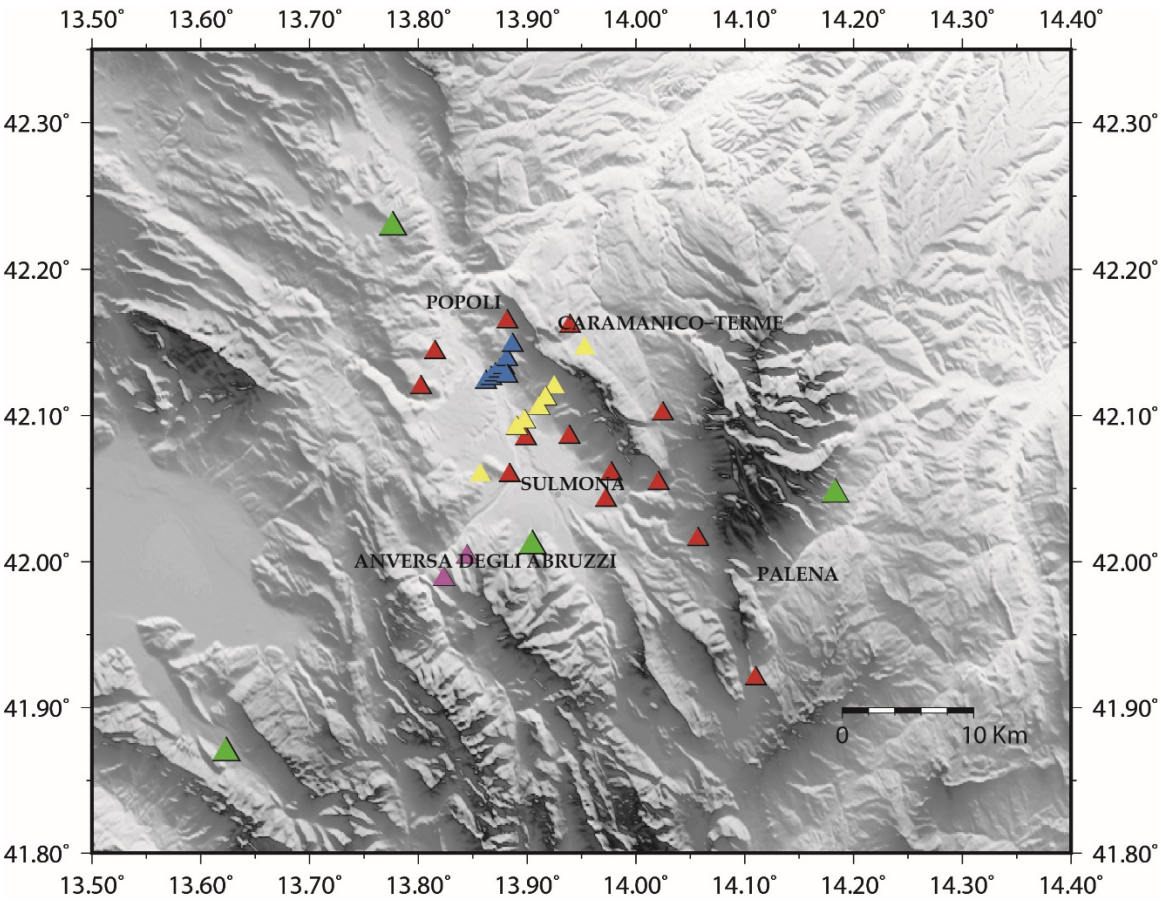

Fig. 1. Map of the seismic station deployed during the experiment: yellow, red, blue, and purple triangles represent stations deployed in different periods during the experiment; green triangles represent the stations of the Permanent seismic stations (RSN).

Corresponding author: mario.anselmi@ingv.it

The many faults of the Messina Straits: A marine geology perspective

Andrea Argnani[1],

[1] *Istituto di Scienze Marine (ISMAR), CNR, Bologna*

The region of the Messina Straits was struck in 1908 by the most destructive earthquake in the history of Italy, and since then it has been the object of many studies dedicated to understand the orgin this large earthquake (Mw 7.1; Argnani and Pino, 2023).

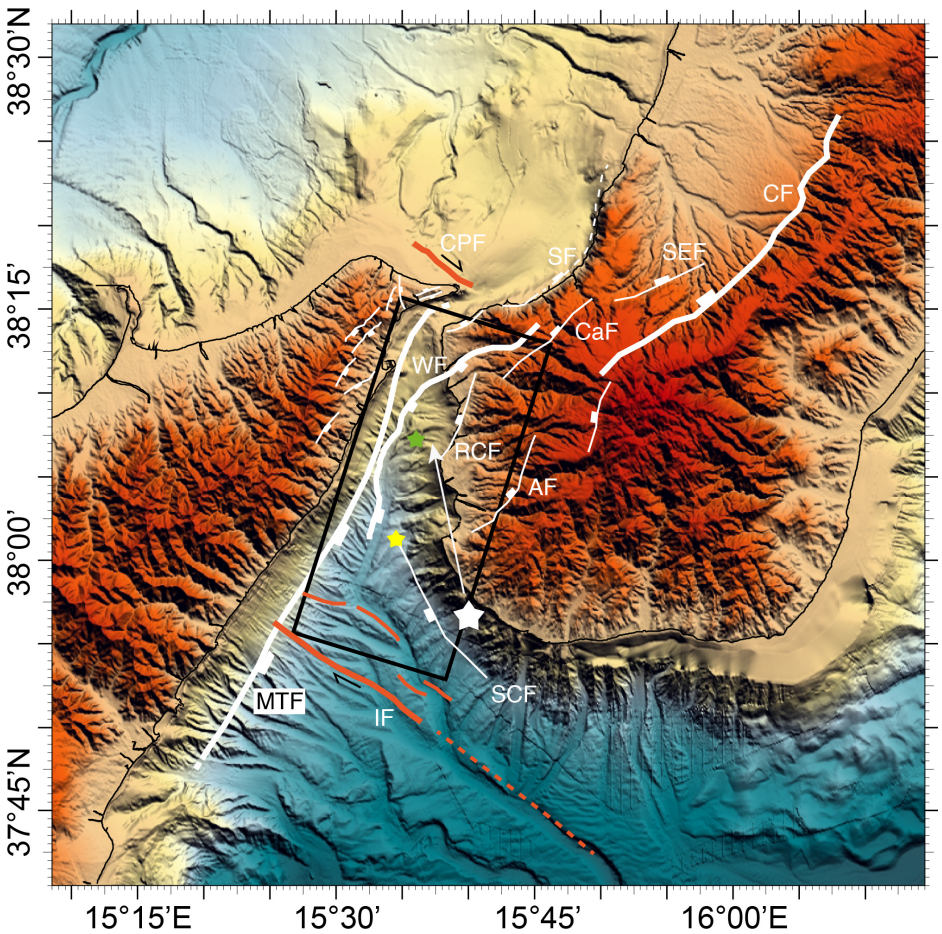

Fig. 1 – Morpho-bathymetry of the Messina Straits region with superimposed the traces of the main faults, with the largest ones indicated with bold lines. The stars indicate the 1908 earthquake epicentral locations of different authors. The black box is the surface projection of the model seismogenic fault and the white arrow shows the rupture directivity (Pino et al., 2009). MTF Messina-Taormina Fault; WF W-Fault; Cittanova Fault CF; Sant'Eufemia Fault SEF; Scilla Fault SF; Calanna Fault CaF; Reggio Calabria Fault RCF; Armo Fault AF; Capo Peloro Fault CPF; Ionian Fault IF; South Calabria Fault SCF.

The search for the seismogenetic fault has produced a wealth of faults and fault systems proposed as potential candidates (Fig. 1). These attempts have often resulted in conflicting interpretations,

where the main fault in one study cannot work in another structural scheme (Fig. 2). In several instances it appears that the studies aim at confirming regional tectonic schemes rather than at better documenting the individual faults. This approach results in a confusing picture where a large number of poorly constrained faults are available, to be selected on demand, in order to support the preferred tectonic model. The seismological studies of the 1908 earthquake can provide only limited information, due to the poor spatial coverage and instrumental technology of the time, although providing useful information regarding the size and orientation of the rupture surface (Fig. 1; Pino et al., 2009). The recent seismicity of the region is characterized by low magnitude earthquakes which confirm the presence of diffuse crustal extension, but do not outline a main fault surface.

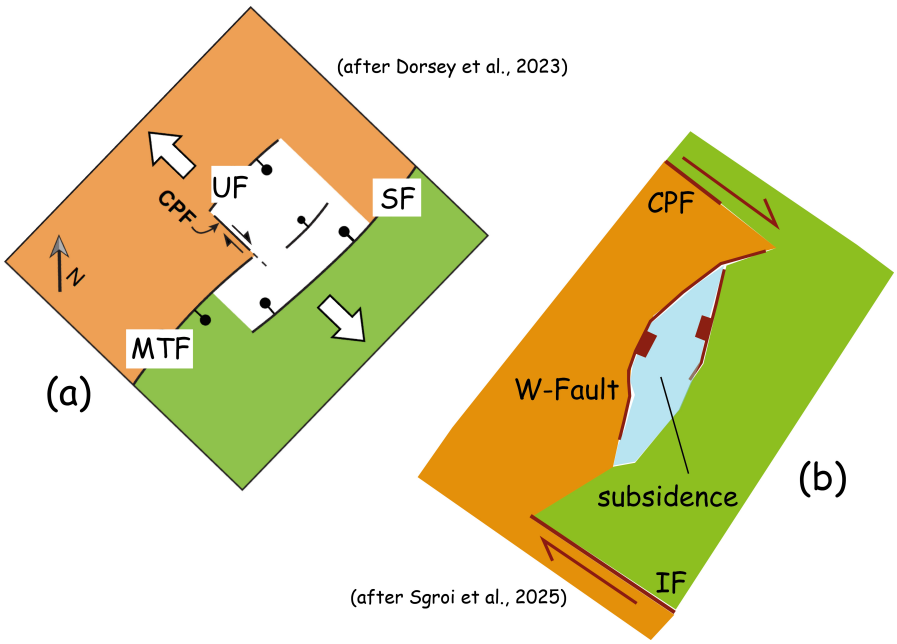

Fig. 2 – Example of two tectonic sketches proposed for the Messina Straits region which give relevance to different faults and different role to the same fault. a) Tectonic sketch of the northern sector of the Messina Straits (after Dorsey et al., 2023). The Capo Peloro Fault (CPF) is interpreted as a transfer fault within two convergent, overlapping extensional faults. The Messina-Taormina Fault (MTF) is interpreted to be the main extensional fault within the straits. SF is the Scilla Fault, and UF is an unnamed fault. b) Tectonic sketch of the Messina Straits (after Sgroi et al., 2025). The CPF and Ionian Fault (IF) are interpreted as lithospheric, strike-slip faults defining a releasing stepover. Within the straits the W-Fault (Barreca et al., 2022) is considered the main extensional fault, responsible of a focused sigmoidal-shaped subsidence.

Although with significantly different locations, it is believed that the epicenter of the 1908 earthquake was located at sea, in the Straits (Fig. 1). Due to the physiographic characteristics of the Straits, the acquisition of geophysical data is difficult, and only a few multichannel seismic surveys have been carried out, with results sometimes affected by the erosive characteristics of the seabed (e.g., Argnani et al., 2009). On the other hand, multibeam acquisitions have provided a high-resolution image of the seafloor morphology in the Straits (Ridente et al., 2014), which has only in some cases been used to interpret the seismic profiles.

A scale issue is also evident when comparing the faults presented in the literature with the fault rupture required to originate the 1908 Messina earthquake. In some cases, high-resolution seismic imaging highlights and correlates small-scale faults which generate structural networks that are difficult to trace back to the large seismogenic fault.

A critical review of published and unpublished data will be presented to address issues related to the major faults in the Messina Straits region. The very existence of some of these faults, although well-established in the literature, may be questioned.

Acknowledgments

N. A. Pino is thanked for the useful discussions on the elusive 1908 fault.

References

Argnani, A., et al.; 2009: Tectonophysics 476, 159–169.

Argnani A., Pino, N.A.; 2023: Seismol. Res. Lett., 94, 557-561, doi: 10.1785/0220220355

Barreca, G. et al.; 2021: 218, 103685 https://doi.org/10.1016/j.earscirev.2021.103685.

Doglioni, C. et al.; 2012: Sci Rep 2:970. https://doi.org/1 0.1038/srep00970

Dorsey, R. J., et al.; 2024: Basin Res., 36(1), https://doi.org/10.1111/bre.12818.

Meschis, M., et al.; 2019: Sci. Rep. 9 (1), 6481.

Pino, N.A., et al.; 2009: Seismol. Res. Lett. 80 (2), 243–259.

Ridente, D., et al.; 2014: Geomorphology 208, 149–159, doi: 10.1016/j.geomorph. 2013.11.021.

Sgroi, T. et al.; 2025: Tectonophysics 230920, https://doi.org/10.1016/j.tecto.2025.2309201

Corresponding author: andrea.argnani@ismar.cnr.it

Site Response Analysis during the 2016 Amatrice–Visso–Norcia Seismic Sequence

A. Attolico[1], M. Anselmi[2], P. De Gori[2] , F.P. Lucente[2], E. Tinti[1]

[1] *Dipartimento di scienze della terra (Università di Roma "La Sapienza", Italy)*
[2] *Istituto Nazionale di Geofisica e Vulcanologia (INGV, Italy)*

The site response is crucial for accurately estimating source parameters, as it directly influences the spectral characteristics of seismic signals. Achieving reliable estimates of these parameters requires clearly distinguishing between source effects, path attenuation, and site response, which are often interdependent and subject to significant trade-offs (*Boatwright et al., 1991; Abercrombie, 2021*). As highlighted in recent studies, site response reflects the amplification or damping effects of the shallow subsurface layers on seismic waves, and its accurate characterization is essential for correcting the observed spectra and improving the source parameter estimations (*Edwards et al. 2008; De Gori et al., 2023*). By accurate analysis of the site response, we aim to mitigate these uncertainties and achieve a more robust parameterization of seismic events, particularly for low-magnitude earthquakes, where these effects are more pronounced.

We analyze the site response of 39,328 seismic events that occurred during the Amatrice–Visso–Norcia (Central Italy) seismic sequence between 24 August and 30 November 2016, focusing on earthquakes with local magnitude Ml < 2.0. All seismograms, recorded by the dense INGV–BGS seismic network, including both permanent and temporary stations installed on different lithological and structural domains, are sampled at 100 Hz. By restricting the analysis to low-magnitude events, we assume that the high-frequency spectral decay is dominated by path attenuation, as corner frequencies (*fc*) are above 40 Hz, the upper limit of our observable frequency range.

We perform a preliminary fit for all events, computing, for each spectrum that exceeds a signal-to-noise ratio (S/N) threshold of 2, the low-frequency level ($\Omega 0$) and the t^* attenuation parameter. This analysis was conducted while neglecting *fc* and assuming that the quality factor (Q) is frequency-independent.

We compute the amplitude residuals between the observed ($U_{ij}^{obs}(f)$) and theoretical ($U_{ij}^{th}(f)$) displacement spectra for P- and S- waves, using the spectral residual technique (*Tsumura et al., 1996; Edwards et al., 2008; Edwards and Rietbrock, 2009 and De Gori et al., 2023*). The site

response spectrum ($\overline{R}_j(f)$) is expressed as the average of residuals obtained at discrete frequencies, considering all the spectra recorded by each station (eq. 1).

$$log_{10}\overline{R}_j(f) = \frac{1}{N_j}\sum_{i=1}^{N_j} log_{10}\frac{U_{ij}^{obs}(f)}{U_{ij}^{th}(f)} \qquad \text{(eq 1)}$$

We investigate the spatial and temporal stability of site response during the ongoing sequence by analyzing individual P- and S-wave site response functions and their S/P amplitude ratio over time. We first assess the stability of site response between the Amatrice (24/08/2016) and Visso (26/10/2016) mainshocks, and then evaluate the impact of the Visso earthquake on the site response.

The results provide valuable insights into site response behaviour, supporting the use of station-specific, invariant site terms to correct observed spectra and achieve more reliable estimates of source parameters.

References

Abercrombie, R. E.; 2021: Resolution and uncertainties in estimates of earthquake stress drop and energy release. Philos. Trans. R. Soc. Lond. A 379.

Boatwright, J., J. B. Fletcher, and T. E. Fumal; 1991: A general inversion scheme for source, site and propagation characteristics using multiply recorded sets of moderate-sized earthquakes. Bull. Seismol. Soc. Am. 81, 1754–1782.

De Gori, P., Pio Lucente, F. and Chiarabba, C; 2023: Source-Parameter Estimation after Attenuation Correction through the Use of Q Tomography. Bull. Seismol. Soc. Am. 113, 1739–1758.

Edwards, B., A. Rietbrock, J. J. Bommer, and B. Baptie; 2008: The acquisition of source, path, and site effects from microearthquake recordings using Q tomography: Application to the United Kingdom. Bull. Seismol. Soc. Am. 98, 1915–1935.

Edwards, B., and Rietbrock A.; 2009: A comparative study on attenuation and source-scaling relations in the Kanto, Tokai, and Chubu regions of Japan, using data from Hi-net and KiK-net. Bull. Seismol. Soc. Am. 99.

Tsumura, N., A. Hasegawa, and S. Horiuchi; 1996: Simultaneous estimation of attenuation structure, source parameter, and site response spectra—Application to the northeastern part of Honshu, Japan. Phys. Earth Planet. In. 93, 105–121.

Corresponding author: andrea.attolico@uniroma1.it

Recent activity of the Tremestieri Fault, Etna volcano: model constraints from integrated seismological, InSAR, tilt and tectonic data

R. Azzaro[1], S. Alparone[1], S. Brooks[1,2], S. Gambino[1], F. Guglielmino[1], A. Iozzia[1], A. Ursino[1]

[1] Istituto Nazionale di Geofisica e Vulcanologia - Osservatorio Etneo, Catania, Italy
[2] Dipartimento di Scienze Biologiche, Geologiche ed Ambientali - Università di Catania, Italy

The Tremestieri fault (TMF) is part of an active tectonic system dissecting a wide sector of the southern flank of Etna. It plays a major role in controlling, through dextral oblique movements, the seaward movement of the volcano's eastern flank, representing a first order structural boundary between the unstable sector to the north and the relatively steady area to the south (Azzaro et al., 2013). The TMF is a ~7 km long, partially hidden structure consisting of broadly NW-SE striking segments arranged in an *en échelon* pattern, and extending from the village of Tremestieri up to Nicolosi (Fig. 1a). The morphological evidence of this fault zone along strike is discontinuous: a ~10 m high fault scarp (downthrown to the northeast) is exposed west of Tremestieri, whereas the downhill termination crossing the village appears as a hidden fault (Azzaro et al., 2012).

From a seismotectonics perspective, this section of the TMF is characterized by near-continuous creep associated with moderate, very shallow seismicity (max M_d 3.2, epicentral intensity I_0 VI EMS). Over recent decades, fault creep has caused significant damage to the buildings and infrastructures located astride the fault trace (Rasà et al., 1996).

On 17-18 November 2025, the INGV seismic network recorded 9 earthquakes located on the southern flank of Etna, mainly between Pedara and Mascalucia, in close proximity to the TMF (Fig. 1b). These low energy events, with M_L between 1.5 and 2.5, were characterized by very shallow focal depth. The strongest shocks - 04:30 UTC, M_L 2.5; 12:12 UTC, M_L 2.5; 12:17 UTC, M_L 2.4 - were clearly felt by people (Int. III-IV EMS) in the area comprising Pedara, Mascalucia, Tremestieri, S. Agata li Battiati and Gravina di Catania (data from HSIT, https://www.hsit.it/).

This minor seismic sequence was accompanied by an acceleration of creep along the southernmost section of the TMF, producing ground fracturing clearly visible within the urban area of Tremestieri.

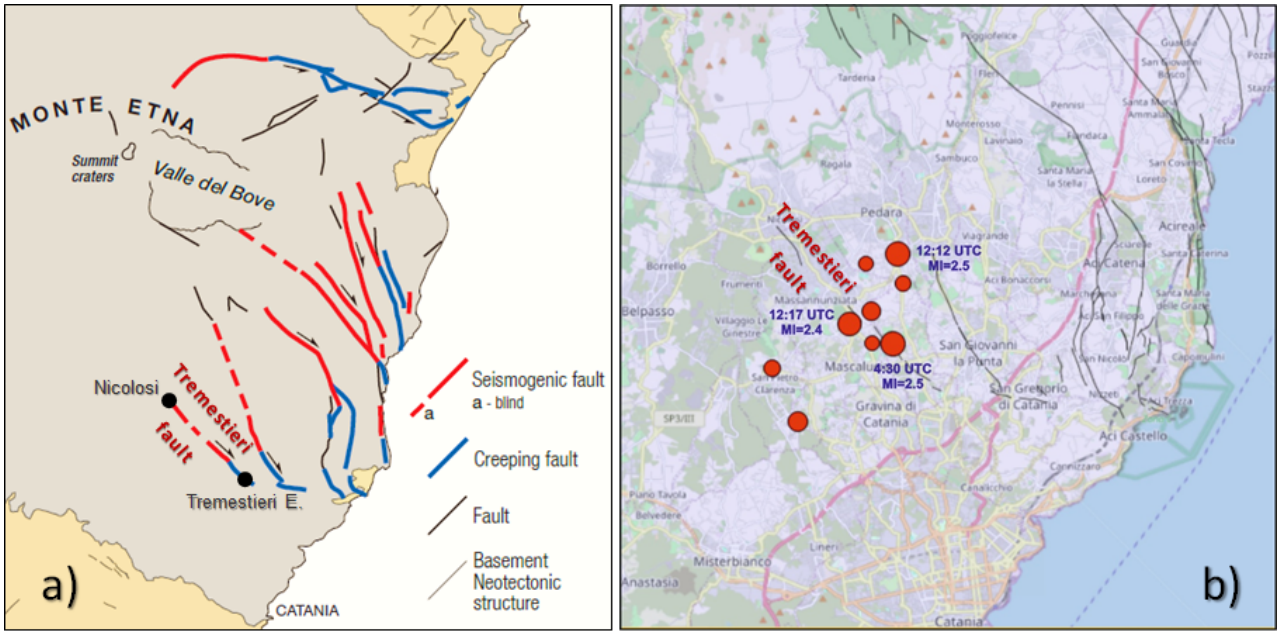

Fig. 1 – a) Seismotectonic model of the Etna region (from Azzaro et al., 2012); b) Preliminary location of the earthquakes recorded on November 17 and 18, 2025 (data from Barberi et al., 2020); the most energetic shocks, felt by people, are indicated with time and magnitude.

Field surveys documented the reactivation of pre-existing ruptures, with prevailing oblique-slip dextral kinematics and measured surface displacements of up to ~1.5 cm (Fig. 2). In addition to tectonic data collected during the field survey and the preliminary earthquake locations routinely produced for surveillance purposes, this seismotectonic activity was also recorded using different types of geophysical data. To characterize the entire seismicity, including very low-energy earthquakes, we integrated data acquired by the permanent INGV-OE seismic network with data recorded by two mobile seismic networks operating in the area since 2025, equipped with 3-C short period and broadband sensors. Accurate hypocentral locations allowed the identification of several clusters attributable to the TMF, enabling the description of the spatio-temporal evolution of the seismicity.

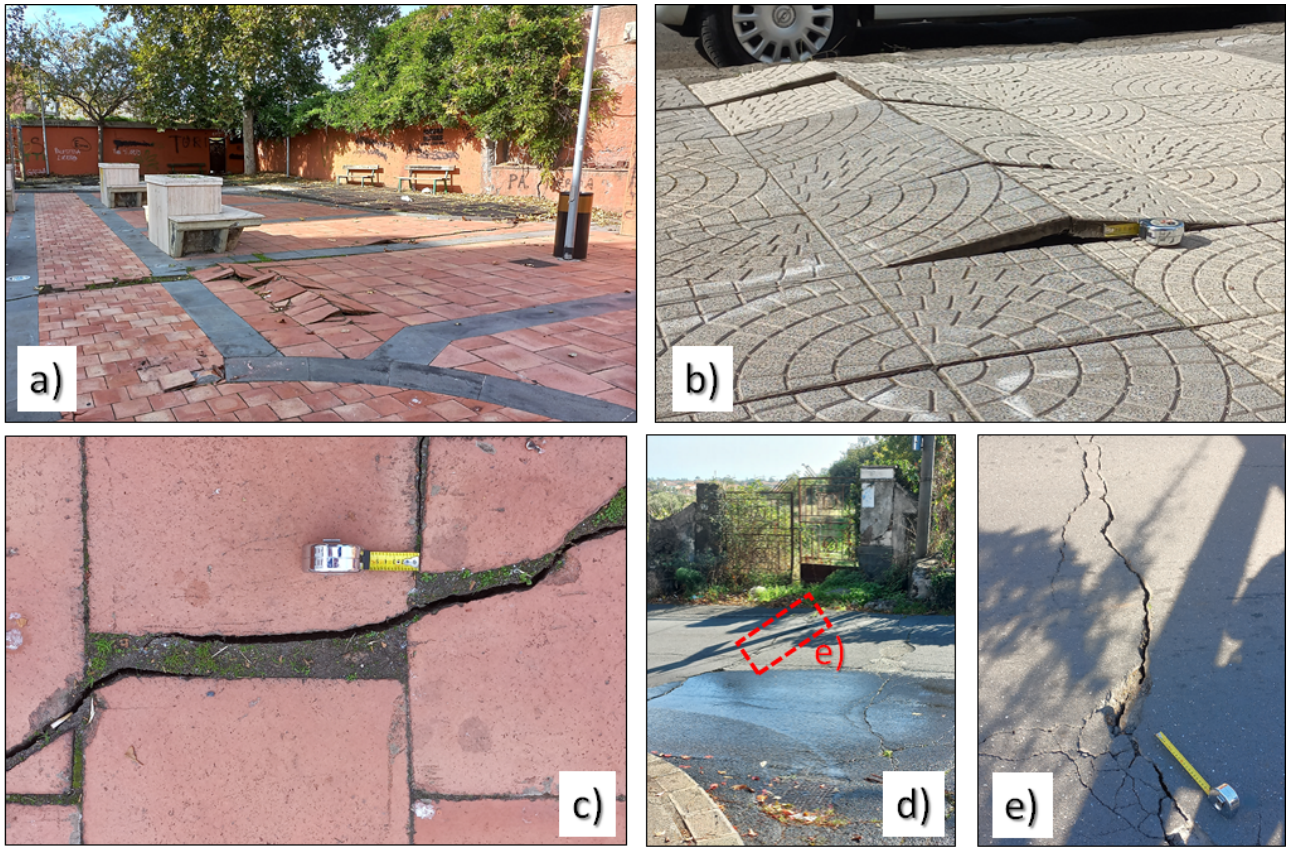

Fig. 2 – Creep effects in the urban area of Tremestieri: a) Fracture system crossing the small square along Via Etnea: the compression structure is determined by the right-component of displacement, the movement being partially hampered by the tessellation of the tiles; b) Compression structure formed on the opposite side of the same street: the shortening has caused a 5 cm uplift; c) Detail of a fracture in which the filling debris is detached from the edges of the fracture, indicative of a reactivation of a pre-existing fracture. Components of movement: horizontal 1 cm, vertical 0.5 cm; d) Fracture system cutting the road SP 3/II "Tremestieri-Mascalucia" and dislocating the gate of "Villa Maria"; note the breakage of a water pipe in the foreground; e) Detail of the main fracture, reactivated on November 17-18, 2025.

The seismotectonic activity was further investigated through geodetic observations using Differential SAR Interferometry (DInSAR). Sentinel-1A and Sentinel-1C SAR images were processed to generate both ascending and descending interferograms, allowing the detection and characterization of ground deformation associated with the Tremestieri Fault. The ascending interferogram covering the period from 15 to 21 November 2025 (Fig. 3a) reveals a well-defined and spatially localized deformation signal, clearly aligned with the mapped trace of the TMF. The observed line-of-sight displacement reaches a maximum value of approximately 2.5 cm across the fault zone, consistent with a shallow creeping process.

Additional independent evidence of fault activity is provided by a tiltmeter station (EMAS) located approximately 0.7 km from the fault on the footwall block. The instrument recorded a clear deformation signal (Fig. 3b), showing a progressive onset beginning in the afternoon preceding the seismic sequence, two more distinct coseismic steps associated with the strongest earthquakes, and a subsequent stabilization marking the end of the deformation episode. The overall deformation recorded at the EMAS station is compatible with a dextral kinematic of a few

centimetres along a fault plane aligned with the mapped trace of the TMF and with a dip-angle of about 70° (as reported in Azzaro et al., 2013).

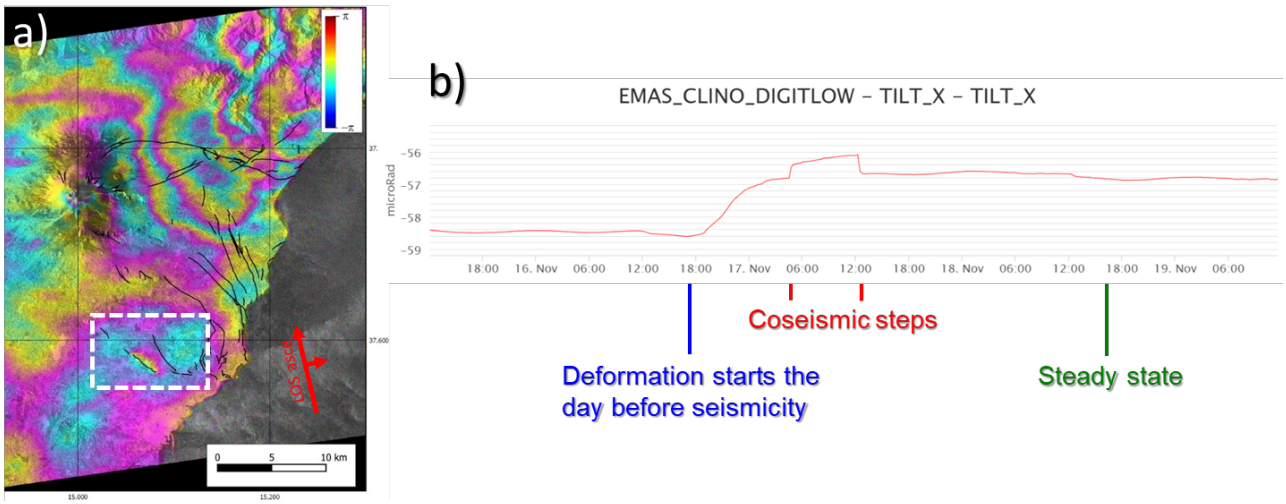

Fig. 3 – a) Tiltmeter signal recorded at the EMAS station, located 0.7 km from the Tremestieri fault, at a depth of 30 m in footwall; b) DInSAR analysis carried out on interferograms of Ascending Sentinel 1 C–A, 20251115_20251121: the white dashed box indicates the fault segment affected by the tectonic activity.

References

Azzaro R., Branca S., Gwinner K. & Coltelli M.; 2012: The volcano-tectonic map of Etna volcano, 1:100.000 scale: morphotectonic analysis from high-resolution DEM integrated with geologic, active faulting and seismotectonic data. It. J. Geosciences (Boll. Soc. Geol. It.), 131 (1), 153-170.

Azzaro R., Bonforte A., Branca S., Guglielmino F., Geometry and kinematics of the fault systems controlling the unstable flank of Etna volcano (Sicily), Journal of Volcanology and Geothermal Research, Volume 251, 2013, Pages 5-15, ISSN 0377-0273, https://doi.org/10.1016/j.jvolgeores.2012.10.001.

Barberi, G., Di Grazia, G., Ferrari, F., Firetto Carlino, M., Giampiccolo, E., Maiolino, V., Mostaccio, A., Musumeci, C., Scaltrito, A., Sciotto, M., Tusa, G., Tuvè, T., & Ursino, A.; (2020): Mt. Etna Revised Seismic Catalog from 2020 (EtnaRSC2020) (Version 1) [Data set]. Istituto Nazionale di Geofisica e Vulcanologia (INGV). https://doi.org/10.13127/ETNASC/ETNARSC2020

Rasà R., Azzaro R. & Leonardi O.; 1996: Aseismic creep on faults and flank instability at Mt. Etna volcano, Sicily. In. W.J. McGuire, A.P. Jones and J. Neuberg (Eds.), "Volcano instability on the Earth and other Planets", Geological Society Special Publication 110, 179-192, ISBN 1-897799-60-8.

Corresponding author: Raffaele Azzaro raffaele.azzaro@ingv.it

Human consequences in the seismic history of Italy

S. Baranello[1], A. Antonucci[2], A. Rovida[2], V. Pessina[2], M. Locati[2]

[1] *Istituto Nazionale di Geofisica e Vulcanologia, Bologna, Italy*
[2] *Istituto Nazionale di Geofisica e Vulcanologia, Milano, Italy*

The estimation of the number of casualties caused by seismic events is a fundamental component in the evaluation of seismic risk, the delineation of loss scenarios and the support of civil protection decisions.
Despite the significant advancement in understanding historical seismicity in Italy, the available data on the human consequences of past earthquakes remains fragmentary, heterogeneous, and challenging to compare due to its infrequent prioritisation in historical seismological research.
The present work sets out a methodological approach that aims to identify, collect and systematically organise information on victims and injuries associated with historical earthquakes in Italy from the published literature. The Italian Archive of Historical Macroseismic Data (ASMI) [Rovida et al., 2017; 2025] is used as a reference framework. ASMI aims to collect, classify and correlate a large number of seismological studies and catalogues, encompassing a time period exceeding a millennium, i.e, from 1000 CE to 2025. This comprehensive collection facilitates critical comparison between diverse seismological studies and datasets pertaining to the same event, thereby enhancing our understanding of each seismic event and its consequences.
The analysis commences with a review of earthquakes from the Italian Macroseismic Database (DBMI) [Locati et al., 2022], characterised by high maximum intensity (i.e., Ix ≥ 8), for which it is reasonable to expect significant consequences for the population. For each event, the studies selected for inclusion in the catalogue were examined, as well as all the alternative ones archived in ASMI, in order to capture the entire spectrum of available information. Particular attention was paid to reports of no casualties, considered significant information for interpretative purposes.
The survey revealed a wide variety of descriptive methods. These ranged from cases in which precise numbers of victims and injured persons were reported, sometimes broken down by locality, to qualitative or approximate indications (e.g. ranges of values or generic expressions), and even to the simple mention of the presence or absence of human consequences. In some cases, the victims were not directly attributable to the collapse of buildings, but to specific situations, such as the collapse of individual structures, or to induced phenomena and factors related to the vulnerability of people (landslides, panic, illness, behaviour during the event).
This heterogeneity makes any immediate quantitative synthesis complex and highlights the limitations of a purely numerical approach. To overcome these critical issues, work has begun on defining a standardised classification scheme capable of translating historical descriptive information into a more concise and parametric form, while maintaining a record of the level of uncertainty and the quality of the sources.
As might be expected, preliminary results indicate that, within the Italian context, the presence and number of victims do not exhibit a straightforward or significant correlation with the magnitude of the earthquake. Rather, they are influenced by a complex set of factors, including the

characteristics of the event, the vulnerability of buildings, the spatial distribution of damage, social conditions, and the manner in which historical sources have documented and transmitted information. Moreover, comparison with global databases highlights the scarcity of this type of information and the consequent necessity and importance of this work.
This research contributes to the ongoing process of enhancing ASMI as a tool for supporting macroseismic reconstruction, while also functioning as a repository of information for the study of the human consequences of historical earthquakes. The integration and systematic structuring of data on victims and injuries is a fundamental step towards making this information more reliable, transparent and usable in future seismic risk and loss scenarios.

References

Locati M., Camassi R., Rovida A., Ercolani E., Bernardini F., Castelli V., Caracciolo C.H., Tertulliani A., Rossi A., Azzaro R., D'Amico S., Antonucci A. (2022). Database Macrosismico Italiano (DBMI15), versione 4.0 [Data set]. Istituto Nazionale di Geofisica e Vulcanologia (INGV). https://doi.org/10.13127/dbmi/dbmi15.4

Rovida A., Locati M., Antonucci A., Camassi R. (a cura di) (2017). Archivio Storico Macrosismico Italiano (ASMI). Istituto Nazionale di Geofisica e Vulcanologia (INGV). https://doi.org/10.13127/asmi

Rovida A. Locati, M., Antonucci A., Camassi R. (2025). The Italian Archive of Historical Earthquake Data, ASMI. Earth System Science Data, 17(6), 3109–3124. https://doi.org/10.5194/essd-17-3109-2025

Corresponding author: sofia.baranello@ingv.it

Enhancing earthquake monitoring with fiber-optic networks via automatic data selection

E. Bozzi[1], G. Pascucci[1], G. Rapagnani[1], G. M. Bocchini[2], R. Harrington[2], A. Ugalde[3], G. Saccorotti[4], F. Grigoli[1]

[1] *Department of Earth Sciences, University of Pisa, Pisa, Italy*
[2] *Institute of Geosciences, Ruhr University Bochum, Bochum, Germany*
[3] *Department of Marine Geosciences, Institut de Ciències del Mar, CSIC, 08003 Barcelona, Spain*
[4] *Istituto Nazionale di Geofisica e Vulcanologia, Pisa, Italy*

Seismic monitoring networks benefit from the integration of conventional sensors with fiber-optic sensing systems such as Distributed Acoustic Sensing (DAS). However, most advantages remain limited to offline analyses as the automated, real-time management of large DAS data volumes remains challenging. To address this, we introduce *ORION*, a tool for rapid and automatic identification of high-quality DAS channels. The workflow consists of two stages: (a) an initial spatial clustering that divides the fiber-optic cable into subsections with similar geometrical attributes, and (b) the subsequent selection of channels within these subsections using waveform-based quality indicators. This procedure ensures both sufficient spatial coverage and the inclusion of a few robust channels, which are essential for a more efficient source characterization. Additionally, automated subsampling can facilitate data transmission and expert review in near real-time.

We test the automatic data selector on various cable geometries and use it to locate events from a seismic sequence that occurred in August 2024 northwest of Kefalonia Island (Greece), comparing its performance with that of an equal number of evenly distributed channels. *ORION* improves location accuracy, demonstrating its potential as a plug-and-play solution for near real-time, fiber-optic–based earthquake monitoring.

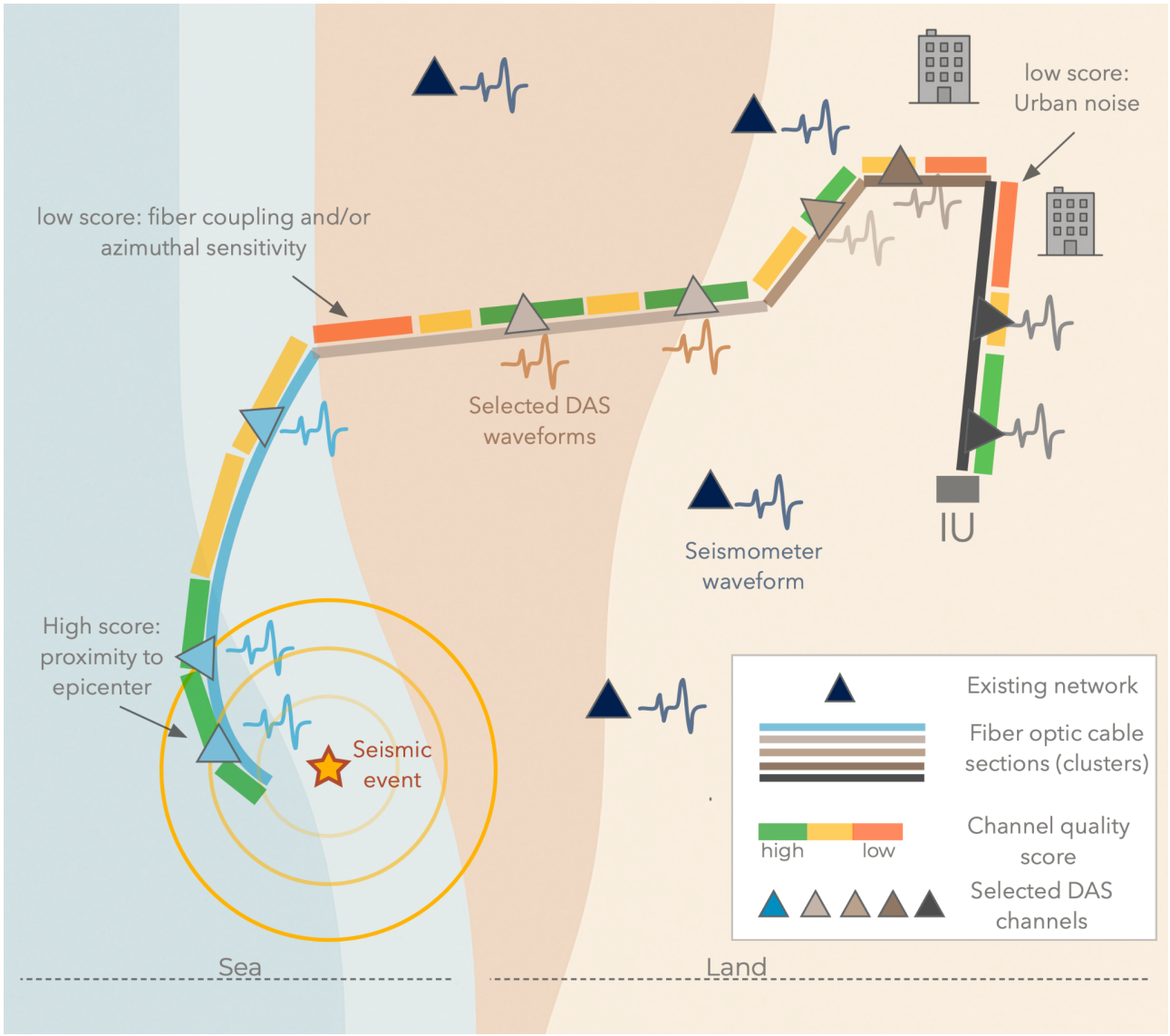

Fig. 1 – Schematic overview of the proposed automatic DAS channel selection workflow (identified as *ORION*) for a hybrid land–marine fiber-optic cable (colored line) and onshore seismic network (dark blue triangles) deployment. The procedure consists of: (1) spatial clustering, represented by color-coded cable segments; (2) channel quality scoring, illustrated with three colors (red, yellow, and green); and (3) final channel selection, shown by triangles. Figure from Bozzi et al., 2025.

References

Bozzi, E., Pascucci, G., Rapagnani, G., Bocchini, G. M., Harrington, R., Ugalde, A., Saccorotti, G., & Grigoli, F. (2025). *Near real-time channel selection for Distributed Acoustic Sensing technology*. arXiv. https://arxiv.org/abs/2512.08845

Corresponding author: emanuele.bozzi@dst.unipi.it

Revealing Seismic Sequence Characteristics in the South-eastern Alps and the Western Dinarides by clustering analysis and refined location

P. Brondi[1], M. Picozzi[1], G. De Landro[2], A. G. Iaccarino[2], G. Rossi[1], A. Lomax[3], A. Magrin[1], L. Zampa[1], M. Michele[4]

[1]National Institute of Oceanography and Applied Geophysics - OGS, Sgonico, Trieste, Italy
[2]Università di Napoli "Federico II", Naples, Italy
[3]ALomax Scientific, Mouans-Sartoux, France
[4]Istituto Nazionale di Geofisica e Vulcanologia – INGV, Rome, Italy

Characterizing seismicity patterns is essential for improving seismic hazard assessments, as temporal and spatial variations in earthquake occurrence reflect changes in fault loading conditions and crustal stress. In this context, analyzing seismic sequences is crucial for investigating the activation of complex fault structures and understanding earthquake triggering processes (Riga and Balocchi, 2015; Petersen et al., 2025).

In this study, we analyzed the seismicity from the past decade (2015-2024) in the South-Eastern Alps and the Western Dinarides regions (SEAWD), an area characterized by moderate to high seismic hazard and the recent occurrence of the high-magnitude Mw 6.5 Friuli earthquake (1976). Using the seismic catalog provided by the Northeastern Italy Seismometer Network, operated by the Seismological Research Center (CRS) of the National Institute of Oceanography and Experimental Geophysics - OGS [international code OX, (Istituto Nazionale di Oceanografia e di Geofisica Sperimentale - OGS 2016)], we applied a clustering analysis (Zaliapin and Ben-Zion, 2013) and the NLL-SSST Coherence algorithm (Lomax and Savvaidis, 2022) to identify the seismic sequences and reconstruct their spatio-temporal evolution with high accuracy.

We identified 75 seismic sequences (Figure 1) that we classified according to Mogi (1963): 49 of the Foreshock-Mainshock-Aftershock sequences (65%), 25 of the Mainshock-Aftershock sequences (32%), and 1 of the Swarm type. Notably, on average, Mainshock-Aftershock sequences exhibit a stronger mainshock than Foreshock-Mainshock-Aftershock sequences. Ongoing analyses aimed at a detailed characterization of the identified sequences are expected to provide further insights into fault interaction processes and the spatio-temporal evolution of stress in the study area.

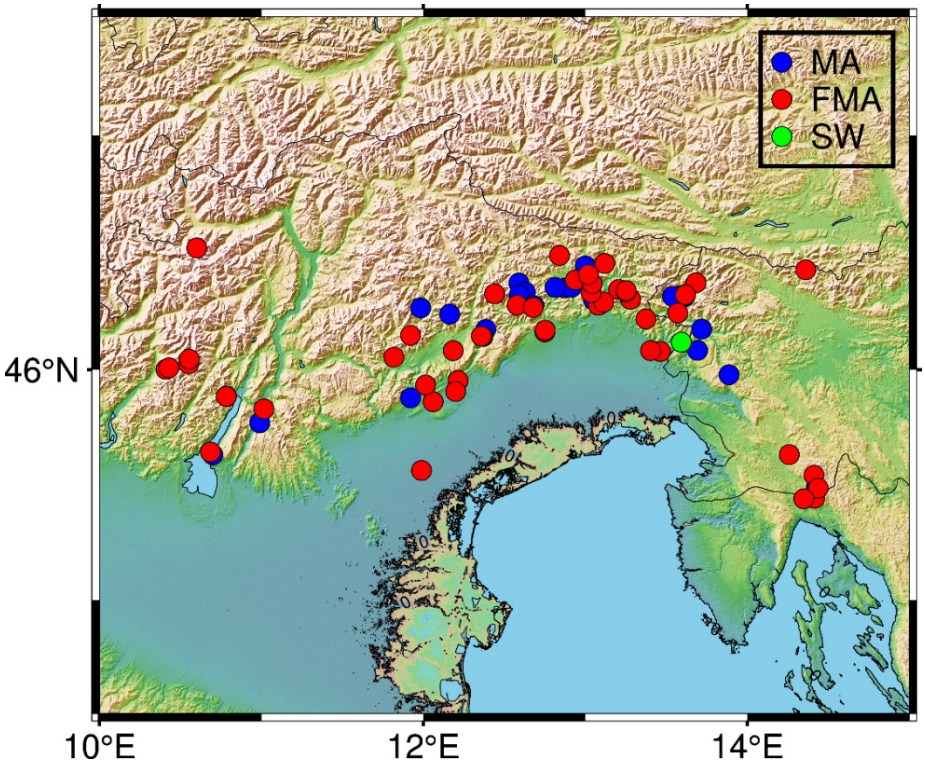

Fig. 1 – Types of the 75 seismic sequences identified during 2015–2024: Foreshock-Mainshock-Aftershock (FMA), Mainshock-Aftershock (MA), and Swarm (SW)

References

Istituto Nazionale di Oceanografia e di Geofisica Sperimentale – OGS; 2016: North-East Italy Seismic Network [Data set]. International Federation of Digital Seismograph Networks. https:// doi.org/10.7914/SN/OX

Lomax, A., & Savvaidis, A.; 2022: High-precision earthquake location using source-specific station terms and inter-event waveform similarity. Journal of Geophysical Research: Solid Earth, 127, e2021JB023190. https://doi.org/10.1029/2021JB023190

Mogi, K.; 1963: Some discussions on aftershocks, foreshocks, and earthquake swarms: the fracture of a semi-infinite body caused by an inner stress origin and its relation to the earthquake phenomenon. Bull. Earthquake Res. Inst., 41, 615-658.

Petersen, G. M., Hofman, L. J., Kummerow, J., & Cesca, S.; 2025: Microseismicity in the large-N Swath-D network: Revealing seismic sequences and active faults in the eastern Alps. Journal of Geophysical Research: Solid Earth, 130, e2024JB030516. https://doi.org/10.1029/2024JB030516

Riga, G., & Balocchi, P.; 2015: Seismic sequence structure and earthquakes triggering patterns. Open Journal of Earthquake Research, 5(1), 20-34.

Zaliapin, I., Ben-Zion, Y.; 2013: Earthquake clusters in southern California I: identification and stability. J. Geophys. Res. Solid Earth 118, 2847–2864. https:// doi.org/10.1002/jgrb.50179.

Corresponding author: pbrondi@ogs.it

Investigating Fault Behaviour on Mt. Etna's Eastern Flank through Sentinel-1 InSAR Time Series (2015–2020)

S. Brooks[1,2], F. Guglielmino[1]

[1] *Istituto Nazionale di Geofisica e Vulcanologia - Osservatorio Etneo, Catania, Italy*
[2] *Dipartimento di Scienze Biologiche, Geologiche ed Ambientali - Università di Catania, Italy*

The eastern flank of Mt. Etna represents one of the most dynamic tectonic environments worldwide, characterized by exceptionally high slip rates, active faulting, and large-scale gravitational flank sliding. Bounded to the north by the Pernicana Fault and to the south by the Tremestieri–Trecastagni Fault system, this sector hosts a complex and dense fault network where locked and creeping segments coexist, resulting in a highly heterogeneous and rapidly evolving pattern of surface deformation (Azzaro et al., 2013). High spatial resolution geodetic observations, such as InSAR, have proven essential for resolving fault behaviour, including the identification of locked and creeping segments (Bürgmann et al., 2000).

To investigate these processes, we analysed a five-year Sentinel-1 SAR time series (2015–2020) acquired in both ascending and descending geometries over Mt. Etna. During this period, the volcano experienced a major dike intrusion starting on 24 December 2018, followed by a Mw 5.0 earthquake on 26 December 2018 along the Fiandaca Fault. Interferograms were generated using ISCE2 (Rosen et al., 2012), and displacement time series were reconstructed with MintPy (Yunjun et al., 2019), producing mean velocity maps with millimetric accuracy (Fig. 1).

The InSAR time series were processed using a dedicated workflow to ensure reliable deformation estimates. Interferograms were unwrapped using optimized phase unwrapping to handle complex topography and connected components. Subsequent processing in MintPy included multilooking, selection of high-coherence reference pixels, and correction of phase unwrapping errors, as well as atmospheric and topographic artefacts and long-wavelength spatial trends. This workflow enabled the computation of distinct pre- and post-event velocities, the isolation of the co-seismic signal from long-term deformation, and the quantification of ground displacement before, during, and after the 26 December 2018 earthquake, providing a comprehensive view of the eastern flank dynamics.

Based on these products, the multi-geometry InSAR results (Fig. 1) reveal detailed deformation patterns across the volcano prior to the 26 December 2018 earthquake (Mw 5.0), several major structures appeared largely locked, exhibiting only minor displacement related to broad-scale flank motion. Following the seismic event, a clear acceleration of motion was observed along multiple fault segments, indicating the activation of previously locked structures and their contribution to post-event deformation.

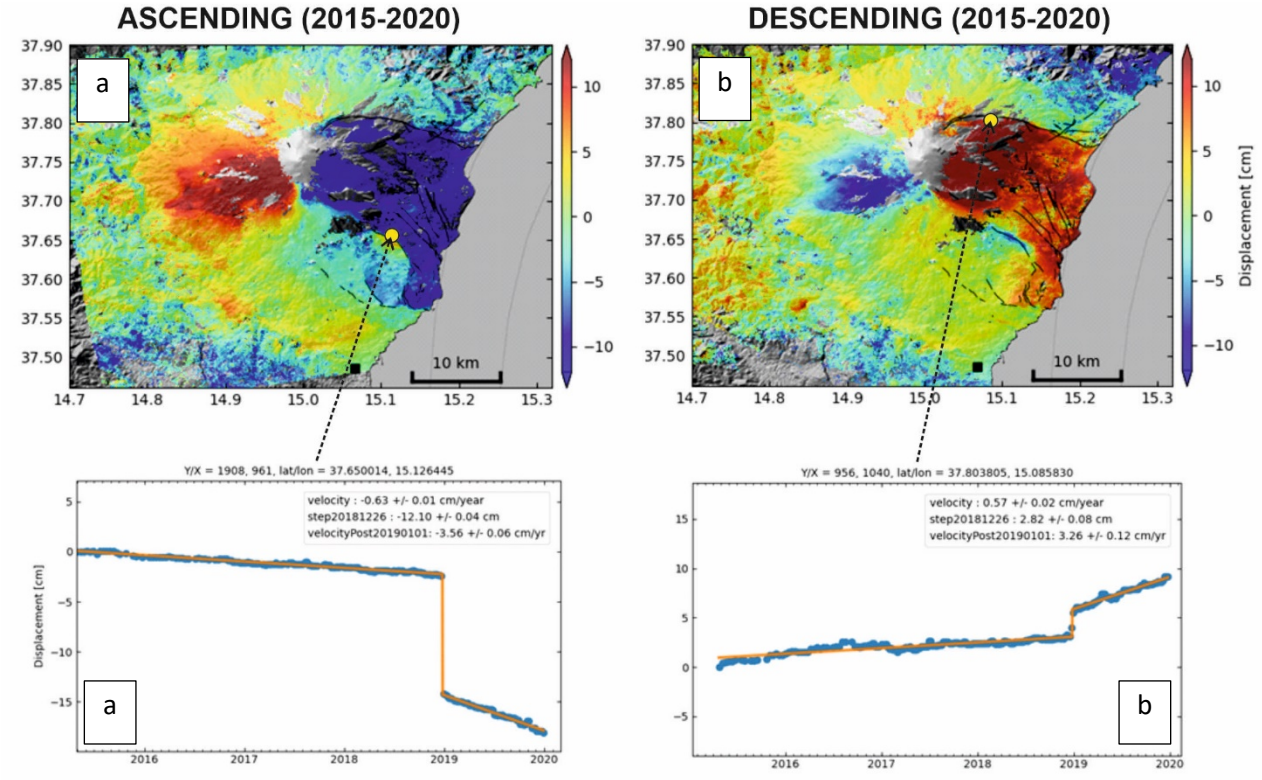

Fig. 1 Ascending (a) and descending (b) Sentinel-1 InSAR time series (2015–2020) illustrating different fault behaviour on Mt. Etna's eastern flank. The ascending example refers to a point located on the Fiandaca Fault (37.650°N, 15.126°E), which shows a jump of 12 cm due to the 26 December 2018 earthquake and a velocity increase in the post-seismic period. The descending example refers to a point located on the Pernicana Fault (37.803°N, 15.085°E), characterized by continuous creep and an increased deformation rate following the earthquake.

To quantify fault-related deformation, we applied a temporal differencing technique within the InSAR time series by comparing the displacement histories of pairs of points located on the hanging-wall and footwall of individual faults (Fig. 2). For each fault, the relative displacement between the two sides is computed as a function of time, providing a direct measure of fault slip across the structure.

While the single-point time series shown in Figure 1 represents the full ground deformation signal resulting from the combined effects of volcanic inflation–deflation cycles, large-scale gravitational flank motion, and fault activity, this differencing approach removes deformation components common to both sides of the fault, isolating the displacement associated with fault slip. This technique provides a clear and geologically meaningful representation of pre-seismic, co-seismic and post-seismic fault slip.

Our observations indicate that deformation is not confined to single structures but involves multiple faults, each characterized by distinct kinematic behaviour, confirming the conceptual models based on historical and field data (Azzaro et al., 2012). Overall, this study demonstrates the potential of multi-geometry InSAR time series to resolve fine-scale fault behaviour in a complex tectonic environment. Although based on a relatively short observation period of five years, the

results highlight the value of extending the analysis to longer time spans. A ten-year dataset, which represents the next step of our ongoing work, will be essential for more robust identification of locked and creeping fault patches and for better constraining their interaction with post-earthquake accelerations. Ultimately, this approach offers valuable constraints on fault kinematics, improves our understanding of Mt. Etna's eastern flank dynamics, and contributes significantly to the advancement of fault-based seismic hazard assessments in this highly exposed area.

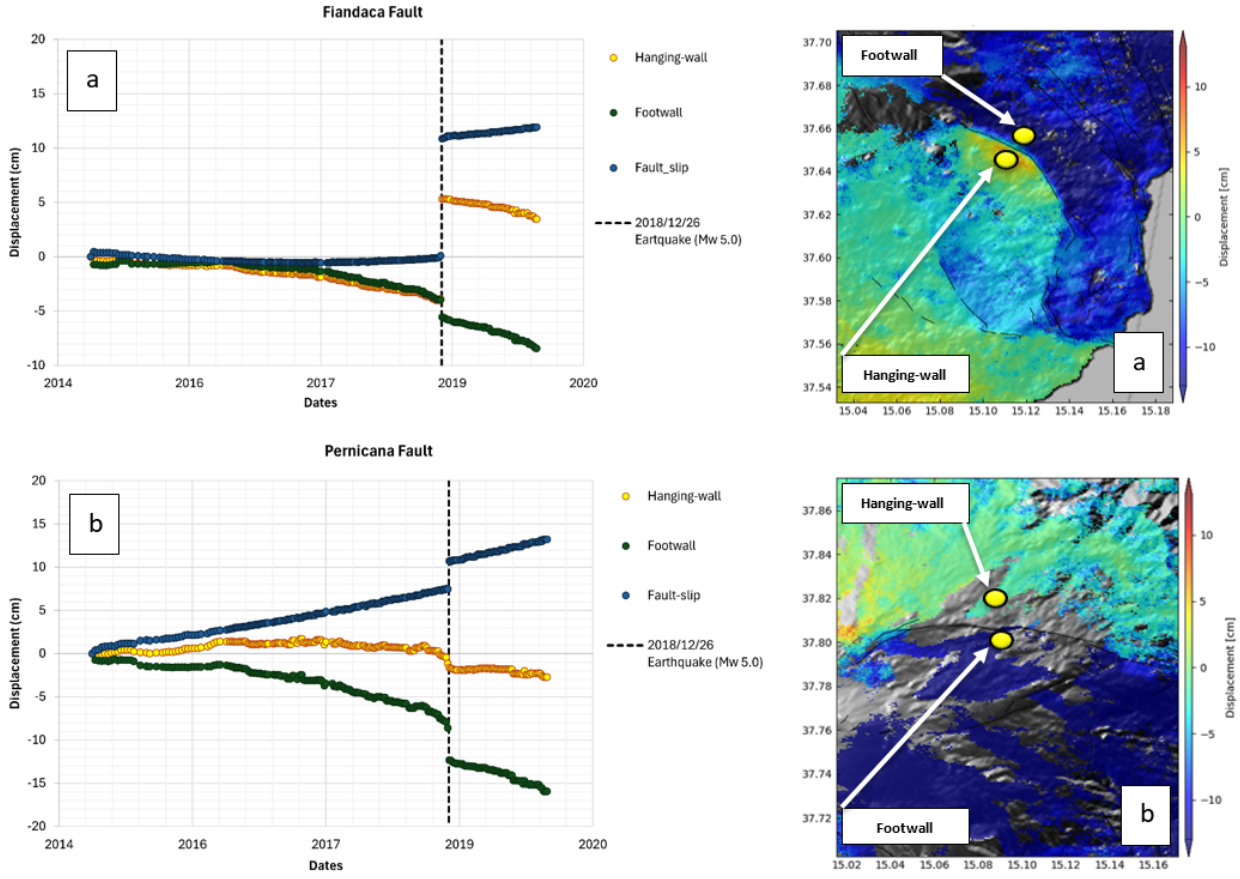

Fig. 2 Fault-related deformation derived from InSAR time series using temporal differencing between hanging-wall and footwall points. Upper panels (a): ascending geometry across the Fiandaca Fault, showing footwall (green), hanging-wall (yellow), and differential fault slip (blue). The dashed black line marks the 26 December 2018 earthquake. The Fiandaca Fault is locked before the event and accelerates afterwards. Lower panels (b): same analysis for the Pernicana Fault, which exhibits continuous creep and a post-earthquake velocity increase.

References

Azzaro R., Branca S., Gwinner K., Coltelli M.; 2012. The volcano-tectonic map of Etna volcano, 1:100.000 scale: morphotectonic analysis from high-resolution DEM integrated with geologic, active faulting and seismotectonic data. It. J. Geosciences (Boll. Soc. Geol. It.), 131 (1), 153-170.

Azzaro R., Bonforte A., Branca S., Guglielmino F.; 2013. Geometry and kinematics of the fault systems controlling the unstable flank of Etna volcano (Sicily), Journal of Volcanology and

Geothermal Research, Volume 251, 2013, Pages 5-15, ISSN 0377-0273, https://doi.org/10.1016/j.jvolgeores.2012.10.001.

Bürgmann R., Rosen, P., Fielding, E.; 2000. Synthetic aperture radar interferometry to measure Earth's surface topography and its deformation: Annual Review of Earth and Planetary Sciences, v. 28, p. 169–209, doi: 10.1146/annurev.earth.28.1.169

Rosen P. A., Gurrola E., Sacco G. F., Zebker H.; 2012. The InSAR scientific computing environment.

Yunjun Z., Fattahi H., Amelung F.; 2019. Small baseline InSAR time series analysis: Unwrapping error correction and noise reduction, Computers & Geosciences, Volume 133, 2019, 104331, ISSN 0098-3004, https://doi.org/10.1016/j.cageo.2019.104331.

Corresponding author: Steven Jeffrey Brooks steven.brooks@phd.unict.it

Structural inheritance still controlling the seismotectonic of the central Apennines (Italy): lessons learned by the last major seismic sequences and implications for seismic hazard assessment

Mauro Buttinelli[1], Francesco Emanuele Maesano[1], Roberta Maffucci[1], Giuseppe Vico[1], Mario Anselmi[1]

[1] *Istituto Nazionale di Geofisica e Vulcanologia, INGV*

The central Apennines (Italy) represent one of the highest seismic hazard areas in the central Mediterranean, characterized by large mainshock-aftershock seismic sequences and a marked geological and structural complexity.

In recent decades, the inner portion of the central Apennine chain has been affected by multiple mainshock-aftershock seismic sequences characterized by several magnitude 6+ events with normal-faulting kinematics related to active post-orogenic extension (e.g., the 1997 Umbria-Marche, 2009 L'Aquila-Campotosto, and 2016-2017 Amatrice-Visso-Norcia-Campotosto events).

This contribution presents a synthetic view of the upper crust across an area of approximately 300 x 100 km² affected by those sequences, extending along the NW-SE direction of the chain to a depth of 15-20 km.

We propose a 3D geological model developed to honor as much as possible the large amount of geological and geophysical observations by gathering updated geological and geophysical data, techniques, and approaches. This unleashes the possibility of making new, robust inferences regarding the relationship between large seismogenic faults and the observed seismicity.

The synoptic view of this large portion of the Apennine crust experiencing such a complex seismic behaviour highlights striking similarities among the last three seismic sequences.

The common thread is the role played by the reactivation and interaction between inherited structures, such as large thrust and normal faults, under the current extensional stress field, which may lie behind the more energetic seismic sequences. Also, crustal fluids trapped between thrusts, acting as mechanical and rheological barriers, control the energy and behavior of most large seismic events.

Such a comprehensive view highlights the central Apennines' distinctive and broad seismogenic character, with significant implications for a more in-depth reassessment of the region's seismotectonics and seismic hazard.

Discriminating the 1688 Sannio earthquake source: ShakeMap-driven validation of competing seismogenic hypotheses

A. Capozzoli[1*], V. Paoletti[1,2], J. Elez[3], P.G. Silva[3], S. Porfido[2], A.M. Michetti[4,2], R. Nappi[2]

[1] Department of Earth, Environmental and Resource Sciences, University of Naples Federico II, Naples, Italy

[2] Istituto Nazionale di Geofisica e Vulcanologia, Naples Section, Osservatorio Vesuviano, Italy

[3] Department of Geology, University of Salamanca, Higher Polytechnic School, Avila, Spain

[4] Dipartimento di Scienza e Alta Tecnologia, Università degli Studi dell'Insubria, Como, Italy

Introduction

The Sannio-Matese area is a high-seismic-risk region of the southern Apennines (Italy), characterized by strong earthquakes ($M_w > 5.5$) in historical records and low-energy instrumental seismicity in the last century. The latter includes isolated events of local magnitude $M_L < 3.0$ with hypocenters up to 20 km depth, seismic sequences and swarms of weak to moderate magnitude, such as the 2013–2014 Matese sequence ($M_L \leq 5.0$) and those from the 1997–2005 ($M_L \leq 4.0$). In contrast, major historical earthquakes have reached M_w up to 7 and are interpreted as associated with NW-SE and E-W faults (e.g., *Mayer Rosa et al., 1993*). Notable examples are the 1456 ($M_w = 7.1$) and 1805 ($M_w = 6.8$) Molise events, the 1688 ($M_w = 7.0$) Sannio earthquake, the 1732 ($M_w = 6.7$) and 1980 ($M_w = 6.9$) Irpinia earthquakes and the 1857 ($M_w = 7.1$) Basilicata event. For several of these, the seismogenic source is identified with reasonable confidence: the 1980 Irpinia earthquake has been attributed to a segmented NW-SE striking fault system (*Porfido et al., 2020*) and the 1805 event is commonly associated with the Bojano Basin fault system, dipping towards NE (*Di Bucci et al., 2005*). In contrast, the fault for the 1688 earthquake ($I_0 = XI\,MCS$), one of the most catastrophic in the region, with over 10,000 victims and total destruction of cities such as Cerreto Sannita (*Rovida et al., 2022*), remains a scientific enigma. Despite macroseismic data from historical archives (*Serva, 1981; Capozzoli et al., 2025 a,b*), its source location and geometry are debated (e.g., *Cinque et al., 2000; Galadini and Galli, 2000; Nappi et al., 2008*). Hypotheses include: i) a SW-dipping, NW-trending normal fault ~30 km long between Cerreto Sannita and Paduli (*Pantosti and Valensise, 1988*); ii) an inferred active system north of Monte Camposauro, ~32 km long and dipping NE (*Di Bucci et al., 2005*); iii) a 45 km long fault system in the Calore River valley, between Apice and Solopaca, with two E–W segments dipping NE connected by a N–S transfer zone near Benevento (*Amato et al., 2025*). These and other proposals derive from the combination of structural geology, historical catalogues and kinematic modelling. Traditional approaches to source discrimination for pre-instrumental earthquakes rely heavily on intensity data inversion or paleoseismological trenching, both suffering from inherent uncertainties. Typical limestone post-glacial bedrock fault scarps which characterize

most active faults in the Southern Apennines (*Sgambato et al., 2025* and reference therein), are lacking in the 1688 epicentral area. Cretaceous to Miocene tectonic melange and Pliocene clays dominate the Benevento Basin; landslides and gravity deformations prevail, masking young normal fault scarps. Macroseismic intensities, typically derived from MCS or EMS-98 scales, are subjective and sparse in epicentral areas, especially in historical contexts, where i) reports were confined to small urban centres existing at the time, often located sparsely and unevenly across the region, leaving vast rural areas undocumented, and ii) construction materials used were far more vulnerable than modern standards, resulting in overestimated intensities not directly comparable to modern conditions. Only the integration of earthquake environmental effects (EEEs) of the ESI-07 scale enables reliable intensity assessment for historic-modern comparisons (e.g., *Michetti et al., 2007*): (i) across time, as landscape impacts persist beyond instrumental periods; and (ii) across areas, independent of socioeconomic or construction variations. Paleoseismological trenching, in contrast, has coarse temporal resolution (± centuries), requiring multiple trenches along a fault to constrain rupture extent. Furthermore, erosion, sedimentation and anthropogenic disturbance often obscure or destroy key stratigraphic and geomorphic (i.e. scarps) markers, with challenging siting in rugged, colluvium-covered terrain yielding inconclusive results. This study introduces a workflow to test competing seismogenic source hypotheses for the 1688 Sannio earthquake. By generating synthetic ShakeMaps for each proposed source and comparing modelled Peak Ground Acceleration (PGA) distributions with macroseismic effects including both building damage (i.e. MCS Scale) and environmental impacts (ESI-07 Scale), we obtain hybrid scenarios as discriminant criterion. The approach leverages Ground-Motion Prediction Equations (GMPEs) for active tectonic regimes used in the USGS ShakeMap Program (*Wald et al., 2005*), incorporating amplification factors and high-resolution topographic datasets proposed by Silva et al. (*2017*). Here, this method discriminates more viable seismic sources, quantitatively demonstrates the inadequacy of certain proposed interpretations, thereby providing a methodological framework for historical earthquakes worldwide, where data scarcity is pervasive.

Methodology

ShakeMaps are typically employed for near-real-time alerting and post-earthquake response to identify shaking-affected areas, or to develop emergency plans and seismic scenarios in populated regions. Another key application involves producing scenarios for future or historical earthquakes. However, existing ShakeMaps for historical events are scarce and generally are applications of standard GMPEs. Research on historical, ancient and prehistoric earthquakes benefits from this modelling tool by integrating catalogued natural effects, paleoseismic and archaeo-seismic data (e.g., *Silva et al., 2023*). These works propose methodological workflows for generating seismic scenarios (in terms of PGA) for historical blind-faulting events, such as the 1688 earthquake. The methodological workflow integrates multiple GIS layers: coseismic EEEs, damage data, high-resolution digital terrain models (DTMs), slope maps and GMPEs. Earthquake models are typically computed using USGS ShakeMap software, requiring key inputs such as epicenter location, fault plane dimensions and geometry, fault type, magnitude (M_w), Joyner-Boore distance (R_{JB}) and site-condition maps (V_{S30}). The latter two parameters are critical for reliable PGA spatialization. The USGS simplified GMPE comprises three terms: 1) a third-order polynomial dependent on faulting

style and magnitude (M) (standardized for various fault types); 2) a logarithmic term tied to Joyner-Boore distance (R_{JB}); and 3) a logarithmic site term based on shear-wave velocity in the upper 30 m (V_{S30}). Site maps are typically derived empirically by correlating terrain slope with V_{S30} (steep slopes → high V_{S30} and so rocky sites; low slopes → low V_{S30} and so soft sediments). This introduces lack of correlation between observed slope failures and modelled PGA, particularly in steep areas where amplification is underestimated, and PGA overestimation in flat areas lacking thick unconsolidated sediments, as slope-based V_{S30} assumes deep deposits. To address these, two correction factors were introduced by Silva et al., 2017: i) a topographic amplification factor, and ii) a sediment thickness correction. The preliminary study presented here applies the full procedure outlined in Figure 1 to the 1688 Sannio earthquake. Lacking fault data, we first tested some of the previously proposed sources (*Pantosti and Valensise, 1988; Gasperini et al., 1999; Cinque et al., 2000; Galadini and Galli, 2000; Valensise and Pantosti, 2001; Di Bucci et al., 2005; Amato et al., 2025)*. For each source, we defined rupture parameters, where absent, using the empirical relationships proposed by Wells and Coppersmith (*1994*). PGA thresholds follow the Faenza and Michelini (*2010*) relations for Italian intensities.

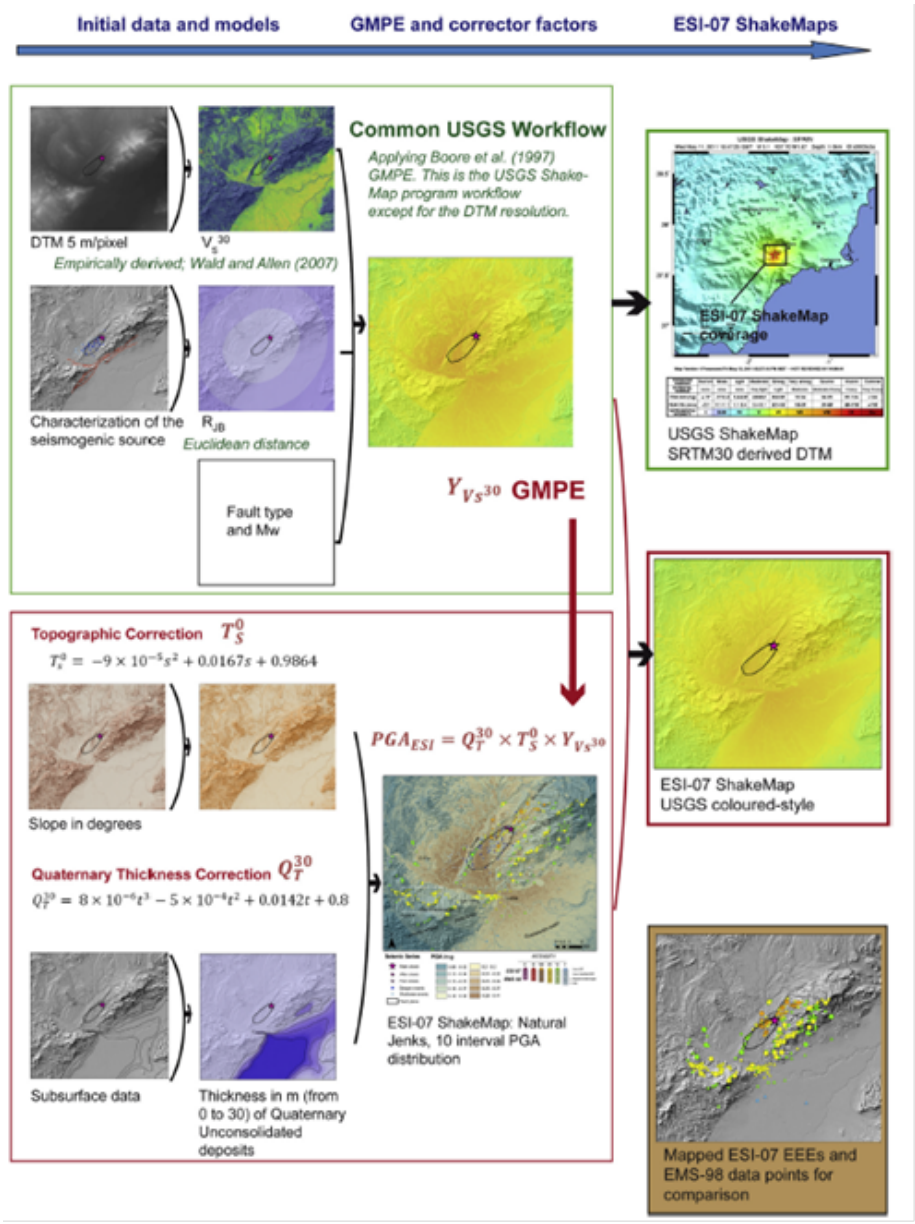

Fig. 1 – Graphical workflow of the methodology used and the differences with the USGS ShakeMap method (without corrections) (*Silva et al., 2017*).

Validation against macroseismic data

Macroseismic damage data were sourced from the *Catalogo dei Forti terremoti in Italia (461 a.C. - 1997) e nell'area mediterranea (760 a.C.-1500)* (CFTI5Med; *Guidoboni et al., 2019*), providing ~170 intensity data points, while environmental effects data derive from Capozzoli et al. (*2025 a,b*), cataloguing 43 coseismic effects of varying ESI-07 intensity. Model fit was assessed through i) spatial correlation between modelled PGA and derived intensities, ii) comparison between expected and modelled maximum PGA values, and iii) directivity alignment between PGA distributions and observed damage patterns.

Results

ShakeMap comparisons with macroseismic and environmental data show no proposed seismogenic sources reproduce observed effects. None of the proposed sources (fault dimensions, geometry, orientation) generate PGA matching intensities, damage patterns and environmental impacts of the 1688 earthquake. Most fail directivity, with mismatches between maxima PGA and coseismic effects or damaged zones. All yield PGA too low for ≥ X MCS (*Faenza & Michelini, 2010*). Our ShakeMap workflow (high-resolution DTMs, site V_{S30}, topographic amplification and quaternary sediment corrections) robustly tests hypotheses. For the 1688 Sannio earthquake ($I_0 = XI\,MCS$), it unequivocally rejects all literature-proposed sources. No proposed source adequately explains this destructive event, highlighting the need for new hypotheses. Critically, this study prompts a revision of the 1688 earthquake's intensities which, based on historical records, is considered one of the southern Apennines' most devastating events and served as a reference for regional seismic hazard and risk assessments. However, if intensities have been overestimated due to methodological limitations, the resulting risk scenario associated with the area changes dramatically. This carries profound implications across seismic hazard mapping, economic planning and building codes for the Campania-Molise region.

References

Amato V.; Ciarcia S.; ... & Giaccio B.; 2025. Unveiling the hidden source of major historical earthquakes: A multi-scale, trans-disciplinary approach to the 1456 and 1688 Sannio earthquakes (Mw 7.0, southern Italian Apennines). Quaternary Science Reviews.

Boore D.M.; Joyner W.; Fumal T.; 1997. Equations for estimating horizontal response spectra and peak acceleration from Western North American earthquakes: a Summary of recent Work. Seismological research letters.

Capozzoli A.; Paoletti V.; … Nappi R.; 2025a. The 1688 Sannio–Matese Earthquake: A Dataset of Environmental Effects Based on the ESI-07 Scale. Data.

Capozzoli A.; Paoletti V.; … Nappi R.; 2025b. Comprehensive Dataset on 1688 Sannio–Matese Earthquake Environmental Impact. Mendeley Data.

Cinque A.; Ascione A.; Caiazzo C.; 2000. Distribuzione spazio-temporale e caratterizzazione della fagliazione quaternaria in Appennino meridionale. Le ricerche del GNDT nel campo della pericolosità sismica.

Di Bucci D.; Massa B.; Tornaghi M.; Zuppetta A.; 2005. Structural setting of the 1688 Sannio earthquake epicentral area (Southern Italy) from surface and subsurface data. Journal of Geodynamics.

DISS Working Group 2025. Database of Individual Seismogenic Sources (DISS), Version 3.3.1: A compilation of potential sources for earthquakes larger than M 5.5 in Italy and surrounding areas. Istituto Nazionale di Geofisica e Vulcanologia (INGV).

Faenza L.; Michelini A.; 2010. Regression analysis of MCS intensity and ground motion parameters in Italy and its application in ShakeMap. Geophysical Journal International.

Galadini F.; Galli P.; 2000. Active tectonics in the central Apennines (Italy)–input data for seismic hazard assessment. Natural Hazards.

Gasperini P.; Bernardini F.; Valensise G.; Boschi E.; 1999. Defining Seismogenic Sources from Historical Earthquake Felt Reports. Bulletin of the Seismological Society of America.

Guidoboni E.; Ferrari G.; … Valensise G.; 2019. CFTI5Med, the new release of the catalogue of strong earthquakes in Italy and in the Mediterranean area, Scientific Data.

Mayer-Rosa D.; Slejko D.; Zonno G.; 1993. Assessment of seismic hazard for the Sannio-Matese area, Southern Italy (Project" TERESA").

Michetti A.; Esposito E.; ... Roghozin E.; 2007. Environmental Seismic Intensity Scale 2007-ESI 2007.

Nappi R.; Alessio G.; … Vilardo G.; 2008. Contribution of the SISCam Web-based GIS to the seismotectonic study of Campania (Southern Apennines): an example of application to the Sannio-area. Natural Hazards.

Pantosti D.; Valensise G.; 1988. La Faglia Sud-Appenninica: Identificazione Oggettiva Di Un Lineamento Sismogenetico Nell'Appennino Meridionale. In Proc. 7th Meeting G.N.G.T.S., Rome, Italy, 28–30 November.

Porfido S.; Alessio G.; … Michetti A. M.; 2020. The 23rd November 1980 Irpinia-Lucania, Southern Italy Earthquake: Insights and Reviews 40 Years Later.

Rovida A.; Locati M.; … Antonucci A.; 2022. Catalogo Parametrico dei Terremoti Italiani (CPTI15), versione 4.0. Istituto Nazionale di Geofisica e Vulcanologia (INGV), Roma, Italy, https://doi.org/10.13127/CPTI/CPTI15.4.

Serva L.; 1981. Il terremoto del 1688 nel Sannio. In Proc. Meeting of Progetto Finalizzato Geodinamica on Sismicità dell'Italia: stato delle conoscenze scientifiche e qualità della normativa sismica.

Sgambato C.; Roberts G. P.; … Shanks R.P.; 2025. Millennial slip-rates variability of along-strike active faults in the Italian Southern Apennines revealed by cosmogenic 36Cl dating of fault scarps. Tectonics.

Silva P. G.; Elez J.; ... Martínez-Graña A.; 2017. ESI-07 ShakeMaps for instrumental and historical events in the Betic Cordillera (SE Spain): An approach based on geological data and applied to seismic hazard. Quaternary international.

Silva P. G.; Elez J.; ... Bardají T.; 2023**.** The AD 1755 Lisbon Earthquake-Tsunami: Seismic source modelling from the analysis of ESI-07 environmental data. Quaternary International.

Valensise G.; Pantosti D.; 2001. Seismogenic Faulting, Moment Release Patterns and Seismic Hazard along the Central and Southern Apennines and the Calabrian Arc. In Anatomy of an Orogen: The Apennines and Adjacent Mediterranean Basin.

Wald D. J.; Worden B.C.; Quitoriano V.; Pankow K.L.; 2005. ShakeMap Manual: Technical Manual, User's Guide, and Software Guide. U.S. Geological Survey.

Wells D. L.; Coppersmith K. J.; 1994. New empirical relationships among magnitude, rupture length, rupture width, rupture area, and surface displacement. Bulletin of the seismological Society of America.

Corresponding author: angelica.capozzoli@unina.it Angelica Capozzoli

Earthquakes without borders. Julian Alps earthquakes at the beginning of the 20th cent.: the March 10th, 1904 event.

C.H. Caracciolo[1]

[1] *Istituto Nazionale di Geofisica e Vulcanologia INGV, sezione di Bologna.*

During the period 1901-1930, according to CPTI15 (Rovida et al. 2021), into the Julian Alps area happened many events with a range of Magnitudes from 3.93 to 6.02.

Some of the more important events of this period were quite well studied (27th march 1928). Yet others deserve a revision. Most of moderate events lack of macroseismic data. Yet, many have a calculated Io and almost all of them have a Mw.

The goal of this paper is to reappraise the seismic activity along the North-Eastern Italian border during the first three decades of the twentieth century. In particular, this study focuses on the event of the early morning of March 10th, 1904.

The CPTI15 (Rovida et al. 2021), records this event on the basis of two different studies. The macroseismic set comes from Molin et al. (2008), who takes the data from Monti (1906). Monti collected the information provided by the macroseismic postcard sent to the Royal Meteorological and Geodynamic Office, in Rome. On the other side, the epicenter location comes from Sandron et al. (2014) and is located in North-West Slovenia and it is the result of the analysis of the coeval seismographs. The seismic portrait that results from these data shows very important lack of information from Slovenia as well from Austria, and also from Italy itself.

The CPTI15 record does not provide any information about magnitude nor the hypocenter's depth. Nevertheless, the respective ASMI record refers to Shebalin et al. (1974), which provides all instrumental parameters:

Ep.: 46,4° 13,2° Depht: 23km.

Io: 6 Magnitudo: 5.1

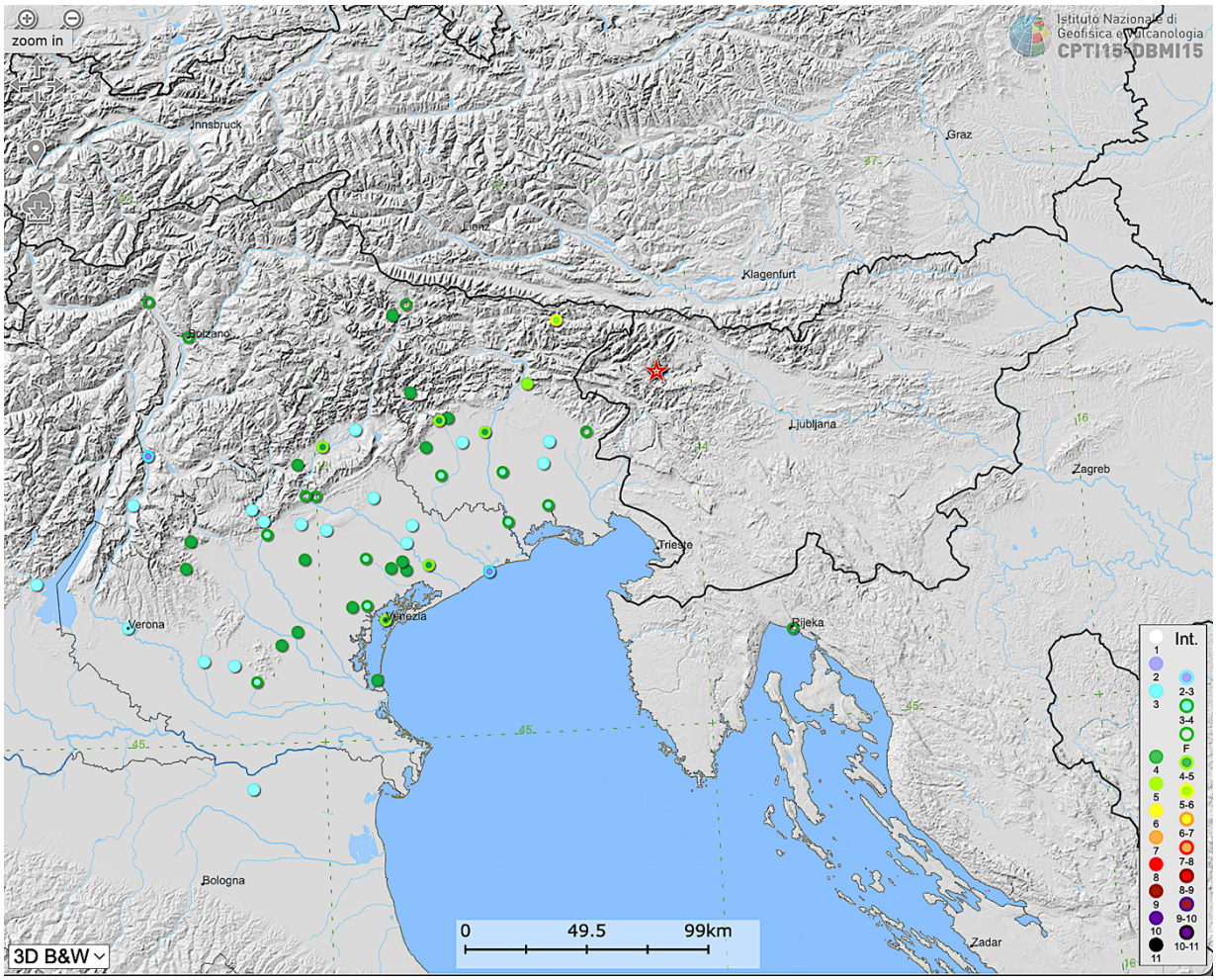

Fig. 1 – The 10th March 1904 earthquake according to CPTI15-DBMI15.

Despite the epicenter was plotted in North-Western Slovenia, up today the only macroseismic data points (mdp) available in DBMI15 (Locati et al., 2021) are situated almost exclusively into the Italian borders. In fact, it shows 57 mdp, and the point with the highest intensity is Pontebba, with an undefined value 5-6 MCS, just on the Italian-Slovenian border. It's easy to gather from these picture that, on one hand, that there is a meaningful lack of data, specially beyond the borders. On the other hand, that the felt zone cover a quite wider area.

In this preliminary work I have gathered many data from Austrian, Italian and Slovenian newspapers about a great deal of localities, as well reports from Slovenian and Austrian seismologist, both belonging to Imperial scientific institutions.

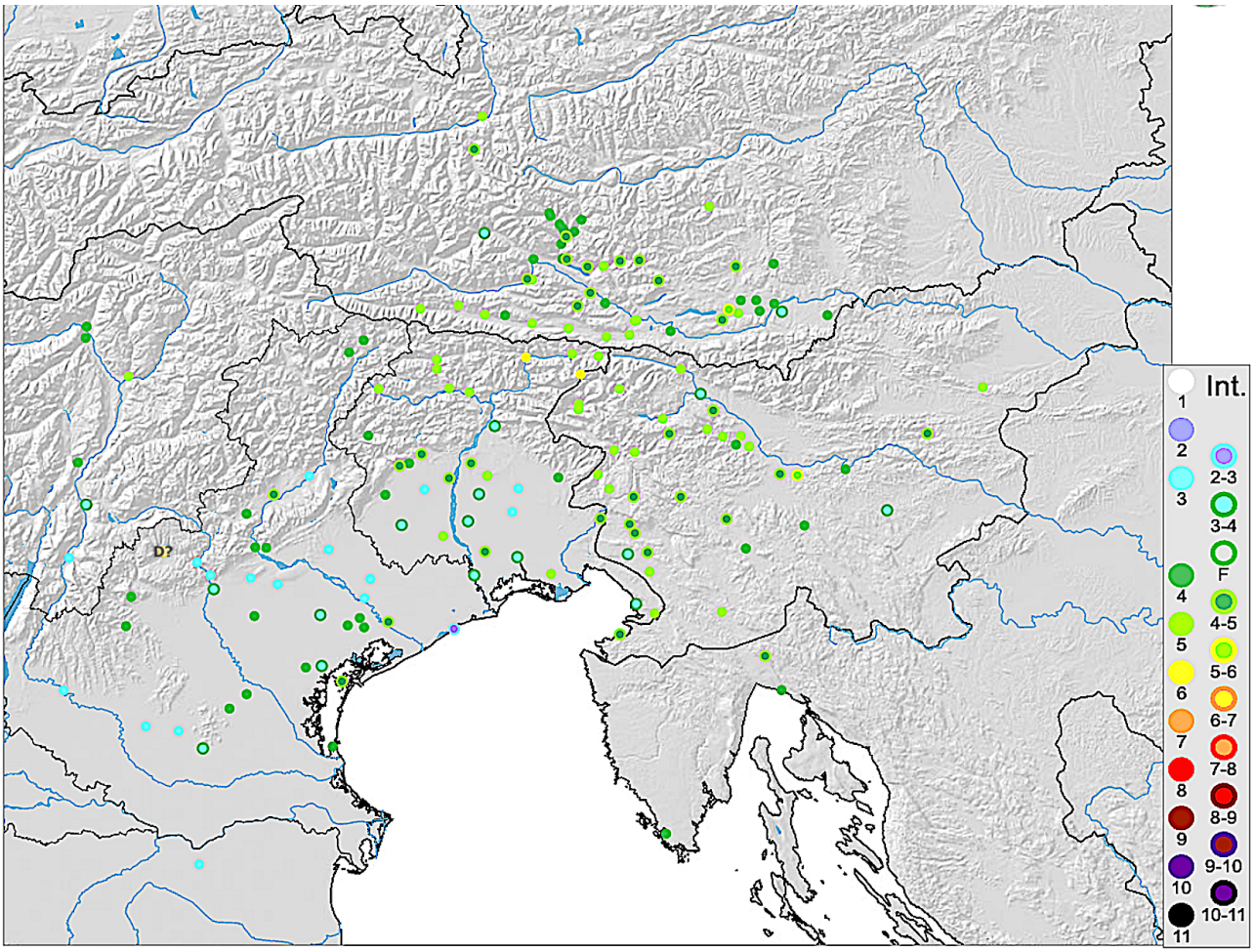

Fig. 2 – The 10th March 1904 earthquake according to this working progress research.

It confirms that the earthquake was felt in a very wide area from, at least, Bolzano to Ljubljana and from Vienna to Padua and beyond. Nevertheless, the higher intensities do not exceed 6 MCS in two localities (Pontebba e Cave del Predil /Raibl). It's worth to mention that, at that time, these two localities were separated by the Italian / Austrian-Hungarian border. Other light damages were reported from the neighborhoods of Klagenfurt and Ljubljana (Vevče). The macroseismic information gathered up to now correspond to 166 MDP (Tab.1).

Tab. 1 Macroseismic Data Set of the 10th March 1904 earthquake.

1904 03 10, 4:23					**Julian Alps**			
Place	**Lat.**	**lon.**	**I MCS**		**Place**	**Lat.**	**lon.**	**I MCS**
Cave del Predil /Raibl	46.438	13.568	6		Abano Terme	45.36	11.79	4
Pontafel/Pontebba	46.506	13.305	6		Auronzo di Cadore	46.552	12.439	4
Klagenfurt	46.626	14.314	5-6		Aviano	46.064	12.585	4
Vevče	46.050	14.593	5-6		Bleiburg	46.583	14.796	4
Altopiano d'Asiago	*45.9*	*11.5*	*D?*		Brandstatt	46.990	13.460	4
Aquileia	45.768	13.370	5		Castelfranco Veneto	45.671	11.926	4
Arnoldstein	46.560	13.706	5		Cermes	46.633	11.146	4

Bate [Batah]	46.045	13.676	5		Chioggia	45.219	12.279	4
Bohinjska Bistrica	46.271	13.956	5		Cividale del Friuli	46.093	13.431	4
Bolzano	46.499	11.352	5		Claut	46.267	12.515	4
Bukovica	46.198	14.244	5		Comelico Superiore	46.591	12.513	4
Camporosso in Valcanale	46.509	13.533	5		Eisentratten	46.922	13.578	4
Cezsoča	46.319	13.548	5		Feltre	46.019	11.906	4
Comeglians	46.514	12.868	5		Fener	45.904	11.942	4
Dolina	45.614	13.859	5		Fischertratten	46.9347	13.523	4
Dutovelj/Duttogliano	45.756	13.847	5		Grafenstein	46.614	14.465	4
Ebenthal in Kärnten	46.611	14.360	5		Karnerau	46.923	13.530	4
Fagagna	46.112	13.086	5		Kellerberg	46.674	13.709	4
Forni di Sopra (Vico)	46.424	12.577	5		Kirchbach in Gailtal	46.652	13.214	4
Fürnitz	46.562	13.819	5		Koschach	46.980	13.465	4
Gemona del Friuli	46.279	13.135	5		Kremsbrücke	46.961	13.617	4
Grades	46.979	14.253	5		Kreuzbichl	46.654	14.376	4
Grafendorf	46.658	13.115	5		Lieseregg	46.833	13.511	4
Jesenice	46.435	14.060	5		Litija /Littai	46.058	14.828	4
Laas	46.694	12.987	5		Malta	46.95	13.507	4
Lind im Drautal	46.768	13.358	5		Maniago	46.167	12.708	4
Marijino Celje nad Kanalom	46.096	13.624	5		Meolo	45.618	12.454	4
Mitschig	46.620	13.345	5		Merano	46.671	11.152	4
Obergail / Obergaital?	46.689	12.799	5		Mezzolombardo	46.211	11.092	4
Ovaro	46.482	12.866	5		Möllbrücken	46.837	13.369	4
Plezzo / Bovec	46.338	13.551	5		Monastier di Treviso (Fornaci)	45.65	12.435	4
Podmelec	46.164	13.810	5		Padova	45.407	11.875	4
Prem	45.605	14.183	5		Poggersdorf	46.651	14.452	4
Radenthein	46.800	13.712	5		Pula / Pola	44.866	13.850	4
Radenthein	46.800	13.713	5		Rakek	45.814	14.319	4
Resiutta	46.112	13.086	5		Rijeka / Fiume	45.327	14.445	4
Reteče	46.158	14.369	5		Roncade	45.627	12.375	4
San Vito al Tagliamento	45.915	12.857	5		Sankt Walburgen	46.770	14.550	4
Sankt Veit im Pongau	47.330	13.154	5		Škofja Loka	46.167	14.305	4
Sv. Lucije na Mostu	46.299	15.526	5		Spinea (Orgnano)	45.49	12.165	4
Tolmezzo	46.398	13.019	5		St. Veit a.d. Glan	46.770	14.361	4
Trenta	46.381	13.754	5		Tainach	46.635	14.539	4
Villa Santina	46.415	12.922	5		Trebesing	46.883	13.510	4
Villach	46.610	13.858	5		Tretto	45.75	11.333	4
Villaco*	46.608	13.850	5		Turjak	45.8779	14.610	4
Volče	46.175	13.710	5		Untergoritschach	46.566	14.022	4
Vorderberg a.d. Gail	46.596	13.522	5		Valdagno	45.651	11.304	4
Weißenfels/Fusine in Valromana	46.496	13.661	5		Valdobbiadene	45.901	11.996	4
Žabnica	46.196	14.331	5		Bassano del Grappa	45.767	11.734	3-4
Železniki	46.226	14.170	5		Codroipo	45.961	12.981	3-4
Capodistria	45.550	13.686	4-5		Este	45.228	11.656	3-4
Cavasso Nuovo	46.196	12.771	4-5		Flattach	46.934	13.134	3-4
Gmünd in Kärnten	46.907	13.536	4-5		Gemona del Friuli	46.279	13.135	3-4
Gorizia	45.946	13.625	4-5		Klopein	46.606	14.574	3-4

Idrija/Idria	46.003	14.020	4-5		Komen na Krasu	45.820	13.747	3-4
Innerteuchen	46.739	13.979	4-5		Latisana	45.777	12.998	3-4
Klana	45.446	14.377	4-5		Mereto di Tomba	46.051	13.041	3-4
Kleblach	46.771	13.333	4-5		Mestre	45.493	12.242	3-4
Kleinkirchheim	46.814	13.795	4-5		Pordenone	45.959	12.658	3-4
Kreuzen	46.670	13.573	4-5		Radovljica	46.347	14.1489	3-4
Kropa	46.288	14.205	4-5		San Giorgio di Nogaro	45.831	13.211	3-4
Loitsch	45.918	14.235	4-5		Treffen / Trebnje	45.909	15.015	3-4
Lokve	46.013	13.791	4-5		Trento	46.067	11.127	3-4
Loške	46.158	15.239	4-5		Treviso	45.666	12.245	3-4
Ljubljana	46.058	14.509	4-5		Trieste	45.650	13.772	3-4
Luggau	47.219	13.105	4-5		Asolo	45.801	11.914	3
Montereale Valcellina	46.16	12.661	4-5		Belluno	46.139	12.218	3
Osek / Ossecca	45.921	13.764	4-5		Cologna Veneta	45.309	11.385	3
Paternion	46.712	13.639	4-5		Conegliano	45.887	12.298	3
Podbrdo	46.219	13.984	4-5		Ferrara	44.835	11.62	3
S. Margarethen i. R.	46.812	13.890	4-5		Montebelluna	45.776	12.045	3
San Daniele del Friuli	46.157	13.010	4-5		Noventa Vicentina	45.29	11.542	3
San Donà di Piave	45.633	12.572	4-5		Oderzo	45.781	12.494	3
Sankt Veit a.d. Glan	46.770	14.363	4-5		Ponte di Piave	45.717	12.462	3
Santa Giustina	46.081	12.042	4-5		Pozzuolo del Friuli	45.985	13.198	3
Seeboden	46.831	13.533	4-5		Rovereto	45.888	11.037	3
Selo/Sella di Bivio/Steinbuchtel	45.890	13.787	4-5		Salò	45.606	10.522	3
Spilimbergo	46.11	12.899	4-5		Solagna	45.815	11.72	3
Spittal an der Drau	46.801	13.633	4-5		Udine	46.063	13.234	3
Stanjel na Krasu	45.822	13.843	4-5		Valstagna	45.86	11.658	3
Teor	45.855	13.056	4-5		Verona	45.439	10.994	3
Venezia	45.438	12.336	4-5		Vivaro	46.076	12.777	3
Viktring	46.592	14.278	4-5		Caorle	45.599	12.887	2-3

In conclusion, the integration of transboundary historical sources has significantly expanded the dataset for the March 10th, 1904 earthquake, reaching a total of 166 macroseismic data points. These updated data will bridge the previous information gap and provide a more accurate seismic characterization of the Julian Alps border region. Nevertheless, because this research is still a work in progress, I prefer not to provide other parameters such as epicentre, magnitude, and focal depth.

References

Locati M., Camassi R., Rovida A., Ercolani E., Bernardini F., Castelli V., Caracciolo C.H., Tertulliani A., Rossi A., Azzaro R., D'Amico S., Antonucci A.; 2022: Database Macrosismico Italiano (DBMI15), versione 4.0 [Data set]. Istituto Nazionale di Geofisica e Vulcanologia (INGV), https://doi.org/10.13127/dbmi/dbmi15.4

Molin D., Bernardini F., Camassi R., Caracciolo C.H., Castelli V., Ercolani E., Postpischl L., 2008: Materiali per un catalogo dei terremoti italiani: revisione della sismicità minore del territorio

nazionale. Quaderni di Geofisica, 57, p. 75+1396 Rom, https://collane-editoriali.ingv.it/index.php/qdg/it/article/view/848.

Monti V.; 1906: Notizie sui terremoti osservati in Italia durante l'anno 1904, s.l., s.n. p. 552.

Rovida A., Locati M., Antonucci A., Camassi R. (a cura di); 2017: Archivio Storico Macrosismico Italiano (ASMI). Istituto Nazionale di Geofisica e Vulcanologia (INGV), https://doi.org/10.13127/asmi

Rovida A., Locati M., Camassi R., Lolli B., Gasperini P., Antonucci A.; 2022: Catalogo Parametrico dei Terremoti Italiani (CPTI15), versione 4.0. Istituto Nazionale di Geofisica e Vulcanologia (INGV), https://doi.org/10.13127/cpti/cpti15.4

Sandron D., Renner G., Rebez A., Slejko D., 2014: Early instrumental seismicity recorded in the Eastern Alps. Bollettino di Geofisica Teorica ed Applicata Vol. 55, n.4, pp. 755-788, https://doi.org/10.4430/bgta0118

Shebalin N. V., Kárnik V., Hadilevski D.; 1974: Catalogue of Earthquakes, Part I, 1901-1970, UNDP/UNESCO, Skopje.

Periodicals

Edinost, Triest.

Freie Stimmen, Klagenfurt.

Giornale di Udine, Udine.

Il Piccolo, Trieste.

Innsbrucker Nachrichten, Innsbruck.

Kärntner Zeitung, Klagenfurt.

Klagenfurter Zeitung, Klagenfurt.

La Patria del Friuli, Udine.

Laibacher Zeitung, Laibach.

Mir, Celovec/Klagenfurt.

Primorski list, Gorizia.

Slovenec, Ljubljana.

Slovenski narod,

Soča, Gorizia.

Villacher Zeitung, Villach.

Wiener Zeitung, Wien.

Corresponding author: carlos.caracciolo@ingv.it

Machine-Learning Forecasting of Strong Aftershocks in New Zealand Using NESTORE: Insights from Two Testing Approaches

L. Caravella[1], S. Gentili[1]

[1] *Istituto Nazionale di Oceanografia e di Geofisica Sperimentale –OGS Centro di Ricerche Sismologiche, Italy*

Located along the active boundary between the Australian and Pacific plates, New Zealand is subject to widespread deformation and high seismicity, with major earthquakes reaching magnitudes up to 7.8. This tectonic setting makes the region well suited for evaluating operational, data-driven forecasting tools such as NESTORE. Improving the understanding and forecasting of seismic activity is essential for rapid hazard assessment, risk evaluation, and mitigation planning.

We therefore applied the machine-learning–based probabilistic forecasting algorithm NESTORE (NExt STRong Related Earthquake, Gentili et al., 2023) to New Zealand's seismicity. NESTORE evaluates nine features related to aftershock occurrence, source area evolution, and temporal trends in magnitude and radiated energy, calculated over progressively longer time windows after each mainshock. Using these features, the algorithm estimates the probability that a mainshock of magnitude Mm will be followed by another event of magnitude ≥ Mm–1 within the spatial and temporal bounds of its seismic cluster. Clusters that experience such a strong aftershock are labelled "Type A," indicating higher potential hazard, while others are labelled "Type B." For each cluster, the algorithm returns the probability of belonging to Type A.

NESTORE's performance was assessed using two approaches. The first was chronological: a cutoff time was selected so that the model was trained on clusters occurring before this cutoff, and then applied to forecast the behaviour of clusters occurring afterwards. The second approach used stratified k-fold cross-validation (Zeng et al., 2000) to test generalisation across multiple randomised partitions of the dataset. To further strengthen model training, we incorporated the outlier-detection procedure REPENESE (RElevant features, PErcentage class weighting, NEighbourhood detection and SElection, Gentili et al. 2025).

Our findings indicate that k-fold cross-validation provides more stable and reliable performance than the chronological approach, although changes in the catalogue may make the newer clusters a more valuable test set. NESTORE correctly classified 88% of seismic clusters 18 hours after the mainshock, including 77% of Type A and 92% of Type B clusters. Importantly, the algorithm successfully identified the Canterbury/Christchurch 2010–2011 sequence – a major, destructive Type A cluster.

Acknowledgments

This work is Co-funded within the RETURN Extended Partnership and received funding from the European Union Next-GenerationEU (National Recovery and Resilience Plan - NRRP, Mission 4, Component 2, Investment 1.3 – D.D. 1243 2/8/2022, PE0000005) and by the grant “Progetto INGV Pianeta Dinamico: Near real-time results of Physical and Statistical Seismology for earthquakes observations, modelling and forecasting (NEMESIS)” - code CUP D53J19000170001 - funded by Italian Ministry MIUR (“Fondo Finalizzato al rilancio degli investimenti delle amministrazioni centrali dello Stato e allo sviluppo del Paese”, legge 145/2018).

References

Gentili S., Brondi P., Di Giovambattista R.; 2023; NESTOREv1.0: A MATLAB Package for Strong Forthcoming Earthquake Forecasting. Seismological Research Letters, ISSN: 0895-0695, doi:10.1785/0220220327

Gentili, S., Chiappetta, G., Petrillo, G., Brondi, P., Zhuang, J., 2025. Forecasting strong subsequent earthquakes in Japan using an improved version of the NESTORE machine learning algorithm. Geoscience Frontiers 16, 102016. doi:https://doi.org/10.1016/j.gsf.2025.102016.

Zeng, Xinchuan, and Tony R. Martinez. (2000) "Distribution-balanced stratified cross-validation for accuracy estimation." Journal of Experimental & Theoretical Artificial Intelligence 12(1), 1-12. https://doi.org/10.1080/095281300146272

Corresponding author: lcaravella@ogs.it

Benchmark tests of Deep Learning pickers at Mount Etna volcano

A. Carducci[1], O. Cocina[2], M. Sciotto[2], A. Cannata[2,3], S. Di Gioia[4], A. Vuan[1], A. Saraò[1], K. Tanaka Hernández[5,1], M. Sugan[1]

[1] *Istituto Nazionale di Oceanografia e di Geofisica Sperimentale – OGS Centro di Ricerche Sismologiche, Italy*

[2] *Istituto Nazionale di Geofisica e Vulcanologia (INGV), Sezione Osservatorio Etneo, Catania, Italy*

[3] *Università di Catania, Dipartimento di Scienze Biologiche, Geologiche e Ambientali, Sezione di Scienze della Terra, Catania, Italy*

[4] *International Center for Theoretical Physics – ICTP, Italy*

[5] *Università degli studi di Trieste, Italy*

This study evaluates the performance of several modern deep learning models, trained on global volcanic and tectonic datasets, for automatic seismic phase picking and event classification in the complex environment of Mount Etna volcano. By using a large dataset of waveforms and reference catalogs, we test the scalability of these models and assess their ability to distinguish Volcano-Tectonic earthquakes from Long-Period events.

A dataset of high-quality waveforms is used, recorded by 38 stations operated by INGV – Osservatorio Etneo in the Etna area between January 2019 and June 2020. Two reference catalogs are also considered: (i) a manually located catalog of Volcano-Tectonic earthquakes, including identified P- and S- phase arrivals (Alparone et al., 2020; Barberi et al., 2020) and (ii) a catalog of Long-Period events detected from summit stations (Sciotto et al., 2022; Cannata et al., 2025). These catalogs provide the benchmark for evaluating the automatic procedures, ensuring consistent assessment of both phase picking and event classification across the network.

The autonomous workflow performs three main steps over the continuous data stream. First, ten pre-trained configurations of two deep learning pickers, PhaseNet (Zhu and Beroza, 2018) and EQTransformer (Mousavi et al., 2020), as available in the SeisBench framework (Woollam et al., 2022), generate probabilistic P- and S-phase picks. The configurations are selected according to event types, source-receiver distances and sampling rates to ensure compatibility with the local Etna waveforms. Second, the GaMMA algorithm (Zhu et al., 2022) associates the machine learning-predicted phases into seismic events. Third, a classification algorithm separates the events into five categories: Pure Long Period, Low-Spectrum, Pure Volcano-Tectonic, Mixed, and Unclassified. The algorithm uses (i) an adaptive filtering workflow, that analyzes the signal-to-noise ratio in the

waveforms, (ii) the spatial coordinates of the associated stations, and (iii) a modified frequency index (Buurman and West, 2010); this last evaluated in selected frequency bands calibrated from representative Volcano-Tectonic and Long-Period events.

Performance is evaluated using the recall score, defined as the fraction of correctly identified positive occurrences relative to the total number of positive samples in the reference catalogs, within specified spatial and temporal tolerances. A 4-month sample, covering a period of intense seismic activity, serves as an initial testbed to benchmark the ten configurations during the picking step. In this test, the PhaseNet Original, PhaseNet Volpick, and EQTransformer Volpick configurations achieve approximately 93% recall for P picks and over 80% recall for S picks, clearly outperforming the other tested variants (Fig. 1a). Based on this preliminary test, the entire 18-month waveform dataset is processed using only the three best configurations, and the recall is analyzed as a function of the probability thresholds. (Fig. 1b). EQTransformer Volpick is the best performing picker, with over 93% for P-picks and over 78% for S-picks, and it maintains robust performance as probability thresholds increase. When the predicted phases from EQTransformer Volpick are associated by GaMMA, the workflow identifies approximately 86% of the Volcano-Tectonic earthquakes in the reference catalog. The resulting filtered events are categorized by frequency index and then analyzed as time and space distributions, compared with the reference Volcano-Tectonic and Long-Period catalogs, demonstrating that the deep learning-based system reproduces the main temporal VT patterns and spatial clustering of volcano seismicity at Mount Etna.

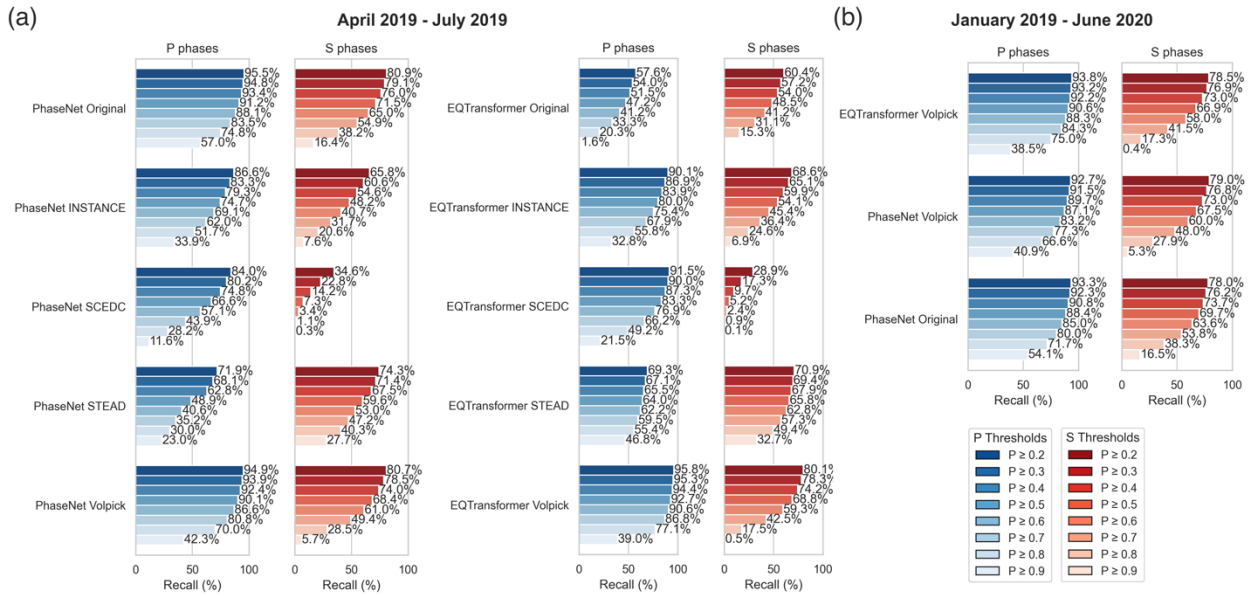

Figure 1 – (a) Recall scores for P-S phase picking (4-month sample test) of the ten tested configurations; (b) Recall scores for P-S phase picking (18-month dataset), configurations: PhaseNet Volpick, EQTransformer Volpick, PhaseNet Original.

References

Alparone S. C., Barberi G., D'Amico S., Di Grazia G., Ferrari F., Giampiccolo E., Maiolino V., Mostaccio A., Musumeci C., Scaltrito A., Scarfì L., Sciotto M., Spampinato S., Tusa G., Tuvè T., Ursino A., Zuccarello L.; 2020: Mt. Etna Revised and Concise Seismic Catalog from 1999 (EtnaRCSC) [Data set], *Ist. Naz. di Geofis. e Vulcanol. (INGV)*, doi: https://doi.org/10.13127/etnasc/etnarcsc

Barberi, G., Di Grazia, G., Ferrari, F., Firetto Carlino, M., Giampiccolo, E., Maiolino, V., Mostaccio, A., Musumeci, C., Scaltrito, A., Sciotto, M., Tusa, G., Tuvè, T., & Ursino, A.: 2020: Mt. Etna Revised Seismic Catalog from 2020 (EtnaRSC2020) (Version 1) [Data set], *Ist. Naz. di Geofis. e Vulcanol. (INGV)*, doi: https://doi.org/10.13127/ETNASC/ETNARSC2020

Buurman, H., and West, M. E.; 2010: Seismic Precursors to Volcanic Explosions During the 2006 Eruption of Augustine Volcano, *US Geol. Surv*., The 2006 eruption of Augustine Volcano, Alaska, pp. 41–57.

Cannata, A., Di Grazia, G., and Sciotto, M.; 2025: Catalog of Long Period seismic events recorded at Mt. Etna during the time interval 2019-2020 (LPSEC2019_2020), *Ist. Naz. di Geofis. e Vulcanol. (INGV)*, doi: 10.13127/ETNA/ELPC/2019_2020.

Mousavi, S. M., Ellsworth, W. L., Zhu, W., Chuang, L. Y., and Beroza, G. C.; 2020: Earthquake transformer—an attentive deep-learning model for simultaneous earthquake detection and phase picking, *Nat. Commun.*, 11, no. 1, 3952, doi: 10.1038/s41467-020-17591-w.

Sciotto, M., Cannata, A., Di Grazia, G., and Montalto, P.; 2022: Volcanic tremor and long period events at Mt. Etna: Same mechanism at different rates or not?, *Phys. Earth Planet. Inter.*, 324, 106850, doi: 10.1016/j.pepi.2022.106850.

Woollam, J., Münchmeyer, J., Tilmann, F., Rietbrock, A., Lange, D., Bornstein, T., et al.; 2022: SeisBench—A Toolbox for Machine Learning in Seismology, *Seismol. Res. Lett.*, 93(3), pp. 1695–1709, doi: https://doi.org/10.1785/0220210324

Zhu, W., and G. C. Beroza; 2018: PhaseNet: A Deep-Neural-Network-Based Seismic Arrival Time Picking Method, *Geophys. J. Int*., 216(1), pp. 261-273, doi: 10.1093/gji/ggy423.

Zhu, W., I. W. McBrearty, S. M. Mousavi, W. L. Ellsworth, and G. C. Beroza; 2022: Earthquake Phase Association Using a Bayesian Gaussian Mixture Model, *J. Geophys. Res. Solid Earth*, 127, no. 5, e2021JB023249, doi: 10.1029/2021JB023249.

Corresponding author: acarducci@ogs.it

Seismic source characterization in Northeastern Italy: insights on stress drop and seismic efficiency distributions

L. Cataldi[1], M. Picozzi[1], M. D'Amico[2], P. Morasca[3], D. Bindi[4], V. Poggi[1], G. Costa[5], A. Viganò[6], D. Spallarossa[1,7]

[1] *National Institute of Oceanography And Applied Geophysics – OGS, Udine, Italy*
[2] *Istituto Nazionale di Geofisica e di Vulcanologia (INGV), OE Catania, Italy*
[3] *Istituto Nazionale di Geofisica e di Vulcanologia (INGV), Milan, Italy*
[4] *GFZ Helmholtz Centre for Geosciences, Potsdam, Germany*
[5] *MIGe, University of Trieste, Trieste, Italy*
[6] *Servizio Geologico, Provincia autonoma di Trento, Trento, Italy*
[7] *DISTAV, University of Genoa, Genoa, Italy*

Regional seismic activity has been recorded in Northeastern Italy since the late 1970s by both local and national networks, with monitoring coverage progressively expanding after the destructive 1976 Friuli earthquake sequence. In the past decade, as the networks in the area have achieved stable configuration and high station density, recorded seismicity has been dominated by low to moderate magnitude earthquakes. This study aims to provide a comprehensive analysis of the source characteristics of recorded seismicity at the regional level, making use of an up-to-date dataset, to expand on the previous studies available for the area (Castro et al. 1996, Malagnini et al. 2002, Franceschina et al. 2006, Klin et al. 2021, Cataldi et al. 2023).

The dataset itself and a description of the Generalized Inversion Technique (GIT; Castro et al. 1990) methodology, that we used to characterize the components contributing to the regional spectral model, have been presented in Cataldi et al. (2025). A broad, high-quality dataset was assembled by selecting all local earthquakes that occurred between 2016 and 2024 within the geographical area of interest ([45 N; 47 N] latitude, [10 E; 15 E] longitude), and recorded by all available stations located within 130 km of each epicentre. Accurate preliminary data selection and processing were performed to ensure the robustness of the results, with constraints applied to azimuthal gap (<200°), minimum number of phases per event (12), minimum number of records per event and per station (8), and signal-to-noise ratio of the corresponding S-wave Fourier amplitude spectra (SNR ≥ 2.5). The resulting dataset (Figure 1) consisted of 1,191 seismic events (1.65 < ML < 4.55) and 172 stations, with over 20,000 spectral amplitude values associated with each frequency in the range 1.2–25 Hz.

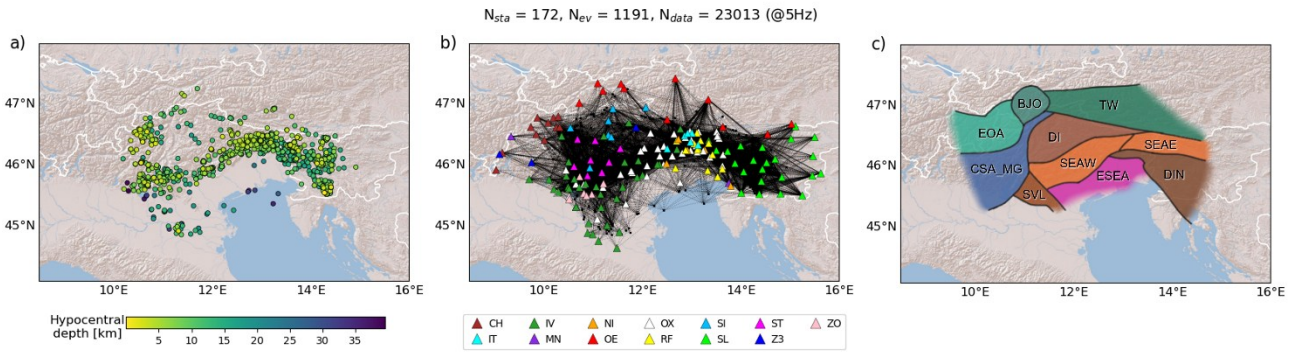

Fig. 1 – a) The 1191 events included in the dataset used for GIT inversion on Northeast Italy, with colour scale corresponding to focal depth. b) A ray map of the same events (black dots) and the associated recording stations (triangles), coloured based on the network they belong to. c) The main seismotectonic domains of interest for the study area. They are, as reported in Villani et al. (2024): BJO, Brenner-Jaufen Oetzal; CSA-MG, Central-Southern Alps and Meran-Giudicarie; DI, Dolomites Indenter; DIN, Dinarides; EOA, Engandine-Ortles Alps; ESEA, External Southeastern Alps; SEAE, Southeastern Alps (eastern sector), SEAW Sourtheastern Southeastern Alps (western sector); SVL, Schio-Vicenza-Lessini; TW, Tauern Window.

A GIT inversion was performed on the dataset using the open source *GITpy* software (D'Amico et al., 2025; Morasca et al., 2025) to separate the source, propagation, and site spectral contributions. We subsequently focused on the analysis of the source spectra, which were fitted to a standard Brune model to obtain estimates for seismic moment and corner frequency source parameters. These estimates were subsequently elaborated to obtain estimates of related source parameters, such as radiated energy, Brune stress drop, and seismic efficiency. The latter two parameters are especially informative of the mechanics of faulting, so we focused on the evaluation of the spatial patterns in their distribution over the different seismotectonic domains of the area. We observed significant spatial variations (Figure 2) revealing distinct mechanical properties of the fault systems that populate the region and suggesting the existence of differences in their dynamic strength.

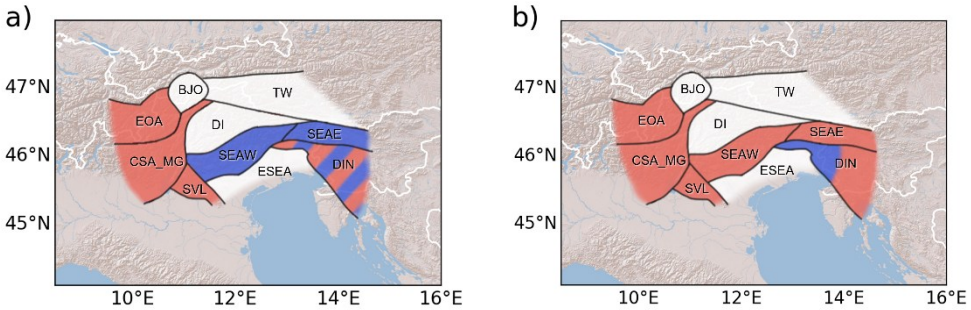

Fig. 2 – a) Characterization of the seismotectonic domains based on stress drop distribution. Domains with no evident stress drop trends are colored in white, domains hosting clusters of events with high or low stress drop ratio are colored in red and blue respectively. Domains hosting both clusters of high and low stress drop ratio events are represented as red and blue striped areas. b) Characterization of the seismotectonic domains based on seismic efficiency distribution. Domains with no evident efficiency trends are colored in white, domains hosting clusters of events with high efficiency are colored in red. The domain DIN hosts both clusters of high and low efficiency events, represented as red and blue areas respectively.

References

Castro R.R., Anderson J.G., Singh S.K.; 1990: *Site response, attenuation and source spectra of S waves along the Guerrero, Mexico, subduction zone*. Bulletin of the Seismological Society of America, 80, 1481–1503, doi:10.1785/BSSA08006A1481

Castro R. R., Pacor F., Sala A., Petrugnaro C.; 1996: *S wave attenuation and site effects in the region of Friuli, Italy*. Journal of Geophysical Research, 101(B10), 22355–22369, doi:10.1029/96JB02295

Cataldi L., Poggi V., Costa G., Parolai S., Edwards B.; 2023: *Parametric spectral inversion of seismic source, path and site parameters: application to northeast Italy*. Geophysical Journal International, 232, 1926–1943, doi:10.1093/gji/ggac431

Cataldi L., Spallarossa D., Picozzi M., D'Amico M., Morasca P., Bindi D., Poggi V., Costa G., Viganò A.; 2025: *Spectral inversion for seismic source characterization in Northeastern Italy*. In: Gruppo Nazionale di Geofisica della Terra Solida, 43° Convegno Nazionale, Riassunti estesi delle comunicazioni.

D'Amico M., Morasca P., Spallarossa D., Bindi D., Picozzi M., Vitrano L.; 2025: *User manual of GITpy: A Python-based tool for the generalized inversion technique*. Rapporti Tecnici INGV, Vol. 494, 146 pp., doi: 10.13127/rpt/494

Klin P., Laurenzano G., Barnaba C., Priolo E., Parolai S.; 2021: *Site Amplification at Permanent Stations in Northeastern Italy*. Bulletin of the Seismological Society of America, 111, 1885–1904, doi:10.1785/0120200361

Franceschina G., Kravanja S., Bressan G.; 2006: *Source parameters and scaling relationships in the Friuli-Venezia Giulia (Northeastern Italy) region*. Physics of the Earth and Planetary Interiors, 154(2), 148–167, doi:10.1016/j.pepi.2005.09.004

Malagnini L., Akinci A., Herrmann R.B., Pino N.A., Scognamiglio L.; 2022: *Characteristics of the Ground Motion in Northeastern Italy*. Bulletin of the Seismological Society of America, 92(6), 2186–2204, doi:10.1785/0120010219

Morasca P., D'Amico M., Spallarossa D., Bindi D., Picozzi M., Oth A., Pacor F.; 2025: *GITpy: A Python Implementation of the Generalized Inversion Technique*. Seismological Research Letters, 96 (6), 3866–3879, doi: 10.1785/0220250042

Villani F., Antonioli A., Pastori M., Baccheschi P., Ciaccio M. G.; 2024: *Stress Patterns and Crustal Anisotropy in the Eastern Alps: Insights From Seismological and Geological Observations*. Tectonics, 43(3), e2023TC008033, doi:10.1029/2023TC008033

Corresponding author: lcataldi@ogs.it

What Small Earthquakes Reveal about Fault Heterogeneity: Insights from Spectral Decomposition of Source Parameters along the East Anatolian Fault Zone, Türkiye

L. Colavitti[1], D. Bindi[2], G. Tarchini[1], D. Scafidi[1], M. Picozzi[3], D. Spallarossa[1]

[1] *University of Genoa, Department of Earth, Environmental and Life Sciences, Genoa, Italy*
[2] *German Research Center for Geoscience – GFZ, Potsdam, Germany*
[3] *National Institute of Oceanography and Applied Geophysics – OGS, Trieste, Italy*

On 6 February 2023, a moment magnitude (M_W) 7.8 earthquake struck near Kahramanmaraş in southern Türkiye along the eastern margin of the Anatolian plate (Wang et al., 2025). The mainshock occurred at 01:17:34 UTC and ruptured about 300 km of the East Anatolian Fault Zone (EAFZ). Dynamic stress transfer from this mainshock triggered cascading failures on adjacent fault segments, and approximately nine hours later an Mw 7.5 event occurred ~100 km to the northeast. Together, these events constitute one of the most complex and energetic earthquake seismic sequences observed along a continental strike-slip fault system

The aim of this study is to assess whether the spatio-temporal variability of small-magnitude earthquake source properties can reveal fault-segment heterogeneity and preparatory processes along the EAFZ.

We analyzed the dataset compiled by Colavitti et al. (2025), which includes seismic events that occurred between January 1, 2019 to February 29, 2024 with local magnitude (M_L) ranging from 2.0 and 5.5, considering a hypocentral distance up to 150 km. The disseminated dataset comprises 9,442 events recorded by 171 seismic stations and includes a total of 270,704 seismic phases.

Source, path, and site contributions were separated through spectral decomposition of Fourier Amplitude Spectra (FAS), using Generalized Inversion Technique (GIT), first introduced by Andrews (1986) and Castro et al. (1990), as implemented in the open-source software GITPy (Morasca et al., 2025) adopting a non-parametric inversion approach.

The linear system is characterized by two unresolved degrees of freedom, so that the solution is not unique and two *a priori* constraints are required to break the trade-offs between the three terms (source, path and sites) and generate solutions relative to the assumptions.

As shown in **Figure 1a**, the average amplification over all stations was set to 1, and stations were selected based on overall amplification median < 1 and 95th percentile < 2.5. All the amplification curves derived from the non-parametric inversion were corrected for the high-frequency (> 10 Hz) decay related to κ, in order to quantify the slope of the high frequency portion of the FAS and ensure consistency with the Ω^2 source model (Brune, 1970). For this study, we assumed a reference amplification model characterized by the site-specific component of high-frequency attenuation parameter κ_0 of 0.035 s, consistent with the findings of Bindi et al. (2023) for the EAFZ area.

Figure 1b shows the results of non-parametric attenuation functions obtained at different frequencies as a function of hypocentral distance. The shapes of the spectral attenuation curves are consistent with those found in previous investigations for the EAFZ (e.g Bindi et al., 2023; Fu et al., 2025). An evident dip is observed in the frequency range at around 2 Hz, which is characterized by an initial decrease followed by an increase at hypocentral distances of approximately 80 km, which may reflect the complex influences of Moho reflections.

The GIT was applied over the frequency range 0.5-25 Hz, and the source spectra appear flat at frequencies above 10 Hz, as shown in **Figure 1c**. As expected, the spectra are grouped by magnitude: the higher the magnitude of the event, the higher the source amplitude. For the source fitting, we anchored the results to an event with a known M_W that is common with the study of Bindi et al. (2023).

Focusing on source properties, our study provides a statistically robust update of the seismic moment - corner frequency ($M_0 - f_c$) scaling relationships for the EAFZ, based on a dataset approximately six times larger than that used by Bindi et al. (2023) and more than twenty times larger than that of Fu et al. (2025). This unified framework bridges the pre- and post-2023 seismicity, revealing continuity in scaling laws and overall stability of source parameters across the sequence.

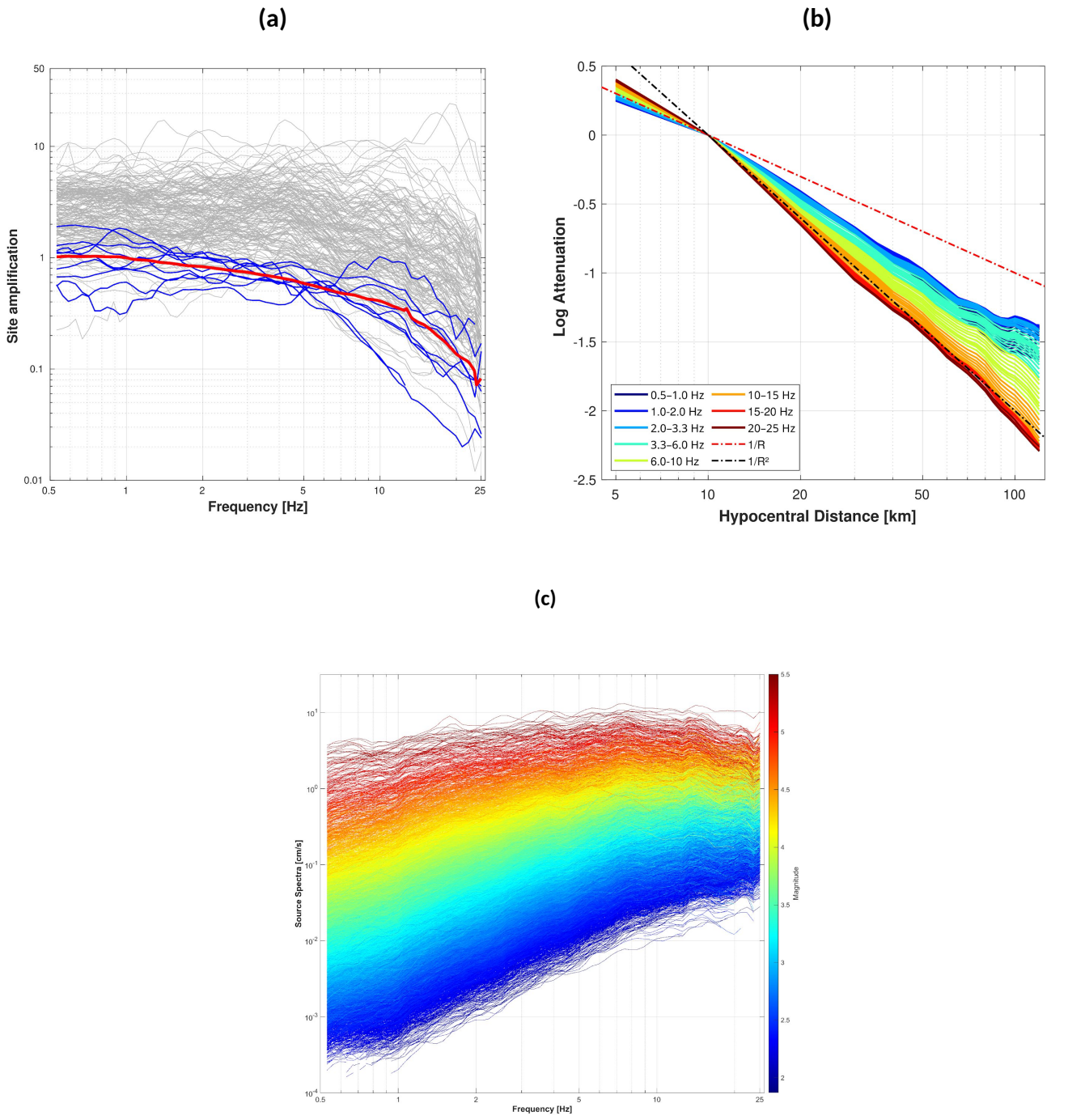

Fig. 1 – **(a)** Site amplification curves obtained from the non–parametric inversion. Grey curves represent the amplification functions of all stations, blue curves correspond to the selected reference sites, and the red curve shows the average response of the reference stations. **(b)** Hypocentral distance versus logarithmic attenuation curves derived from the non-parametric inversion, with colored lines indicating different frequency bands. **(c)** Empirical source spectra obtained from the non-parametric inversion, with curves color-coded according to event magnitude.

The relation between seismic moment and energy radiated ($M_0 - E_r$) for EAFZ is consistent with observations from other tectonic settings and faulting regimes worldwide, with minor differences that could be related to the dataset characteristics and the different assumptions used in the source parametrization. From a spatio-temporal perspective, using fault information from the works of

Melgar et al. (2023) and the Zaliapin and Ben-Zion (2016) clustering algorithm, we have shown that for the analyzed events, no significant pattern are evident if we use canonical scaling through the classical $M_0 - f_c$ relationship.

Following an approach similar to the one proposed for other tectonic settings (Bindi et al., 2024; Bindi et al., 2025), we therefore examined the distribution of stress drop anomalies $\varepsilon\Delta\sigma$ and scaled energy anomalies $\varepsilon\frac{E_R}{M_0}$ associated with the seismic rupture. Cross-sections across the main fault zones highlight the possible presence of a mechanical barrier capable of accumulating stress without releasing it through small-magnitude earthquakes, thereby favoring stress build-up until the occurrence of the mainshock. The contrast between $\varepsilon\Delta\sigma$ and $\varepsilon\frac{E_R}{M_0}$ may indicate that the two parameters weight source heterogeneities differently: while $\Delta\sigma$ reflects large-scale variations in source conditions, $\frac{E_R}{M_0}$ more effectively captures small-scale heterogeneity an the processes occurring along distinct fault segments (e.g. Allen et al., 2004).

In conclusion, this research demonstrates that classical source-scaling relations alone are not sufficient to capture the complexity of fault-zone behavior along the EAFZ. By leveraging a large, high-quality dataset and alternative source-parameter proxies, we show that small-magnitude seismicity contains valuable information on fault heterogeneity and stress accumulation processes. These findings highlight the potential of source-parameter anomalies as diagnostic tools for identifying mechanically distinct fault segments and for improving our understanding of earthquake preparation processes in complex tectonic settings.

References

Allen T. I., Gibson G., Brown A., and Cull J. P.; 2004: Depth variation of seismic source scaling relations: implications for earthquake hazard in southeastern Australia. Tectonophysics 390, 5-24. https://doi.org/10.1016/j.tecto.2004.03.018.

Andrews D. J.; 1986: Objective determination of source parameters and similarity of earthquakes of different size. In S. Das, J. Boatwright, and C. H. Scholz (Eds.), Earthquake Source Mechanics. Am. Geophys. Union, Washington DC. https://doi.org/10.1029/GM037p0259.

Bindi D., Zaccarelli R., Cotton F., Weatherill G., and Kotha S. R.; 2023: Source Scaling and Ground Motion Variability along the East Anatolian Fault. The Seismic Record, 34, 311-321. https://doi.org/10.1785/0320230034.

Bindi D., Spallarossa D., Picozzi M., and Tarchini G.; 2024. Scaling and Depth Variability of Source Parameters in Central and Southern Italy Using Regional Attenuation Models. Bulletin Seismological Society of America, 115 (3), 983-999. https://doi.org/10.1785/0120240144.

Bindi D., Picozzi M., Oth A., and Spallarossa D.; 2025. Impact of Seismic Attenuation Corrections on Source Parameter Estimation. Seismica, 4(2). https://doi.org/10.26443/seismica.v4i2.1651.

Brune J. N.; 1970: Tectonic stress and the spectra of seismic shear waves from earthquakes. Journal of Geophysical Research, 75 (26). https://doi.org/10.1029/JB075i026p04997.

Castro R. R., Anderson J. G., and Singh S. K.; 1990: Site response, attenuation and source spectra of S waves along the Guerrero, Mexico, subduction zone. Bulletin Seismological Society America, 80, 1481-1503. https://doi.org/10.1785/BSSA08006A1481.

Colavitti L., Bindi D., Tarchini G., Scafidi D., Picozzi M., and Spallarossa D.; 2025: A high-quality Data Set for seismological studies in the East Anatolian Fault Zone, Türkiye. Earth Science System Data, https://doi.org/10.5194/essd-2024-448.

Fu L., Chen K., and Li X.; 2025. Strong ground-motion spectral statistical properties of the East Anatolian fault region, Türkiye: heterogeneous attenuation, stress drop, and site variations. Bulletin Earthquake Engineering, 23: 3239-3267. https://doi.org/10.1007/s10518-025-02175-0.

Melgar D., Taymaz T., Ganas A., Crowell B., Öcalan T., Kahraman M., Tsironi V., Yolsal-Çevikbilen S., Valkaniotis S., Irmak T. S., Eken T., Erman C., Özkan B., Dogan A. H. and Altuntaş C.; 2023: Sub- and super-shear ruptures during the 2023 Mw 7.8 and Mw 7.6 earthquake doublet in SE Türkiye. Seismica, 2(3). https://doi.org/10.26443/seismica.v2i3.387.

Morasca P., D'Amico M., Spallarossa D., Bindi D., Picozzi M., Oth A., and Pacor, F.; 2025: GITpy: A Python Implementation of the Generalized Inversion Technique. Seismological Research Letters, 96 (6), 3866-3879. https://doi.org/10.1785/0220250042.

Wang Z., Qui Q., Fu Y., Lin J., and Pei, S.; 2025: Distinct triggering mechanism of the 2023 Türkiye earthquake doublet. Communications Earth Environment 6, 287. https://doi.org/10.1038/s43247-025-02266-5.

Zaliapin I. and Ben-Zion Y.; 2016: A global classification and characterization of earthquake clusters, Geophysical Journal International, 207 (1), 608-634. https://doi.org/10.1093/gji/ggw300.

Corresponding author: leonardo.colavitti@edu.unige.it

Physics-Based Broadband Ground Motion Simulations of the Mw 6.2 April 2025 Istanbul Earthquake

A. Cuius[1], A. Akinci[1], P. Artale Harris[1], A. Pitarka[2] , A. Askan[3], S. Karimzadeh[4], G. Muratoglu[3] , U. Hancilar[5]

[1] *Istituto Nazionale di Geofisica e Vulcanologia, Rome, Italy*
[2] *Lawrence Livermore National Laboratory, Livermore, CA, USA*
[3] *Middle East Technical University, Ankara, Türkiye*
[4] *University of Minho, Braga, Portugal*
[5] *Dept. of Earthquake Engineering, Kandilli Observatory&Earthquake Res. Inst., Istanbul, Türkiye*

On April 23, 2025, at 09:49:11 UTC, an Mw 6.2 earthquake struck the Marmara Sea, Türkiye (Figure 1). This region, marking the western termination of the North Anatolian Fault Zone, is characterized by a complex fault system . Owing to this complexity, a reliable reconstruction of the rupture process, particularly its directivity and fault heterogeneity, is critical, as both strongly influence near-fault ground motion characteristics. Rupture directivity effects are especially important for densely populated areas such as Istanbul, because they can substantially amplify ground motion intensity.

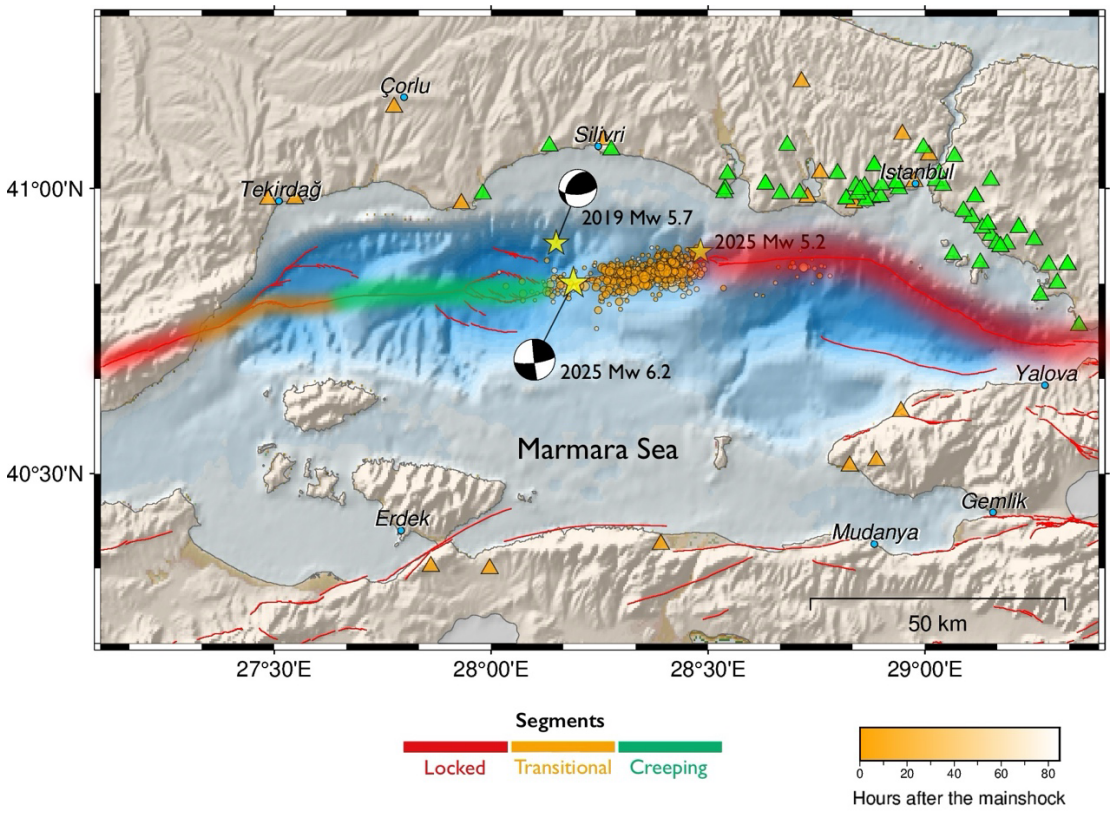

Fig 1 – Location of the Mw 6.3 Magnitude earthquake occurred in Marmara sea on 23th April 2025. The epicenter is located in a transitional zone between a locked zone and a creeping zone.

To address this problem, we performed broadband ground motion simulations using the representation theorem and the Frequency–Wavenumber (FK) technique. By adopting suitable source rupture models, the FK-based approach enables efficient and accurate computation of synthetic time histories. First, we applied the Graves and Pitarka (2016) method to generate kinematic rupture models for this event (Figure 2). FK Green's functions were then computed using the propagator matrix method of Zhu and Rivera (2002), based on a one-dimensional velocity model for the Marmara region (Tan et al., 2022).

Because reliable rupture models for this earthquake were not yet available, we adopted a fully stochastic framework to generate a suite of kinematic rupture models representing plausible rupture scenarios. These models capture source complexity through stochastic slip distributions.

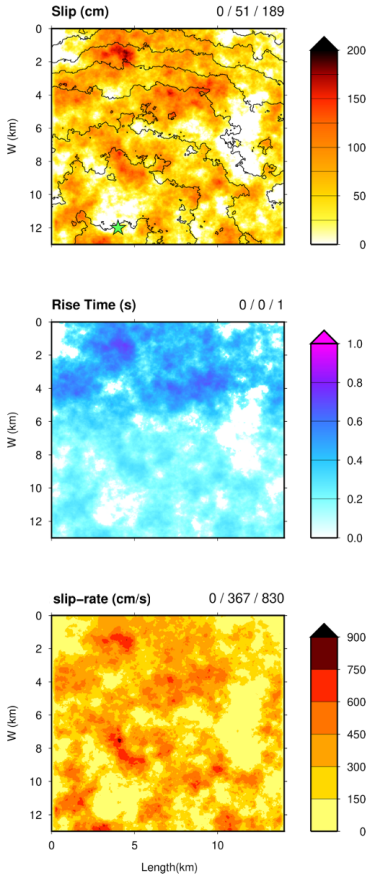

Fig. 2 – Kinematic rupture model used for the simulation. Top: stochastic slip distribution and hypocenter location. Center**:** rise-time distribution. Bottom: slip-rate distribution.

The simulations were evaluated through goodness-of-fit (GoF) analyses by comparing synthetic waveforms with available recordings using selected seismological and engineering intensity measures, allowing us to assess the robustness of the rupture models (Figure 3).

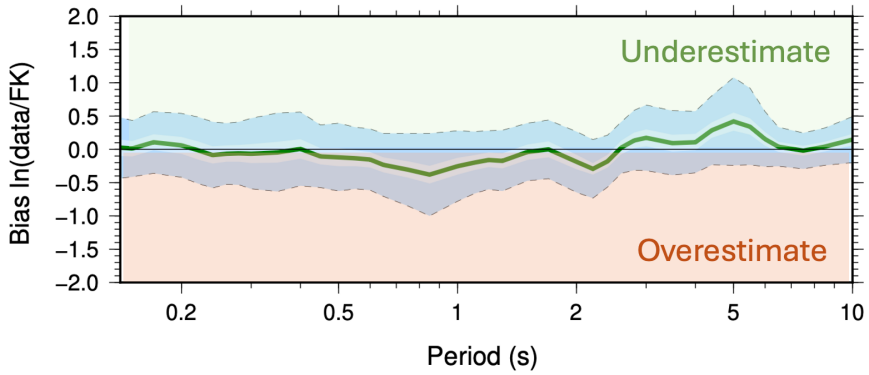

Fig 3 – Goodness of Fit (GoF) analysis using 43 seismic stations. In green the bias and in light blue the standard deviation.

Finally, ground motions computed at approximately 9,000 nodes on a uniform 1 km grid were used to examine the spatial variability of ground motion and its relationship to rupture kinematics, including forward-directivity effects. The results demonstrate the capability of this approach to capture the seismic complexity of the Marmara Sea region and highlight its potential for ground motion prediction in tectonically complex settings, providing valuable insights for seismic hazard assessment and risk mitigation in the greater Istanbul area.

References

Graves, R., & Pitarka, A.; 2016: Kinematic ground motion simulations on rough faults including effects of 3D stochastic velocity perturbations. *Bulletin of the Seismological Society of America*, *106*, 2136–2153.

Tan, O., Karagöz, Ö., Ergintav, S., & Duran, K.; 2023: The neglected Istanbul earthquakes in the North Anatolian Shear Zone: tectonic implications and broad-band ground motion simulations for a future moderate event. *Geophysical Journal International*, *233*(1), 700-723.

Zhu, L., & Rivera, L. A.; 2002: A note on the dynamic and static displacements from a point source in multilayered media. *Geophysical Journal International*, *148*(3), 619–627.

Preliminary seismicity patterns at Ischia Island revealed by Machine-Learning detection and relative relocation

S. Danesi[1], S. Carlino[2], N.A. Pino[3]

[1] *Istituto Nazionale di Geofisica e Vulcanologia, Sezione Bologna, IT*
[2] *Istituto Nazionale di Geofisica e Vulcanologia, Osservatorio Vesuviano, IT*
[3] *Università di Camerino, Scuola di Scienze e Tecnologie, Sezione di Geologia, IT*

Ischia Island, southern Italy, is an active volcanic area characterised by shallow seismicity within a hydrothermally active crust. The magnitude 3.9 earthquake that struck the northern sector of the island in August 2017 renewed awareness of the seismic hazard associated with shallow volcano-tectonic structures. In this study, we analyse the seismic activity of the Ischia area between 2018 and 2024 through the detection and relative location of seismic events. Continuous seismic waveforms were retrieved from the Italian node of the European Integrated Data Archive (EIDA) and processed using a machine-learning-based approach for earthquake detection (Zhu and Beroza, 2019). The detected events were subsequently relocated using the HypoDD double-difference algorithm (Waldhauser, 2001) to improve relative hypocentral accuracy. Preliminary results reveal coherent spatial patterns of seismicity, providing a refined dataset for future investigations of shallow fault activity and its potential relationship with geothermal systems at Ischia.

References

Zhu W. and Beroza G.C.; 2019: PhaseNet: a deep-neural-network-based seismic arrival-time picking method, Geophysical Journal International, 216, 1, 261–273, https://doi.org/10.1093/gji/ggy423

Waldhauser F.; 2001: hypoDD—A Program to Compute Double-Difference Hypocenter Locations: U.S. Geological Survey Open-File Report 01-113, 25 pp., https://pubs.usgs.gov/of/2001/0113/.

Corresponding author: stefania.danesi@ingv.it

Investigating earthquakes with Distributed Acoustic Sensing at the Irpinia Near Fault Observatory

G. Festa[1,2], C. Strumia[1], F. Scotto di Uccio[1], A. Suresh[1], A. Trabattoni[3], L. Elia[4], G. Saccorotti[5], R. Pegna[5]

[1] Dipartimento di Fisica "Ettore Pancini", Università di Napoli Federico II, Italy
[2] Istituto Nazionale di Geofisica e Vulcanologia, Osservatorio Nazionale Terremoti, Roma, Italy
[3] Geoazur, Université de Nice Sophia Antipolis, Valbonne, France
[4] Istituto Nazionale di Geofisica e Vulcanologia, Osservatorio Vesuviano, Napoli, Italy
[5] Istituto Nazionale di Geofisica e Vulcanologia, Sezione di Pisa, Italy

The Irpinia Near Fault Observatory is a multidisciplinary infrastructure located in the Southern Apennines, designed to monitor the fault system responsible for the 1980 Mw 6.9 Irpinia earthquake. The observatory integrates seismic, geodetic, and geochemical instrumentation and has recently been expanded with two Distributed Acoustic Sensing (DAS) systems within the PNRR project MEET – Monitoring Earth Evolution and Tectonics.

The DAS interrogator is connected to two fiber-optic cables: a 20-km-long cable deployed in the southern Campania–Lucania Apennines, and a 60-km-long cable installed in the central sector of the region, following the surface projection of the main fault segments of the 1980 earthquake. Since the beginning of its operation, the DAS network has recorded approximately 100 earthquakes, many of which are clearly observed along large portions of one or both cables.

To assess the detection capability of the DAS network, we analyzed ambient seismic noise by investigating the temporal variability of power spectral density (PSD). During quiet nighttime conditions, the system reaches the instrumental noise level at several locations, limiting the recording of ambient seismic noise. Detection threshold was estimated by comparing PSD levels with theoretical earthquake spectra, calibrated using real events. Results indicate that the DAS system can detect earthquakes with local magnitude Ml 1 up to hypocentral distances of ~25 km and Ml 2 up to ~60 km, enabling detailed observation of microseismicity beneath the fiber-optic cables.

Earthquake detection and phase picking are performed using the deep-learning model PhaseNet (Zhu and Beroza, 2019), demonstrating that existing seismic models can be effectively transferred to DAS measurements. The procedure yields a large number of phase picks, with event association carried out using at least 50 picks, which are then used for earthquake location through NNLoc (Lomax, 2000).

Local magnitude is estimated by integrating strain-rate data in space and time to retrieve short-wavelength displacement, subsequently convolved with the Wood–Anderson instrumental response to measure peak displacement. Magnitude is then computed using the empirical relation of Bobbio et al. (2009). Moment magnitude and source parameters are derived directly from native strain data following the model proposed by Strumia et al. (2024). After double integration, amplitude spectra of the strain-integral are computed and inverted. Estimates of both local and moment magnitudes are consistent with those obtained from the conventional seismic network, and corner frequency and spectral fall-off parameters can be reliably retrieved for events with Mw larger than 2.

References

Bobbio, A., Vassallo, M., Festa, G.; 2009. A local magnitude scale for southern Italy. Bulletin of the Seismological Society of America, 99(4), 2461-2470.

Lomax, A., Virieux, J., Volant, P., Berge-Thierry, C. ; 2000. Probabilistic earthquake location in 3D and layered models: Introduction of a Metropolis-Gibbs method and comparison with linear locations. In Advances in seismic event location (pp. 101-134). Dordrecht: Springer Netherlands.

Strumia, C., Trabattoni, A., Supino, M., Baillet, M., Rivet, D., Festa, G.; 2024. Sensing optical fibers for earthquake source characterization using raw DAS records. Journal of Geophysical Research: Solid Earth, 129(1), e2023JB027860.

Zhu, W., Beroza, G. C.; 2019. PhaseNet: a deep-neural-network-based seismic arrival-time picking method. Geophysical Journal International, 216(1), 261-273.

Corresponding author: gaetano.festa@unina.it

Seismotectonic Framework of the Northern Apennines: Insights from deep earthquake along the Livorno-Sillaro alignment (Central Italy)

Fiaschi A.[1], Pauselli C.[2], Morelli M.[3],

[1] Istituto Geofisico Toscano, Fondazione Parsec, Prato
[2] Dipartimento di Fisica e Geologia Università di Perugia
[3] Museo Italiano di Scienze Planetarie, Fondazione Parsec, Prato.

The seismology of the Northern Apennines reveals a complex, depth-dependent tectonic regime, as evidenced by the analysis of 30 deep earthquakes (with magnitude between 1.9 and 3.1) that occurred between 2005 and 2025 in the inner sector of the Apennine chain, southwest of the Apennine watershed.

Deep seismicity of this area had already been studied in the past (Selvaggi et al. 1992), but the development of the Italian national seismic network allow for the acquisition of previously unavailable, high-quality data. The dataset, downloaded from the INGV database between latitude 43.8°/44.2°N and longitude 10.5°/11.2°E, with depth exceeding 30 km, was relocated after manually reviewing the arrival times of P and S waves and first-motion polarities. To locate seismic events, we chose the linearized approach by Lahr, 1999 (Hypoellipse code) using a best 1D velocity model for the area (from Ciaccio et al., 2021), but exploring the hypocenter solutions space by changing Vp/Vs ratio.

For each earthquake we got the focal solutions using the grid-search FPFIT code (Reasenberg and Oppenheimer, 1985), which is based on the P first-motion pattern. For each event we required a minimum number of 10 P-polarities. The results are then plotted with classic beach ball representation.

The seismic data were then compared with the Moho depth trend along the Tuscan section of the Livorno-Sillaro line (Piana Agostinetti and Amato, 2009; DI Stefano et al., 2009; Rosenbaum and Piana Agostinetti, 2015) and with the tomographic studies performed in previous works (Paffrath et al 2021). The same data were also compared with the gravimetric and thermal data for the same area.

The focal mechanisms of these earthquakes are fairly evenly distributed among compressional, extensional, and strike-slip mechanisms. However, in the immediate vicinity of the Livorno-Sillaro line, a greater presence of strike-slip mechanisms, often with a transpressional or transtensional component, is observed. These deeper earthquakes are not associated with evidence of surface

faulting, but are likely related to the regional displacement of major tectonic units. In particular, the spatial distribution and kinematics of these events is well correlate with the more internal position of the tectonic fronts north of the Livorno-Sillaro line, suggesting differential motion and internal deformation between the major crustal blocks.

References

Ciaccio MG, Di Stefano R, Improta L, Mariucci MT and BSI Working Group (2021) First-Motion Focal Mechanism Solutions for 2015–2019 M ≥ 4.0 Italian Earthquakes. Front. Earth Sci. 9:630116. doi: 10.3389/feart.2021.630116

Di Stefano, R., E. Kissling, C. Chiarabba, A. Amato, and D. Giardini (2009), Shallow subduction beneath Italy: Three-dimensional images of the Adriatic-European-Tyrrhenian lithosphere system based on high-quality P wave arrival times, J. Geophys. Res., 114, B05305, doi:10.1029/2008JB005641.

Lahr, J. C. (1999). HYPOELLIPSE: A Computer Program for Determining Local Earthquake Hypocentral Parameters, Magnitude, and first-Motion Pattern. U.S. Geological Survey Open-File Report 99–23, version 1.1. Reston, VA: USGS, 119.

Paffrath, M., Friederich, W., Schmid, S. M., Handy, M. R., and the AlpArray and AlpArray-Swath D Working Group: Imaging structure and geometry of slabs in the greater Alpine area – a P-wave travel-time tomography using AlpArray Seismic Network data, Solid Earth, 12, 2671–2702, https://doi.org/10.5194/se-12-2671-2021, 2021.

Piana Agostinetti, N., and A. Amato (2009), Moho depth and Vp/Vs ratio in peninsular Italy from teleseismic receiver functions, J. Geophys. Res., 114, B06303, doi:10.1029/2008JB005899

Reasenberg, P. A., and Oppenheimer, D. (1985). FPFIT, FPPLOT and FPPAGE: FORTRAN Computer Programs for Calculating and Displaying Earthquake Fault-Plane Solutions. US Geological Survey Open-File Report 85-739. Italy: USGS, 109.

Rosenbaum, G., and N. Piana Agostinetti (2015), Crustal and upper mantle responses to lithospheric segmentation in the northern Apennines, Tectonics, 34, 648–661, doi:10.1002/2013TC003498.

Corresponding author: fiaschi@fondazioneparsec.it

b-value estimation at Campi Flegrei (Italy) as indicator of seismic and volcanic activity

A.Figlioli[1], S.Azhideh[2], S.Barani[2], N.AlessandroPino[3], S.Danesi[4], M.Massa[1]

[1]Sezione Milano, Istituto Nazionale di Geofisica e Vulcanologia, Milano , Italia
[2]Dipartimento di Scienze della Terra, dell'Ambiente e della Vita, Università degli Studi di Genova, Italy
[3]Università di Camerino, Scuola di Scienze e Tecnologie,Sezione di Geologia
[4]Sezione Bologna, Istituto Nazionale di Geofisica e Vulcanologia, Bologna , Italia

Campi Flegrei is a complex volcanic region, located near Naples (Southern Italy), characterized by significant geophysical and geochemical activity. The analysis of the seismicity occurred in the last few years provides critical insights into the underlying volcanic processes and the potential associated hazards. One of the key parameters investigated in this analysis is the b-value of the Gutenberg-Richter Frequency-Magnitude Distribution (FMD), which describes the relative abundance of large earthquakes with respect to small ones. Here we study the spatial and temporal variations of the b-value within the Campi Flegrei. Using space gridding and time binning, along with different techniques for b-value estimation, we aim to add information to existing literature results (Danesi et al., 2024; Tramelli et al., 2024).

To carry out the analysis, we restricted earthquakes to occur in the period 2020-2024, which marks a significant increase in the geophysical and geochemical parameters. Data was downloaded from the GOSSIP website, which is managed by Istituto Nazionale di Geofisica e Vulcanologia-Osservatorio Vesuviano (INGV-OV). The analysis is conducted using well-known different statistical approaches: the Maximum Likelihood Estimation (MLE) and the b-positive methods. Each technique provides distinct advantages. MLE is well known for its robustness in handling large datasets while the b-positive method is not affected by changes in the completeness magnitude Mc and better highlights spatial and temporal variations of the b-value. A new analysis method proposed by (Azhideh et al., 2025) will then be applied.

The spatial analysis is performed by splitting the target area into a grid of smaller subregions and computing the b-value in each sub-region, while the temporal analysis focuses on tracking b-value variations over different time periods by applying a sliding-window technique. Thus, we examine the results in the light of both the geological-structural characteristics and the ongoing volcanological phenomena. This approach aims to identify localized anomalies and better understand the spatial and time heterogeneity of seismic activity within the caldera. In particular, the spatial distribution of the b-value might highlight volumes characterized by higher differential stress, potentially associated with specific subsurface structures, while its variation with time could reveal localized changes in the seismogenic process, possibly related to migration of magmatic fluids.

References

Azhideh, S., Barani, S., Ferretti, G., Taroni, M., Resta, M., and Massa, M.: Optimization of rolling window approach to analyze earthquake time series and identify possible precursors, EGU General Assembly 2025, Vienna, Austria, 27 Apr–2 May 2025, EGU25-17245, https://doi.org/10.5194/egusphere-egu2517245, 2025.

Stefania Danesi, Nicola Alessandro Pino, Stefano Carlino, Christopher R.J. Kilburn: Evolution in unrest processes at Campi Flegrei caldera as inferred from local seismicity,Earth and Planetary Science Letters,Volume 626,2024,118530,ISSN 0012-821X,https://doi.org/10.1016/j.epsl.2023.118530.

Tramelli, A., Convertito, V. & Godano, C. b value enlightens different rheological behaviour in Campi Flegrei caldera. Commun Earth Environ 5, 275 (2024). https://doi.org/10.1038/s43247-024-01447-y

Corresponding author: anna.figlioli@ ingv.i t

Deep learning phase-picking analysis and seismic catalog building applied to the Amatrice-Visso-Norcia seismic sequence

Rossella Fonzetti[1], Daniele Bailo[1], Luisa Valoroso[1], Pasquale De Gori[1] and Claudio Chiarabba[1]

[1] Istituto Nazionale di Geofisica e Vulcanologia, Rome (RM), Italy

Deep learning methods for seismic catalogs computation are nowadays widely used in the seismological community. In particular, convolutional neural networks (CNN) trained on specific datasets have shown a significant increase in the P- and S- phase recognition on continuous data streams, increasing the overall quality of the seismic catalogs, in terms of location errors and number of events obtained, lowering by more than one unit the completeness magnitude of the traditional hand-made catalogues. However, CNN may produce several false positives (non-real) P or S phase identifications, and the procedures that allow us to distinguish between a false positive and a real event are still poorly understood. Another issue concerns the choice of the probability threshold that constrains the prediction of discrete arrival times.

Here we present a Python workflow that allows creating a seismic catalog starting from P- and S-waves phase picking and association, with a subsequent selection of the best data for seismic event location using the linear localization algorithm Hypoellipse (Lahr, 1980) and the double-difference relocation method HypoDD (Waldhauser, 2001).

We present a preliminary application of this workflow to the 2016-2017 Amatrice-Visso-Norcia seismic sequence, analyzed using the PhaseNet convolutional neural network (Zhu and Beroza, 2019) for picking and the GaMMA unsupervised clustering associator (Zhu et al., 2022). The neural network was trained using the AQ2009 dataset (Bagagli et al., 2023), which contains the aftershocks of the 2009 L'Aquila sequence, to optimize the recognition of arrival times for events occurring during the seismic sequence of the Apennines, using the Seisbench Python platform (Wollam et al., 2022).

We tested different picking prediction thresholds (from 0.1 to 0.9) and GaMMA associator configurations. The threshold was evaluated based on the percentage of real seismic events compared to false events, trying to balance the trade-off between false events and completeness of the catalog.

The choice of the best threshold depends on the characteristics of the study area and how the data is to be managed (whether a high number of events is desirable or not). In the future, this choice can be automated by means of statistical methods.

Acknowledgments

We thank Jannes Münchmeyer and Frederik Tilmann from the GFZ research center for their suggestions and support of this research.

References

Bagagli, M., Valoroso, L., Michelini, A., Cianetti, S., Gaviano, S., Giunchi, C., Jozinović, D., & Lauciani, V. (2023). AQ2009 - The 2009 Aquila Mw 6.1 earthquake aftershocks seismic dataset for machine learning application. Istituto Nazionale di Geofisica e Vulcanologia (INGV). https://doi.org/10.13127/AI/AQUILA2009

Lahr, J. C. (1980). Hypoellipse. *A computer program for determining local earthquakes hypocentral parameters magnitude, and first-motion pattern: US Geological Survey Open-File Report*, 99-23.

Waldhauser, F. (2001). *HypoDD-A program to compute double-difference hypocenter locations* (No. 2001-113).

Woollam, J., Münchmeyer, J., Tilmann, F., Rietbrock, A., Lange, D., Bornstein, T., ... & Soto, H. (2022). SeisBench—A toolbox for machine learning in seismology. *Seismological Society of America*, *93*(3), 1695-1709.

Zhu, W., & Beroza, G. C. (2019). PhaseNet: a deep-neural-network-based seismic arrival-time picking method. *Geophysical Journal International*, *216*(1), 261-273.

Zhu, W., McBrearty, I. W., Mousavi, S. M., Ellsworth, W. L., & Beroza, G. C. (2022). Earthquake phase association using a Bayesian Gaussian mixture model. *Journal of Geophysical Research: Solid Earth*, *127*(5), e2021JB023249.

Corresponding author: rossella.fonzetti@ingv.it

A novel GNSS-based crustal velocity field for western Sicily

Martina Gennuso[1], Riccardo Cassataro[1], Mimmo Palano[1,2,3], Mauro Agate[1], Maurizio Gasparo Morticelli[1], Giuseppe Avellone[1], Luigi Ferranti[4], Attilio Sulli[1]

[1] Dipartimento di Scienze della Terra e del Mare, Università degli Studi di Palermo;
[2] Istituto Nazionale di Geofisica e Vulcanologia, Osservatorio Etneo - Sezione di Catania;
[3] Istituto di Geologia Ambientale e Geoingegneria, Consiglio Nazionale delle Ricerche;
[4] Dipartimento di Scienze della Terra, dell'Ambiente e delle Risorse, Università Federico II di Napoli;

Western Sicily (WS) is part of the Sicilian Fold and Thrust Belt, a sector of the SE-verging orogenic belt in the central Mediterranean. This part of the complex Apennine-Maghrebian chain has been described as a thick embricate wedge of Mesozoic carbonate (platform and deep-water) and siliciclastic rocks formed during the Neogene-Quaternary. According to deep seismic explorations in the area, the tectonic belt is composed of tectonically overlapping imbricate thrust-stack systems separated by regional basal detachments (Catalano et al., 2013 and references therein).
Active tectonic deformation is well documented in the northern offshore of Sicily, where geodetic, geological, and earthquake focal mechanisms highlight a near continuous E-W-oriented belt characterized by a significant crustal shortening (Billi et al., 2023 and reference therein). Conversely, the few available geodetic data suggest that WS is characterized by a contractional pattern occurring at rates lower than 1-2 mm/yr (Palano et al., 2012). Moreover, WS has been historically hit by significant earthquakes (M≥5) as the two occurred close at Selinunte (between the fourth and third centuries B.C., and between the sixth and thirteenth century A.D., respectively) (Guidoboni et al., 2002), Sciacca (1578) with estimated magnitude of 5 (Scarfi et al., 2024), as well as the one (M ~ 6) occurred in 1968 in the Belice region (Barreca et al., 2014) (Fig. 1a).
Despite this last event is considered as the most destructive earthquake hitting WS, the available seismic and geological data do not allow the identification of a specific seismogenic structure. The scientific debate about the possible source, its geometry, and its movement is still ongoing. The focal mechanisms do not provide unambiguous solutions, showing results that range from pure strike-slip to pure reverse faulting.
Given these still-present uncertainties, we established a new geodetic network of 24 episodic benchmarks crossing the main tectonic system of the Belice region. In addition, we collected all available episodic and continuous GNSS observations to provide a dense velocity field in a wide area encompassing the study region. Such a large dataset includes data acquired by continuous (RING, ASI, NETGEO, and ITALPOS) and episodic (IGM95, PTGA, and TYRGEONET) GNSS networks (Fig. 1b). RING (https://webring.gm.ingv.it) and ASI (http://geodaf.mt.asi.it) networks have been established for geodynamic and monitoring purposes, while NETGEO https://shop.netgeo.it) and ITALPOS (https://hxgnsmartnet.com) have been developed for general navigation and cadastral purposes. The IGM95 network was established and surveyed by the Italian Istituto Geografico Militare during the time span 1992-1996 to provide a set of 3D coordinates based on the GPS reference system for cartographic and civil applications. The TYRGEONET (Achilli et al., 1993) and PTGA (Ferranti et al., 2008) networks have been developed to study crustal deformation of central mediterranean and southern Italy, respectively. We re-surveyed most of these episodic sites in order to i) extend over the time their time series and ii) provide a fine refinement of site velocity estimation. All raw observations have been processed by using the GAMIT/GLOBK software and adopting the approach

described in Billi et al. (2023). The achieved crustal velocity field have been framed into the ongoing geodynamic of the study area.

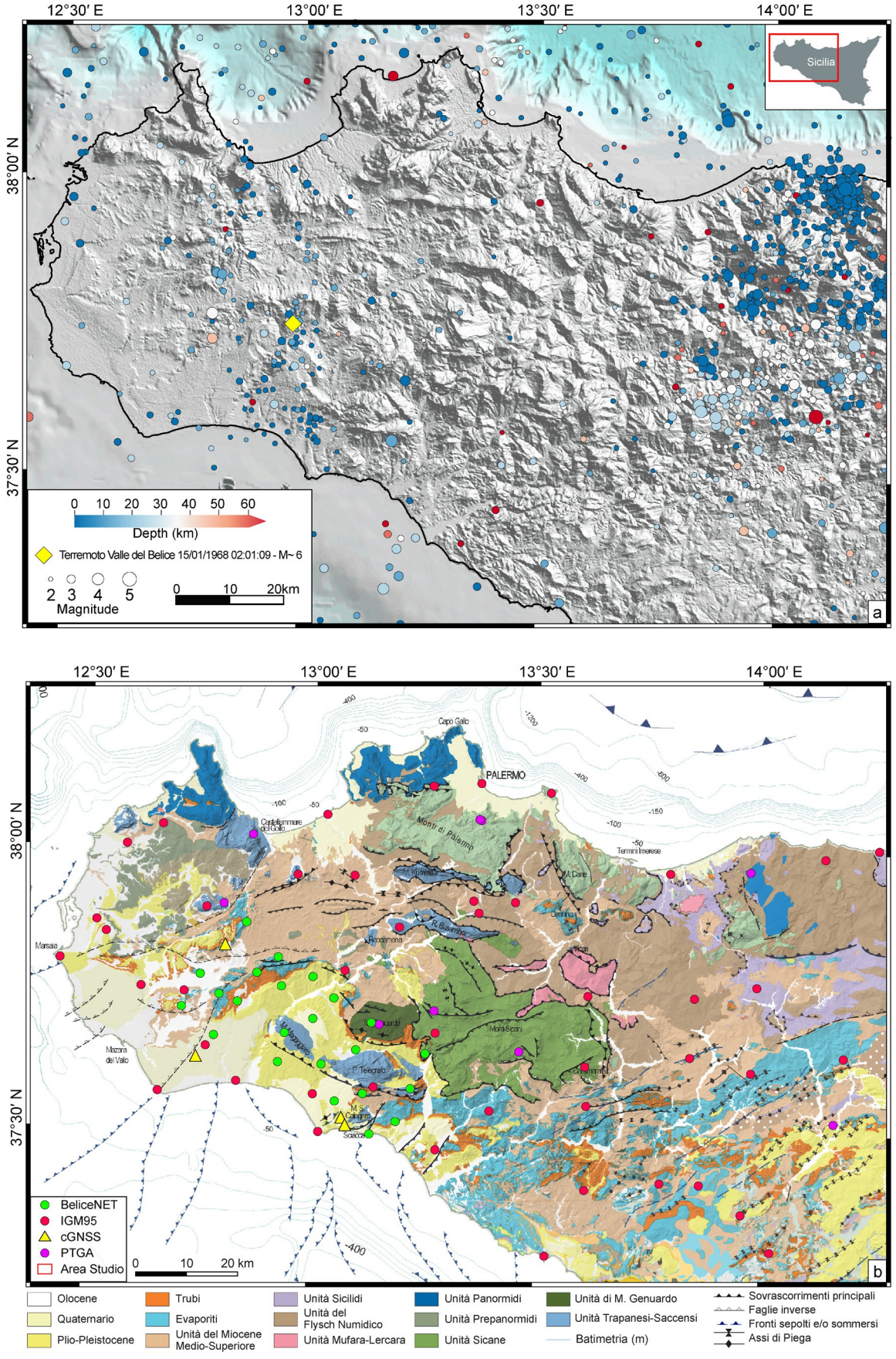

Fig. 1 - Figure shows the study area of the present work (Western Sicily). (a) Earthquake locations from 1981 to 2018 (CLASS Catalogue) and from 2019 to the present (ISIDE Catalogue). (b) Regional geological map showing the locations of geodetic networks with episodic measurements (BeliceNET, IGM95, PTGA, and TYRGEONET), indicated by colored points, and continuous GNSS (cGNSS) stations (RING, ASI, NETGEO, and ITALPOS), shown as yellow triangles.

References

Achilli, V., Anzidei, M., Baldi, P., Marsella, M., Salemi, G., & Vespe, F. (1993). The TYRGEONET project. In Permanent Satellite Tracking Networks for Geodesy and Geodynamics: Symposium No. 109 Vienna, Austria, August 11–24, 1991 (pp. 81-94). Berlin, Heidelberg: Springer Berlin Heidelberg.

Barreca, G., Bruno, V., Cocorullo, C., Cultrera, F., Ferranti, L., Guglielmino, F., ... & Pepe, F. (2014). Geodetic and geological evidence of active tectonics in south-western Sicily (Italy). Journal of Geodynamics, 82, 138-149.

Billi, A., Cuffaro, M., Orecchio, B., Palano, M., Presti, D., & Totaro, C. (2023). Retracing the Africa–Eurasia nascent convergent boundary in the western Mediterranean based on earthquake and GNSS data. Earth and Planetary Science Letters, 601, 117906.

Catalano R., Valenti V., Albanese C., Sulli A., Gasparo Morticelli M., Avellone G. & Basilone L. (2013) - Sicily's Foreland Fold/thrust Belt and Slab Roll-back: The SI. RI. PRO. Seismic Crustal Transect. In: "AAPG European Regional Conference & Exhibition".

Ferranti, L., Oldow, J. S., D'Argenio, B., Catalano, R., Lewis, D., Marsella, E., ... & Sulli, A. (2008). Active deformation in southern Italy, Sicily and southern Sardinia from GPS velocities of the Peri-Tyrrhenian Geodetic Array (PTGA). Boll. Soc. Geol. Ital, 127(2), 299-316.

Guidoboni, E., Muggia, A., Marconi, C., & Boschi, E. (2002). A case study in archaeoseismology. The collapses of the Selinunte temples (Southwestern Sicily): two earthquakes identified. Bulletin of the Seismological Society of America, 92(8), 2961-2982.

Corresponding author: martina.gennuso@unipa.it

Spatiotemporal Clustering of the New Zealand Catalog: A Comparative Study of ST-DBSCAN and Window-Based Methods – Preliminary results

S. Gentili[1], L. Caravella[1], E. Piegari[2]

[1] National Institute of Oceanography and Applied Geophysics - OGS, Italy
[2]Dipartimento di Scienze della Terra, dell'Ambiente e delle Risorse, Università degli Studi di Napoli Federico II, Italy

Earthquakes often occur in spatio-temporal clusters, reflecting complex physical processes within the Earth's crust. While background seismicity results from long-term tectonic loading and typically behaves as a temporally independent Poisson process, large earthquakes can generate aftershock sequences that develop into multi-stage cascades. Seismic catalogues contain both independent (background) and dependent (clustered) events, and distinguishing between these populations is crucial for scientific interpretation and hazard forecasting. Background seismicity underpins long-term seismic hazard models, whereas clustered events provide information on stress transfer, fault interactions, and aftershock evolution. Many seismic hazard frameworks require, or benefit from, catalogues in which independent events are separated and clusters are accurately identified (Gentili et al., 2019, 2025).

A major development in seismic cluster analysis in recent years has been the introduction of machine learning techniques. Among these, density-based algorithms such as DBSCAN (Ester et al., 1996) and OPTICS (Ankerst et al., 1999) have been widely used to identify arbitrarily shaped seismicity clusters based on spatial density criteria (Cesca, 2020; Piegari et al., 2022). However, classical DBSCAN does not differentiate between spatial and temporal coordinates, often requiring time to be treated independently from space, which limits its suitability for aftershock identification, where simultaneous space–time clustering is essential (Nicolis et al., 2024). An improvement to this limitation is ST-DBSCAN (Birant and Kut, 2007), which uses separate spatial and temporal search radii, allowing more flexible treatment of space–time relationships.

In this preliminary study, we compare two clustering approaches applied to the New Zealand earthquake catalogue: a window-based method commonly used in operational seismology, and ST-DBSCAN. We selected clusters containing more than 100 events and focused our analysis on pairs of clusters identified by both methods whose centroids lie within 10 km of each other. Fifteen clusters were found to overlap, providing a consistent basis for comparison.

Cluster quality metrics indicate broad agreement between the two approaches, with an Adjusted Rand Index of approximately 0.79. Preliminary results show that ST-DBSCAN tends to resolve fine-scale structure more effectively, whereas the window-based method forms tighter and more distinct large-scale groupings.

To assess correspondence with an independent reference, we carried out an initial analysis of the 2010–2013 Canterbury–Christchurch sequence. Using the event list from Herman et al. (2014), which includes 150 earthquakes of magnitude Mw ≥ 3.5, we compared sequence membership and structural consistency.

Acknowledgments

This work is Co-funded within the RETURN Extended Partnership and received funding from the European Union Next-GenerationEU (National Recovery and Resilience Plan - NRRP, Mission 4, Component 2, Investment 1.3 – D.D. 1243 2/8/2022, PE0000005) and by the grant “Progetto INGV Pianeta Dinamico: Near real-time results of Physical and Statistical Seismology for earthquakes observations, modelling and forecasting (NEMESIS)” - code CUP D53J19000170001 - funded by Italian Ministry MIUR (“Fondo Finalizzato al rilancio degli investimenti delle amministrazioni centrali dello Stato e allo sviluppo del Paese”, legge 145/2018).

References

Ankerst M.; Breunig M.M.; Kriegel H.P.; Sander J.; 1999. OPTICS: ordering points to identify the clustering structure, ACMSIGMOD Record, 28(2), 49–60.

Birant D.; Kut A.; 2007: ST-DBSCAN: An algorithm for clustering spatial-temporal data. Data & Knowledge Engineering, 60(1), 208–221. doi:10.1016/j.datak.2006.01.013

Cesca S.; 2020. Seiscloud, a tool for density-based seismicity clustering and visualization, J. Seismol., 24, 443–457.

Ester M.; Kriegel H.; Sander J.; Xu X.; 1996: A density-based algorithm for discovering clusters in large spatial databases with noise. In Proceedings of the 2nd International Conference on Knowledge Discovery and Data Mining (KDD), 226–231. doi:10.1145/3001460.3001507.

Herman M. W.; Herrmann R. B.; Benz H. M.; Furlong . P.; 2014: Using regional moment tensors to constrain the kinematics and stress evolution of the 2010–2013 Canterbury earthquake sequence, South Island, New Zealand. Tectonophysics, 633, 1-15, doi:10.1016/j.tecto.2014.06.019.

Gentili S.; Chiappetta G.D.; Petrillo G.; Brondi P.; Zhuang J.; 2025: Forecasting strong subsequent earthquakes in Japan using an improved version of NESTORE machine learning algorithm, Geoscience Frontiers, 16(3). https://doi.org/10.1016/j.gsf.2025.102016.

Gentili S.; Peresan A.; Talebi M.; Zare M.; Di Giovambattista R; 2019: A seismic quiescence before the 2017 Mw 7.3 Sarpol Zahab (Iran) earthquake: Detection and analysis by improved RTL method. Physics of the Earth and Planetary Interiors, 290, 10-19, https://doi.org/10.1016/j.pepi.2019.02.010.

Nicolis O.; Delgado L.; Peralta B.; Díaz M.; Chiodi M.; 2024: Space-time clustering of seismic events in Chile using ST-DBSCAN-EV algorithm. Environ Ecol Stat 31, 509–536. https://doi.org/10.1007/s10651-023-00594-3

Piegari E.; Herrmann M.; Marzocchi W.; 2022: 3-D spatial cluster analysis of seismic sequences through density-based algorithms. Geophys J Int 230(3), 2073–2088, doi:10.1093/gji/ggac160

Corresponding author: sgentili@ogs.it

Earthquake parameters of historical events: influence of alternative macroseismic fields on the seismogenic source determination

Gironelli V.[1], Luzi L.[1], Antonucci A.[1], Rovida A.[1]

[1] *Istituto Nazionale di Geofisica e Vulcanologia (INGV), Milano, Italy*

The investigation of 3D seismogenic sources of historical earthquakes, requires an integrated methodological approach that combines geological, seismological, and historical data. The primary input for the characterisation of these events is the geographic distribution of earthquake effects quantified in terms of macroseismic intensities.

The common practice involves determining the key seismological parameters (epicentral location and magnitude) of historical events from these macroseismic data. This procedure implies several uncertainties in both the data, such as the assessment of the intensity degrees from descriptive information, and the methods used for their inversion. These uncertainties propagate to subsequent elaborations, such as the reconstruction of seismogenic source geometries. Therefore, the spatial homogeneity and completeness of the intensity distribution can impact on the reliability of the derived macroseismic parameters. An additional factor of uncertainty lies in the features of the macroseismic field selected for parameterization.

In the Italian Parametric Earthquake Catalogue (CPTI15, Rovida et al., 2020, 2022), the parametrization of historical events is based on the Boxer algorithm to derive the macroseismic epicentre, which is assumed as the barycentre of the data with the maximum observed intensities (Imax), and the macroseismic magnitude is derived by combining epicentral intensity (I0) and the isoseismal areas and computed as the weighted average of the values obtained from each intensity class.

CPTI15 selects the input intensity distributions from the Italian Archive of Historical Earthquake Data (ASMI; Rovida et al., 2017, 2025), a comprehensive repository that provides various seismological studies and alternative intensity datasets for historical events. The selection of one macroseismic field takes into account its recentness, completeness and representativeness of the available historical information, i.e, solely “macroseismological” criteria. Such a choice inherently influences the subsequent parameter estimates the resulting seismogenic source geometry might not fully match the known geological structures.

In this contribution, we analyse the impact of the selection of alternative, although plausible and reliable, macroseismic fields on historical earthquake parametrisation and 3D source reconstruction through two case studies: the 1781 Cagli and the 1599 Valnerina earthquakes. For the latter, we

additionally test the consistency of the inferred source geometries with the fault model proposed in a recent geological study by Galli et al. (2020). The results highlight how different macroseismic fields can lead to significantly different epicentral locations, magnitude estimates, and source dimensions, and the selection of the most reliable hypothesis should be supported by a multiparametric approach, considering geologic, tectonic and seismological constraints.

References:

Galli, P., Galderisi, A., Marinelli, R., Messina, P., Peronace, E., & Polpetta, F. (2020). A reappraisal of the 1599 earthquake in Cascia (Italian Central Apennines): Hypothesis on the seismogenic source. Tectonophysics, 774, 228287. https://doi.org/10.1016/j.tecto.2019.228287.

Locati M., Camassi R., Rovida A., Ercolani E., Bernardini F., Castelli V., Caracciolo C.H., Tertulliani A., Rossi A., Azzaro R., D'Amico S., Antonucci A. (2022). Italian Macroseismic Database (DBMI15), version 4.0 [Data set]. Istituto Nazionale di Geofisica e Vulcanologia (INGV). https://doi.org/10.13127/dbmi/dbmi15.4

Rovida A., Locati M., Antonucci A., Camassi R. (a cura di) (2017). Archivio Storico Macrosismico Italiano (ASMI). Istituto Nazionale di Geofisica e Vulcanologia (INGV). https://doi.org/10.13127/asmi

Rovida A., Locati M., Camassi R., Lolli B., Gasperini P. (2020). The Italian earthquake catalogue CPTI15. Bulletin of Earthquake Engineering, 18(7), 2953-2984. https://doi.org/10.1007/s10518-020-00818-y

Rovida A., Locati M., Camassi R., Lolli B., Gasperini P., Antonucci A. (2022). Italian Parametric Earthquake Catalogue (CPTI15), version 4.0 [Data set]. Istituto Nazionale di Geofisica e Vulcanologia (INGV). https://doi.org/10.13127/cpti/cpti15.4

Rovida A. Locati, M., Antonucci A., Camassi R. (2025). The Italian Archive of Historical Earthquake Data, ASMI. Earth System Science Data, 17(6), 3109–3124. https://doi.org/10.5194/essd-17-3109-2025

Corresponding author: veronica.gironelli@ingv.it

Interseismic coupling degree of the Northern Apennine Arc in Emilia Romagna region, (Italy).

Salvatore Giuffria[1-2], Shannon Graham[3], Letizia Anderlini[4], Francesco Carnemolla[1-2], Fabio Brighenti[5-2], Giorgio de Guidi[1-2], Flavio Cannavò[6], Riccardo Caputo[2-5]

[1] Department of Biological, Geological and Environmental Sciences, University of Catania, Italy
[2] CRUST - Interuniversity Center for 3D Seismotectonics with territorial applications. U.R. Catania, Italy
[3] The College of New Jersey - TCNJ, Physics Department, NJ
[4] INGV, National Institute of geophysics and Volcanology, Bologna, Italy
[5] Department of Physics and Earth Sciences, University of Ferrara, Italy
[6] INGV-OE, National Institute of Geophysics and Volcanology-Etnean Observatory, Catania, Italy

1.Introduction

The Emilia- Romagna portion of the Po Plain hosts part of the outermost sector of the Northern Apennines orogenic front formed in the context of the Europe-Africa relative convergence (Fig.1a). The low strain rate and the compressional velocity gradient acting in these areas are well documented through recent studies, although it is still unknown which fault segment plays the dominant role in accommodating the recognized deformation during the interseismic period. Some of these faults, such as the Mirandola and the Ferrara thrusts System (Fig. 1b), are considered the causative sources of the 2012 Emilia seismic sequence (e.g., Cheloni et al., 2016). In this work we propose a comprehensive kinematic block modeling approach (McCaffrey, 2002) to identify which fault segment effectively accommodate the ongoing compressive geodetic velocity pattern by uniform slip rates in the long term. We therefore investigate the seismic potential of the Northern Apennine front by discretising it as a 3D Triangular Dislocation Elements (TDEs) mesh which includes the seismogenic sources of the May 2012 seismic events. In the analysis, we also estimate the slip deficit rate (Savage, 1983) and the interseismic coupling coefficient to discriminate possible locked asperity capable of generating earthquakes.

2. Seismotectonic of the Po Plain

The Northern Apennines front can be grouped in three different NE verging thrust and fold related systems: The Monteferrato, the Emilian, and the Ferrara-Romagna Arcs. The latter is structured in two major fold and thrust groups: The Mirandola fault (MI) and the Ferrara Thrust System (Fig.1a). The Ferrara Thrust System (Fig. 1b), is composed of various active thrusts (Cheloni et al., 2016): The Inner Ferrara thrusts (IF, Quarantoli thrust), the Middle Ferrara thrust (MF) and the Outer Ferrara thrust (OF). Activity of the Ferrara Thrust System and Mirandola thrust is evidenced by

historical and instrumental seismicity, for instance the mainshocks of the May 20 and 29, 2012 seismic

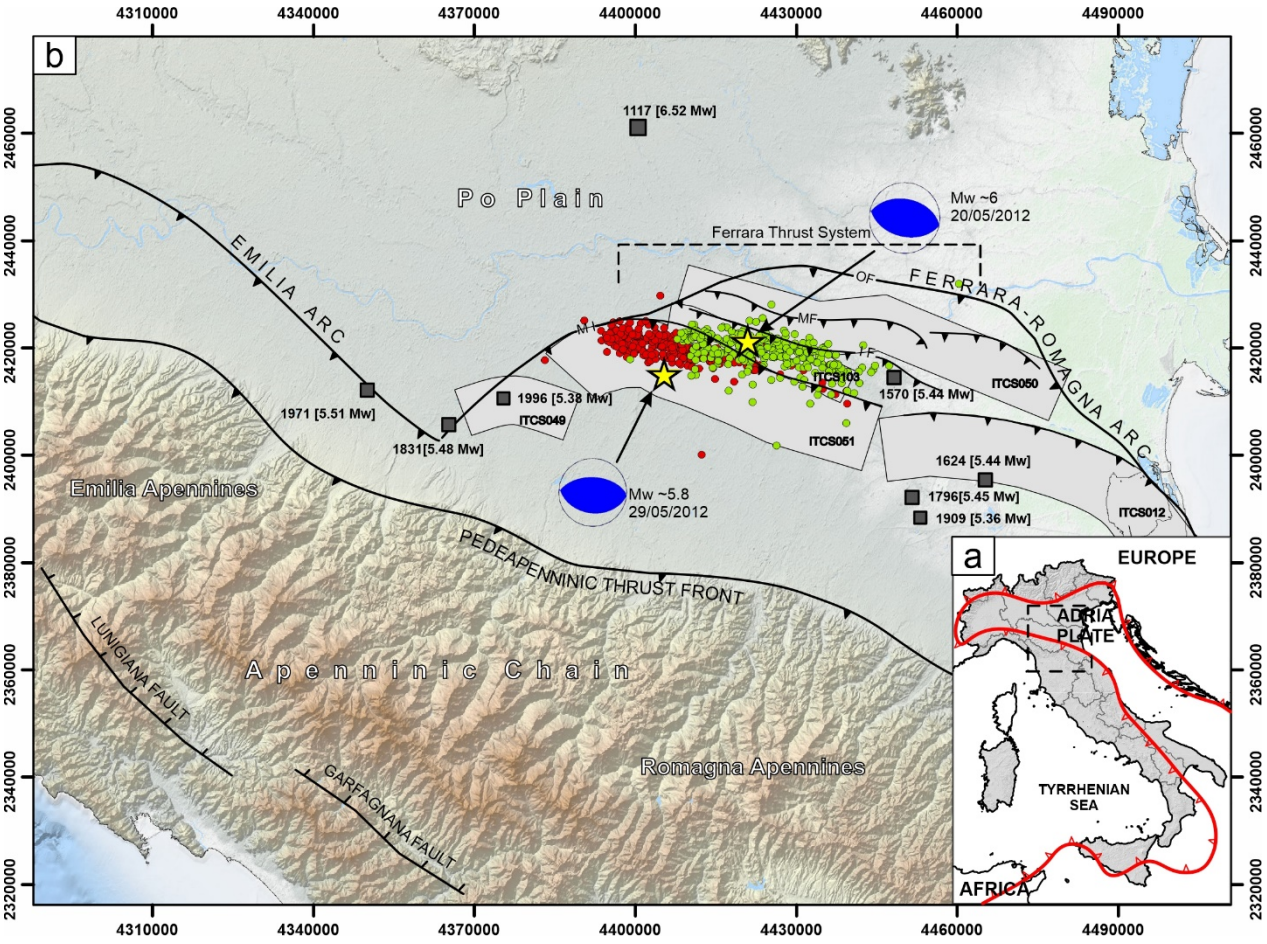

Fig. 1 – a) Europe-Africa relative convergence in the context of the Central mediterranean area, (red line represents the front of the collisional domain). b) Simplified seismotectonic map of the Emilia region. Seismogenic sources (in grey) are from DISS. The green and red dots are the microseismicity associated with the 20th and 29th May 2012 seismic event respectively, (from CLASS Database).

sequence, Mw ~6 and ~5.8 respectively (focal plane solutions in Fig. 1b), and the 1570 Ferrara earthquakes of Mw ~5.4, (see Fig. 1b for epicentral location of historical earthquakes in the Po Plain from CPTI15, Rovida et al., 2022). According to DISS database and literature, the Po Plain is bordered to the south by an active thrust front belonging to the Northern Apennines, these N-verging blind thrusts are also called Pedeapenninic Thrust Front (PTF, Fig. 1b). The available focal mechanisms for the PTF show a predominant reverse kinematic referred to earthquakes within the first 20 km of depth. Moving toward South-West, other remarkable faults are present in correspondence of the Intramontane area. This area belongs to a belt running on the Tyrrhenian side of the studied region, close to the main topographic divide of the Apenninic chain. It is characterized by various extensional faults, such as the Garfagnana and Lunigiana and spread seismicity with prevalent extensional focal mechanisms for the first 15-20 km of depth.

3. Data and methods

3.1 Geodetic data

We used GNSS data and solutions from Serpelloni et al., (2022) that provides time series longer than 2.5 years. We additionally reoccupied 12 IGM-95 (Istituto Geografico Militare) campaign stations during March 2023 accurately selected across the studied faults; these sites have GNSS time series starting in 1994. Campaign data were processed using GAMIT/GLOBK (Herring et al., 2015), and time series were computed in the ITRF2014 reference frame (Eurasia fixed). We used the co-seismic and post-seismic source models of Cheloni et al. (2016) for the 2012 Emilia seismic sequence to correct the long-term interseismic motion of the IGM-95 points. Specifically, we used GAME (Ground deformAtion ModElling MatLab tool, Cannavò, 2019) software to forward model surface displacements by activating the Okada-type patch sources for the Middle Ferrara (20 May) and Mirandola (29 May) thrusts (Fig. 2a). Finally, we removed these modelled co-/post-seismic contributions from the observed time series (Fig. 2b). The obtained velocities were used together with that of Serpelloni et al., (2022) to implement a kinematic block modeling.

3.2 Kinematic block modeling

According to the Block modeling theory (McCaffrey, 2002 and reference therein), the velocity gradient observed at surface, assumed to be representative of the interseismic period, can be modelled considering the lithospheric layer divided into rigid blocks, bordered by rectangular fault planes embedded in a homogeneous, isotropic and elastic half space. Accordingly, the interseismic deformation can be modelled as the sum of the long-term velocity, related to the blocks motion, and a shallow long term slip rate with a negative sign (acting in opposite directions with respect to the coseismic slip sense), called back slip or slip deficit, which is representative of the amount of the expected slip on the fault that is not released steadily by creeping mechanisms and accumulates in the shallow part of the crust during the interseismic period (Savage, 1983; McCaffrey, 2002). As a first approach we opted to build a simple model including 2 blocks, considering the seismogenic sources belonging to the Emilia Arc, to the Ferrara Romagna arc and the Mirandola thrust (MI and MF in figure 1b). For these faults we constrained a locking depth of 12 km and an average dip angle of 30° according to DISS database and previous seismotectonic studies. We therefore passed through more complicated models in which we included the intramountain faults (Garfagnana and Lunigiana faults), and the Pedeapenninic Thrust Front (PTF), defined by three and four blocks respectively. Following the DISS database, we used a locking depth of 15 km and an average dip angle of 40° for the PTF, whereas a 10 km of locking and an average 60° dip angle for the Intramountain faults.

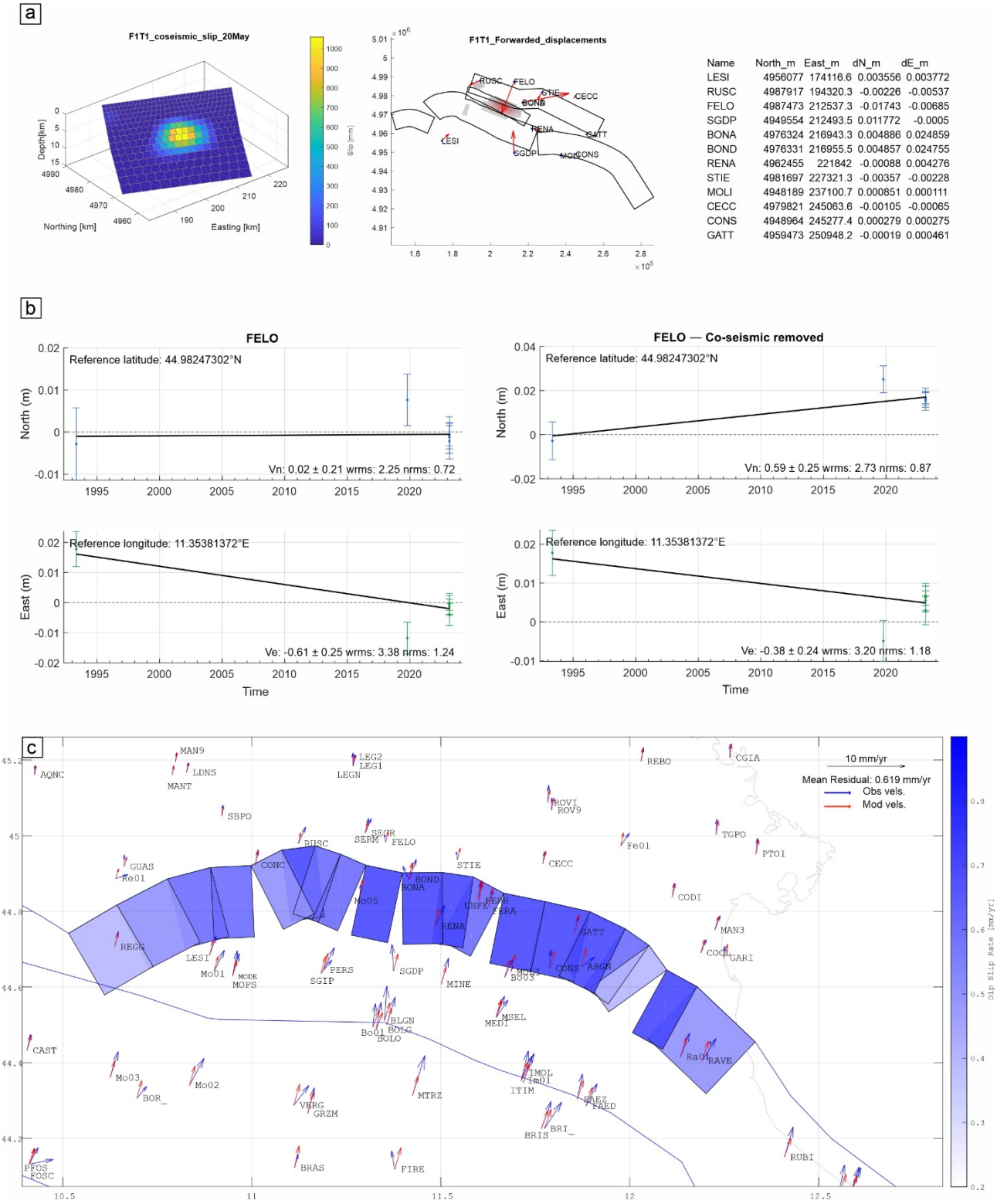

Fig. 2 – a) Example of the modelled patches (Cheloni et al., 2016), used to forward coseismic displacement components (dE_m and dN_m) on the measured IGM-95 stations. b) example of time series (FELO) epurated from coseismic displacement. c) optimal block model setting for the study region and long-term dip slip rates on the modelled northern Apennine Arc.

We consider the model that includes the PTF, MF and MI as the best candidate (WRMS = 0.538 mm/yr) to reproduce the observed velocity gradient in Emilia Romagna region (Fig. 2c). The latter allowed us to infer contractional slip rate at most equal to 1 mm/yr on the modelled Northern

Apennine front (Fig. 2c) and slip rate of ~1-1.5 mm/yr for the PTF consistent with the slip rate known in literature.

3. Results

We discretised the fault planes as a single TDE mesh, honouring the known fault trends, dip directions, dip angles, and a maximum depth of 13 km, to compute the slip-deficit rate (SDR) distribution. The resulting SDR pattern is useful for discriminating along-strike and downdip variations in fault behaviour and for identifying regions of high interseismic coupling (Meade and Loveless, 2009). Within the block modelling framework, highly coupled fault areas are interpreted as “locked asperities” that accommodate the velocity gradient elastically and may fail seismically, whereas low-coupling portions are inferred to accommodate deformation predominantly through aseismic processes (e.g., long-term creeping behaviour).

3.1 Slip deficit and velocity gradient

The SDR reaches a value at most equal to 1 mm/yr and depicts one large two central portion of the mesh with high slip deficit (from 0.8 mm/yr to 1.0 mm/yr), potentially coupled to some degree along its entire extension. Additionally, we denoted high slip deficit areas at the margin of the model, which we do not treat in the following since these need more resolution analysis. To investigate the velocity gradient across the two central high slip deficit areas and verify how the modelled front accommodates it, we built a regular grid of experimental points (EPs). For each EPs we computed the corresponding velocities derived from the direct model of the optimal block model. Furthermore, we built 2 sections slicing across the modelled mesh surface (section s_1 and s_2 in figure 3 b-c). For each section we plotted the parallel observed and modelled parallel velocity components and used a polynomial function to build the fit curves of the forwarded velocity field for each section. Accordingly, the velocity field shows a predominant compressional pattern across the modelled mesh: in s_1 exhibits a gradient of 0.97 ± 0.23 mm/yr, while in s_2 a gradient of 0.81 ± 0.22 mm/yr.

3.2 Coupling degree

The interseismic coupling coefficient (IC) is a dimensionless number defined as the ratio of the slip-deficit rate in the interseismic period and the long-term slip rates across the fault due to the relative motion of the adjacent blocks (McCaffrey, 2002). According to our inversion (Fig. 3d), we detected one large, coupled asperity (IC ≥ 0.5) located near the epicentral location of the May 20th, 2012, seismic event. This asperity fit well with the seismicity associated with the mainshock, whereas the epicentral areas near the May 29th event are characterized by low coupling values. The coupling distribution highlights another area with IC higher than 0.5 located to the east with respect to the 2012 events, that is smaller than the previously observed around the May 20th event, around Ferrara and another asperity located near Ravenna, in the sallowest portion of the modelled mesh.

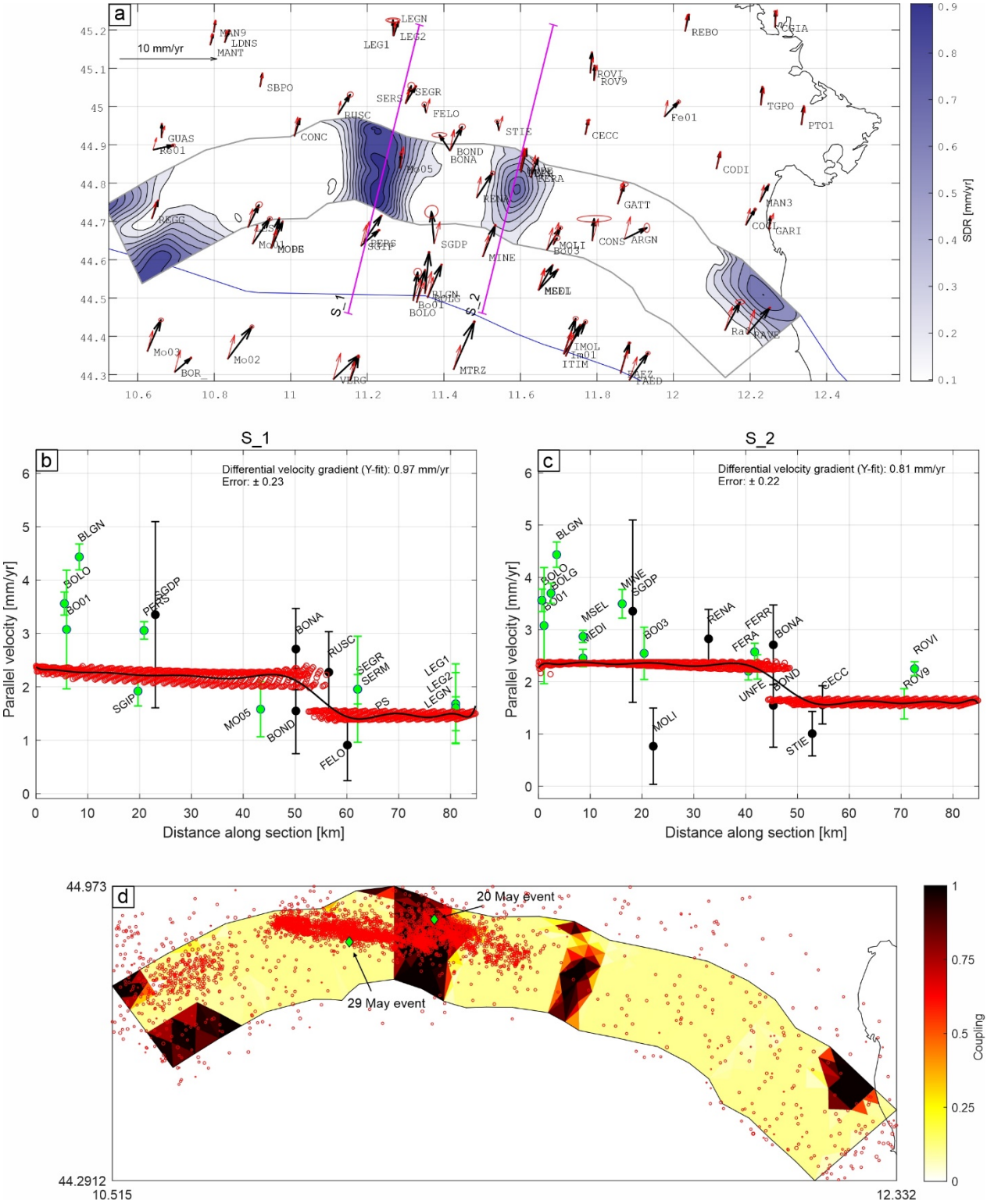

Fig. 3 –a) Slip deficit on the modelled TDEs mesh. b-c) S_1 and S_2 showing the parallel component of the forwarded velocity across the; green and black circles are the permanent and campaign stations respectively; red circles are the modelled velocity. d) obtained coupling degree compared with available seismicity of the area (from HORUS database).

4.1 Discussion and conclusion

The spatial pattern of IC that we obtain along the Emilia–Romagna sector of the Northern Apennines front shows both expected and new features. The main coupled asperity (IC ≥ 0.5)

beneath the May 20th, 2012, epicentral area confirms the interpretation of this segment as an elastic strain accumulation and seismic release areas, in agreement with the instrumental seismicity pattern. In contrast, the low to moderate coupling inferred in correspondence of the May 29th, 2012, events should be interpreted with caution. In this sector, the GNSS network is sparser, and the velocity field is less constrained, so the apparent reduction in coupling is likely influenced, at least in part, by data coverage and model resolution rather than reflecting a truly decoupled fault patch. A particularly relevant result of our inversion is the identification of a second high-coupling asperity, located to the east of the 20 May rupture zone, near Ferrara, where IC values again exceed 0.5 and the SDR is 0.5 – 0.8 mm/yr. This feature does not coincide with any previously ruptured large event in the instrumental record and may therefore represent a locked asperity capable of generating future moderate to strong earthquakes. Similarly, we detect an additional locked asperity near Ravenna, clustered in the shallowest portion of the modelled thrust front, further supporting the presence of along-strike segmentation with potentially distinct seismic potential.

Acknowledgments

We thank all co-authors for their valuable contributions to this work. We are particularly grateful to D. Cheloni for kindly providing the Okada patch solutions for the 2012 seismic events used in his previously published study.

References

Boccaletti, M. (1985) - Report of the Working Group on Paleogeography and Geodynamics Part I: Western Mediterranean. In Rogl F., ed., Report on activity of the RCMNS Working Groups and Bibliography 1979-1984, Mediterranean and Paratethys Neogene. Hungarian Geological Survey, Budapest, pp. 41-43.

Cannavò, F. (2019). A new user-friendly tool for rapid modelling of ground deformation. Computers & Geosciences, 128, 60–69. https://doi.org/10.1016/j.cageo.2019.04.002

Cheloni D., Giuliani R., D'Agostino N., Mattone M., Bonano M., Fornaro G., Lanari R., Reale D. and Atzori S. (2016): New insights into fault activation and stress transfer between en echelon thrusts: The 2012 Emilia, Northern Italy, earthquake sequence, J. Geophys. Res., 121, 4742–4766, doi: 10.1002/2016JB012823.

DISS Working Group (2025). Database of Individual Seismogenic Sources (DISS), Version 3.3.1: A compilation of potential sources for earthquakes larger than M 5.5 in Italy and surrounding areas. Istituto Nazionale di Geofisica e Vulcanologia (INGV). https://doi.org/10.13127/diss3.3.0

Herring, T. A., King, R. W., Floyd, M. A., and McClusky, S. C. (2015). Introduction to GAMIT/GLOBK, Release 10.6. Available at: gpsg.mit.edu/~simon/gtgk/ Intro_GG.pdf.

McCaffrey, R. (2002) Crustal Block Rotations and Plate Coupling, in Plate Boundary Zones, a cura di S. Stein & J. Freymueller, AGU Geodynamics Series, Vol. 30, pp. 101–122. https://doi.org/10.1029/GD030p0101.

Meade, B.J. and Loveless, J.P. (2009) 'Block modeling with connected fault-network geometries and a linear elastic coupling estimator in spherical coordinates', Bulletin of the Seismological Society of America, 99(6), pp. 3124–3139. Available at: https://doi.org/10.1785/0120090088.

Rovida A., Locati M., Camassi R., Lolli B., Gasperini P., Antonucci A. (eds), 2022. Italian Parametric Earthquake Catalogue (CPTI15), version 4.0. Istituto Nazionale di Geofisica e Vulcanologia (INGV). https://doi.org/10.13127/CPTI/CPTI15.4

Savage, J.C., 1983. A dislocation model of strain accumulation and release at a subduction zone, J. geophys. Res., 88, 4984–4996.

Serpelloni, E., Cavaliere, A., Martelli, L., Pintori, F., Anderlini, L., Borghi, A., Randazzo, D., Bruni, S., Devoti, R., Perfetti, P., & Cacciaguerra, S. (2022). Surface velocities and strain-rates in the Euro-Mediterranean region from massive GPS data processing. Frontiers in Earth Science, 10, Article 907897. https://doi.org/10.3389/feart.2022.907897

Corresponding author: salvatore.giuffrida@phd.unict.it

Seismic potential of the Crati Valley (northern Calabria, Italy) in the context of the ongoing geodetic velocity field.

Salvatore Giuffrida[1-2], Francesco Carnemolla[1-2], Giorgio de Guidi[1-2], Letizia Anderlini[3], Fabio Brighenti[4-2], Mario La Rocca[5], Carlo Tansi[6].

[1] Department of Biological, Geological and Environmental Sciences, University of Catania, Italy
[2] CRUST - Interuniversity Center for 3D Seismotectonics with territorial applications. U.R. Catania, Italy
[3] INGV, National Institute of geophysics and Volcanology, Bologna, Italy
[4] Department of Physics and Earth Sciences, University of Ferrara, Italy
[5] University of Calabria, unical, Italy
[6] CNR, Centro Nazionale per le Ricerche, Calabria Italy

1.Introduction

The Study of active faults is fundamental to assess the seismic potential of a given area, this kind of knowledge is achievable by using geodetic measurements, such as GNSS data (Global Navigation Satellites System), which have been highly exploited during the last decades due to their recent improvement and their capability of detecting millimeters ground deformation (Segall & Davis, 1999). This approach is adopted by several authors to infer the seismic potential of active faults and explain ground deformation related to these during the interseismic period (Meade & Hager, 2005). Areas characterized by high deformation rates are those where strong earthquakes (Mw higher than 7) are likely to occur, for example near plate boundaries (i.e., areas of collision and subduction zones). However, high magnitude seismic events can also occur near faults that accommodate the large-scale dynamic led by tectonic plates. An example is the Calabrian Arc (CA) (Fig. 1), in Southern Italy, where the high level of crustal seismicity in the last years (Rovida et al., 2025) is mainly defined by the activity of ~ NS and ~ NE-SW striking faults (Fig 3a) which accommodate the ongoing WNW-ESE extensional stress regime due to the relative movement of the European and African plates (Malinverno & Ryan, 1986; Monaco et al., 1996; Faccenna et al., 2011) (Fig. 3b-c). In this work we conduct an enhanced seismotectonic study to determine the seismic potential of the Border faults of the Crati Valley (Northern Calabria). Several authors agree in considering the West Crati fault (WCF) as causative of the 1184, Mw ~ 6.8 and the 1854, Mw ~ 6.3 Earthquakes (i.e., Postpischl, 1985; Rovida et al 2025), however, the capacity of this fault of determining future earthquakes is still unknown, nevertheless the WCF is considered as a debated seismogenic source (DISS working group, 2025) and its role in accommodating the actual stress regime is still matter of questions.

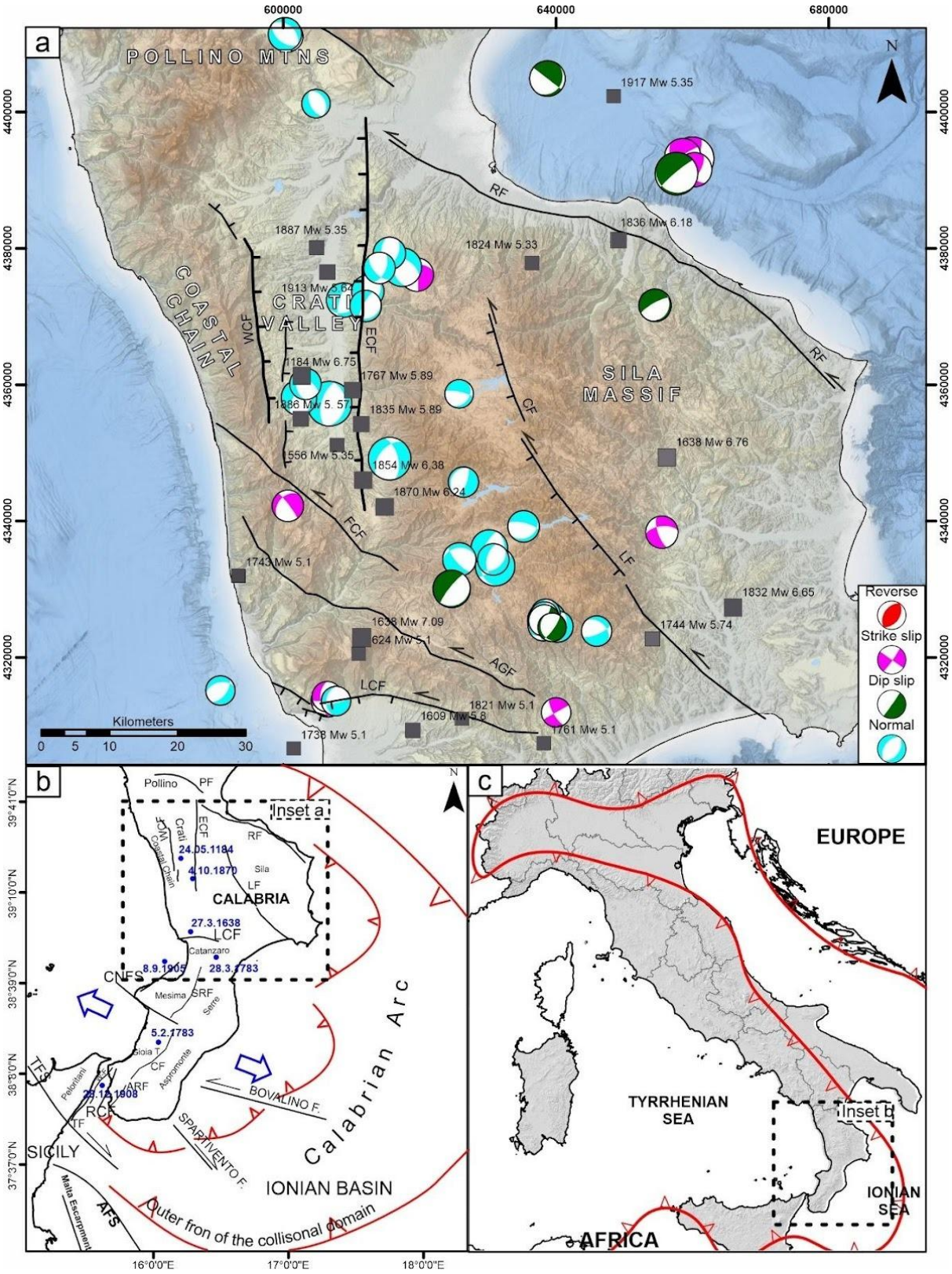
a
POLLINO MTNS
COASTAL CHAIN
CRATI VALLEY
SILA MASSIF
WCF
ECF
RF
CF
FCF
LF
AGF
LCF
1917 Mw 5.35
1836 Mw 6.18
1824 Mw 5.33
1887 Mw 5.35
1913 Mw 5.64
1184 Mw 6.75
1767 Mw 5.89
1886 Mw 5.57
1835 Mw 5.89
1638 Mw 6.76
1556 Mw 5.35
1854 Mw 6.38
1870 Mw 6.24
1743 Mw 5.1
1832 Mw 6.65
1638 Mw 7.09
1624 Mw 5.1
1744 Mw 5.74
1821 Mw 5.1
1609 Mw 5.8
1738 Mw 5.1
1761 Mw 5.1
Reverse
Strike slip
Dip slip
Normal
Kilometers
0 5 10 20 30
600000
640000
680000
4400000
4380000
4360000
4340000
4320000
b
Pollino
PF
Inset a
Crati
ECF
RF
Coastal Chain
WCF
24.05.1184
4.10.1870
Sila
LF
CALABRIA
27.3.1638
LCF
Catanzaro
CNFS
8.9.1905
28.3.1783
Mesima
SRF
Serre
5.2.1783
Gioia T.
CF
Aspromonte
TTF
Peloritani
ARF
23.10.1908
RCF
TF
BOVALINO F.
SPARTIVENTO F.
Calabrian Arc
SICILY
IONIAN BASIN
Malta Escarpment
AFS
Outer fron of the collisonal domain
16°0'0"E
17°0'0"E
18°0'0"E
39°41'0"N
39°10'0"N
38°39'0"N
38°8'0"N
37°37'0"N
c
EUROPE
TYRRHENIAN SEA
Inset b
IONIAN SEA
AFRICA

Fig. 1 – a) *a) Seismotectonic map of the Northern Calabria Arc (Modified after Tansi et al., 2007), black lines are the main faults slicing across the area, grey squares are historical earthquakes from CPTI15 4.0 (Catalogo Parametrico dei Terremoti Italiani; https://emidius.mi.ingv.it/CPTI15-DBMI15/ accessed on 29/07/2025), Digital elevation model is from EmodNet (https://emodnet.ec.europa.eu/) WCF: West Crati Fault; ECF: East Crati Fault; CF: Cecita Fault; LF: Lake Fault; FCF: Falconara-Carpanzano Fault; AGF: Amantea-Gimigliano Fault; LCF: Lamezia Catanzaro Fault. b) Tectonic Sketch of the studied area with location of major earthquakes, red lines represent the actual front of the collisional belt (Giuffrida et al., 2023 Modified). SRF: Serre Fault; CNFS: Coccorino-Nicotera Fault System; CF: Cittanova Fault; ARF: Armo Fault; RCF: Reggio Calabria Fault; TF: Taormina Fault; TFS: Tindari Fault System; AFS: Alfeo.Etna Fault System. c) Geodynamic Framework of the Calabrian Arc in the context of the Europe-Africa relative convergence. b) tectonic sketch of the Calabrian Arc after Giuffrida et al. (2025); blue dots are the location of main historical earthquakes. c)Location of the Calabrian Arc in the context of the Europe -Africa relative convergence. The red line represents the nowadays compressional orogenic front.*

2. Data and method

To better understand the role of the border faults of the Crati Valley in the complex seismotectonic context in which they are located, we first investigated the geodetic horizontal velocity field by using available GNSS data and solution of INGV (RING/RDN Network). We moreover improved the density of the dataset by including GPS Points of IGM 95 network reoccupied during the 2024 (Fig. 2). We also build three velocity cross sections which depict a clear extensional velocity pattern across the studied faults (s1, s2 and s3 in Fig. 2). The obtained velocity field was then inverted to analyse possible strain rate gradients across the Crati valley, we moreover applied a kinematic Block Modeling Approach (BM, MccAffrey 2002; Meade & Loveless, 2009) to infer which fault plays a major role in accommodating the obtained extensional velocity gradient by long term slip rates. From recent analysis of high-quality seismic reflection profiles (Brozzetti et al., 2017; Lines L1, L2 and L3, Vi.D.E.P.I. project), the geometry at depth of the WCF was enlightened, exhibiting an East dipping low angle plane representing the main tectonic structure which controls the evolution of the Crati Basin, in line with the tectonic style of the Southern Apennine region, whereas the antithetic SW dipping faults are considered as secondary structures, merging at depth with the WCF. Following Brozzetti et al., (2017), we challenge to better clarify the seismic potential of the WCF, since the role of low angle normal faults in determining high magnitude seismic events is largely questioned within the scientific community (Chiaraluce et al., 2007). We first discretized the WCF as a 3D triangular dislocation element mesh, for which we solved the slip deficit rate (Savage, 1983), we moreover defined the interseismic coupling coefficient (IC) on the modelled mesh as the ratio of the slip deficit and the long-term slip rate for each triangle. According to MccAffrey, (2002), fault portions with high IC, are those ones that reproduce the observed geodetic velocity gradient by elastic responses and are considered as ‘locked asperities’ which accumulate energy during the interseismic period. Accordingly, we propose a possible set of rupture scenarios considering the activation of the detected coupled fault portions (see also Graham et al., 2021), estimating the moment magnitude and the related recurrence interval for each increment of coupling.

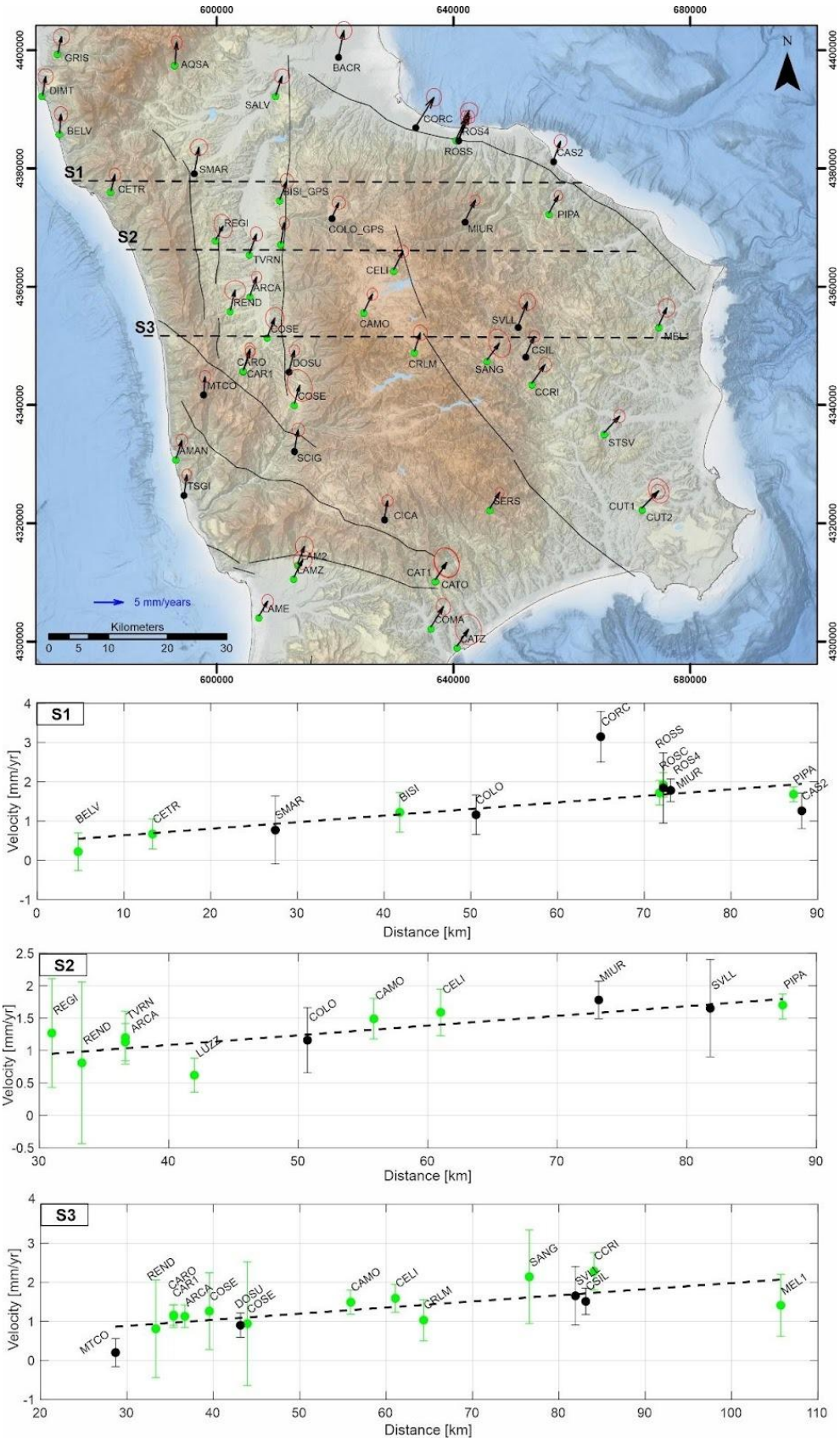

Fig. 2 -velocity field and velocity sections in ITRF 14 (Eurasia fixed) reference frame. Black dots are the campaign GNSS station of IGM-95 network; green dots are the permanent GNSS stations.

3. Results

The horizontal GNSS velocity field, obtained by combining the INGV (RING/RDN) solutions with the 2024 re-occupation of benchmarks from the IGM95 network, highlights a coherent extensional pattern across the Crati Valley. Inversion of the velocity field, together with a kinematic Block Modeling approach, suggests that the observed interseismic gradient is primarily accommodated by long-term dip-slip extension on the West Crati Fault (WCF) and the East Crati Fault (ECF) (Fig. 3a), with rates on the order of ~2–1 mm/yr. Secondary strike-slip components are also inferred, reaching up to ~0.8 mm/yr, with opposite kinematics on the two main faults (dextral on the ECF and sinistral on the WCF). Additional structures contribute to the regional budget: the Amantea–Gimigliano Fault (AGF) and the Lamezia–Catanzaro Fault (LCF) show extensional dip-slip rates of ~1 mm/yr with subordinate left-lateral motion of ~0.5 mm/yr, whereas the RF (Rossano Fault)exhibits a more complex behaviour with both extensional and contractional dip-slip components (ranging between 0.6 and 0.3 mm/yr) and a dominant strike-slip rate of ~1.5 mm/yr. Using the fault geometry constrained by high-quality seismic reflection profiles (Brozzetti et al., 2017), the WCF was discretized as a 3-D triangular dislocation elements (TDEs) mesh, and the slip deficit rate (SDR) was solved following the classic interseismic slip-deficit framework. The resulting SDR distribution ranges from ~0.2 to ~1.8 mm/yr (Fig. 3b). The derived interseismic coupling coefficient (IC, Fig. 3c), defined as the ratio between slip deficit and long-term slip rate for each triangular element, suggests the presence of a potentially locked portion within the upper ~8 km of the fault, located in the central–northern sector of the modelled plane. This patch constitutes the most plausible candidate for a locked asperity capable of accumulating elastic strain during the interseismic period.

4. Conclusions

Our geodetic and kinematic modelling results indicate that the present-day extensional velocity gradient across the Crati Valley is primarily accommodated by dip-slip motion on the West and East Crati faults (~2–1 mm/yr), with subordinate strike-slip components. The inferred slip-deficit rate suggests a broadly coupled behaviour of the WCF along its modelled surface, supporting its potential role as a significant seismogenic structure. By translating the geodetically constrained coupling fractions into moment accumulation, we obtain a range of earthquake scenarios (Fig.3d); for an average coupling fraction of 0.5 the expected event size is Mw ~ 6.2 with a recurrence time of 460 ± 80 years. At the same time, the modeled coupling pattern and the inferred seismic scenarios remain subject to uncertainties related to the role of antithetic structures that may share deformation with the main low-angle fault. Therefore, further analyses are required to strengthen the assessment of seismic potential, including: (i) slip-tendency or Coulomb-style mechanical evaluations to test whether the identified patches are favourably oriented for failure under the current stress field; (ii) explicit meshing and modeling of the antithetic ECF W-dipping fault to quantify their contribution to the observed velocity gradient and possible slip partitioning; and (iii) sensitivity analyses on data and coupling parameter.

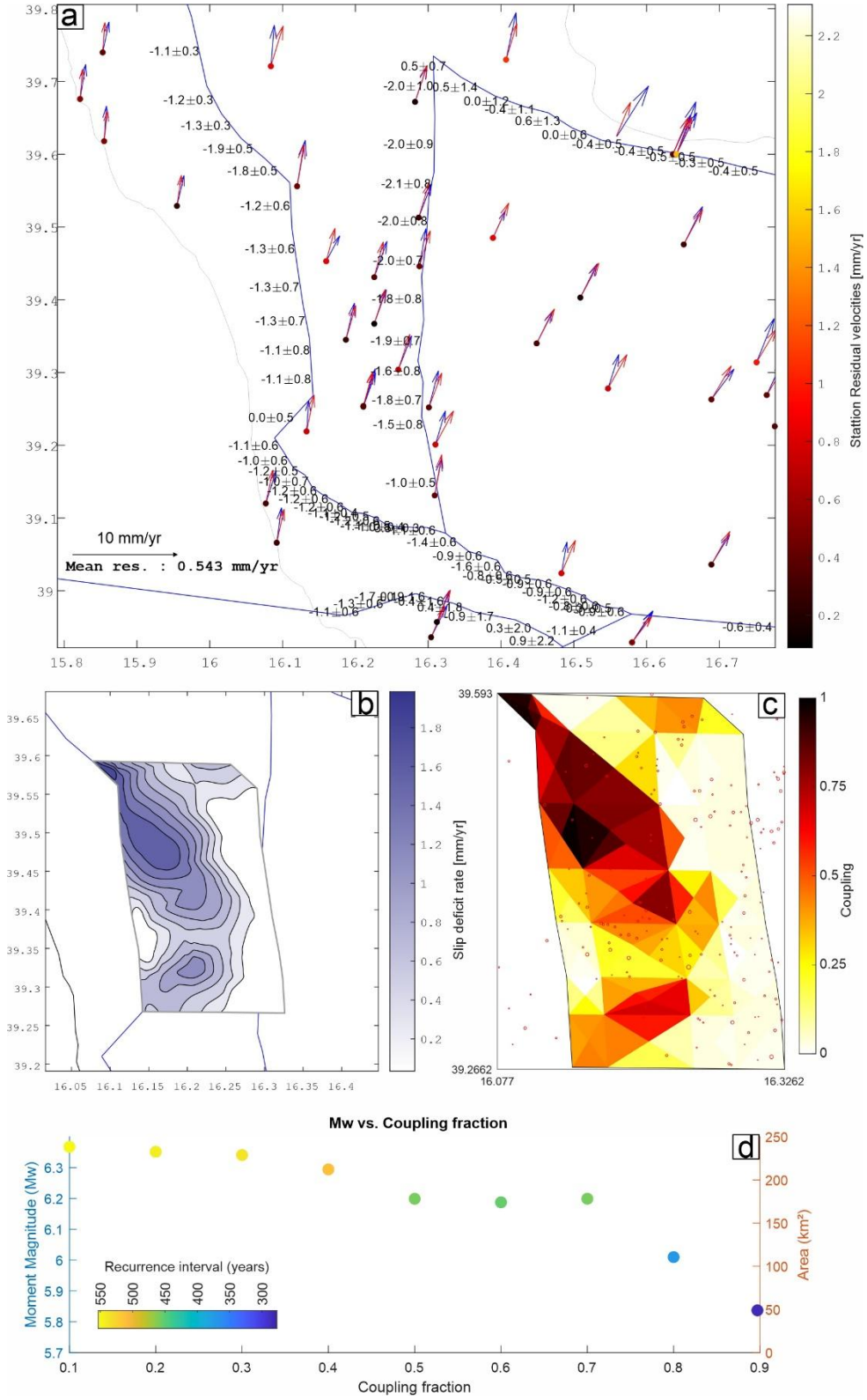

Fig. 3 –a) Observed and modelled velocity field (black and red arrows, respectively) and model residuals. Long term slip rate (Dip slip component) for each fault segment. b) slip decific rate on the modelled WCF 3D mesh. c) interseismic coupling coefficient on the modelled WCF 3D mesh. d) Summary of the rupture scenarios involving each coupling fraction (from 0.1 to 0.9), estimated Mw and related recurrence intervals.

References

Brozzetti, F., Cirillo, D., Liberi, F., Piluso, E., Faraca, E., De Nardis, R., & Lavecchia, G. (2017). Structural style of Quaternary extension in the Crati Valley (Calabrian Arc): Evidence in support of an east-dipping detachment fault. *Italian Journal of Geosciences, 136*(3), 434–453. https://doi.org/10.3301/IJG.2017.11

Chiaraluce, L., Chiarabba, C., Collettini, C., Piccinini, D., & Cocco, M. (2007). Architecture and mechanics of an active low-angle normal fault: Alto Tiberina fault (northern Apennines, Italy). *Journal of Geophysical Research: Solid Earth, 112*, B10310. https://doi.org/10.1029/2007JB005015

DISS Working Group (2025). Database of Individual Seismogenic Sources (DISS), Version 3.3.1: A compilation of potential sources for earthquakes larger than M 5.5 in Italy and surrounding areas. Istituto Nazionale di Geofisica e Vulcanologia (INGV). https://doi.org/10.13127/diss3.3.1

EMODnet Bathymetry Consortium (2025). EMODnet Digital Bathymetry (DTM). https://emodnet.ec.europa.eu/ (accessed 29/07/2025).

Faccenna, C., Molin, P., Orecchio, B., Olivetti, V., Bellier, O., Funiciello, F., Minelli, L., Piromallo, C., & Billi, A. (2011). Topography of the Calabria subduction zone (southern Italy): Clues for the origin of Mt. Etna. *Tectonics, 30*, TC1003. https://doi.org/10.1029/2010TC002694

Giuffrida, S., Carnemolla, F., De Guidi, G., Anderlini, L., Brighenti, F., La Rocca, M., & Tansi, C. (2025). Interseismic coupling degree of Serre and Cittanova faults surface in Southern Calabria (Italy): new constraints from geodetic data observations. *Geophysical Journal International, 241*(2), 954–? https://doi.org/10.1093/gji/ggaf087

Graham, S. E., Loveless, J. P., & Meade, B. J. (2021). A global set of subduction zone earthquake scenarios and recurrence intervals inferred from geodetically constrained block models of interseismic coupling distributions. *Geochemistry, Geophysics, Geosystems, 22*, e2021GC009802. https://doi.org/10.1029/2021GC009802

Malinverno, A., & Ryan, W. B. F. (1986). Extension in the Tyrrhenian Sea and shortening in the Apennines as a result of arc migration driven by sinking of the lithosphere. *Tectonics, 5*(2), 227–245. https://doi.org/10.1029/TC005i002p00227

McCaffrey, R. (2002). Crustal block rotations and plate coupling. In S. Stein & J. Freymueller (Eds.), *Plate Boundary Zones* (AGU Geodynamics Series, Vol. 30, pp. 101–122). American Geophysical Union. https://doi.org/10.1029/GD030p0101

Meade, B. J., & Hager, B. H. (2005). Block models of crustal motion in southern California constrained by GPS measurements. *Journal of Geophysical Research: Solid Earth, 110*, B03403. https://doi.org/10.1029/2004JB003209

Meade, B. J., & Loveless, J. P. (2009). Block modeling with connected fault-network geometries and a linear elastic coupling estimator in spherical coordinates. *Bulletin of the Seismological Society of America, 99*(6), 3124–3139. https://doi.org/10.1785/0120090088

Monaco, C., Tortorici, L., Nicolich, R., Cernobori, L., & Costa, M. (1996). From collisional to rifted basins: an example from the southern Calabrian Arc (Italy). *Tectonophysics, 266*(1–4), 233–249. https://doi.org/10.1016/S0040-1951(96)00192-8

Postpischl, D. (Ed.). (1985). *Catalogo dei terremoti italiani dall'anno 1000 al 1980*. Quaderni della Ricerca Scientifica, 114(2B). CNR, Bologna.

Rovida, A., Locati, M., Camassi, R., Lolli, B., Gasperini, P., & Antonucci, A. (Eds.). (2022). *Italian Parametric Earthquake Catalogue (CPTI15), version 4.0*. Istituto Nazionale di Geofisica e Vulcanologia (INGV). https://doi.org/10.13127/CPTI/CPTI15.4

Savage, J. C. (1983). A dislocation model of strain accumulation and release at a subduction zone. *Journal of Geophysical Research: Solid Earth, 88*(B6), 4984–4996. https://doi.org/10.1029/JB088iB06p04984

Segall, P., & Davis, J. L. (1997). GPS applications for geodynamics and earthquake studies. *Annual Review of Earth and Planetary Sciences, 25*, 301–336. https://doi.org/10.1146/annurev.earth.25.1.301

Serpelloni, E., Cavaliere, A., Martelli, L., Pintori, F., Anderlini, L., Borghi, A., Randazzo, D., Bruni, S., Devoti, R., Perfetti, P., & Cacciaguerra, S. (2022). Surface velocities and strain-rates in the Euro-Mediterranean region from massive GPS data processing. *Frontiers in Earth Science, 10*, 907897. https://doi.org/10.3389/feart.2022.907897

Tansi, C., Muto, F., Critelli, S., & Iovine, G. (2007). Neogene–Quaternary strike-slip tectonics in the central Calabrian Arc (southern Italy). *Journal of Geodynamics, 43*(3), 393–414. https://doi.org/10.1016/j.jog.2006.10.006

Corresponding author: salvatore.giuffrida@phd.unict.it

Integration of field and web-based macroseismic surveys in Italy

L. Graziani[1], P. Sbarra[1], M. Locati[1], A. Rovida[1], V. De Rubeis[1], D. Sorrentino[1], A. Tertulliani[1], P. Tosi[1]

[1] *Istituto Nazionale di Geofisica e Vulcanologia, Italy*

Macroseismology is the only tool for obtaining seismological data from historical earthquakes and is essential for comparing historical earthquakes with modern ones. Thanks to Citizen Science and the use of web platforms, it is nowadays possible to collect data on the effects of earthquakes in real time. However, traditional macroseismic surveys, conducted by specialised personnel to assess the severity of damage to buildings on site, remain the most viable approach for assessing high intensities. For these reasons, coupled with time constraints and personnel availability, field surveys mostly cover the near-field and are less comprehensive for intensities driven by transient effects. In contrast, web-based, citizen-contributed surveys mainly collect information on low intensities based on transient effects.

Currently, INGV is one of the few research institutions in the world that collects state-of-the-art macroseismic data with both field and web-based surveys, the former collected by the "Quick Earthquake Survey Team" (QUEST, https://quest.ingv.it/), the latter by the "Hai Sentito Il Terremoto" (HSIT, https://www.hsit.it/) group. To date, the two sets of macroseismic data have always been kept separate (Figure 1), and their integration, which would provide a complete picture of the effects of the earthquake, has never been attempted until now.

We examined a set of earthquakes for which both macroseismic intensity datasets are available, to derive a unified intensity map through the integration of the two data types. This operation cannot be performed by simply merging the two datasets, as several critical issues must first be addressed in order to establish a robust and reproducible methodology that can be applied to future events.

As a first step, we defined a strategy to resolve the dissimilarity of the geographic scale at which intensities are estimated by the two types of macroseismic surveys (municipalities, localities, hamlets). To make the two datasets comparable, the data were homogenised. The

HSIT macroseismic questionnaires, initially aggregated by Italian municipalities, were aggregated at the same scale as the direct surveys, i.e. by localities.

Once the datasets were homogenised and referred to a common geographic gazetteer, the analyses focused on the critical issues that emerge, for both the European Macroseismic Scale (EMS-98) and the MCS scale, in the overlap range of the two intensity data sets.

In order to overcome the discrepancies between the two methodologies, we addressed the following key aspects:

- evaluate the consistency of intensity estimates where both datatypes are available;
- identification of a threshold, or range of intensity, that defines the domains of best performance of each methodology;
- evaluate the minimum number of questionnaires required in the web-based survey to assign a reliable intensity, possibly depending on the intensity level;
- calibrate the methodology for the web-based assignment in the presence of damage by the detailed comparison with field-assessed intensities;

To this end, data relating to earthquakes for which both field surveys and online questionnaires were collected have been analyzed to define the most effective integration methodology.

In this study, we present the preliminary results using the 24 August 2016 earthquake as a case study, illustrating the integration of the QUEST and HSIT datasets. This preliminary work aims to develop operational guidelines to be applied to both past earthquakes and future events, enabling an integrated QUEST-HSIT macroseismic field. The integration of the two approaches is expected to compensate for their respective limitations, resulting in a complete and robust macroseismic intensity distribution.

We believe the co-operation between the INGV working groups operating QUEST and HSIT is essential to obtain, following a strong earthquake, a comprehensive macroseismic picture that is univocal and a more accurate estimate of the earthquake's impact. The possibility of obtaining a comprehensive overview following an earthquake, based on extensive data and with complete coverage of the territory, represents a significant advantage. This would have notable impacts in several subjects, such as ground motion estimates and attenuation models.

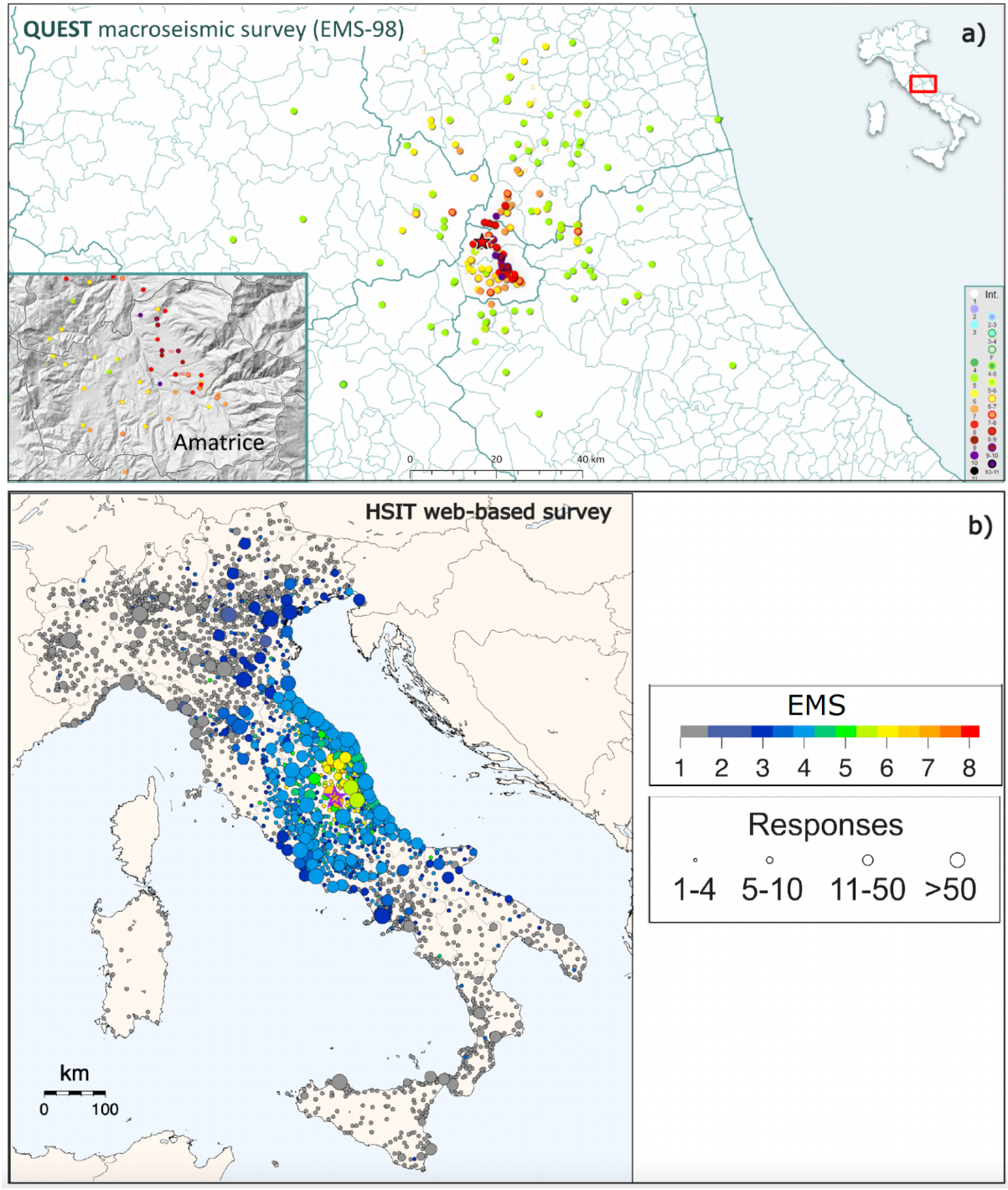

Fig. 1 - Macroseismic fields of the Mw 6.0 earthquake of August 24, 2016 processed considering a) QUEST's direct survey b) HSIT's web-based survey.

Corresponding author: laura.graziani@ingv.it

A Review of 40 Years of Instrumental Seismicity for the Study of Hidden Seismogenic Structures in Southeastern Piedmont

F. Guiñez-Rivas[1], S.C. Vinciguerra[1], C. Comina[1], F. Bosco[2], G.M. Adinolfi[1]

[1] Dipartimento di Scienze della Terra, Universitá degli Studi di Torino, Italy
[2] ARPA Piemonte, Regional Agency for the Protection of the Environment, Department Natural and Environmental Risks, Turin.

Accurately identifying and characterizing active seismogenic structures is fundamental for seismic hazard assessment, particularly in regions with low to moderate seismicity rates, where fault detection remains a complex challenge (Shaw and Shearer 1999; Panara et al. 2021; Vannoli et al. 2015; Bonasera et al. 2022). The southeastern Piedmont region of northwest Italy presents a particularly intricate case due to its tectonic complexity. Located at the intersection of the Western Alps, the Northern Apennines, and the Po Plain foreland basin, this area is shaped by the interactions between several major tectonic systems (Mathey et al. 2021; Schwartz et al. 2024). These include the Alpine orogeny, the past subduction of the Adria microplate beneath Europe and current anticlockwise rotation, and the tectonic activity of the Po Plain. Additionally, the region is characterized by a thick sedimentary cover that obscures fault structures, making it challenging to observe and directly assess active faults through traditional geological methods.

Despite the region's complex tectonic framework, active seismogenic structures have not been fully mapped, and many of the faults in the area are poorly constrained. Historical records (Rovida et al. 2020) indicate moderate seismicity, with several large earthquakes in the past centuries, such as the 1564 Lantosque (Mw 5.8), 1808 Pinerolo (Mw 5.6), 1828 Tortona (Mw 5.7), and 1887 Diano Marina (Mw 6.3), but the specific seismogenic sources remain debated. Instrumental seismicity, particularly since the late 20th century, has provided valuable data, but the detection of active faults in this area remains a challenge due to the region's thick sedimentary cover and the complex interaction between the Alpine and Apenninic tectonic domains.

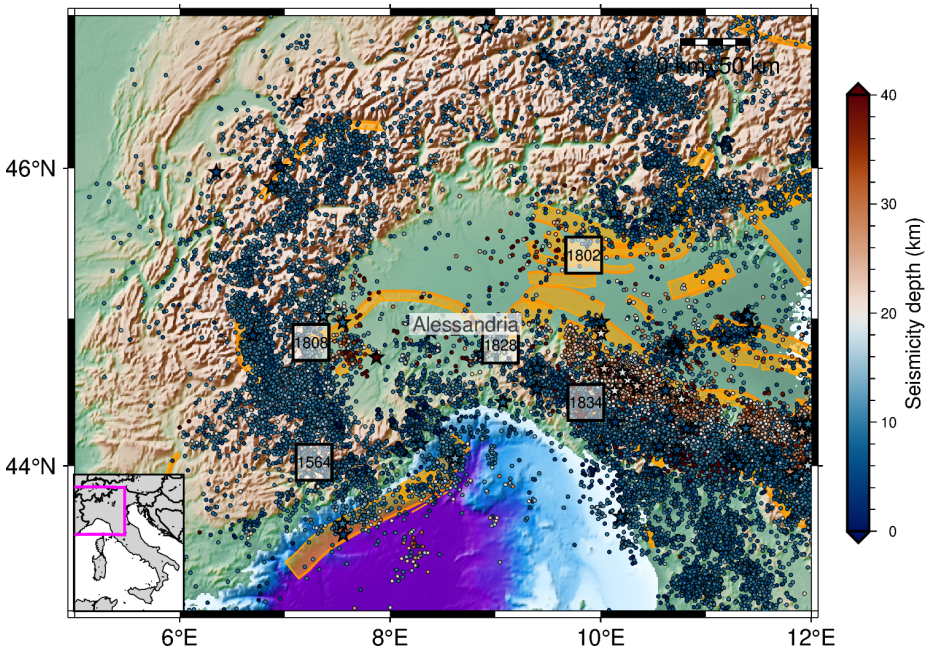

Figure 1: North-Western Italy map with instrumental seismicity (circles) from 1980 to 2025 represented by depth. Events with magnitude higher than 4 are represented as stars. Historical seismicity with an estimated magnitude higher than 5 is shown by black squares. Composed and individual seismogenic sources inferred for the area are drawn via orange rectangles.

This study aims to address the gap in knowledge by leveraging more than 40 years of instrumental seismicity data, which includes over 20,000 phase arrivals and more than 1,300 seismic events. These data are used to map and investigate the active fault systems in southeastern Piedmont, contributing new insights into the region's seismic potential. By applying advanced seismic relocation methods, cluster analysis, and focal mechanism computation, we provide a refined understanding of the region's seismotectonic behaviour, revealing both previously unrecognized and poorly mapped active fault systems. These results will be crucial for improving seismic hazard assessment in this tectonically active and densely populated region.

We compiled a comprehensive seismicity dataset by merging three independent seismic catalogues, CLASS (1981-2008) (Latorre et al. 2023), RSNI (2012-present) (University of Genoa 1967), and INGV (1980-present) (INGV Data Management Office 2020), which provided both parametric event information and phase arrivals from a network of stations with varying coverage. This dataset includes over 20,000 phase arrivals and 1,330 seismic events within a 50 km radius of Alessandria, the area of focus for this study. The phase arrival times database was subjected to a robust quality control procedure based on the simil-Wadati criterion, ensuring consistency and accuracy in the arrival times. The final dataset offers a detailed temporal and spatial distribution of seismicity, including events ranging from microearthquakes to moderate magnitudes ($M \leq 4.8$).

Advanced seismic event relocation techniques, including absolute (Lomax et al. 2000) and double-difference methods (Waldhauser and Ellsworth 2000), were employed to enhance the precision of event locations. The application of a 3D regional velocity model (Scafidi et al. 2009), which accounts for lateral variations in crustal structure, resulted in a well-constrained seismicity catalogue. To ensure the reliability of depth estimates, events were filtered based on the hypocentral distance to the closest recording station, retaining only earthquakes for which the

station coverage provides sufficient depth resolution. Our relocation analysis revealed that most seismicity occurs at depths between 10 and 20 km, with deeper events (>60 km) observed in the northwestern part of the study area, aligning with the eastward deepening of the European Moho. In addition, temporal clustering of seismicity was analysed using the HDBSCAN (Hierarchical Density-Based Spatial Clustering of Applications with Noise; Campello et al. 2013) algorithm, identifying multiple spatial and temporal clusters that reflect episodic activation of fault systems across the region.

Focal mechanisms were computed for 45 well-located earthquakes with magnitudes greater than 2, providing constraints on the regional stress field and faulting styles. Mechanisms were obtained through the joint inversion of P-wave first-motion polarities and low-frequency spectral amplitude ratios. First-motion polarities were determined automatically using a clustering-based analysis of waveform features, while spectral level ratios were computed with TESLA (Tool for Automatic Spectral Level Analysis; Adinolfi et al. 2023). The joint inversion was performed within a Bayesian framework using the BISTROP software (De Matteis et al. 2016), yielding posterior probability distributions for the admissible fault-plane solutions. Solution quality was subsequently evaluated using the median Kagan angle between the preferred solution and all solutions with an a posteriori probability greater than 90%. Only focal mechanisms with Kagan angles smaller than 30° were considered well constrained (Adinolfi et al. 2022). The resulting dataset reveals a predominance of strike-slip faulting in central Piedmont, consistent with a regional transcurrent deformation regime driven by the interaction between the Alpine and Apenninic tectonic systems. In contrast, the northwestern Apennines display a wider range of faulting styles, including normal and reverse mechanisms, suggesting more complex and locally controlled tectonic processes.

Spatial cluster analysis revealed 13 distinct seismic clusters, each showing varying activation patterns over time. Notably, the area around Alessandria exhibits clear clustering of seismic events following the 2000 (Md 4.8) and 2001 (Md 4.0) earthquakes, with a reactivation of faults between 2000 and 2003, followed by sporadic events in subsequent years. The Tortona and Asti regions also displayed significant seismic activity, with focal mechanisms supporting the hypothesis of active strike-slip and normal faulting in these areas. Furthermore, seismicity in the northern Apennines, though continuous, demonstrated a highly time-dependent behaviour, with migration of seismic activity between 2008 and 2020 and varying fault kinematics.

The study's methodology, which integrates advanced seismic event relocation, cluster analysis, and focal mechanism computation, provides a refined understanding of the seismotectonic behaviour of southeastern Piedmont. The results highlight the heterogeneous nature of seismicity in the region, with fault systems exhibiting complex and episodic activation. This study not only improves our understanding of the tectonic processes governing the region but also contributes to the identification of previously unrecognized or poorly mapped active faults.

Our findings contribute to improving the understanding of regional seismic hazard, particularly in densely populated areas such as Alessandria and Tortona, where the potential for moderate to strong seismic events remains significant. Furthermore, this research underscores the importance of continued and expanded seismic monitoring, as well as the integration of additional geophysical

and geological data, to refine the characterization of active fault systems in this complex tectonic region. As demonstrated, high-quality seismic data combined with advanced analysis techniques can significantly improve the resolution of active fault identification and contribute to more accurate seismic hazard models in areas of low to moderate seismicity.

References

Adinolfi, Guido Maria, Vincenzo Convertito, and Raffaella De Matteis. 2023. 'TESLA, A Tool for Automatic Earthquake Low-Frequency Spectral Level Estimation: The Study of 2013 St. Gallen Earthquake Fault-Plane Solutions'. *Seismological Research Letters* 94 (5): 2441–55. https://doi.org/10.1785/0220230033.

Adinolfi, Guido Maria, Raffaella De Matteis, Rita De Nardis, and Aldo Zollo. 2022. 'A Functional Tool to Explore the Reliability of Micro-Earthquake Focal Mechanism Solutions for Seismotectonic Purposes'. *Solid Earth* 13 (1): 65–83.

Álvarez-Gómez, José A. 2019. 'FMC—Earthquake Focal Mechanisms Data Management, Cluster and Classification'. *SoftwareX* 9: 299–307.

Bonasera, Mauro, Giandomenico Fubelli, Cesare Comina, et al. 2022. 'A Multidisciplinary Approach to Detect the Seismogenic Source of the Tortona 1828 Earthquake (Piedmont, Northwest Italy)'. *ITALIAN JOURNAL OF GEOSCIENCES* 141 (2022) f.1 (February). https://doi.org/10.3301/IJG.2022.07.

Campello, Ricardo J. G. B., Davoud Moulavi, and Joerg Sander. 2013. 'Density-Based Clustering Based on Hierarchical Density Estimates'. In *Advances in Knowledge Discovery and Data Mining*, edited by Jian Pei, Vincent S. Tseng, Longbing Cao, Hiroshi Motoda, and Guandong Xu. Springer. https://doi.org/10.1007/978-3-642-37456-2_14.

De Matteis, Raffaella, Vincenzo Convertito, and Aldo Zollo. 2016. 'BISTROP: Bayesian Inversion of Spectral-Level Ratios and P-Wave Polarities for Focal Mechanism Determination'. *Seismological Research Letters* 87 (4): 944–54.

INGV Data Management Office. 2020. 'INGV Open Data Registry, the Metadata Catalogue of the Istituto Nazionale Di Geofisica e Vulcanologia'. With Mario Locati, Francesco Mariano Mele, Salvatore Mazza, et al. Istituto Nazionale di Geofisica e Vulcanologia (INGV), November 18. Text/xml,text/html,application/json,application/ld+json,application/x-turtle,text/xml, hundreds of metadata records related to geophysical data. https://doi.org/10.13127/DATA-REGISTRY.

Latorre, Diana, Raffaele Di Stefano, Barbara Castello, Maddalena Michele, and Lauro Chiaraluce. 2023. 'An Updated View of the Italian Seismicity from Probabilistic Location in 3D Velocity Models: The 1981–2018 Italian Catalog of Absolute Earthquake Locations (CLASS)'. *Tectonophysics* 846 (January): 229664. https://doi.org/10.1016/j.tecto.2022.229664.

Lomax, Anthony, Jean Virieux, Philippe Volant, and Catherine Berge-Thierry. 2000. 'Probabilistic Earthquake Location in 3D and Layered Models'. In *Advances in Seismic Event Location*, edited by Clifford H. Thurber and Nitzan Rabinowitz. Springer Netherlands. https://doi.org/10.1007/978-94-015-9536-0_5.

Mathey, Marguerite, Christian Sue, Colin Pagani, et al. 2021. 'Present-Day Geodynamics of the Western Alps: New Insights from Earthquake Mechanisms'. *Solid Earth* 12 (7): 1661–81. https://doi.org/10.5194/se-12-1661-2021.

Panara, Yuri, Francesco Emanuele Maesano, Chiara Amadori, Jakub Fedorik, Giovanni Toscani, and Roberto Basili. 2021. 'Probabilistic Assessment of Slip Rates and Their Variability Over Time of Offshore Buried Thrusts: A Case Study in the Northern Adriatic Sea'. *Frontiers in Earth Science* 9 (May). https://doi.org/10.3389/feart.2021.664288.

Rovida, Andrea, Mario Locati, Romano Camassi, Barbara Lolli, and Paolo Gasperini. 2020. 'The Italian Earthquake Catalogue CPTI15'. *Bulletin of Earthquake Engineering* 18 (7): 2953–84. https://doi.org/10.1007/s10518-020-00818-y.

Scafidi, Davide, Stefano Solarino, and Claudio Eva. 2009. 'P Wave Seismic Velocity and Vp/Vs Ratio beneath the Italian Peninsula from Local Earthquake Tomography'. *Tectonophysics* 465 (1): 1–23. https://doi.org/10.1016/j.tecto.2008.07.013.

Schwartz, Stéphane, Yann Rolland, Ahmed Nouibat, et al. 2024. 'Role of Mantle Indentation in Collisional Deformation Evidenced by Deep Geophysical Imaging of Western Alps'. *Communications Earth & Environment* 5 (1): 17. https://doi.org/10.1038/s43247-023-01180-y.

Shaw, John H., and And Peter M. Shearer. 1999. 'An Elusive Blind-Thrust Fault Beneath Metropolitan Los Angeles'. *Science* 283 (5407): 1516–18. https://doi.org/10.1126/science.283.5407.1516.

University of Genoa. 1967. 'Regional Seismic Network of North Western Italy'. International Federation of Digital Seismograph Networks. SEED data. https://doi.org/10.7914/SN/GU.

Vannoli, Paola, Pierfrancesco Burrato, and Gianluca Valensise. 2015. 'The Seismotectonics of the Po Plain (Northern Italy): Tectonic Diversity in a Blind Faulting Domain'. *Pure and Applied Geophysics* 172 (5): 1105–42. https://doi.org/10.1007/s00024-014-0873-0.

Waldhauser, Felix, and William L. Ellsworth. 2000. 'A Double-Difference Earthquake Location Algorithm: Method and Application to the Northern Hayward Fault, California'. *Bulletin of the Seismological Society of America* 90 (6): 1353–68.

Corresponding author: Francisca Guiñez Rivas, francisca.guinezrivas@unito.it

Preparatory Phase of Major Earthquakes during Campi Flegrei Unrest (2020-2024)

Antonio Giovanni Iaccarino[1], Matteo Picozzi[2,1], Grazia De Leandro[1], Daniele Spallarossa[3]

[1] Department of Physics "Ettore Pancini", University of Naples Federico II, Naples, Italy.
[2] National Institute of Oceanography and Applied Geophysics – OGS, Trieste, Italy.
[3] DISTAV, University of Genoa, Genoa, Italy.

The ongoing unrest at Campi Flegrei is posing significant challenges for hazard assessment and risk mitigation. This densely populated region has experienced more than 20,000 shallow earthquakes since 2020, driven by hydrothermal fluid accumulation beneath a mechanically strong caprock (Fig. 1b). In this work, we analyze the seismic activity characterizing the ongoing crisis, also including the magnitude Md 4.4 occurred in May 2024 in correspondence of a cumulative caldera uplift of 130 cm at the RITE GPS station.

Here, we demonstrate that the joint interpretation of micro-seismicity evolution and deformation trend reveals the preparatory phase of major earthquakes. Our analysis of 20 seismic sequences from 2015 to 2024 highlights for larger earthquakes a consistent preparatory phase, with a strong correlation between deformation rates, cumulative seismic moment, and earthquake magnitudes. Residual strain, representing the difference between deformation-driven input and seismic output, emerges as a critical parameter associated with the maximum earthquake magnitudes (Fig. 1a). Unveiling the preparation phase of larger earthquakes in the densely populated Campi Flegrei area has the potential to significantly contribute to seismic risk mitigation. Preliminary, simple predictive models based on strain dynamics (Fig. 1c-d) show promising results, leading the way to developing novel approaches to forecast earthquake magnitudes and event rates days in advance.

Our insights provide a crucial foundation for improving seismic risk mitigation strategies at Campi Flegrei and other volcanic systems worldwide.

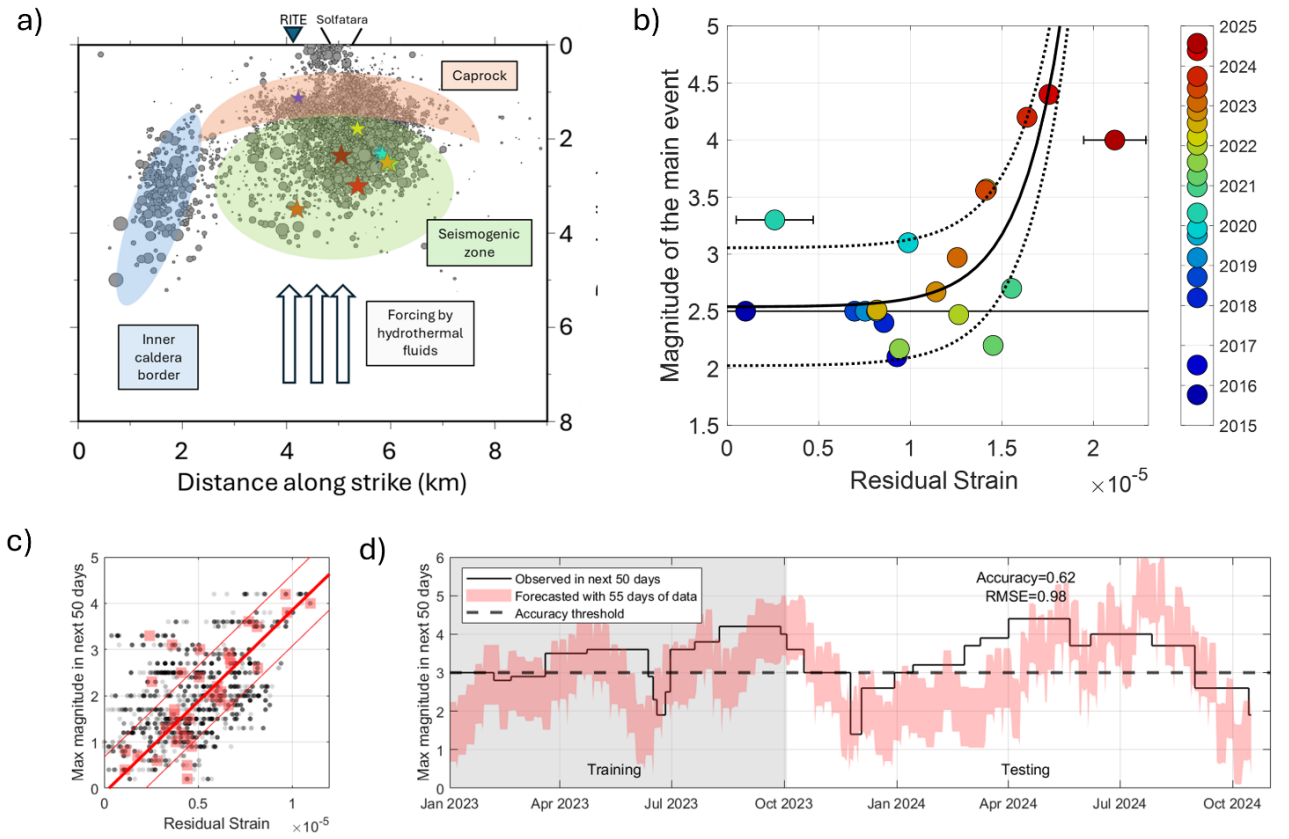

Fig. 1 – **a)** Section of the events with schematization of the caldera. The events are represented by grey circles sized by magnitude. Stars represent the location of the main events. Orange area refers to the caprock. Green area corresponds to the gas reservoir. Blue area refers to the offshore inner caldera border. **b)** Magnitude of the main event versus residual strain for all the sequences in the 100 days preceding the main event. **c)** Maximum magnitude recorded in the next 50 days versus Residual Strain measured in the last 55 days. Black shaded dots refer to daily data. Red shaded squares refer to data binned in along the y-axis. Red solid lines refer to the fit and to the confidence interval. **d)** Prediction of the Maximum magnitude recorded in the next 50 days using data from the last 55 days. Black line represents the observed value of Maximum magnitude. The red area represents the confidence interval of the prediction. The black dashed line refers to the threshold used to compute accuracy.

Corresponding author: antoniogiovanni.iaccarino@unina.it

Automated Spectral Analysis of Hydroseismograms by means of a Neural Network Based ML Approach: Preliminary Results on the Gran Sasso Aquifer (Italy)

D. Isaya[1], A. Pignatelli[2], G. De Luca[2], V. Guerriero[1], C. Petrucci[1-2], M. Tallini[1]

[1] *Department of Civil, Construction-Architectural and Environmental Engineering (DICEAA), University of L'Aquila, Italy*
[2] *National Institute of Geophysics and Volcanology (INGV), Italy*

Introduction

Hydroseismograms, are high-frequency pore pressure measurements acquired in well by means of hydraulic pressure devices (HPD) (Figure 1). Utilizing these records for seismic monitoring has emerged as a promising methodology for deciphering earthquake physics and enhancing monitoring and identification of potential earthquake precursors (De Luca et al., 2016, 2018; Isaya et al., 2025).
Isaya et al. (2025) examined the earthquake detection capabilities of a HPD situated within the Gran Sasso Aquifer, in Central Italy. Its strategic placement in a deep horizontal well, which intersects a primary fault system, combined with a high-frequency sampling rate, provides a highly sensitive instrument for tracking both seismic events and pore pressure anomalies.
Earlier investigations by De Luca et al. (2016, 2018) identified anomalous signals in two boreholes (conventionally named S13 and S14) throughout the 2016 Amatrice seismic sequence, in pre-seismic (potential precursors) and co-seismic conditions.
While high-magnitude seismic events are readily identifiable (in co-seismic condition) within a hydroseismogram (Fig. 1), low-magnitude or far earthquakes may be difficult to distinguish, requiring detailed spectral analysis of the signal (Fig. 2). Isaya et al. (2025) analysed 1,068 recorded events, by means of a notably time-consuming procedure. Consequently, we are interested in developing an automated classification method utilizing a dedicated algorithm.
In this contribution, we present the preliminary results of a spectral approach for hydroseismogram analysis, based on neural networks. This methodology holds significant potential for real-time, continuous seismic monitoring via HPD. Future research will focus on assessing the performance of this approach with larger datasets, as well as, exploring its application also in detecting pre-seismic signals (potential precursors) and post-seismic effects, such as permanent aquifer modifications.

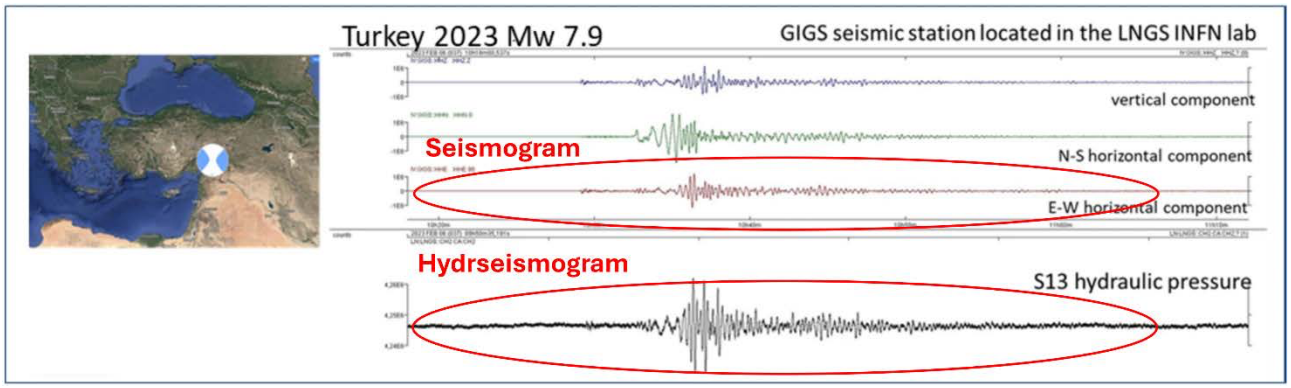

Fig. 1 – Example of seismogram recorded by a traditional seimic station and hydorseismogram recorded by a HPD.

Methods

Hydroseismogram classification was conducted via neural network image recognition, more specifically by means of the pre-trained convolutional neutral network Alexnet (Han et al., 2017; Krizhevsky et al., 2017; Indolia et al., 2018) applied to the corresponding spectrograms, each representing a duration of six hours. To replicate the manual classification process previously performed by a human operator (Isaya et al., 2025), the neural network was trained on a dataset of 176 images, comprising 81 images labeled as 'operator-detected' and 95 images labeled as 'not detected.' The sample was partitioned into a training set (80%) and a test set (20%). A 5-fold cross-validation (k-fold) approach was employed, in which the algorithm utilized five different combinations of training and testing sets extracted from the same sample (i.e., detected vs. not detected). The final accuracy parameters were calculated averaging the five results.

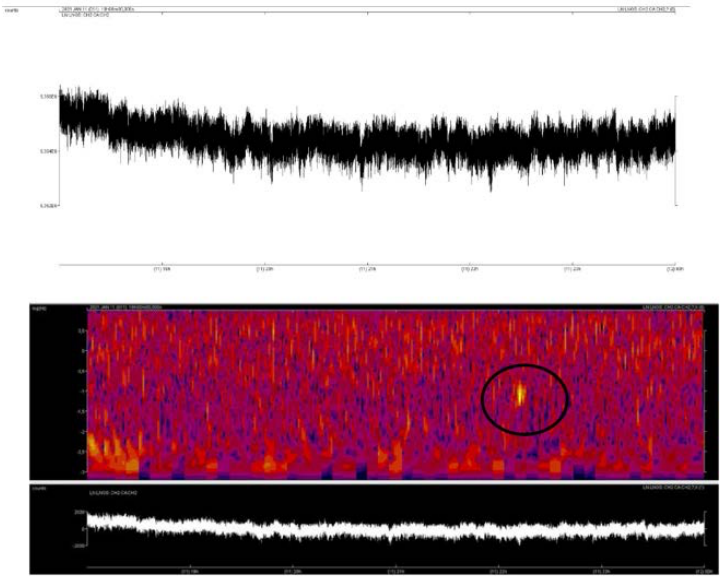

Fig. 2 – Hydroseismogram and related spectrogram.

Results

Preliminary findings from the analysis performed on the aforementioned start sample were assessed using two confusion matrices obtained from k-fold cross-validation: the first one normalized by columns and the second by rows. These results indicate that the classification algorithm achieved a sensitivity of approximately 85% and a specificity of 82%, with an overall mean accuracy of roughly 83%.

		True	
		Undetected	Detected
Predicted	Undetected	**82.4%**	14.9%
	Detected	17.6%	**85.1%**

		True	
		Undetected	Detected
Predicted	Undetected	**88.4%**	11.6%
	Detected	22.2%	**77.8%**

Conclusions and perspectives for future research

These preliminary results indicate that, even with a limited sample size, the adopted classification method yielded reasonable levels of accuracy, specificity and sensitivity. Although these levels might appear not yet fully satisfactory at this stage, it is expected that analyses performed on large datasets, such as those acquired in case of continuous seismic monitoring, will result in significantly improved performance.

A primary objective of ongoing research will be the calibration of the threshold values used to categorize a spectrogram as either ‘detected’ or ‘undetected,’ with the aim of establishing the optimal trade-off between sensitivity and specificity. Furthermore, future research will involve the implementation of training and test sets in which each spectrogram is labeled as an ‘existing seismic event’ or a ‘non-existent event’ based on whether the national (traditional) seismic network recorded an event during the same time interval. In this manner, the neural network will not merely replicate the classification process performed by a human operator but will instead be trained to perform autonomous detection.

Finally, with appropriate modifications, the illustrated classification framework could potentially be adapted to analyze hydroseismograms for identifying signal anomalies in pre-seismic conditions. The investigation and analysis of potential seismic precursors represent a compelling objective for future study.

Acknowledgments: The research leading to these results has received funding from the ArtEmis Project funded by the European Union, under Grant Id: 101061712. The research described in this paper has been developed in the framework of the research project National Centre for HPC, Big Data and Quantum Computing - PNRR Project, funded by the European Union - Next Generation EU. As concerns the ArtEmis Project, views and opinions expressed are however those of the author(s) only and do not necessarily reflect those of the European Union or European Commission-Euratom. Neither the European Union nor the granting authority can be held responsible for them.

References

De Luca G., Di Carlo G., Tallini M.; 2018: A record of changes in the Gran Sasso groundwater before, during and after the 2016 Amatrice earthquake, central Italy. Scientific Reports, G:15982. https://doi.org/10.1038/s41598-018-34444-1.

De Luca G., Di Carlo G., Tallini M.; 2016: Hydraulic pressure variations of groundwater in the Gran Sasso underground laboratory during the Amatrice earthquake of August 24, 2016. Annals of Geophysics 59, Fast Track 5. https://doi.org/10.4401/AG-7200.

Han, X., Y. Zhong, L. Cao and L. Zhang; 2017: Pre-trained AlexNet architecture with pyramid pooling and supervision for high spatial resolution remote sensing image scene classification, Remote Sensing, 9, 848, https://doi.org/10.3390/rs9080848.

Indolia, S., A.K. Goswami, S.P. Mishra and P. Asopa; 2018: Conceptual understanding of convolutional neural network – a deep learning approach, Procedia Computer Science, 132, 679–688, https://doi.org/10.1016/j.procs.2018.05.069.

Isaya D., De Luca G., Di Carlo G., Guerriero V., Martorana R., Tallini M.; 2025: Hydroseismograms at Gran Sasso aquifer, central Italy, for earthquake hydrology studies. Scientific Reports, 15, 13162. https://doi.org/10.1038/s41598-025-96113-4.

Krizhevsky, A., I. Sutskever and G.E. Hinton; 2017: ImageNet classification with deep convolutional neural networks, Communications of the ACM, 60, 84–90, https://doi.org/10.1145/3065386.

Corresponding author: domenico.isaya@graduate.univaq.it

Fault System Interaction and Deformation Partitioning at the NE Adria Indenter: Insights from Eastern Friuli and Western Slovenia

V. Kastelic[1], M. M. C. Carafa[1], G. Rajh[2], B. Vičič[2]

1 Istituto Nazionale di Geofisica e Vulcanologia – INGV, Roma1, L'Aquila, Italy
2 Slovenian Environment Agency, Seismology Office – ARSO, Ljubljana, Slovenia

The eastern Southern Alps and Pre-Alps represent a region of complex active deformation within the northeastern margin of the Adria microplate, where tectonic convergence between Adria and Eurasia results in a mixture of thrust and strike-slip faulting. This area exhibits prominent deformation partitioning between NW–SE striking subvertical dextral strike-slip faults in western Slovenia, and E–W oriented, north-dipping thrust faults in eastern Friuli. Our study addresses the structural and seismotectonic interplay of these systems, aiming to determine whether they act as independent structures or are mechanically and/or kinematically linked in accommodating the regional strain field.

The Ravne Fault, belonging to the broader Idrija fault zone represents one of the principal active strike-slip structures in western Slovenia and is seismically active along well-defined segments (Kastelic et al., 2008. Bajc et al. (2001) detail the 1998 Mw 5.6 Krn Mountain earthquake along this fault, showing clear right-lateral kinematics and rupture along a steeply dipping plane, consistent with the broader regional pattern. The segmentation and distinct mechanical behavior of the Ravne Fault system suggest its ability to accumulate and release deformation independently but also raise the question of how such structures interact at depth or near major structural boundaries.

On the other side of the region, the 1976 Friuli earthquake sequence, characterized by a main Mw 6.4 thrust event followed by significant aftershock activity (e.g., Slejko et al., 1999), ruptured the frontal north-dipping ramps of the Alpine thrust belt. The focal mechanisms of these events, and their spatial confinement to the thrust domain, illustrate a more partitioned behavior. However, the spatial proximity of these systems, separated in some areas by less than 10–15 km, creates conditions in which stress transfer or even rupture interaction may occur.

A critical element of our analysis is the geometric and kinematic correspondence between fault orientation, surface morphology, and deep crustal structure. Using crustal and upper mantle tomography (Magrin and Rossi, 2020), we observe that the orientations of both strike-slip and thrust fault systems correspond closely with the margins of the Adria indenter, particularly in its lower crust. The NW–SE trending strike-slip faults follow the lateral edges of the indenter, while the thrusts reflect the frontal geometry of its northern margin. This correspondence is also expressed in the surface morphology: elongated topographic ridges, fault-parallel valleys, and structural scarps align with the mapped traces of these active faults, indicating a long-term tectonic imprint on the landscape.

Kinematic analysis of regional seismicity supports this interpretation. Focal mechanism solutions (Saraò et al., 2021, ARSO dataset) show that the maximum principal compressive stress (σ1) is oriented N–S to NNW–SSE, consistent with the overall convergence direction of Adria into Eurasia. The derived kinematic P-axes (σ1) from these focal mechanisms exhibit systematic spatial variability across the study area. In eastern Friuli, P-axes of thrust events are generally horizontal and strike ~N–S to NNW–SSE, while in western Slovenia, P-axes from strike-slip events are similarly oriented but show a slight clockwise rotation toward NW–SE. Correspondingly, the T-axes (σ3) are sub-horizontal and oriented roughly E–W in the Friuli region and shift toward NE–SW across the strike-slip domain.

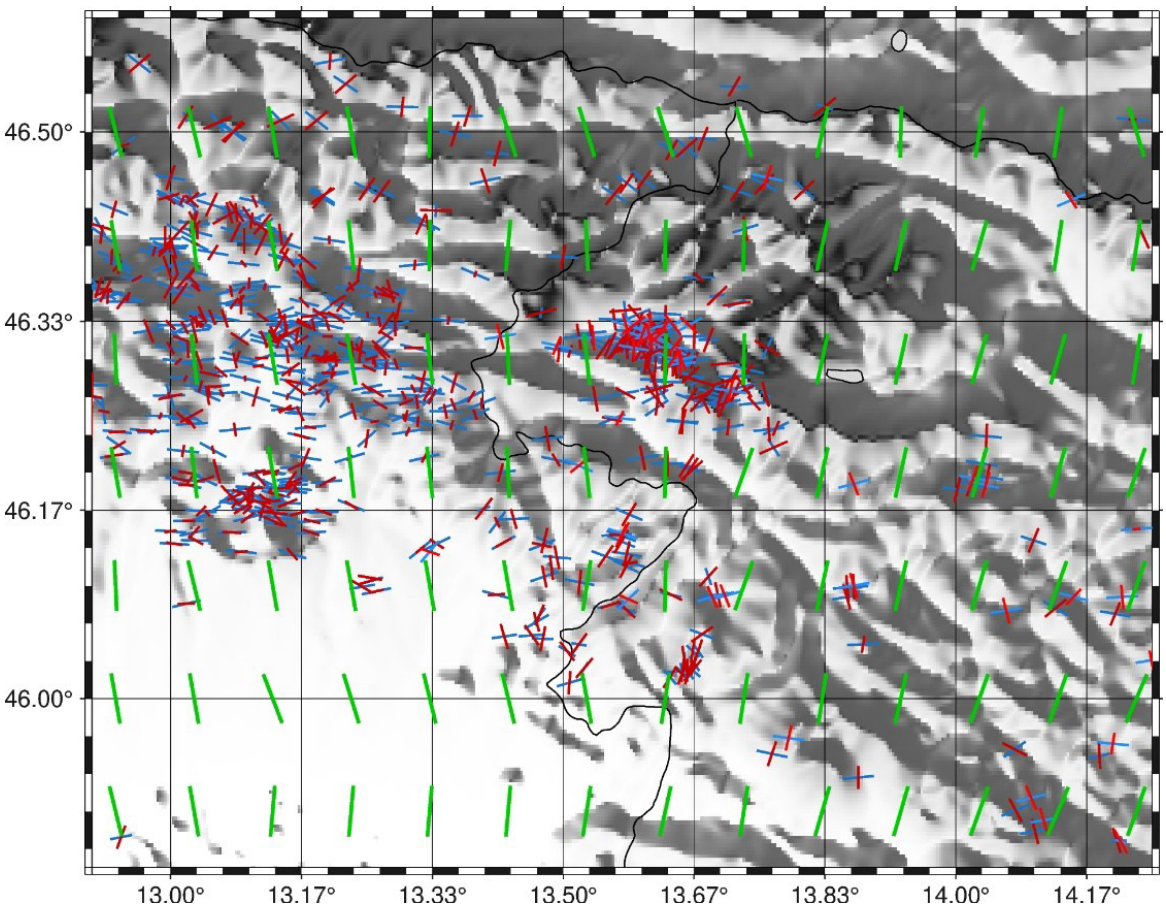

Fig. 1 – Orientations of P- (blue) and T-axes (red) derived from focal-mechanism solutions (Saraò et al. and the ARSO earthquake catalogue), together with the interpolated SHmax directions from the regional stress compilation (green; from Carafa et al., 2015), in western Slovenia–eastern Friuli.

These spatial trends in kinematic axes correspond closely with the dominant orientations of surface morphotectonic features and crustal deformation patterns. The alignment of P-axes with topographic ridges and structural trends supports the idea that crustal stress is imprinted on surface morphology. To quantify this relationship further, we compare the focal mechanism-derived stress orientations with the interpolated maximum horizontal stress (*SHmax*) (Carafa et al., 2015) which broadly confirm the P-axis patterns, showing an NNW–SSE trend across eastern Friuli and a clockwise rotation to N-S and NNE-SSW in western Slovenia. The match between interpolated *SHmax* and earthquake-derived P-axes indicates consistency between long-term and short-term deformation fields.

While the two fault systems accommodate different components of deformation, strike-slip shear versus compressional shortening, their relative proximity and consistent structural orientations raise the question of mechanical and kinematic interaction. Our synthesis of tomographic models, fault maps, and focal mechanism data suggests that in key transitional zones, especially in eastern Friuli, these systems may be interconnected. Certain NW–SE faults appear to terminate into or branch off E–W thrusts, forming composite transpressive structures that can potentially rupture together. This hypothesis is supported by the spatial coincidence of historical earthquake epicenters with mapped fault intersections and transitions.

Our results advocate for a tectonic model where the orientation and interaction of active faults are dictated by the geometry of the Adria indenter from the lower crust upwards, and where localized structural linkages may allow for partial or full coseismic coupling between systems. These findings have direct implications for regional seismic hazard: if strike-slip and thrust faults can rupture together, larger rupture areas and higher moment release may occur than anticipated by conventional segmented models.

References

Bajc, J., Živčić, M., & Gosar, A. (2001). The 1998 Bovec–Krn mountain earthquake sequence (NW Slovenia): Monitoring and preliminary results. Geologija, 44(2), 405–418.

Carafa, M. M. C., Tarabusi, G., & Kastelic, V. (2015). SHINE: Web application for determining the horizontal stress orientation. Computers & Geosciences, 74, 39–49.

Kastelic, V., Vrabec, M., Cunningham, D., & Gosar, A. (2008). Neo-Alpine structural evolution and present-day tectonic activity of the eastern Southern Alps: The case of the Ravne Fault, NW Slovenia. Journal of Structural Geology, 30(8), 963–975.

Magrin, A., & Rossi, G. (2020). Lithospheric structure and deformation in the Eastern Alps–Dinarides region. Journal of Geodynamics, 135, 101713.

Saraò, A., Sugan, M., Bressan, G., Renner, G., & Restivo, A. (2021). A focal mechanism catalogue of earthquakes that occurred in the southeastern Alps and surrounding areas from 1928–2019. Earth System Science Data, 13(5), 2245–2258.

Slejko, D., Renner, G., & Rebez, A. (1999). Seismotectonics of the eastern Southern Alps: a review. Bollettino di Geofisica Teorica ed Applicata, 40(3–4), 229–302.

Corresponding author: vanja.kastelic@ingv.it

Detection and Characterization of the Recent Seismicity Clusters Along the Africa-Eurasia Plate Boundary in the Southern Tyrrhenian region

T. Mancuso[1], S. Cesca[2], F. Grigoli[3], D. Presti[1], C. Totaro[1], B. Orecchio[1]

[1] Department of Mathematical and Computer Sciences, Physical Sciences and Earth Sciences (MIFT), University of Messina, Messina, Italy
[2] GFZ Helmholtz Centre for Geosciences, Potsdam, Germany
[3] Department of Earth Sciences, University of Pisa, Pisa, Italy

The Southern Tyrrhenian region, crossed by the Africa-Eurasia plate-boundary segment, is a geodynamically complex area where the plate convergence coexists with extensional processes occurring between Sicily and Calabria (Cuffaro et al., 2024). The presence of large offshore areas along with the lack of permanent ocean-bottom seismometers and a recent low-to-moderate magnitude seismicity often reduce the capability to derive reliable constraints for the characterization of seismogenic sources. In this context, we have conducted a comprehensive study of recent seismicity along the Africa-Eurasia plate boundary segment of the Southern Tyrrhenian region, providing an analysis of earthquake clusters recorded in the period 2010-2025 and a detailed investigation of the most recent offshore sequence identified. To achieve this aim, we first implemented a space-time metric (Frohlich and Davis, 1990) into a DBSCAN clustering algorithm (Cesca, 2020) to detect seismicity clusters from a high-resolution relocated earthquake catalog. We then used several statistical parameters describing the seismic moment distribution over time (e.g., skewness, kurtosis) to properly classify the identified clusters as swarms or mainshock-aftershock sequences (Mesimeri et al., 2019; Passarelli et al., 2025), in order to assess the different seismic behaviors along the margin. Finally, we focused on the 2025 Alicudi sequence (M_{max} 4.7) by proposing and applying an integrated workflow aimed at improving the characterization of offshore seismicity (Mancuso et al., under review). This approach takes advantage of advanced algorithms by combining Bayesian inference for accurate absolute hypocenter location (Presti et al., 2004), machine learning technique for phase picking and event detection (Zhu and Beroza, 2019), Distance Geometry Solvers for relative location (Grigoli et al., 2021) and probabilistic inversion framework for source mechanism estimation (Heimann et al., 2018). The results demonstrate the effectiveness of our integrated approach for defining seismogenic source geometry and kinematics even under not-optimal network conditions.

References

Cesca S.; 2020. Seiscloud, a tool for density-based seismicity clustering and visualization. Journal of Seismology, 24(3), pp.443-457.

Cuffaro M., Petricca P., Conti A., Palano M., Billi A. and Bigi S.; 2024. Fault kinematic modeling along a widely deformed plate boundary in southern Italy. Geophysical Research Letters, 51, e2023GL106854.

Frohlich C. and Davis S.D.; 1990. Single-link cluster analysis as a method to evaluate spatial and temporal properties of earthquake catalogues. Geophysical Journal International, 100(1), pp.19-32.

Grigoli F., Ellsworth W.L., Zhang M., Mousavi M., Cesca S., Satriano C., Beroza G.C. and Wiemer S.; 2021. Relative earthquake location procedure for clustered seismicity with a single station. Geophysical Journal International, 225(1), pp.608-626.

Heimann S., Isken M., Kühn D., Sudhaus H., Steinberg A., Daout S., Cesca S., Bathke H. and Dahm T.; 2018. Grond: A probabilistic earthquake source inversion framework. GFZ Data Services.

Mancuso T., Cesca S., Grigoli F., Presti D., Totaro C. and Orecchio B.; under review. High-Resolution Analysis of the 2025 Offshore Seismic Sequence in the Aeolian Archipelago (Southern Tyrrhenian Sea, Italy). Geophysical Journal International.

Mesimeri M., Karakostas V., Papadimitriou E. and Tsaklidis G.; 2019. Characteristics of earthquake clusters: Application to western Corinth Gulf (Greece). Tectonophysics, 767, p.228160.

Passarelli L., Petersen G., Mizrahi L. and Cesca S.; 2025. Detecting and Characterizing Swarm-Like Seismicity. Seismological Research Letters.

Presti D., Troise C. and De Natale G.; 2004. Probabilistic location of seismic sequences in heterogeneous media. Bulletin of the Seismological Society of America, 94(6), pp.2239-2253.

Zhu W. and Beroza G.C.; 2019. PhaseNet: a deep-neural-network-based seismic arrival-time picking method. Geophysical Journal International, 216(1), pp.261-273.

Corresponding author: thomas.mancuso@studenti.unime.it

High-precision close-range photogrammetry of paleoseismological trenches for 3D modelling, monographs and synthetic images from rendering.

A. Marchesini

Department of Agricultural, Food, Environmental and Animal Sciences (DI4A) (University of Udine, Italy)

The University of Udine's Structural Geology Research Group dug, in the framework of the Seismic Microzonation National Project (MS), many paleoseismological trenches (20÷30 m long, 2÷2.5 m deep, 3÷4 m wide) in the eastern Southern Alps (Veneto and Friuli Regions), which are currently affected by a low strain rate compressive regime. Paleoseismological study always predicted photogrammetric surveys in order to create a 3D model of the trench walls with geometric validity constraints as a basis for integration with the field log.

During the capture phase, direct lighting of the wall (even with masking on fences, Fig. 1a) and variations in light quality and intensity exceeding the sensor's dynamic range are avoided. The aim is to avoid cast shadows and minimize the objects' own shadows.

In an excavation, the color of the light reflected by the surrounding vegetation, the material of the opposite wall and the bottom mixes with the color of the light refracted by the atmosphere; therefore, the temperature of the incident light is calibrated (white balance), without automatic mechanisms or on-camera presets, that fail to correct the color casts.

We use professional photographic studio color charts on spot-color media that do not suffer from metamerism, meaning the color patches return the same ratio between their RGB components under any wavelength (Fig. 1a).

Our tools for photogrammetric survey of paleoseismological trenches

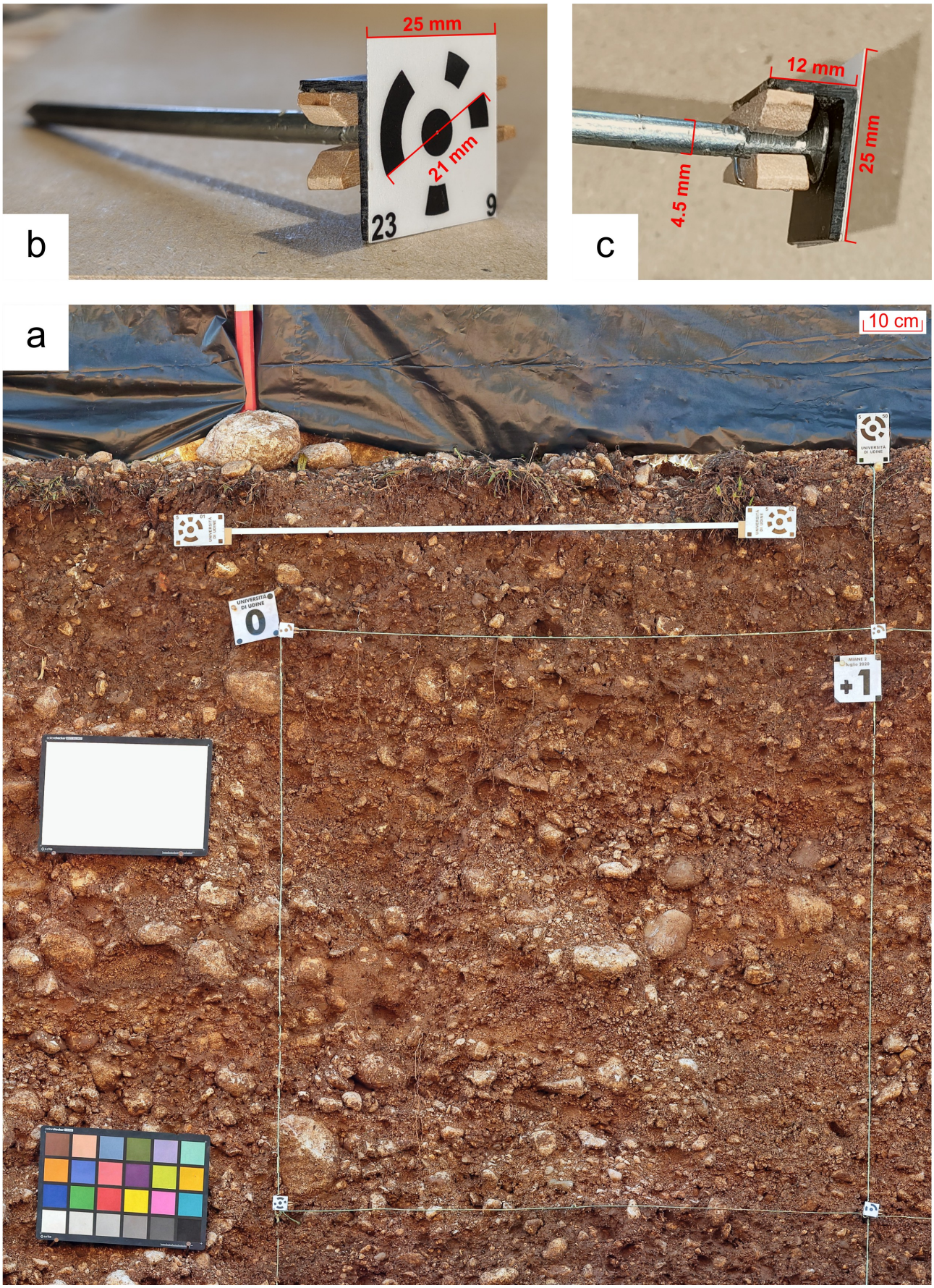

Fig. 1 - (a) Paleoseismological trench wall equipped with masking, color charts, scale bar and coded markers for benchmark or fixed to nails for metric grid; (b and c) Clip fixing system for markers on nails.

Perceptual psychology explains how we, live, try to trace the constancy of color and the effect of shadows by comparing consolidated patterns in our experience, whether past or from an hour before.

When viewing photographs, we notice excessive "unwelcome" shadows that obscure information, but on-site our perception integrates these shadows or filters them out during orientation and volumetric analysis processes. Furthermore, we enjoy a broader "exposure latitude" compared to the more limited "recoveries" provided by the dynamic range of sensors. Sometimes, photographic rendering leads the observer to recognize different volumetric effects than what was perceived stereoscopically on-site, or rather, noticing cases such as shadows from the bottom up (e.g. due to a significant contribution from light reflected from a light-colored sandy bottom).

A high-class non-metric camera equipped with a full-frame sensor (Leica format) with one of the largest single photodiode sizes among professional products (6.6 μm) is used, in order to obtain excellent results even at medium sensitivities if necessary. In winter and in occluded excavations, ISO 500 is also used (instead of the preferred ISO 100) at an aperture of /5.6 or /6.3 and a shutter speed around 1/80 s. The resolution of 20M pixels comes from a non-dense sensor to avoid diffraction at closed apertures, for the necessary depth of field in the case of stepped walls.

The camera is radio-controlled with a remote shutter (with a 2-second delay if necessary) to prevent camera micro-shake and is mounted on a three-axis gimbal (motorized inertial stabilizer) capable of handling heavy loads. It provides horizontal alignment and maintains a direction perpendicular to the mean vertical plane of the wall in awkward positions at various heights from the bottom of the excavation and from the edge, from where angled shots are also taken.

Downstream of the photogrammetric processing, for the shots orthogonal to the ideal vertical plane of the wall, the means and medians are < 1° for roll and 2° ± 0.4° for pitch, both with standard deviations < 1°. The yaw is between -5° and 5° with standard deviations of approximately 3°, depending on the operator's manual orientation for each vertical strip. At the end of each strip, the gimbal is recalled to its initial state to reset a slow pitch drift (depending on the different calibrations, it accumulates from 0.2° and sometimes we have reported up to 2°).

The 35 mm fixed focal length lens, stabilized and produced by the same company, is the most suitable for distances between 2÷4 m and panoramas up to approximately 6÷8 m. It has been pre-calibrated to pre-impose the calibration coefficients for internal orientation in photogrammetric processing. Mainly in summary: absolute value of the coefficients k1, k2 < 0.1 with average uncertainty 0.005 from a posteriori adjustment; p1 and p2 negligible; uncertainty f: 0.07 px, Cx and Cy: 0.07, b1 and b2: 0.05 from a posteriori adjustment; b1 and b2 are more impactful (1 order of magnitude with respect to k). The off-diagonal values of the parameter correlation matrix are very low where expected, except for f with b1.

For a wall with a linear development of 25 m, 2.2 m high and variable shot distances between 2 and 3.5 m, we have approximately 700÷800 frames with 80% overlaps, with an indicative movement of the camera of approximately every 30 cm in a vertical direction and approximately 50 cm in the direction of the progression of the wall, resulting in 9 or more frames for each point on the wall.

The usability, quality and white balance of the RAW format shots are checked on a native-10 bit profiled display (using a calibrating device) and developed in tif or jpg formats using the manufacturer's management software. The sRGB colour space is sufficient, given the shades of the deposits and the final use in GIS environment.

Colleagues equip the cleaned wall with nails to which a cord-square mesh is attached at 1 m intervals, as far as possible to insert the nails in their target position between the clasts (Fig. 1a).

Horizontality is checked with a 1 m long spirit level and a green laser level (more suitable than red due to the color of the deposits) as an absolute reference with a declared accuracy of ± 3 mm at 10 m distance.

For practical information, the laser plane was followed with the naked eye for 6+6 m from the center in a time window of approximately 1.5 hours before dark: in mid-February at 4:40 PM local time at 45° latitude, the amount of light measured in the trench without direct light was 300 lux. Using a sensor on the wall, the laser plane can be followed in broad daylight up to approximately 15+15 m from the center, with the operational limitation of avoiding full direct sunlight on the sensor and considering that as the distance increases, the angle of incidence becomes too small and the plane can increasingly be intercepted by wall overhangs.

If possible, the metric offset on the vertical is constrained to the vertical sliding pole of the laser level, as the wall is not vertical for safety reasons. The coordinates of the opposite walls are comparable because the coordinates of the central nail of origin on one wall have been transferred to the opposite wall by means of the crosshair of two each other-orthogonal laser planes, having oriented the laser level orthogonal to the vertical reference plane.

I designed and built around one hundred 25 mm square PVC supports for photogrammetric circular-coded markers (21 mm diameter) with a clip for quickly fixing to the nail shank, so as to adapt to different sizes: up to a diameter of 6 mm for the shank and 12 mm for the head (Fig. 1b, 1c). For special uses, we know we have a fixed 6 mm horizontal offset, remembering however that the fixing of the nail to the wall is not guaranteed to be orthogonal. The markers are facing the camera. The dimensions are calibrated for automatic recognition of the coding in shots taken from the bottom of the excavation. In the least favourable situation of a shot from a distance of 2 m, there is a wall coverage of approximately 2 x 1.4 m (2.8 m^2); therefore each shot in the central portions of the wall typically has at least 2 markers.

The marker coding is such that the last digit indicates the relative metric height (exception: 9 indicates -1 m), while the preceding digits indicate the metric chainage. For example, marker 53 is

on the nail at chainage coordinate 5 m and relative height 3 m (5,3); marker 239 is on the (23,-1) nail (Fig. 1b); marker 500 on the (0.0) nail.

These pairs of plane coordinates are only used to identify the nail and are never imposed on the model, which lives in its own 3D environment in local coordinates.

Markers with a code greater than 500 are larger (42 mm diameter, Fig. 1a) for automatic recognition even when shooting from outside the trench. They are used for temporary benchmarks on the walking surface at the edge and end of a dozen square-section aluminium bars with a finished length of 1 m. These are positioned positioned, with arbitrary orientation, in the the wall frame and serve as a metric and verification constraint.

The absolute orientation of the wall can be defined by a 20 x 20 cm “L-shaped” rigid set of three markers, with known and fixed chainage (x-axis), relative height (y-axis), depth (z-asix) coordinates in 3D cartesian system (here using the acronym: Ch-rE). It is positioned in a vertical plane, on a mini-tripod with head leveling base and oriented according to the azimuth of the established vertical median plane of the wall. It is interesting to note that the coordinate constraints of this set of markers alone already verify, to within a few millimeters, the actual distances of the metric bars.

Instead, when it is necessary to directly reference the direction of part of the physical grid, the orientation can be defined by the line joining markers on two specific nails at the same height and two markers on a plumb line. If possible, this is immersed in a container of water and silt to dampen the oscillations caused by the wind sail effect on the markers attached to the plumb line.

In the example case of a 25 m wall, approximately 13÷14B pix are processed, usually with 2x downsampling (to speed up the process and still obtain an adequately dense cloud), with a maximum limit of 400 k constraint points and 2.5M projections, with a 0.4÷0.5 pix reprojection RMS error. By cautiously imposing an error of 1 mm for the constraint references, an average error of 2 mm is obtained on the verification samples. The ground sampling distance (the distance between adjacent pixel centers measured in reality) is 0.4÷0.5 mm/pix and therefore indicates the minimum identifiable distance. The dense cloud, after light filtering, is in the order of 170M points.

The precision of about 2 mm is achieved on the wall (ground classification) but not on wires with a diameter of 1.4÷1.6 mm. If necessary, even for aesthetic reasons, very heavy processing without downsampling restores the continuity and geometry of the wires as “a granular set” of a 3D object (0.3 pix reprojection RMS error), for an estimated 85% of the length of approximately 150 m of wires.

The depth model is calculated (on the vertical plane that approximates the wall) and is like a DEM in x- and y-axis of Ch-rE system; the value is the depth of the wall with respect to the observer, with a conventional value of convenience on the plane of rigid set of three markers.

Generally, the bottom is removed from the 3D model, as in orthometric view the debris covers the often over-excavated base of the wall. Special cases involve cleaning the bottom to highlight deformations on the horizontal plane. The bottom model is managed together with the two walls

and separate orthomosaics are produced for each wall and the bottom. It follows that it is very useful to use the same chainage origin and scale for each orthomosaic (Fig. 2).

The orthomosaic is a true orthophoto in Ch-rE system with a resolution of 0.4÷0.6 mm/pix, with occasional artefacts on objects outside the wall, due to light filtering. It is translated to fit the intersection of two wires, adjacent to the wall, to its corresponding Ch-rE coordinates. This nail is chosen arbitrarily, preferably at the center of the wall or in the most interesting area.

The accuracy of the photogrammetric product is at least one order of magnitude greater than the approximation with which the individual wire quadrangles on the wall identify the vertical planes of side 1 m. Therefore, the wire crossing coordinates in the Ch-rE system are not guaranteed to be integer values, as assumed in the log drawing. Depending on the difficulty of placing the nails, accuracy is often verified to be within a few cm, which can be degraded for nails at the ends of the wall due to cumulative errors.

The orthomosaic is a “finished” raster product, ready to be easily loaded into a GIS environment, ideally in the same local coordinates as the log, which is then adjusted based on the orthomosaic. In the example, depending on different shot distances and resolutions, the orthomosaic and depth model consist of approximately 50k x 9k pixels to 75k x 12k pixels. For overviews and small-format prints, downsizing is performed using contrast and equalization processing.

The 2D vector drawing of the log adjusted on the orthomosaic can be back-translated and recalculated as 3D polylines on the wall model. The accuracy of the result with respect to 3D shapes depends on the limitations of drawing on a specific 2D view; however, the 3D vertices can be subsequently edited by snapping to the dense cloud or mesh.

The quality of the 50 cm grid spacing DEM from the 2017-2020 LiDAR aerial survey carried out by Regione Autonoma Friuli Venezia Giulia can be appreciated by comparing the topographic profile derived from the mesh and point cloud on the trace of the trench edge both with the shape of the orthomosaic profile and with the orthometric elevations from GNSS-RTK (in reference to the temporary benchmarks that appear in the model). In Fig. 2 an example for the SW wall of trench POL 1.

The difference in elevation between benchmarks measured on the orthomosaic generally has an uncertainty of about ±3 cm compared to the GNSS-RTK survey performed after excavation and about ±10 cm compared to the reading from LiDAR DEM from 5 or more years ago. Assuming that we subtract a systematic difference here of about 6 cm between altitudes from the GNSS-RTK (2025) survey and LiDAR DEM (2018), the uncertainty would be about 4 cm. These are good values, considering specificities and precision of the different methods and that we are talking about the topographic surface of rural fields altered by excavation activities.

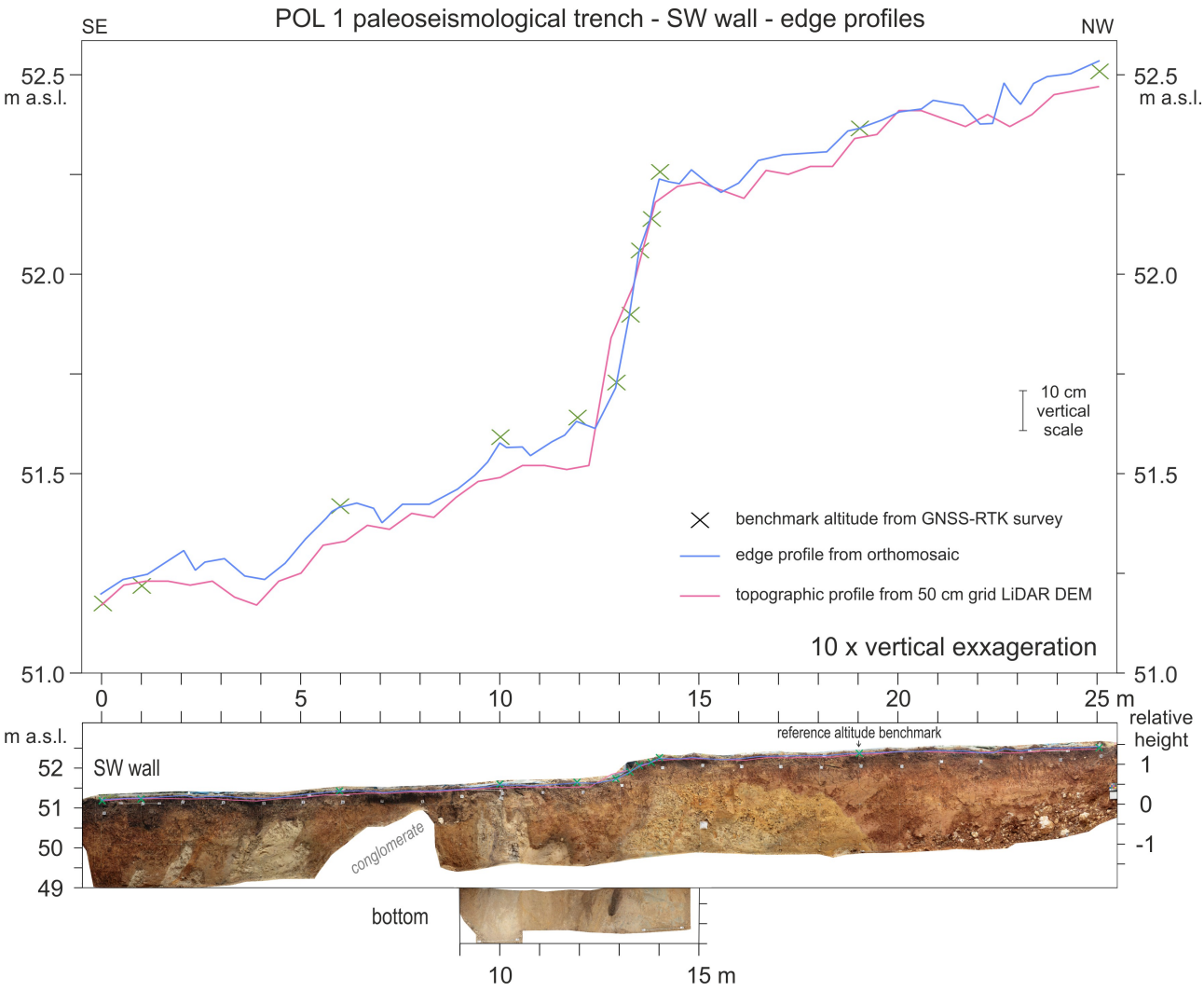

Fig. 2 - POL 1 trench: profiles of the SW wall edge from GNSS-RTK survey, orthomosaic, DEM LiDAR methods. Accuracy considerations in the text. Orthomosaics of the SW wall and bottom (same chainage coordinates).

The orthomosaic derived from soft-light shots makes roughness, overhangs, and clast alignments less evident than on-site experience. Therefore, synthetic images are created with rendering techniques, imposing controlled lighting, similar to hill shading effect created from a planimetric DEM (Fig. 3). Since we have a subvertical wall, given its coordinates, orientation, date, and time, we can simulate shading on the orthomosaic, as well as from any useful direction. Working with the tonal range helps avoid over- and underexposure defects. To understand the direction of the light, it is also useful to simply consider the orientation of the shadow of the nail holding the metric chainage label, which protrudes approximately 1 cm.

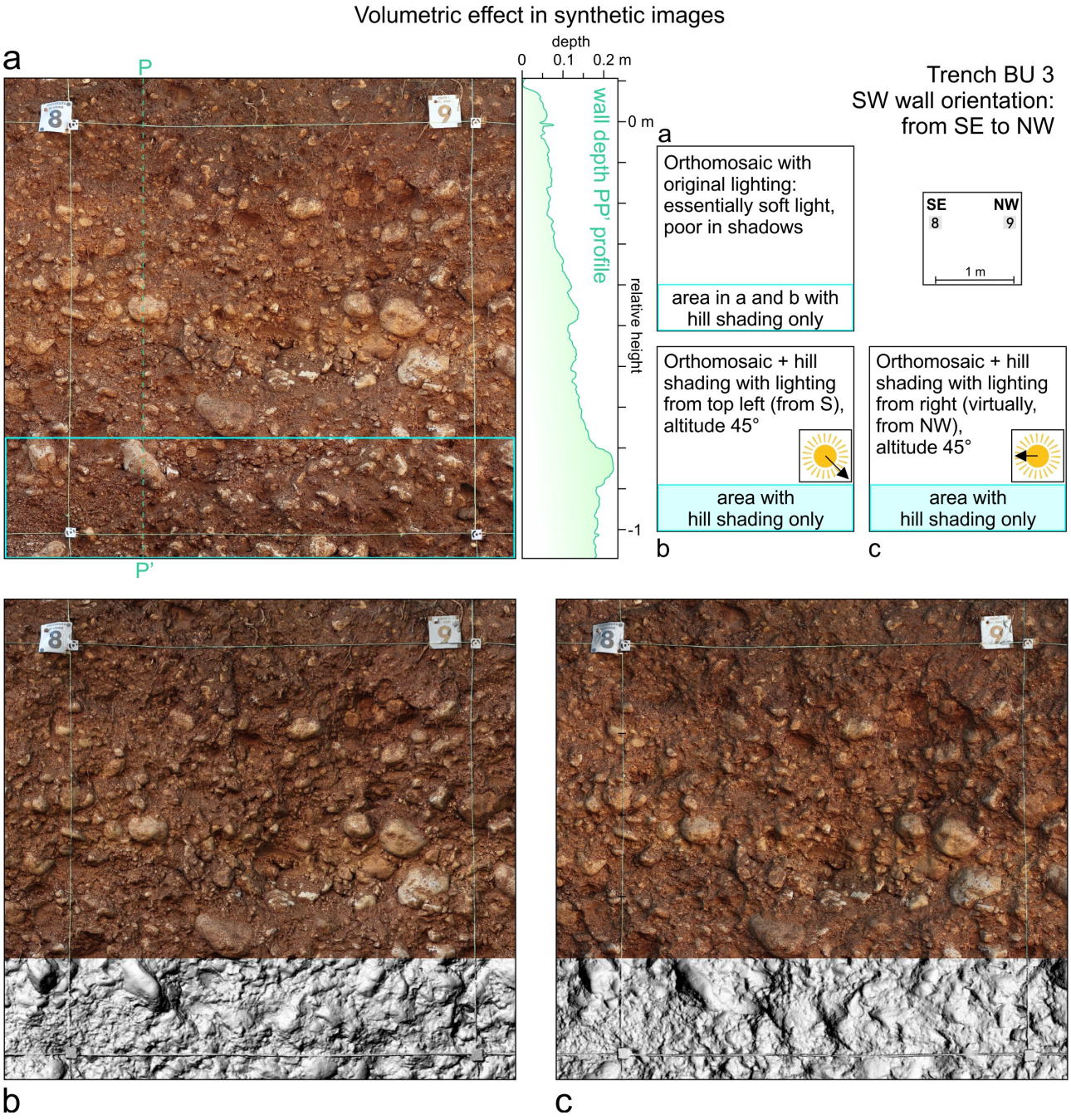

Fig. 3 - Synthetic images to recreate volumetric effects starting from a neutral model in soft light (note: the "8" label is actually curved, a root covers the "9" label).

Corresponding author: andrea.marchesini@uniud.it

Modeling Block Kinematics and Interseismic Coupling in the Central Mediterranean Region

R. Nucci[1,2], E. Serpelloni[1], A. Armigliato[2]

[1] *Istituto Nazionale di Geofisica e Vulcanologia – Bologna, Italy*
[2] *Dipartimento di Fisica e Astronomia – Università di Bologna, Italy*

The Mediterranean region is a diffuse deformation zone involving the African, Arabian, and Eurasian tectonic plates, located at the western edge of the Alpine–Himalayan orogen (McKenzie, 1972; Jackson, 1994). Within this region, a complex interaction of microplates occurs largely independently of the overall oblique convergence rate between the African and Eurasian plates (Faccenna and Becker, 2010; Nocquet, 2012). Several subduction systems, including the Hellenic and Calabrian subductions, have played, and continue to play, a key role in the geodynamic and tectonic evolution of the Mediterranean, as well as in its seismic and tsunami hazard (Malinverno and Ryan, 1986; Faccenna et al., 2014).

In the Central Mediterranean, interactions between distant tectonic domains, the regional continuity of strain accumulation, and the distribution of slip rates on seismogenic and tsunamigenic structures remain critical to understanding. In this work, we construct a new kinematic block model inverting horizontal GNSS velocity data in the Central Mediterranean region. The model is more detailed in the southern Adriatic and Ionian seas, along the southern Dinarides–Balkans thrust belts, and across the Calabrian and Aegean arcs, providing new insights into interseismic strain buildup and associated seismogenic potential of the involved structures. The primary objective is to evaluate the interseismic coupling (IC), defined as the degree of kinematic locking during the interseismic phase, along major subduction interfaces. Additionally, we assess its imprint on surface velocities and strain rates.

An integrated horizontal GNSS velocity field is constructed by combining several published velocity solutions to obtain a dense spatial coverage of GNSS stations within the entire study area (Figure 1). The implemented block model incorporates three-dimensional representations of subduction interfaces and thrust systems, and inverts surface velocities to estimate rigid block rotations, slip rates (Figure 2), and IC along major tectonic structures (Figure 3). This is achieved by leveraging a new inversion strategy implemented in this study and used within the *Blocks* code (Meade and Loveless, 2009).

These findings provide a new synoptic view of geodetic strain accumulation and slip rates across the Central Mediterranean, and represent a first attempt to map IC on major structures at the scale of the entire region, including the Albanides–Dinarides margin. In Greece, low but non-zero IC takes place along the Hellenic subduction zone beneath Crete, while high IC is observed along the southeastern margin of the Cephalonia Transform Fault. High IC patches are also identified in

the Albanides and along the Montenegrin coast. IC along the Calabrian subduction zone is also investigated; however, its spatial distribution remains weakly constrained due to the presence of only onshore GNSS data. Moreover, in this region, the uncertain kinematics of the Ionian Sea (i.e., whether its motion is coherent with Apulia or Nubia) and the location of the Nubia–Apulia plate boundary play a key role in controlling the kinematics along the Calabrian arc (Figures 2 and 3).

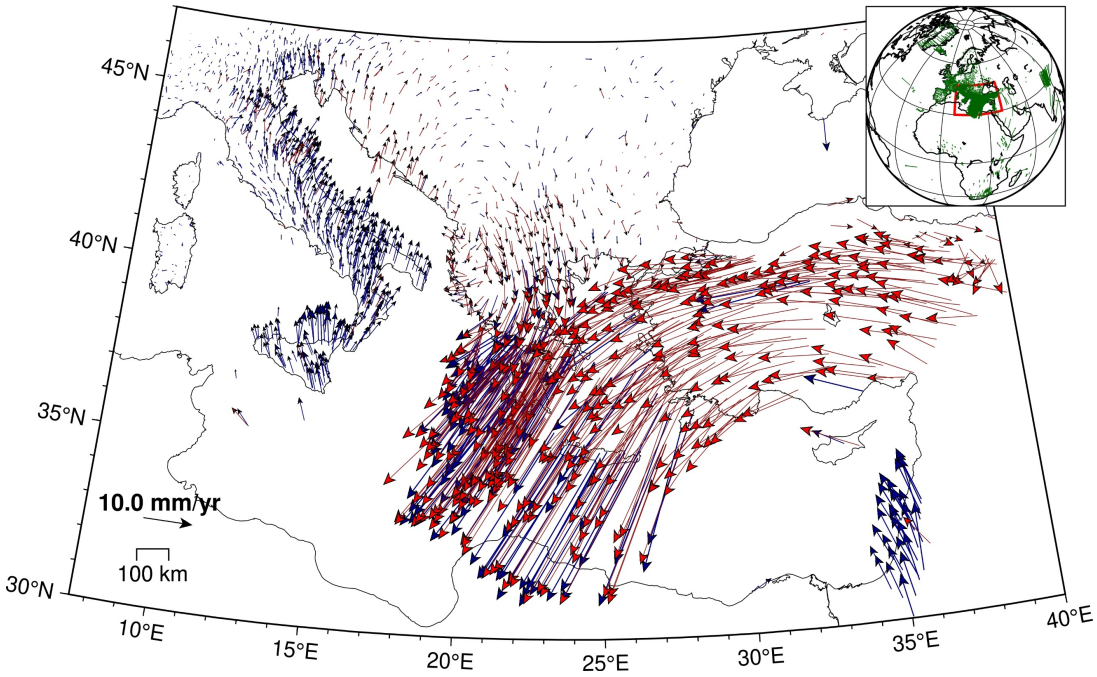

Fig. 1 – Map of the GNSS velocity field used in this study, shown in an Eurasian-fixed reference frame. Blue: INGV velocity field; Red: integrated velocity fields from different authors.

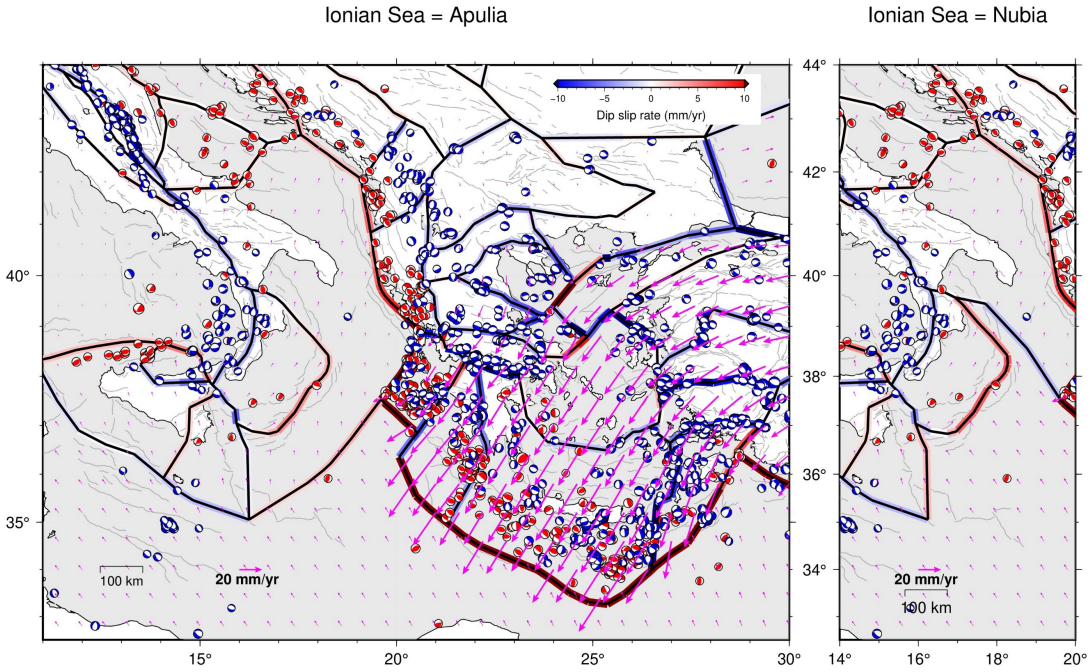

Fig. 2 – Dip-slip rates along block boundaries, superimposed on focal mechanisms colored according to tectonic style. Negative values (blue) indicate extension, whereas positive values (red) indicate shortening. Results for the alternative

boundary condition in Calabria (Ionian Sea = Nubia) are shown on the right. Magenta arrows indicate the estimated surface velocities.

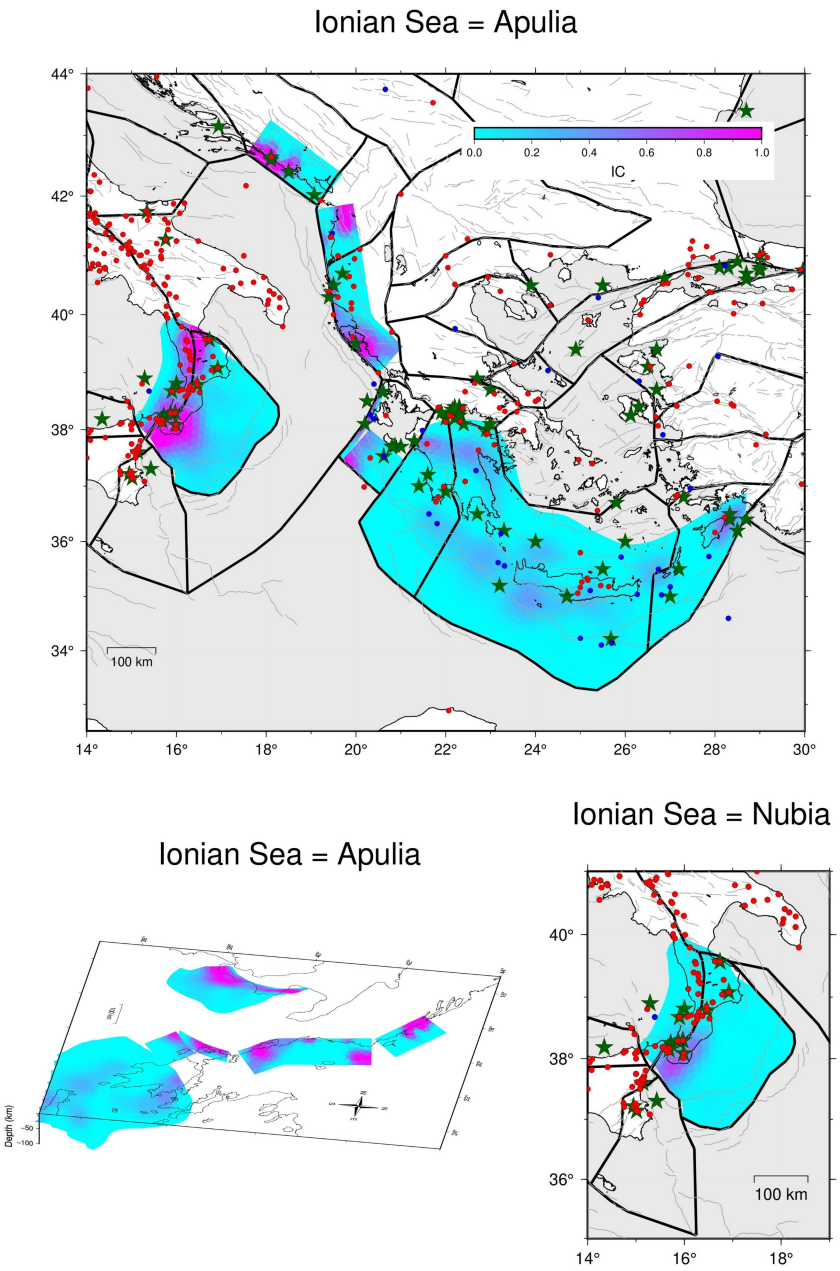

Fig. 3 – IC distribution on boundary meshes for both boundary conditions (Ionian Sea = Apulia and Ionian Sea = Nubia). Green stars represent tsunamis from the EMTC catalog (only events with reliability ≥ 3 and caused by earthquakes; Maramai et al., 2019). Red dots indicate seismic events from the CFTI5Med catalog for the Euro-Mediterranean region (Guidoboni et al., 2019), and blue dots indicate the events with magnitude ≥ 6 from the EMSC seismic catalog (Haslinger et al., 2022).

References

Faccenna, C., Becker, T.W., 2010. Shaping mobile belts by small-scale convection. Nature 465, 602–605. URL: https://doi.org/10.1038/nature09064 .

Faccenna, C., Becker, T.W., Auer, L., Billi, A., Boschi, L., Brun, J.P., Capitanio, F.A., Funiciello, F., Horvàth, F., Jolivet, L., et al., 2014. Mantle dynamics in the mediterranean. Reviews of Geophysics 52, 283–332. URL: https://doi.org/10.1002/2013RG000444.

Guidoboni, E., Ferrari, G., Tarabusi, G., Sgattoni, G., Comastri, A., Mariotti, D., Ciuccarelli, C., Bianchi, M.G., Valensise, G., 2019. Cfti5med, the new release of the catalogue of strong earthquakes in italy and in the mediterranean area. Scientific Data 6, 80. URL: https://doi.org/10.1038/s41597-019-0091-9 .

Haslinger, F., Basili, R., Bossu, R., Cauzzi, C., Cotton, F., Crowley, H., Custódio, S., Danciu, L., Locati, M., Michelini, A., et al., 2022. Coordinated and interoperable seismological data and product services in europe: the epos thematic core service for seismology. Annals of Geophysics 65. URL: https://gfzpublic.gfz-potsdam.de/pubman/item/item_5012231 .

Jackson, J., 1994. Active tectonics of the aegean region. Annual Review Of Earth And Planetary Sciences, Volume 22, pp. 239-271. 22, 239–271. URL: https://doi.org/10.1146/annurev.ea.22.050194.001323 .

Malinverno, A., Ryan, W.B., 1986. Extension in the tyrrhenian sea and shortening in the Apennines as result of arc migration driven by sinking of the lithosphere. Tectonics 5, 227–245. URL: https://doi.org/10.1029/TC005i002p00227 .

Maramai, A., Graziani, L., Brizuela, B., 2019. Euro-mediterranean tsunami catalogue (emtc), version 2.0. URL: https://doi.org/10.13127/tsunami/emtc.2.0. Istituto Nazionale di Geofisica e Vulcanologia (INGV).

Meade, B.J., Loveless, J.P., 2009. Block modeling with connected fault-network geometries and a linear elastic coupling estimator in spherical coordinates. Bulletin of the Seismological Society of America 99, 3124–3139. URL: https://doi.org/10.1785/0120090088 .

McKenzie, D., 1972. Active tectonics of the mediterranean region. Geophysical Journal International 30, 109–185. URL: https://doi.org/10.1111/j.1365-246X.1972.tb02351.x .

Nocquet, J.M., 2012. Present-day kinematics of the mediterranean: A comprehensive overview of gps results. Tectonophysics 579, 220–242. URL: https://doi.org/10.1016/j.tecto.2012.03.037 .

Corresponding author: riccardo.nucci9@gmail.com

New macroseismic intensity data for the earthquakes of the 1783 seismic sequence in Calabria (Italy)

M. Orlando[1,2], A. Tertulliani[1], L. Graziani[1]

[1] *Istituto Nazionale di Geofisica e Vulcanologia (INGV), Roma, Italia*

[2] *Dipartimento di Scienze, Università Roma Tre, Roma, Italia*

Between February and March 1783, Calabria was struck by one of the most devastating seismic sequences in Italian history. The crisis began on February 5 and lasted for over three years, characterized by five mainshocks (occurring on February 5, 6, and 7, and March 1 and 28) with macroseismic magnitudes between 5.9 and 7.1, according to the Parametric Catalogue of Italian Earthquakes (CPTI15; Rovida et al., 2022) and maximum epicentral intensities ranging from IX–X to XI on the Mercalli-Cancani-Sieberg (MCS) scale, with epicenters located in the provinces of Reggio Calabria, Vibo Valentia, and Catanzaro.

These earthquakes, followed by hundreds of minor aftershocks, produced catastrophic cumulative effects over an area of thousands of square kilometers.

Despite the wealth of documentary evidence and the extensive literature that has emerged, significant gaps remain in our understanding of this seismic sequence. These limitations arise primarily from the inherent challenge of distinguishing between the effects of individual earthquakes and assessing the cumulative impact of successive shocks (Stucchi and Rovida, 2008; Guidoboni and Valensise, 2015; Tertulliani et al., 2018).

In this context, this study proposes a macroseismic revision of the sequence through the following methodological approach:
(i) Systematic collection and critical analysis of historical sources (including Catalogue of Strong Earthquakes in Italy and in the Mediterranean Area data, archives, etc.);
(ii) Reconstruction of the source chronology to trace the spatio-temporal evolution of the sequence;
(iii) Identification and georeferencing of the affected localities;
(iv) Definition of cause-and-effect relationships by critically associating, where possible, damage descriptions with individual seismic events;
(v) Assignment of macroseismic intensity according to the MCS and EMS-98 scales. A cumulative intensity was introduced in cases where damage exceeded intensity VII for subsequent earthquakes and it was impossible to distinguish the specific event responsible for the damage.

This revision work resulted in a 30% increase in macroseismic data points compared to the Italian Macroseismic Database (DBMI15; Locati et al., 2022), covering a total of 558 localities.

A distinctive feature of this work is the clear-cut separation between intensity and cumulative intensity, allowing for a more accurate assessment of the relative contribution of overlapping destructive effects.

These new evaluations could improve the characterization of the 1783 sequence and, more broadly, contribute to refining the seismic hazard assessment of this critical area.

References:

Guidoboni E., Ferrari G., Mariotti D., Coastri A., Tarabusi G., Sgattoni G., Valensise G., 2018. CFTI5Med, Catalogo dei Forti Terremoti in Italia (461 a.C.-1997) e nell'area Mediterranea (760 a.C.-1500). Istituto Nazionale di Geofisica e Vulcanologia (INGV). https://doi.org/10.6092/ingv.it-cfti5.

Guidoboni, E., & Valensise, G. (2015). On the complexity of earthquake sequences: a historical seismology perspective based on the L'Aquila seismicity (Abruzzo, Central Italy), 1315-1915. *Earthquakes and Structures*, *8*(1), 153–184. https://doi.org/10.12989/EAS.2015.8.1.153

Locati M., Camassi R., Rovida A., Ercolani E., Bernardini F., Castelli V., Caracciolo C.H., Tertulliani A., Rossi A., Azzaro R., D'Amico S., Antonucci A. (2022). Italian Macmroseismic Database (DBMI15), version 4.0. Istituto Nazionale di Geofisica e Vulcanologia (INGV). https://doi.org/10.13127/dbmi/dbmi15.4

Rovida A., Locati M., Camassi R., Lolli B., Gasperini P., Antonucci A. (2022). Italian Parametric Earthquake Catalogue (CPTI15), version 4.0. Istituto Nazionale di Geofisica e Vulcanologia (INGV). https://doi.org/10.13127/cpti/cpti15.4

Stucchi M. e Rovida A., (2008). Investigating Historical Earthquake Sequences. MERCEA'08 Seismic Engineering International Conference, Messina e Reggio Calabria, 8-11 luglio 2008.

Tertulliani A., Graziani L., Rovida A., Antonucci A., (2018). Effetti cumulativi nelle sequenze sismiche e stima dei parametri macrosismici: cosa abbiamo imparato dalla sequenza del centro Italia del 2016-2017. 370 convegno GNGTS, Bologna

Unveiling the segmentation of the Montello Front and the role of inherited margins in the Eastern Southern Alps (NE Italy): insights from the CARG Project – 084 Vittorio Veneto Sheet

G. Patricelli[1], M.E. Poli[1], G. Monegato[2], P. Mozzi[3], J. Boaga[3], I. Barone[3], L. Rettig[3,4,5], S. Rossato[2], G. Toffolon[6], L. Crocitto[7], S. Papa[3], N. Preto[3], A. Franceschet[1,8], C. Stefani[3]

[1] Department of Agricultural, Food, Environmental and Animal Sciences, University of Udine, Italy
[2] Institute of Geosciences and Earth Resources, National Research Council of Italy, Padova, Italy
[3] Department of Geosciences, University of Padua, Italy
[4]Laboratory of Hydraulics, Hydrology and Glaciology (VAW), ETH Zürich, Zürich, Switzerland.
[5]Swiss Federal Institute for Forest, Snow and Landscape Research (WSL), Bâtiment ALPOLE, Sion, Switzerland.
[6] Geologo Libero professionista, Motta di Livenza (TV), Italy
[7] Geologo Libero professionista, Teolo (PD), Italy
[8] Department of Life Sciences, University of Trieste, Italy

Introduction

This contribution presents a new structural interpretation of the Montello sector, developed within the framework of the CARG Project (Sheet 084 – Vittorio Veneto). Our reconstruction focuses on the geometry and segmentation of the Montello Thrust, previously described as a laterally continuous, ~30 km long SE-verging thrust fault (Galadini et al., 2005; Picotti et al., 2022). The results provide new insights into the structure and evolution of the frontal sector of the Eastern Southern Alps (ESA), highlighting the importance of paleogeographic structural inheritances, and its associated seismotectonic implications.

The Montello Thrust belongs to the Pliocene–Quaternary front of the ESA, a SSE-verging fold-and-thrust belt that developed during the Neogene in response to the convergence between the Adria and European plates. However, the compressive tectonics superimposed on the inherited paleogeographic framework controlled by pre-existing tectonic structures. During the Mesozoic, the Venetian Prealpine area represented the transitional margin between the carbonate platform to the southeast and the deep-marine pelagic domain of the Belluno Basin to the northwest (Bosellini et al., 1981; Masetti et al., 2012). Until the late Cretaceous, a complex system of normal and strike-slip faults accommodated subsidence in the northwestern sector, controlling sedimentation. Following this tectonic phase, the study area was only marginally affected by the southwestward propagation of the External Dinarides during the Paleocene-Eocene Dinaric orogenic phase (Doglioni and Bosellini, 1987; Castellarin and Cantelli, 2000). Similarly, starting from the Oligocene, the study area was peripherally influenced by the development of the Alpine Chain *s.s.*, representing its distal foreland (Fantoni et al., 2002). In the Venetian area, the main structuring of the Southalpine Chain started during the Serravallian with the Neogene Valsugana event, but the propagation of the SE-

verging fold and thrust belt affected the investigated Venetian prealpine sector since the Messinian-Pliocene with the development of the Bassano–Valdobbiadene Thrust (Castellarin and Cantelli, 2000). Subsequently, deformation propagated outward, producing the more external Montello and Arcade fronts (Ferrarese et al., 1998, Benedetti et al., 2000; Mozzi et al., 2015;), which still accommodate crustal shortening in the northeastern Venetian Plain.

Seismic activity within the map area is relatively low (Fig. 1). The epicenters of the largest historical earthquakes (M > 6) are located farther in the inner portion of the chain: the 1695 Asolo earthquake (Mw 6.4) affected the region located west of the study area, while both the 1873 Alpago (Mw 6.3) and 1936 Cansiglio (Mw 6.1) macroseismic epicenters are placed northeastward (CPTI15 v4.0, Rovida et al., 2022). Instrumental seismicity is also moderate, with local magnitudes generally not exceeding 4.5 (Romano et al., 2019). Despite the low seismicity, the dimensions of the mapped thrust structures—which exceed 25 km in length— suggest a significant theoretical seismogenic potential (M > 6.5, Galadini et al., 2005). In this regard, Barba et al. (2013) proposed that the Bassano-Valdobbiadene Thrust is a locked, potentially seismogenic structure, whereas the Montello Thrust predominantly accommodates deformation through aseismic creep.

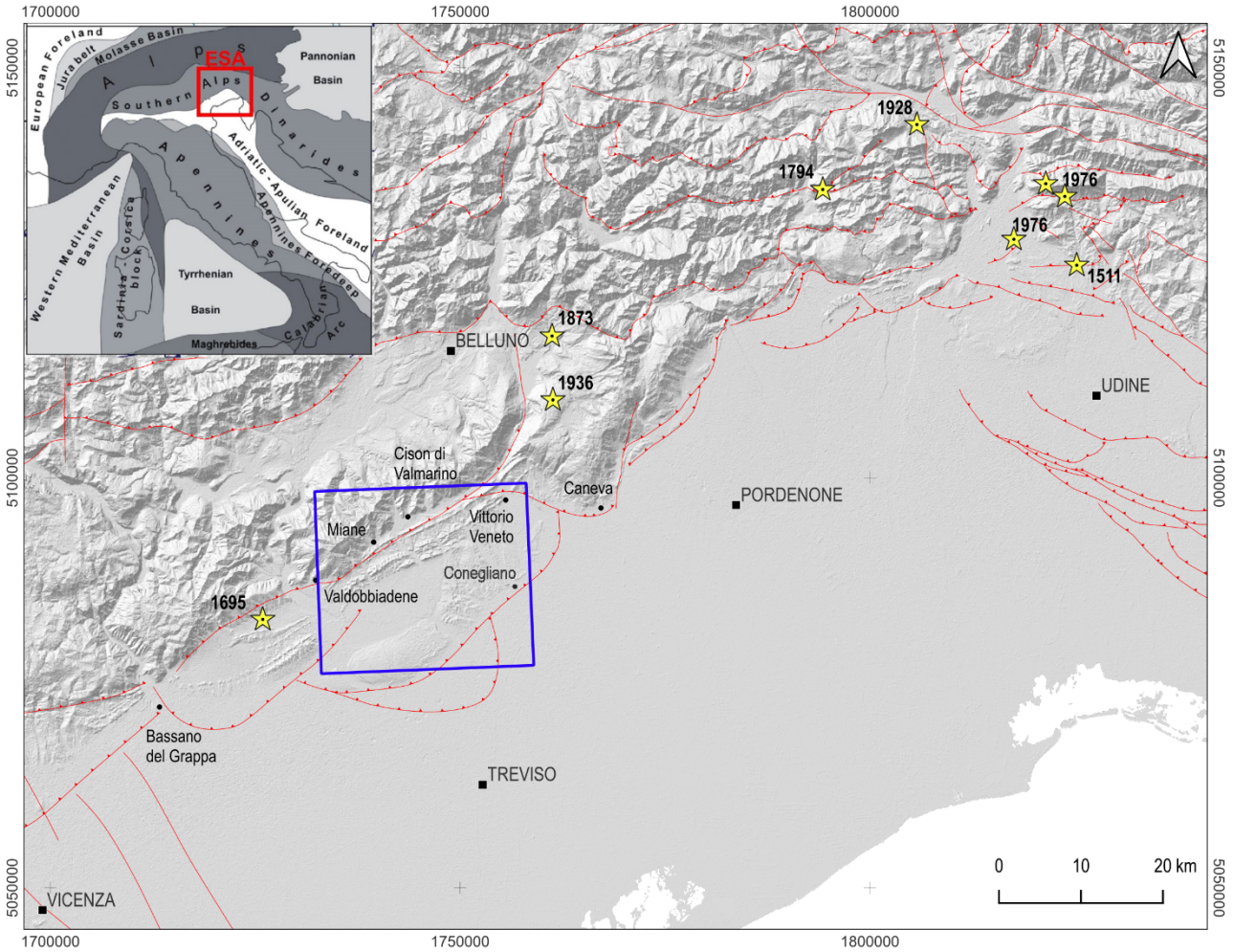

Fig. 1 – *Structural map of Eastern Southern Alps (modified after Galadini et al., 2005). Yellow stars indicate M>5.5 earthquakes from CPTI15. Blue box represents the CARG Vittorio Veneto Sheet map area. Faults acronyms: AR: Arcade, BC: Bassano-Cornuda th., BL: Belluno th., BV: Bassano-Valdobbiadene th., CA: Cansiglio th., MT: Montello th., PM: Polcenigo-Montereale th., SV: Schio-Vicenza Fault System.*

Methods and Results

Focusing on the outermost portion of the Southalpine front, we reconstructed the deep structural architecture of the northeastern Veneto Plain by integrating subsurface and surface geological data. In particular, the analysis of industrial seismic profiles (gently supplied by ENI and British GAS), calibrated with wells stratigraphy, allowed us to identify the main subsurface stratigraphic units and to reconstruct their geometry. A velocity model was derived from British Gas well-log velocities and integrated with published data; it was then used to perform time-to-depth conversion in Move software. The resulting deep geological sections were integrated with surface geological information, including both unpublished field data acquired during the survey for the CARG Vittorio Veneto sheet and published geological data from existing CARG 063 Belluno Sheet (Costa et al., 1996). Interpolation of stratigraphic horizons and thrust planes across the sections enabled the reconstruction of the three-dimensional geometry of major stratigraphic surfaces and tectonic structures down to depths of about 6 km.

The resulting structural model shows that the northwestern part of the study area is affected by the Valdobbiadene-Vittorio Veneto Thrust, which represents the eastern segment of the Bassano-Valdobbiadene Thrust. Here, the thrust front emplaces the southern limb of the Mt. Cesen–Mt. Visentin anticline, composed of Jurassic–Cretaceous successions of the Belluno Basin, over the Paleocene–Eocene turbidites and Miocene Molasse units. At the footwall of the Valdobbiadene-Vittorio Veneto Thrust, the stratigraphic succession is folded into broad syncline–anticline structures, which are further cut and uplifted by the more external thrust fronts. The fundamental structural element common to the entire frontal sector is the deep Mesozoic paleogeographic margin marking the transition from the shallow-water Friuli Carbonate Platform domain to the southeast and the deeper Belluno Basin to the northwest. Our model indicates that the southeastward propagation of the external Neogene front reused the pre-existing deep structural inheritance, reactivating the Mesozoic normal fault systems with reverse kinematics.

Focusing on the structural architecture of the thrust systems, the reconstructed model suggests that the external front of the Chain is segmented: there is no lateral continuity between the Montello sector (western study area), where the Montello-Arcade Thrust System develops, and the Conegliano sector (eastern area) affected by the Conegliano Thrust System. In detail, the western sector is characterized by the Montello anticline, which is supported by the homonymous thrust. The Montello Thrust offsets the pre-Quaternary succession up to the lower-middle Miocene Cavanella Group, at depths of roughly 1 km, with a middle-to-low angle geometry. Upwards, it causes the anticlinal folding of the upper Miocene-Pliocene Molasse, which forms the Montello elongated hill. A further reverse splay develops at the hangingwall of the Montello Thrust: the Arcade Thrust, which propagates to near-surface levels as a medium- to high-angle ramp cutting the entire stratigraphic sequence. In contrast to the Montello sector, the eastern portion of the study area is affected solely by the Conegliano Thrust System, composed of two medium-angle reverse faults (Conegliano 1 and Conegliano 2 Thrusts), which cut the entire stratigraphic succession and propagate upward to near-surface levels, clearly offsetting the Pliocene–Quaternary deposits. The analyzed data suggest that the lateral continuity between the Montello–Arcade and Conegliano Thrust Systems is interrupted at the Nervesa narrow, presently occupied by the Piave River. Here, the exposed Pliocene–Pleistocene deposits exhibit a pervasive NNW–SSE-oriented cleavage, likely representing the surface expression of the lateral ramp of the Conegliano System, which structurally overrides the Montello block.

Considering the structural complexity of the external thrust system from a seismogenic perspective, the presence of a segmented thrust front, rather than a single continuous source, would reduce the maximum earthquake potential of the study area. This interpretation also accounts for the absence of moderate-to-strong historical earthquakes within the completeness interval of the catalog.

Considering the overall low rate of instrumental seismicity, it is consistent to assess that the outermost frontal sector accommodates deformation predominantly through aseismic creeping (Barba et al., 2013; Romano et al., 2019).

References

Barba, S., Finocchio D., Sikdar E., Burrato P. (2013). Modelling the interseismic deformation of a thrust system: Seismogenic potential of the Southern Alps, Terra Nova 25, 221–227. doi: 10.1111/ter.12026.

Benedetti, L., Tapponnier, P., King, G. C., Meyer, B., Manighetti, I. (2000). Growth folding and active thrusting in the Montello region, Veneto, northern Italy. Journal of Geophysical Research: Solid Earth 105(B1), 739-766. https://doi.org/10.1029/1999JB900222.

Bosellini A., Masetti D., Sarti M. (1981). A Jurassic "tongue of the ocean" infilled with oolitic sands: the Belluno Trough, Venetian Alps, Italy. Marine Geology 44, 59-95. https://doi.org/10.1016/0025-3227(81)90113-4.

Castellarin, A., Cantelli, L. (2000). Neo-Alpine evolution of the Southern Eastern Alps. Journal of Geodynamics 30, 251-274.

Costa V. and Doglioni C. (1996). Foglio Geologico e Note illustrative della Carta Geologica d'Italia, alla scala 1:50000. Foglio 063-Belluno. Servizio Geologico d'Italia. Istituto Poligrafico dello Stato.

Doglioni, C. and Bosellini, A. (1987). Eoalpine and mesoalpine tectonics in the Southern Alps. Geologische Rundschau 76, 735-754. https://doi.org/10.1007/BF01821061.

Fantoni, R., Catellani, D., Merlini, S., Rogledi, S., Venturini, S. (2002). La registrazione degli eventi deformativi cenozoici nell'avampaese Veneto-Friulano. Memorie della Società Geologica Italiana 57, 301-313.

Ferrarese, F., Sauro, U., Tonello, C. (1998). Karst evolution of an alpine neotectonic morphostructure. Zeitschrift für Geomorphologie. Supplementband 109, 41-62.

Galadini, F., Poli, M.E., Zanferrari, A. (2005). Seismogenic sources potentially responsible for earthquakes with M > 6 in eastern Southern Alps (Thiene-Udine sector, NE Italy). Geophysical Journal International 161, 739-762. https://doi.org/10.1111/j.1365-246X.2005.02571.x.

Masetti D., Fantoni R., Romano R., Sartorio D., Trevisani E. (2012). Tectonostratigraphic evolution of the Jurassic extensional basins of the eastern southern Alps and Adriatic foreland based on an integrated study of surface and subsurface data. Aapg Bulletin 96(11), 2065-2089. 10.1306/03091211087.

Mozzi P., Rossato S., Pascucci V., Andreucci S., Monegato G., Fontana A., Sechi D. (2015). Aggradation of the Montebelluna Megafan (NE Italy) at the MIS 3-2 transition, problems and perspectives. Abstracts Volume AIQUA Congress 2015: "The Plio-Pleistocene continental record in

Italy: highlights on Stratigraphy and Neotectonics". Torino, February 24 | 26, 2015, pag. 33. Miscellanea INGV.

Picotti, V., Romano, M. A., Ponza, A., Guido, F. L., Peruzza, L. (2022). The Montello thrust and the active mountain front of the eastern Southern Alps (northeast Italy). Tectonics 41(12), e2022TC007522.

Romano, M. A., Peruzza, L., Garbin, M., Priolo, E., Picotti, V. (2019). Microseismic portrait of the Montello thrust (Southeastern Alps, Italy) from a dense high-quality seismic network. Seismological Research Letters 90(4), 1502-1517. https://doi.org/10.1785/0220180387.

Rovida, A., Locati, M., Camassi, R., Lolli, B., Gasperini, P., Antonucci, A. (2022). Catalogo Parametrico dei Terremoti Italiani (CPTI15), versione 4.0. Istituto Nazionale di Geofisica e Vulcanologia. https://doi.org/10.13127/CPTI/CPTI15.4.

Corresponding author: giulia.patricelli@uniud.it

THE "ETNA FAC-MS3" PROJECT: PROBLEMS AND IMPLICATIONS OF CAPABLE FAULTS ON MICROZONATION IN A VOLCANIC AREA

E. Peronace[1], R. Azzaro[2], S. Catalano[1,3], M. Mancini[1], A. Torrisi [4]

[1] Istituto di Geologia Ambientale e Geoingegneria, Consiglio Nazionale delle Ricerche, Rome.
[2] Istituto Nazionale di Geofisica e Vulcanologia, Osservatorio Etneo, Catania, Italy.
[3] Dipartimento di Scienze Biologiche, Geologiche e Ambientali (DSBGA) – Sezione di Scienze della Terra, Università di Catania.
[4] Dipartimento Regionale della Protezione Civile della Presidenza della Regione Siciliana (DRPC Sicilia), Nicolosi (CT).

The *Guidelines for the study of Active and Capable Faults (FAC) in the Etna region (LG_FAC_Etna*) represent the core objective of the "**Etna FAC-MS3 Project**", established through a scientific collaboration agreement between the *Dipartimento Regionale della Protezione Civile della Presidenza della Regione Siciliana* (DRPC Sicilia) and the *Istituto di Geologia Ambientale e Geoingegneria del Consiglio Nazionale delle Ricerche* (CNR IGAG), on behalf of the *Center for Seismic Microzonation and its applications* (CentroMS). The development of specific guidelines for FAC studies in the Etna region is due to the characteristics of these active tectonic structures (Azzaro et al., 2012), requiring a proper contextualization within the methodological framework of Seismic Microzonation (SM) analyses, to ensure the correct application of definitions and representation standards already adopted at a national scale (MS Technical Commission, 2020). These are outlined in the "*Guidelines for the Management of Territory in Areas Affected by Active and Capable Faults (FAC)*" (LG FAC, 2015), approved by the National Civil Protection Department and the Conference of Regions and Autonomous Provinces of Italy.

The LG_FAC_Etna are based on the extensive scientific knowledge matured over decades, integrating geological-structural, geomorphological, seismological (both macroseismic and instrumental), and paleoseismological data collected by universities and research institutions, now parts of CentroMS. These new guidelines do not replace the LG FAC (2015), which remain the national reference for SM studies, but provide an essential, context-specific integration to support technicians involved in SM studies at Etna. Moreover, they also offer an interpretative framework for study outcomes, aiding technicians in territorial planning, management, and population protection.

Seismicity on Mt. Etna is extremely shallow, with hypocentres confined to the uppermost kilometres of the crust and causative faults undergoing continuous topographic rejuvenation due to frequent emplacement of new lava fields. These features strongly influence the effects of the

coseismic surface ruptures, predisposing the system to a much wider areal dispersion of ground fracturing than that typically observed in other geological settings. FAC at Etna (Fig. 1) rarely expose their main fault planes at the surface; instead, they are expressed through sets of secondary conjugate faults and fractures. Their periodic reactivation does not necessarily produce spatially focused or cumulatively stable surface ruptures. However, identifying a surface trace of fault—whether certain or uncertain—is essential for defining FACs in SM, as it underpins the delineation of associated Respect Zones (ZR) and Susceptibility Zones (ZS). Uncertainties in trace localization comparable to the width of these zones, or fracturing dispersion exceeding the zoning predicted by FAC Guidelines (2015), significantly limit the development of reliable predictive models of coseismic surface ruptures. For the classification of Etna's FACs, the ability to identify a fault trace with decametric precision has therefore been adopted as a discriminating criterion. Surface exposure of fault planes is feasible only where lava flows have long shielded the structures, and even when exposure is short-lived due to rapid erosion of the uplifted lava layers. Consequently, in the absence of direct geological evidence, the surface traces of active and capable faults have been inferred from associated morpho-structural elements (fault scarps), allowing the use of established fault datasets in the local geological literature (Azzaro and D'Amico, 2024). These elements correspond to three tectonic morpho-types that characterize the active faults of Mt. Etna or specific segments of them (Fig. 2).

A comprehensive database (DB_FAC_Etna) cataloguing all fault segments and associated zoning relevant to SM level 3 studies, accompanies the guidelines (Fig. 1). The active lineaments at Etna, identified as capable faults in national and local archives (ITHACA Working Group, 2019; Azzaro and D'Amico, 2024), were classified basing on their surface expression into categories, some aligning with the classical LG FAC (2015) definitions. Only the faults with documented seismic history and observed ground displacement/fracturing were considered in the database and relevant for SM studies. Eligible FACs must demonstrate cyclic seismic activity with morpho-structural evidence, sufficient to identify either the principal fault trace (FAC_a, certain) or its probable location when buried (FAC_b, uncertain), critical for establishing Respect Zones (ZR) or Susceptibility Zones (ZS) as defined in LG_FAC (2015).

Considering the peculiar features, a new distinct category of FAC — the Active Fracturing Zones (ZFA) — was introduced for the Etna in order to consider the historically documented co-seismic fracturing along hidden faults (Azzaro et al., 2012), the latest occurring on 26 December 2018 (Civico et al., 2019; Villani et al., 2020; Romagnoli et al., 2021; Tortorici et al., 2021; Tringali et al., 2021; Azzaro et al., 2022). In these cases, surface fracturing may also occur at significant distances from the vertical projection of the main buried fault, making it impractical the longitudinal zoning of likely surface rupture. Finally, tectonic lineaments identified as active through geodetic data, but lacking surface rupture were excluded from SM studies, as well as linear features associated with volcanic activity (e.g. eruptive fissures).

The LG_FAC_Etna focuses exclusively on surface ruptures associated with co-seismic displacement, excluding other secondary phenomena such as near-fault shaking effects. However, the lineaments not considered remain potential sources of local seismic events capable of significant damage,

maintaining relevance for SM and for regional seismic hazard assessment. In addition, an important contribute of this study is the geophysical characterization of FACs at Etna, that involved different research groups and methodological approaches. Standard and advanced techniques have been tested in different local geo-tectonic settings to evaluate the best performances and to give professionals hints and indications for correct geophysical field investigations.

The LG_FAC_Etna for professional users is being published in a special volume in the *CNR Edizioni* series edited by the CentroMS (BookMS series), whereas the related scientific basis is the subject of a Special Issue in the journal Annals of Geophysics.

Finally, the project will be continued thanks to a new cooperation agreement between DRPC Sicilia and CNR IGAG on behalf of the CentroMS, to align previous SM studies to the LG_FAC_Etna.

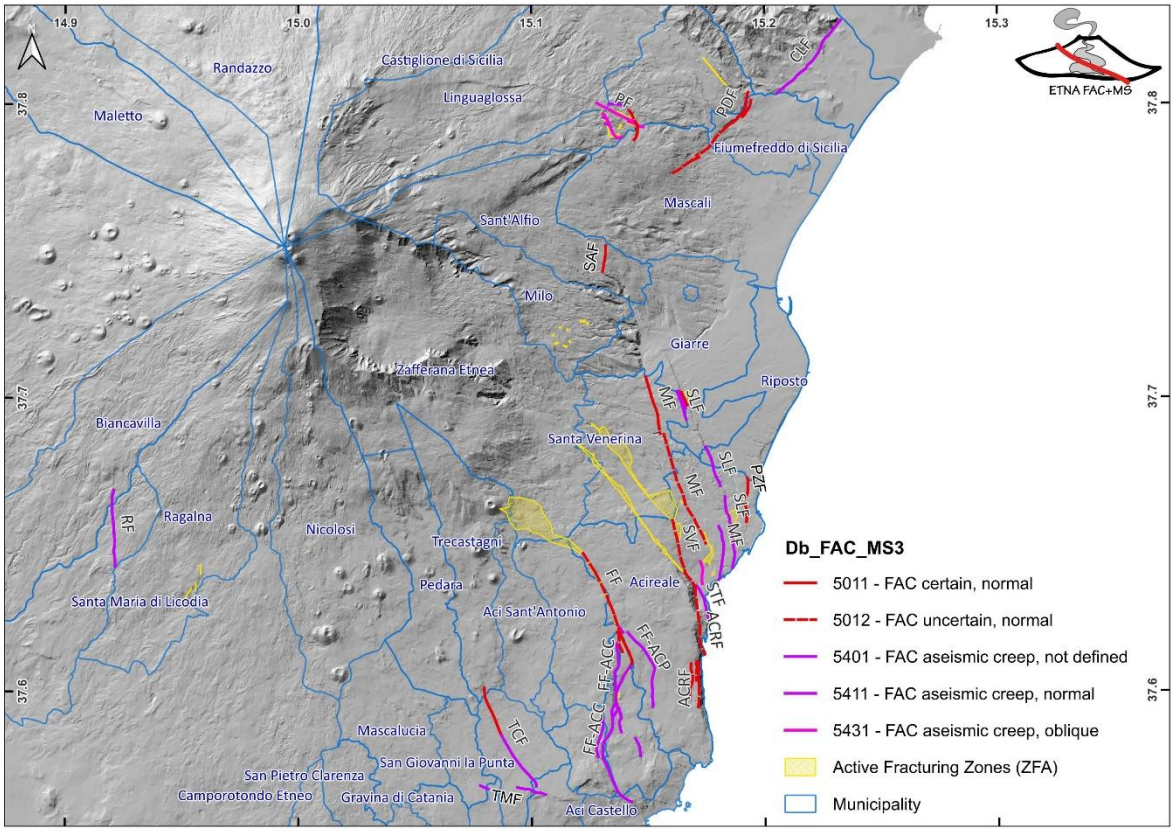

Fig. 1 – Active and capable faults (FAC) defined in the "ETNA FAC-MS3" project; faults: PF, Pernicana; RF, Ragalna TMF, Tremestieri; TCF, Trecastagni; FF, Fiandaca; ACC, Acicatena; ACP, Aciplatani; ACRF, Acireale; STF, S. Tecla; MF, Moscarello; SLF, S. Leonardello; SVF, S. Venerina; PZF, Pozzillo; SAF, S. Alfio; PDF, Piedimonte; CLF, Calatabiano.

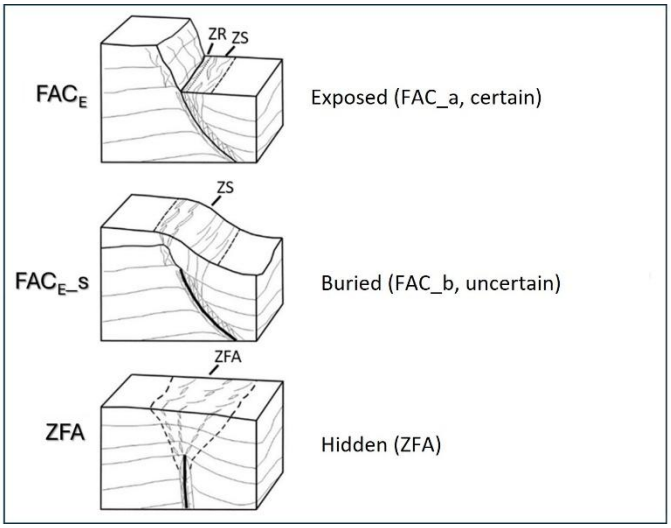

Fig. 2 – Types of active and capable faults identified on Mount Etna, related classification and zoning proposal for MS3 studies. ZR = Respect Zone; ZS = Susceptibility Zone; ZFA = Active Fracturing Zone.

Acknowledgments

We would like to sincerely thank all members of the ETNA FAC+MS group whose expertise and efforts contributed to the success of this project.

References

Azzaro R., Branca S., Gwinner K. & Coltelli M.; 2012: The volcano-tectonic map of Etna volcano, 1:100.000 scale: morphotectonic analysis from high-resolution DEM integrated with geologic, active faulting and seismotectonic data. It. J. Geosciences (Boll. Soc. Geol. It.), 131 (1), 153-170.

Azzaro R. & D'Amico S.; 2024: Database delle Faglie Attive Etnee (DFAE). Versione beta 0.5. Istituto Nazionale di Geofisica e Vulcanologia (INGV), https://www.ct.ingv.it/macro/dfae/index.html.

Civico R., Pucci S., Nappi R., Azzaro R., Villani F., Pantosti D., Cinti F., Pizzimenti L., Branca S., Brunori C.A. Caciagli M., Cantarero M., Cucci L., D'Amico S., De Beni E., De Martini P.M., Mariucci M.T., Montone P., Nave R., Ricci T., Sapia V., Smedile A., Tarabusi G., Vallone R. & Venuti A.; 2019: Surface ruptures following the 26 December 2018, Mw 4.9, Mt. Etna earthquake, Sicily (Italy). Journal of Maps, 15, 831–837. https://doi.org/10.1080/17445647.2019.1683476.

ITHACA Working Group; 2019: ITHACA (ITaly HAzard from CApable faulting), A database of active capable faults of the Italian territory. ISPRA Geological Survey of Italy.

Linee Guida FAC; 2015: Linee guida per la gestione del territorio in aree interessate da Faglie Attive e Capaci (FAC). Versione 1.0. Commissione tecnica per la Microzonazione sismica. Conferenza delle Regioni e Province autonome – Dipartimento della protezione civile, Roma. 61 pp. https://www.centromicrozonazionesismica.it/documents/22/Linee_guida_per_la_gestione_del_territorio_interessato_da_faglie_attive_e_capaci.pdf

MS Technical Commission, (2020): Microzonazione Sismica - Standard di Rappresentazione e Archiviazione Informatica, Versione 4.2, dicembre 2020. A cura di: Bramerini F., Carbone G., Castenetto S., Coltella M., Naso G., Pietrosante A., Romagnoli G., Catalano S., Nocentini M., Porchia A. Programma per il supporto al rafforzamento della governance in materia di riduzione del rischio ai fini di protezione civile (PON governance e capacità istituzionale 2014-2020). Dipartimento della Protezione Civile, Roma. 138 pp. https://www.centromicrozonazionesismica.it/documents/1/StandardMS_4_2.pdf

Romagnoli G., Pavano F., Tortorici G. & Catalano S.: 2021: Field dataset of the 2018 Mount Etna earthquake (Mw 4.9). Mendeley Data. https://doi.org/10.17632/rzmdnj8j2w.4.

Tortorici G., Pavano F., Romagnoli G. & Catalano S.; 2021: The effect of recent resurfacing in volcanic areas on the distribution of co-seismic ground deformation due to strike-slip earthquakes: new insights from the 12/26/2018 seismic event at Mt. Etna. J. Struct. Geol., 145, https://doi.org/10.1016/j.jsg.2021.104308.

Tringali G, Bella D., Livio F.A., Ferrario M. F., Groppelli G., Blumetti A.M., Di Manna P., Vittori E., Guerrieri L., Porfido S., Boso D., Pettinato R., Paradiso G., Michetti A.M.; 2021: Fault rupture and aseismic creep accompanying the December 26, 2018, Mw 4.9 Fleri earthquake (Mt. Etna, Italy): factors affecting the surface faulting in a volcanotectonic environment. Quaternary International. https://doi.org/10.1016/j.quaint.2021.124.019.

Villani F., Pucci S., Azzaro R., Civico R., Cinti F., Pizzimenti L., Tarabusi G., Branca S., Brunori C.A., Caciagli M., Cantarero M., Cucci L., D'Amico S., De Beni E., De Martini P.M., Mariucci M.T., Messina A., Montone P., Nappi R., Nave R., Pantosti D., Ricci T., Sapia V., Smedile A., Vallone R. & Venuti A.; 2020: Surface ruptures database related to the 26 December 2018, Mw 4.9, Mt. Etna earthquake, southern Italy. Sci. Data, 7 (42), 1-9, Doi: https://doi.org/10.1038/s41597-020-0383-0.

Corresponding author: edoardo.peronace@cnr.it

Linking thrust fault maturity and coseismic behaviour: evidence from the 2022 Mw 5.8 Adriatic offshore earthquake

L. Petracchini[1], S. Tavani[1,2], M. Brandano[1,3], E. Carminati[3], C. Chiarabba[4], A. Conti[1], R. Devoti[4], P. Galli[1,5], M. Palano[6], G. Pezzo[4], L. Scognamiglio[4], E. Tinti[3,4], A. Billi[1]

[1]*CNR-IGAG, Rome, Italy*
[2]*University of Florence, Italy*
[3]*Sapienza University of Rome, Italy*
[4]*INGV, Rome, Italy*
[5]*Dipartimento della Protezione Civile, Italy*
[6]*University of Palermo, Italy*

Fault maturity, defined as the degree of structural and mechanical evolution accumulated through fault slip history, is increasingly recognized as a controlling factor on coseismic behaviour (Choy and Kirby, 2004; Manighetti et al., 2007; Perrin et al., 2016). Mature faults typically develop localized slip surfaces, reduced roughness, and well-organized damage zones, favouring fast rupture propagation. Conversely, immature faults, characterized by limited cumulative displacement and poorly developed fault cores, are expected to exhibit distinct seismic patterns, including slower rupture velocities and heterogeneous slip (Guo et al., 2023). While these relationships have been widely explored for strike-slip and extensional faults, their investigation in compressional settings remains limited.

In thrust belts, deformation is partitioned between faulting and folding, and along-strike variations in cumulative displacement, ramp geometry, and interaction with adjacent structures may lead to strong lateral variations in fault maturity (Bergen and Shaw, 2010). The 9 November 2022 Mw 5.8 Adriatic offshore earthquake (Italy) provides a rare opportunity to investigate the link between thrust maturity and coseismic behaviour in compressional setting, thanks to the availability of high-quality multidisciplinary datasets, including seismic reflection profiles, well data, instrumental and historical seismicity, and GNSS measurements (Fig. 1).

The earthquake occurred along the outermost active front of the Northern Apennines fold-and-thrust belt. Interpretation of seismic reflection profiles (Figs. 1, 2) allowed reconstruction of the regional tectonic framework and the identification of the Cornelia thrust as the most likely seismogenic source (Maesano et al., 2023; Petracchini et al., 2025).

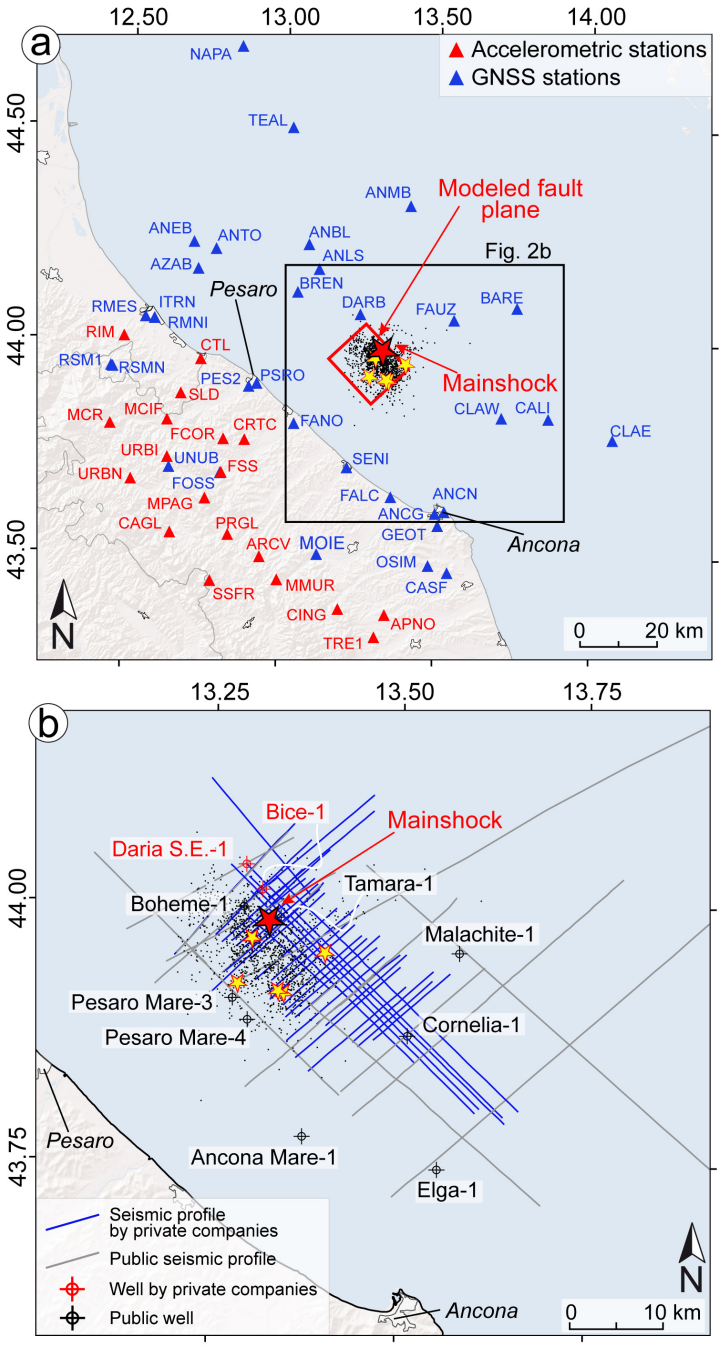

Fig. 1 – Location of measurement stations and datasets. (a) Map showing GNSS stations and accelerometric stations. The red polygon represents the surface projection of the modeled fault plane from the kinematic finite-fault inversion. (b) Map of seismic reflection profiles and wells (from Petracchini et al., 2025).

The Cornelia thrust displays a pronounced along-strike variation in cumulative displacement and structural style (Fig. 2). Its central sector is characterized by a well-developed fault-propagation fold and cumulative displacement of up to ~3 km, whereas to the northwest, the thrust segment retains an embryonic fault-propagation fold setting and the displacement decreases to less than ~0.3 km. The 2022 mainshock nucleated and ruptured this northwestern segment, which corresponds to the lateral tip of the structure, where the thrust is structurally immature.

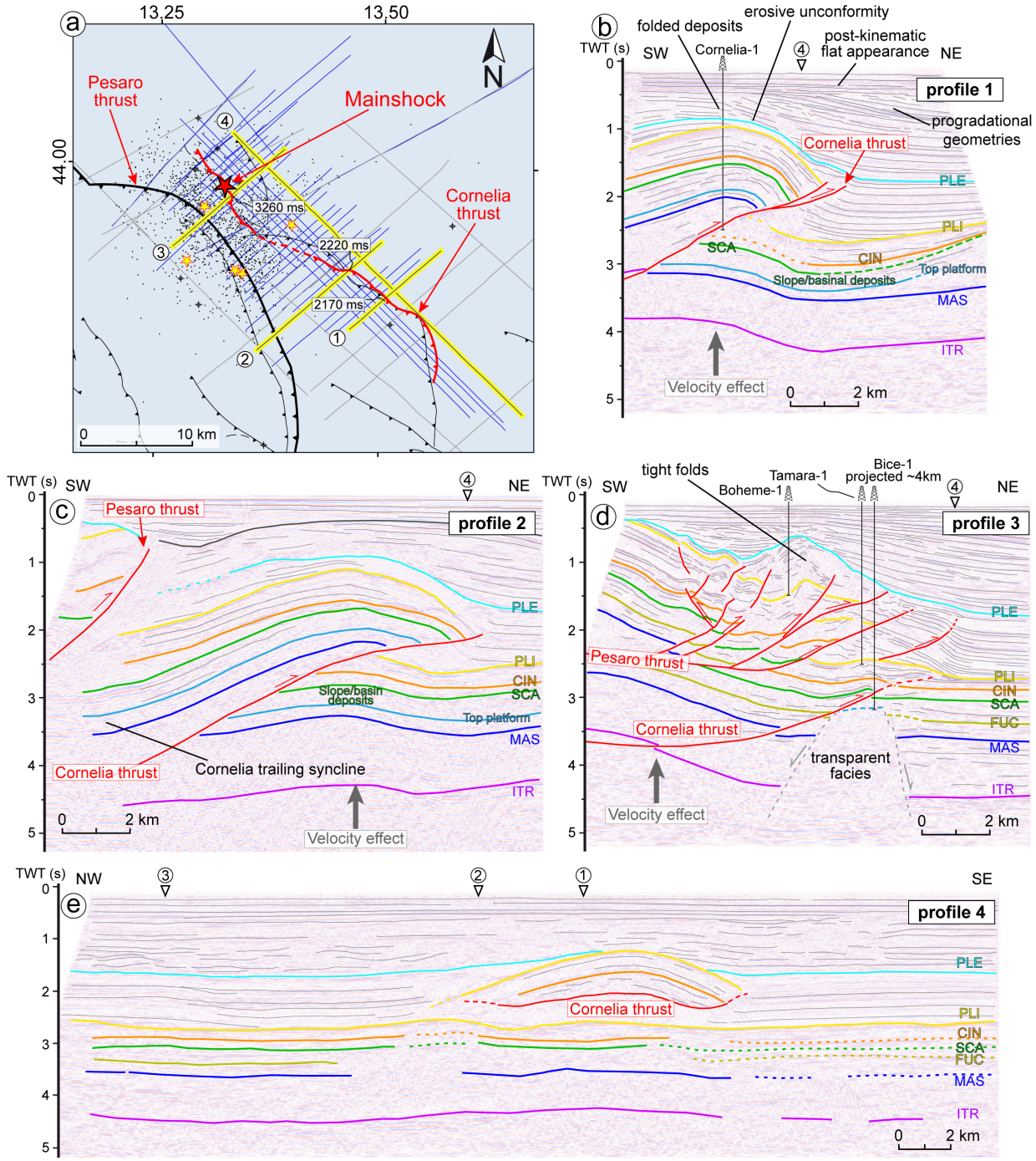

Fig. 2 – Selected seismic reflection profiles and related interpretation (from Petracchini et al., 2025).

Seismological analyses further support this interpretation. The kinematic finite-fault inversion, constrained by the geometry derived from seismic reflection data, reveals a rupture propagating downdip from the hypocenter characterized by an unusually low rupture velocity of ~1.3 km/s (Fig. 3; Chounet et al., 2018; Petracchini et al., 2025). This value is significantly lower than rupture velocities typically reported for large strike-slip earthquakes (Guo et al., 2023) and lies near the lower bound documented by Chounet et al. (2018) for 96 Mw ≥5.6 thrust, strike–slip, and normal faulting events. The coseismic slip patch is confined to the thrust ramp and does not propagate upward, consistent with rupture propagating downdip into velocity-weakening, calcite-rich, and mechanically stronger lithologies.

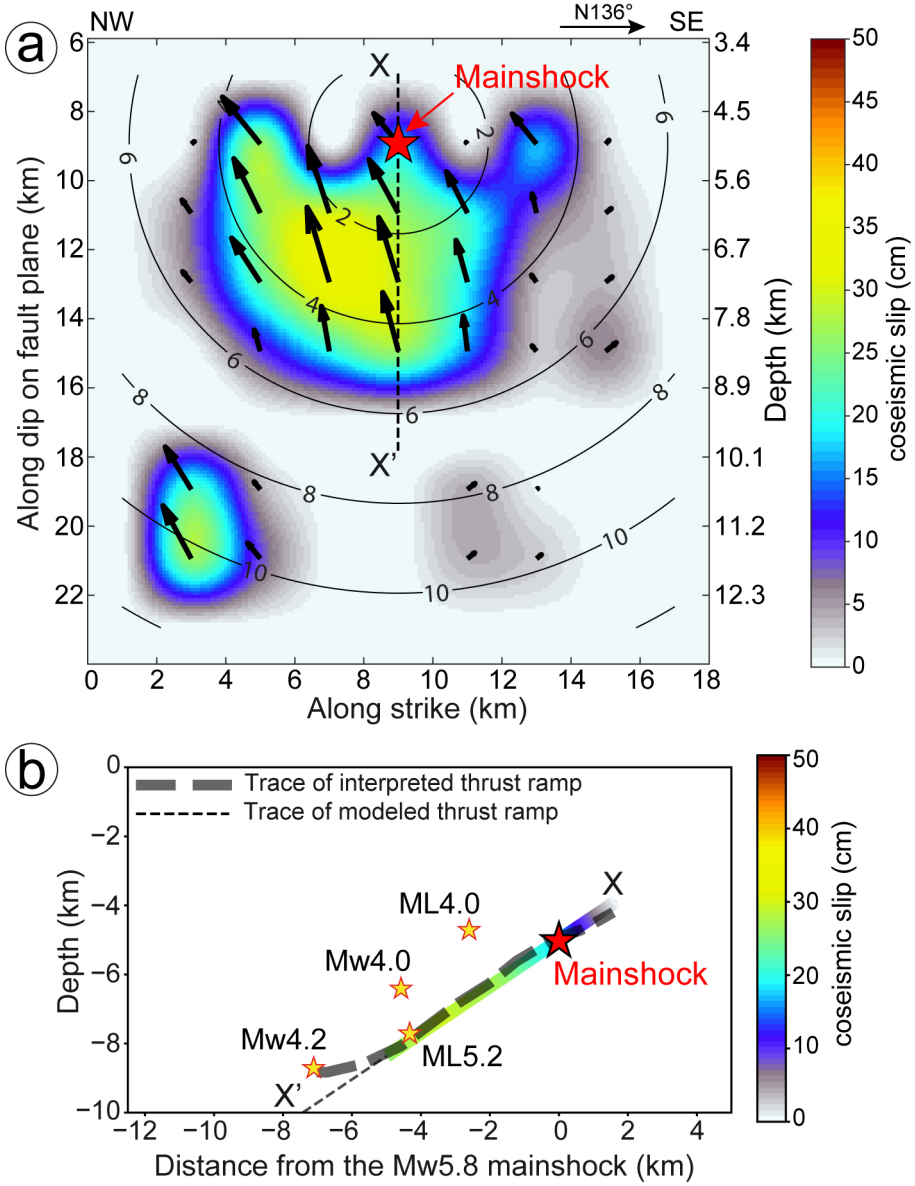

Fig. 3 – Coseismic slip model from finite-fault inversion (from Petracchini et al., 2025).

The integration of geological and seismological observations highlights a clear relationship between thrust fault maturity and coseismic behavior: low cumulative displacement and structural immaturity correspond to slow rupture propagation. This represents one of the few documented examples of such a relationship in a compressional, offshore setting.

GNSS data provide additional constraints on long-term deformation. Horizontal velocities indicate a long-term slip rate of approximately 1 mm/yr across the thrust system. Comparison between coseismic slip and long-term strain accumulation provides first-order estimates of the seismic cycle in this offshore setting.

The integration of geological observations with seismological and geodetic results indicates that structural immaturity correlates well with slow rupture velocity, establishing a direct connection between fault maturity and coseismic dynamics even in compressional settings. Recognizing along-strike changes in structural maturity is therefore crucial for accurately assessing seismic hazard,

especially in offshore fold-and-thrust belts where active faults are difficult to identify and characterize. The results emphasize the need to integrate structural geology, seismology, and geodesy to better constrain seismic potential and associated risks in compressional tectonic settings.

References

Bergen K.J., Shaw J.H.; 2010: Displacement profiles and displacement-length scaling relationships of thrust faults constrained by seismic-reflection data. GSA Bulletin 122 (7–8), 1209–1219.

Chounet A., Vallée M., Causse M., Courboulex F.; 2018: Global catalog of earthquake rupture velocities shows anticorrelation between stress drop and rupture velocity. Tectonophysics 733, 148–158.

Choy G.L., Kirby S.H.; 2004: Apparent stress, fault maturity and seismic hazard for normal-fault earthquakes. J. Geophys. Res.

Guo H., Lay T., Brodsky E.E.; 2023: Seismological indicators of geologically inferred fault maturity. J. Geophys. Res. 128.

Maesano F.E., Buttinelli M., Maffucci R., Toscani G., Basili R., Bonini L., Burrato P., Fedorik J., Fracassi, U., Panara Y., Tarabusi G., Tiberti M.M., Valensise G., Vallone R., Vannoli P.; 2023: Buried alive: imaging the 9 November 2022, Mw5.5 earthquake source on the offshore Adriatic blind thrust front of the Northern Apennines (Italy). Geophys. Res. Lett. 50 (11).

Manighetti I., Campillo M., Bouley S., Cotton F.; 2007: Earthquake scaling, fault segmentation, and structural maturity. Earth Planet. Sci. Lett. 253, 429–438.

Perrin C., Manighetti I., Ampuero J.-P., Cappa F., Gaudemer Y.; 2016: Location of largest earthquake slip and fast rupture controlled by along-strike change in fault structural maturity due to fault growth. J. Geophys. Res. 121, 3666–3685

Petracchini L., Tavani S., Brandano M., Carminati E., Chiarabba C., Conti A, Devoti R., Galli P., Palano M., Pezzo M., Scognamiglio L., Tinti E., Billi, A.; 2025: Thrust fault maturity and coseismic behavior: Insights from the 2022 Mw5. 8 Adriatic offshore earthquake. Earth and Planetary Science Letters, 669.

Acknowledgements

We gratefully acknowledge Eni S.p.A. for providing seismic reflection profiles, well logs, and GNSS data, and AleAnna Italia S.p.A. for granting permission to publish the data. Financial support from the Ministry of the Environment and Energy Security (MASE) to DST, Sapienza Università di Roma, and CNR-IGAG is also acknowledged.

Corresponding author: Lorenzo Petracchini - lorenzo.petracchini@cnr.it

Analysis of the preparatory phase of the 7 January 2025 (Mw 7.1) earthquake in Dingri, Tibet

Franco Pettenati[1], Matteo Picozzi[1,2], Denis Sandron[1], Alessandro Vuan[1,3]
[1]Istituto Nazionale di Oceanografia e di Geofisica Sperimentale – OGS, Trieste
[2]Università degli Studi di Napoli Federico II - Corso Umberto I 40 - 80138 Napoli, Italy, [3]Istituto Nazionale di Geofisica e Vulcanologia – INGV, Rome, Italy

On 7 January 2025, an earthquake of magnitude Mw 7.1 struck the Dingri region in southwestern Xizang (Tibet). Although classified as intraplate, this area is subject to complex crustal deformation associated with the India-Asia convergence. The scarcity of seismic stations near the epicentre makes it challenging to investigate the preparatory phase. To address this limitation, we analysed the continuous signal from the three components of the OGS IO.EVN station, located at the EvK2CNR Pyramid observatory south of Mount Everest, approximately 6 km from the mountain and 80 km from the earthquake epicentre. The dataset spans from January 2023 until the mainshock on 7 January 2025. The results reveal a space-time evolution consistent with a critical nucleation process, underscoring the potential of single station analysis for seismic monitoring within the Tibetan Rift Valley extensional system. When enhanced by AI techniques, single-station monitoring proves valuable for detecting early warning signs of fault activation, even in data-sparse regions.

The Tibetan Plateau is one of the most tectonically active regions in Asia (Li et al. 2025; Pietrolungo et al. 2024), characterised by normal faults that develop in response to progressive post-collisional extension and are offset by east-west strike-slip fault systems. Despite the complex fault configuration, most crustal deformation is currently concentrated along the Himalayan arc and is caused by the high rate of convergence between the Indian and Eurasian plates. The Dingri earthquake in January 2025 (Yao et al. 2025) was one of the strongest recent normal fault events in the Tibetan Plateau. Previous studies, conducted mainly on interplate events (Bouchon et al. 2013), have highlighted the importance of the nucleation phase and seismic precursors in understanding fault activation processes.

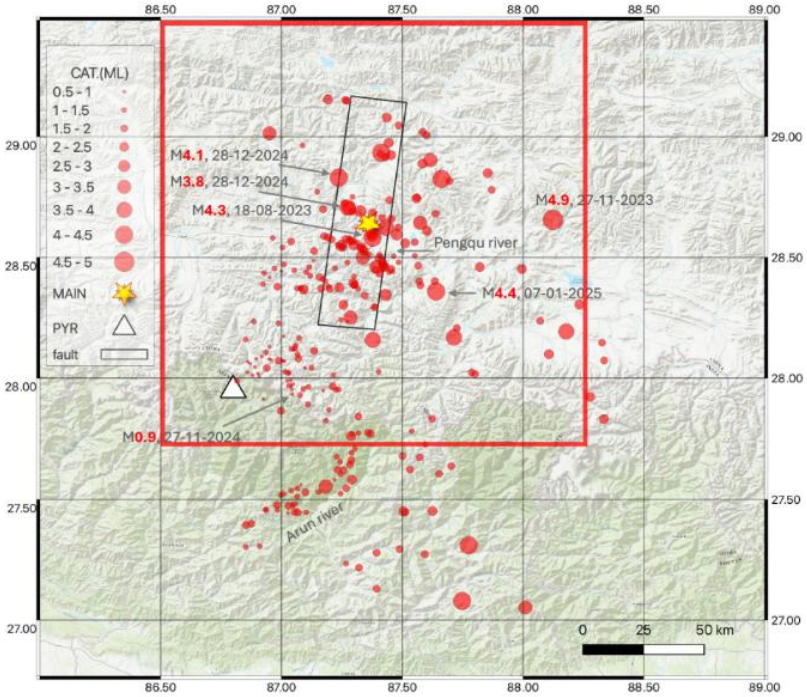

Fig. 1: Map of the 289 foreshocks identified by PhaseNet. The white triangle marks the location of the EvK2cnr pyramid (white triangle), where the IO.EVN (OGS) seismic station is installed. The yellow star indicates the epicentre.

The signal from the single IO.EVN station was processed using an automatic AI-based workflow, PhaseNet (Zhu, W. & Beroza 2019), with quality criteria based on polarisation analysis (Vidale 1986) to locate relevant events and calculate epicentral distances. This analysis produced a catalogue of 289, enabling the study of seismicity evolution before the mainshock (Fig. 1). Subsequently, a template matching procedure (Vuan 2018) was used to identify families of repetitive events. For each selected event, the seismic moment was calculated.

Several analyses were conducted. Among the most significant, the b-positive analysis (van der Elst 2021) shows stable values around 0.7 for distances greater than 30 km, with increasing values up to approximately 1.2 for events located in the epicentral area. This behaviour is consistent with an interpretation involving local weakening of the crust, possibly linked to microfracturing processes. The cumulative release of seismic moment shows continuous growth up to the mainshock (Fig. 2). The growth curve was compared with the Omori inverse (Mignan 2011) and log-logistic (Ley and Simone, 2020) models, confirming an acceleration and a progressive approach to the future epicentre starting about 45 days before the main earthquake. In particular, an ML 2.4 event on 23 November 2024, located about 26 km from the epicentre, appears to mark the beginning of an acceleration phase.

Conclusions

1. The use of an AI-based workflow and filter matching has proven useful for constructing an analysable seismic catalogue in a single-station context.

2. The data show a localised preparatory phase with three clusters and acceleration beginning in late November.

3. The increase in b+ and the inverse Omori law support a critical nucleation model.

4. The proposed approach may be useful in other remote and intraplate contexts, with implications for seismic prediction.

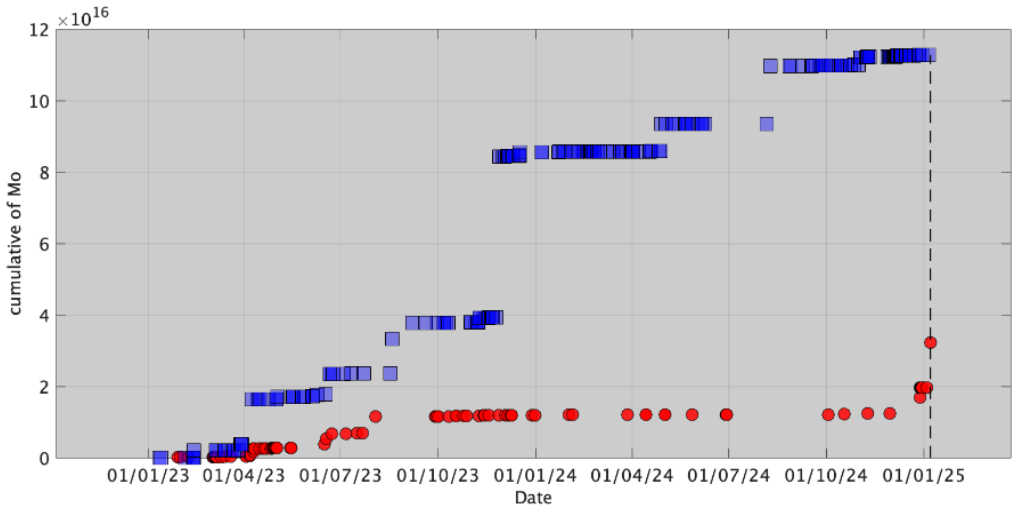

Fig. 2: development of the cumulative moment release with a radius of 70 km around the epicentre of the Dingri earthquake (within 70 km red dots, beyond 70 km blue dots).

Riferimenti

Bouchon M., Durand V., Marsan, D., Karabulut H. & Scmittbuhl J.; 2013: The long precursory phase of most large interplate earthquakes. *Nat. Geosci*. 6, 299–302. https://doi.org/10.1038/ngeo1770.

Ley C., & Simone R.; 2020: Modelling Earthquakes: Characterizing Magnitudes and Inter-Arrival Times. In A. Bekker et al. (Eds.), *Computational and Methodological Statistics and Biostatistics* (pp. 29–50). Springer. https://doi.org/10.1007/978-3-030-42196-0_2.

Li Y., Shan, X., Qu C., Zhang G., Wang X. and Xiong H.; 2025: Slip deficit rate and seismic potential on crustal faults in Tibet. *Geophys. Res. Lett.* 52, e2024GL112122. https://doi.org/10.1029/2024GL112122.

Mignan A.; 2011: Retrospective on the Accelerating Seismic Release (ASR) hypothesis: Controversy and new horizons. *Tectonophysics* 505. 1–16. https://doi.org/10.1016/j.tecto.2011.03.010.

Pettenati F., Sandron D., Verza G., Plasencia Linares M.P., Percacci R., Bistia, K. and Cravos C.; 2025: The seismic station IO.EVN at Pyramid EvK2CNR (Everest): 10 years of activity. *Seismol. Res. Lett.* 96, 1733–1746. https://doi.org/10.1785/0220240111

Pietrolungo F., Lavecchia G, Madarieta-Txurruka A., Sparacino F., Srivastava E,Cirillo C., de Nardis R., Andrenacci C., Bello S. Parrino N., Sulli A. and Palano M. 2024: Comparison of crustal stress and strain fields in the Himalaya–Tibet region: geodynamic implications. *Remote Sens.* 16, 4765. https://doi.org/10.3390/rs16244765.

van der Elst N. J.; 2021: B-positive: a robust estimator of aftershock magnitude distribution in transiently incomplete catalogs. *J. Geophys. Res. Solid Earth* 126, e2020JB021027. https://doi.org/10.1029/2020JB021027.

Vidale J.E.; 1986: Complex polarization analysis of particle motion. *Bull. Seismol. Soc. Am.* 76, 1393–1405.

Vuan A., Sugan M. Amati G. & Kato A.; 2018: Improving the Detection of Low-Magnitude Seismicity Preceding the Mw 6.3 L'Aquila Earthquake: Development of a Scalable Code Based on the Cross Correlation of Template Earthquakes. *Bull. Seism. Soc. Am*, 108 (1): 471–480. doi: https://doi.org/10.1785/0120170106.

Wu X. Yu G., Ren J., Yang X., Chen G., Xu C., Du K., Huang X., Yang H, L, K. and Hao. H. ; 2024 : The China Active Faults Database (CAFD) and its web system. *Earth Syst. Sci. Data* 16, 3391–3417. https://doi.org/10.5194/essd-16-3391-2024.

Yao J., Yao D., Chen F., Zhi M., Sun L. & Wang D.; 2025: A preliminary catalog of early aftershocks following the 7 January Mw 6.8 Dingri, Xizang earthquake. *J. Earth Sci.* XX, 1–15. https://doi.org/10.1007/s12583-025-0210-9.

Zhu W. & Beroza G.C.; 2019: PhaseNet: a deep-neural-network-based seismic arrival-time picking method. *Geophys. J. Int.* 216, 261–273. https://doi.org/10.1093/gji/ggy423.

Corresponding author: dsandron@ogs.it

A possible Kinematic Model of the Friuli Earthquake from Macroseismic data

Franco Pettenati[1], Denis Sandron[1], Paolo Harabaglia[2]
[1]Istituto Nazionale di Oceanografia e di Geofisica Sperimentale – OGS, Trieste
[2]Università degli Studi della Basilicata – via dell'Ateneo Lucano n.10 - Potenza

We propose a model that reconciles the essence of the CMT (Ekström et al. 2012) mechanism, the ISC location (https://www.isc.ac.uk/iscbulletin/search/catalogue/), and the key result of the macroseismic inversion of the Mw 6.4, 6 May 1976 earthquake by Pettenati et al. 2018.

Our model is based on macroseismic data from the CPTI15 (Rovida et al. 2022) catalogue, integrated with data from Austria (Drimmel et al. 1979) and Slovenia [ARSO Cecić (2002)], and is computed using an updated version of the kinematic function KF (Sirovich 1996; Sirovich et al. 2001). This new version allows for a rupture propagation direction different from the strike, respect the previous version. Consequently, the linear source we used also becomes progressively shallower as the rupture progresses.

We used the focal mechanism parametres of the CMT model, but we did not constraint the fault geometry, meaning that the hypocentre, fault length and fault width are free to vary. We also allowed the Mach numbers to vary freely, as well as the angle of rupture propagation, which represents the improvement in our model KF.

The interesting fact is that only our new epicentre location is similar to ISC and obviously to Pettenati et al. 2018, but the rupture propagation vector almost coincides with the strike of Pettenati et al. 2016 (Fig. 1). This because the old KF version it only provided for propagation in the direction of the strike. In the Table 1 you can see the focal mechanism parametres and the ipocentre coordinates of the two versions.

Table 1

Parametres	Pettenati et al. 2018	New version
Strike [◦]	266±10	284
Dip [◦]	53±8	18
Rake [◦]	71±11	119
Epicentre latitude [◦] N	46.38	46.40
Epicentre longitude [◦] E	13.30	13.38
Depth [km]	21.9±3.6	20

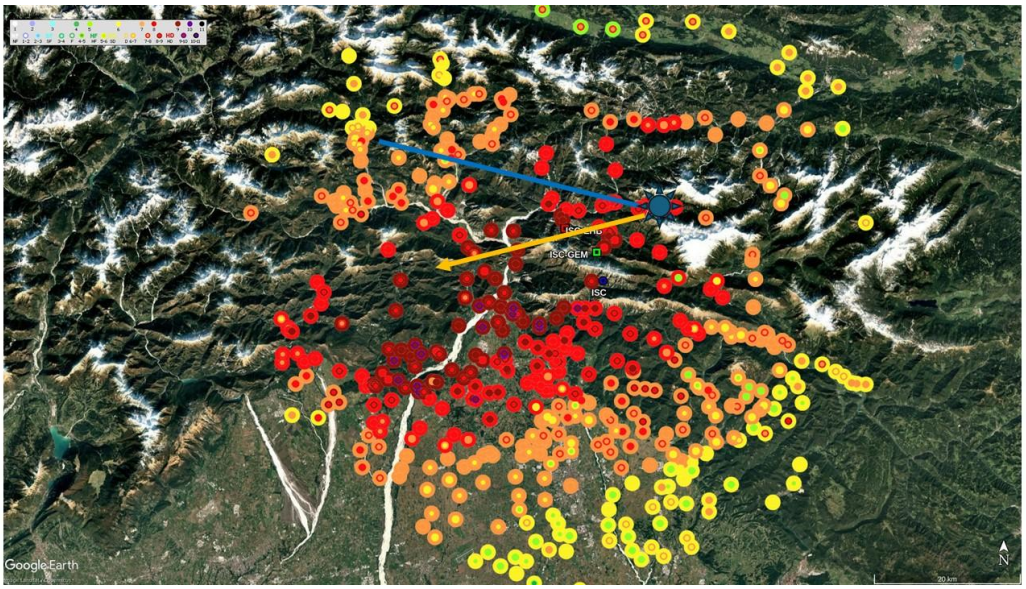

Fig. 1 – map of macroseismic intensities of Mw 6.4, 6 May 1976 earthquake. Inner dots are the observed intensities; outer portion of the dots the calculated intensities. The blue asterix is the epicentre of the inversion solution and the blue line represents the strike. The orange arrow represents the main rupture propagation.

References

Cecić I.; 2002: Potres 6 maja 1976 v Furlaniji: inventarizacija in prevrednotenje makroseizmičkih podatkov za Slovenijo. ARSO, Ljubljana, Slovenia, Internal report.

Drimmel J., Fiegweil E. and Lukeschitz G.; 1979: Die auswirkung der Friauler Beben in Österreich; makroseismische bearbeitung der starkbeben der jahre 1976/1977 samt historischem rückblick. Zentralanstalf für Metereologie und Geodynamik, Wien, Austria, Publ. n. 236, 83 pp.

Ekström G., Nettles G. M. & Dziewonski A. M.; 2012: The global CMT project 2004-2010: Centroid-moment tensors for 13,017 earthquakes, *Phys. Earth Planet. Inter.*, 200-201, 1-9, doi:10.1016/j.pepi.2012.04.002.

Pettenati F., Sirovich L. & Sandron D.; 2018: Modern techniques of treating damage patterns (intensity) to retrieve information on the 6 May 1976 M 6.4 earthquake. *Bollettino di Geofisica Teorica e Applicata,* Vol. 59, 445-462, December 2018, https://doi.org/10.4430/bgta0250.

Rovida A., Locati M., Camassi R., Lolli B. Gasperini P., Antonucci, A.; 2022: Catalogo Parametrico dei Terremoti Italiani (CPTI15), versione 4.0 [Data set]. Istituto Nazionale di Geofisica e Vulcanologia (INGV). https://doi.org/10.13127/cpti/ cpti15.4.

Sirovich L.; 1996: A simple algorithm for tracing out synthetic isoseismals. Bull. Seismol. Soc. Am., 86, 1019-1027.

Sirovich L., Pettenati F. & Chiaruttini C.; 2001: Test of Source-Parameter Inversion of Intensity Data. *Natural Hazards*, vol.**24**, 105-131, 2001, https://doi.org/10.1023/A:1011856522161.

Corresponding author: fpettenati@ogs.it

Fault-Propagation Folding and Holocene Faulting Along the 123-km-Long Kur Fault: Field Evidence from the Greater Caucasus (Azerbaijan)

G. Piccio[1], F. L. Bonali[1,2], T. Pánek[3], V. A. Bracchi[1], E. Dell'Era[1], F. Pasquarè Mariotto[4], M. Březný[3], L. Panzeri[5], A. Galli[5], A. Tibaldi[1,2]

[1] Department of Earth and Environmental Sciences, University of Milan-Bicocca, Milan, Italy
[2] CRUST-Interuniversity Center for 3D Seismotectonics with Territorial Applications, Chieti Scalo, Italy
[3] University of Ostrava, Department of Physical Geography and Geoecology, Ostrava, Czech Republic
[4] Department of Human and Innovation Sciences, Insubria University, Varese, Italy
[5] Department of Materials Science, University of Milano-Bicocca, Milan, Italy

In this work, we present the results of a field study carried out along the Holocene 123-km-long Kur Fault (Fig. 1), the frontal structure of the Plio-Quaternary Kura Fold-and-Thrust Belt (KFTB) in the Greater Caucasus (Azerbaijan) (Forte et al., 2010). The Kur Fault has been investigated through geological–structural, geomorphological, and paleontological surveys conducted along its entire length (Fig. 1B). A detailed examination of the frontal structure can: i) provide insights into the shallow propagation of a regional reverse fault, ii) enhance our understanding of the early stages of a young continent–continent collision, and iii) offer important implications for seismic hazard assessment, given that the area is seismically active and hosts some of the country's most critical energy-production infrastructures (e.g., the Shamkir Dam).

Starting from the analysis of satellite images on Google Earth, several sites of interest were identified for detailed investigation. Field studies at these sites allowed us to document deformation structures related to recent tectonic activity. Among the various observed morphostructures there are uplifted areas (including recent river deposits) with aligned scarps (Fig. 2A), triangular facets, suspended valleys and gullies, layering of Pliocene-Pleistocene deposits tilted from a few degrees to nearly vertical, and folded strata in late Pleistocene-Holocene deposits (Fig. 2C). Our work was therefore based on the collection of quantitative data and samples to better characterize the surface deformation of the fault zone and its age.

Among the various methods used to study these deformation-affected locations, DSMs and 3D models of the outcrops were created using photogrammetric techniques, the uplift of the fluvial deposits was quantified using field GPS and laser rangefinders, and finally a paleoseismological trench was opened (Fig. 2D) along a scarp of the Kur Fault identified at the Tovuz site (Fig. 2A).

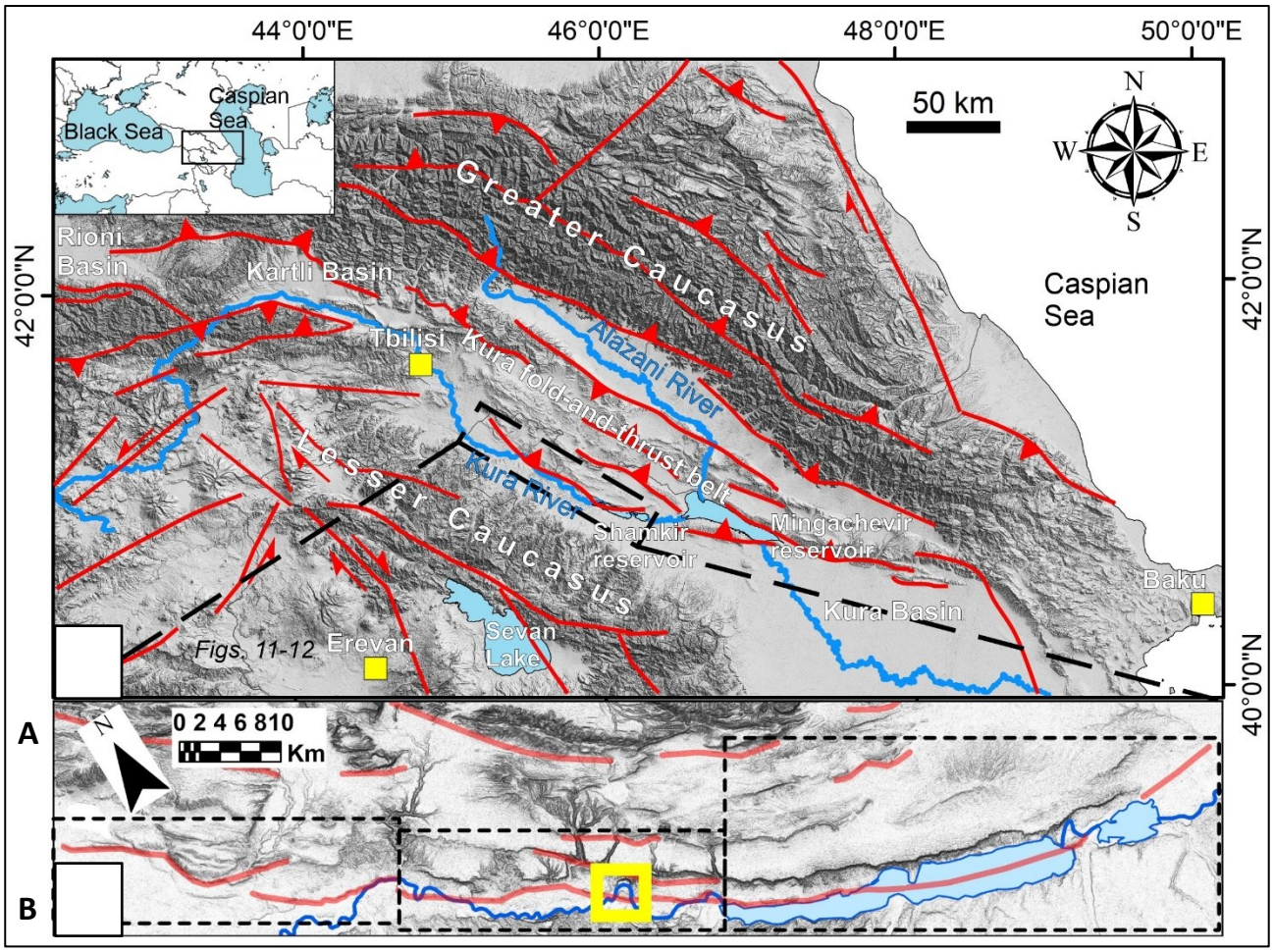

Figure 01. (A) Location of the Kura fold-and-thrust belt between the Greater and Lesser Caucasus ranges. Major Quaternary faults are shown in red, modified from Tibaldi et al. (2021). (B) Detailed structural map of the Kur Fault, showing the classification of the fault segment following Tibaldi et al. (2024). The yellow rectangle indicates the area of the Tovuz paleoseismological trench study. DEM from NASADEM (30 m) - https://lpdaac.usgs.gov/products/nasadem_hgtv001/.

On a larger scale, the shallow expression of the Kur Fault, striking WNW–ESE, consists of four main scarp segments arranged in a right-stepping pattern (Fig. 1B), each with distinct structural significance. These segments correspond to an alternation of fault-propagation folds, folds with offset frontal limbs, and shallow faulting, in agreement with Tibaldi et al. (2024). Analyses of the age of deformed deposits and landforms indicate activity up to Holocene. The outcrop of the Kur Fault shows that its orientation and pure reverse kinematics are consistent with the Holocene and present-day stress field, characterized by a N–S to NNE–SSW-trending horizontal σ_1 as confirmed by paleostress tensor obtained by kinematic indicators in Lower Pleistocene faulted deposits (Fig. 2B), suggesting the potential for seismic reactivation.

Calculations of the potential Mw of the fault, based on the length of the four fault segments, yield values in the range 6.7–7.1 following the Wells & Coppersmith (1994) relationship, and 6.6–7.2 following the Blaser et al. (2010) relationship, whereas for the entire Kur Fault the Mw is 7.5 and 7.9, respectively. The KFTB front is therefore an area of fundamental importance for seismic hazard assessment in Azerbaijan, with possible implications for the country's strategic infrastructure.

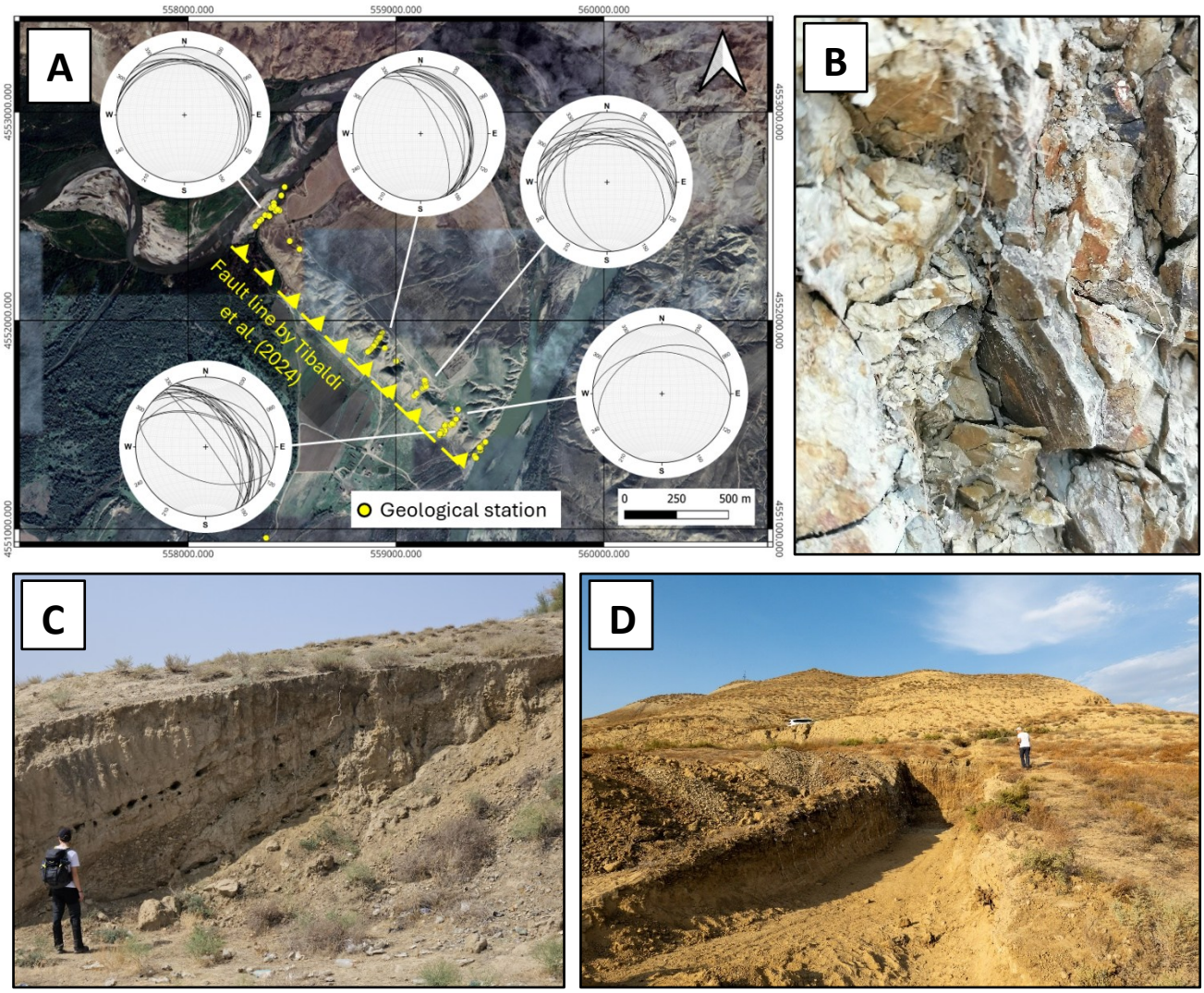

Figure 02. (A) Map of the Tovuz site, characterised by a topographic high in the fault hanging-wall block, with both topographic surface and stratigraphic bedding tilted at a low angle towards the NE. (B) Photo of a fault plane in Lower Pleistocene deposit showing striae. (C) Tilted strata representing the flank of a fold in recent deposits. (D) Photograph of the paleoseismological trench excavated perpendicular to the fault scarp.

The work was carried out entirely through field data collected during two dedicated campaigns within the framework of the NATO Project G5907 – Science for Peace and Security Programme, which focuses on geohazard assessment around the Shamkir Hydroelectric Power Station (https://shamkirproject.unimib.it/).

References

Blaser, L., Krüger, F., Ohrnberger, M., & Scherbaum, F. (2010). Scaling Relations of Earthquake Source Parameter Estimates with Special Focus on Subduction Environment. *Bulletin of the Seismological Society of America*, *100*(6), 2914–2926. https://doi.org/10.1785/0120100111

Forte, A. M., Cowgill, E., Bernardin, T., Kreylos, O., & Hamann, B. (2010). Late Cenozoic deformation of the Kura fold-thrust belt, southern Greater Caucasus. *GSA Bulletin*, *122*(3–4), 465–486. https://doi.org/10.1130/B26464.1

Tibaldi, A., Babayev, G., Bonali, F. L., Pasquaré Mariotto, F., Russo, E., Tsereteli, N., & Corti, N. (2021). Active kinematics of the greater Caucasus from seismological and GPS data: a review. Building Knowledge for Geohazard Assessment and Management in the Caucasus and other Orogenic Regions, NATO Series Book, 33-57.

Tibaldi, A., Bonali, F. L., Pasquaré Mariotto, F., Oppizzi, P., Tsereteli, N., Havenith, H., Babayev, G., & Pánek, T. (2024). Structural expression of the frontal thrust of an active fold-and-thrust belt: The Holocene 123-km-long Kur fault, Greater Caucasus, Azerbaijan. *Journal of Structural Geology*, *180*, 105085. https://doi.org/10.1016/j.jsg.2024.105085

Wells, D. L., & Coppersmith, K. J. (1994). New empirical relationships among magnitude, rupture length, rupture width, rupture area, and surface displacement. *Bulletin of the Seismological Society of America*, *84*(4), 974–1002. https://doi.org/10.1785/BSSA0840040974

Corresponding author: g.piccio@campus.unimib.it

Seismic Energy from Small Earthquakes Maps Fault Segmentation in the Southeastern Alps

M. Picozzi[1], L. Cataldi[1], A. Viganò[2], G. Ferretti[3], P. Brondi[1], D. Bindi[4], A. Magrin[1], G.D. Chiappetta[1], A.G. Iaccarino[5], D. Scafidi[3], P. Comelli[1], D. Spallarossa[3]

[1] National Institute of Oceanography and Applied Geophysics – OGS, Trieste, Italy.
[2] Servizio Geologico, Provincia autonoma di Trento, Trento, Italy
[3] DISTAV, University of Genoa, Genoa, Italy.
[4] Helmholtz Centre Potsdam, GFZ German Research Centre for Geosciences, Potsdam, Germany.
[5] University of Naples Federico II, Naples, Italy.

Fault strength spatial variability controls how earthquakes initiate, propagate, and arrest, yet remains poorly resolved in complex tectonic settings. The southeastern Alps constitute one of the most seismically hazardous regions in Central Europe, with active fault systems, a history of damaging earthquakes, and ongoing tectonic deformation. We analyze more than 9,600 small-to-moderate earthquakes ($0 \leq M_L \leq 4.5$) recorded between 2016 and 2025 to image lateral variations in crustal stress using the Energy Index (EI), a moment-energy parameter sensitive to rupture efficiency. By extending the RAMONES framework to this region, we detect pronounced east–west contrasts in fault mechanical behaviour: high EI values in the west mark zones of reduced frictional strength, whereas low EI in the east suggests mechanically stronger, segmented fault domains. These spatial patterns align with independent geophysical indicators (V_P/V_S, Q_P), indicating a strong link between mechanical segmentation, material properties, and permeability structure. Our results demonstrate that small earthquakes carry diagnostic signatures of fault-zone strength and segmentation, providing a scalable tool to resolve stress heterogeneity and refine seismic hazard models in structurally complex regions.

Corresponding author: mpicozzi@ogs.it

New hints for the seismic hazard assessment of the Venetian Prealps between Vittorio Veneto and Valdobbiadene (eastern Southern Alps, NE Italy).

M. E. Poli [1], G. Patricelli [1], G. Paiero [1], A. Marchesini [1], E. Farinatti [2]

[1] Department of Agricultural, Food, Environmental and Animal Sciences, Udine University, Italy
[2] INDAGO snc Rovigo

In the framework of the Italian Seismic Microzonation Project (Gruppo di lavoro MS, 2008), we investigated the eastern segment of the Bassano-Valdobbiadene Thrust *Auct.* (i.e. the Vittorio Veneto-Valdobbiadene segment) which runs at the base of the Venetian prealpine foothill between Miane, Follina and Cison di Valmarino municipalities (NE Italy). The Bassano-Valdobbiadene Thrust belongs to the SW-NE striking, SE-verging Neogene front of the eastern Southern Alps (Castellarin and Cantelli, 2000) which at present, accommodates deformation with velocities of the order of 2-3 mm/yr (Serpelloni et al., 2016).

According Castellarin (1981) and Antonelli et al. (1990) the Bassano Valdobbiadene Th. is segmented into three main compressive structures: the Caltrano-Bassano del Grappa (BV1 in Fig. 1), the Bassano del Grappa-Alano di Piave (BV2 in Fig. 1) and the Valdobbiadene-Vittorio Veneto (VVV in Fig. 1). Moreover, according to Costa and Doglioni (1996), the easternmost portion of the Bassano Valdobbiadene Th. gives rise to a left lateral ramp (the Longhere-Fadalto-Cadola line, LCF in Fig. 1), located in the correspondence of the NNE-SSW trending Mesozoic inherited paleogeographical boundary between the Friuli Carbonate Platform in the east and the Belluno Basin in the west (Fig. 1). The prominent geological and morphological expression (Asiago - Monte Grappa-Monte and Cesen-Monte Visentin anticlines) underlies the Neoalpine tectonic activity of the Bassano-Valdobbiadene segments. However, the Quaternary tectonic activity of VVV Th. is scarcely constrained.

Historical seismicity reveals that few destructive earthquakes (M≥5.5) hit the Venetian prealpine region. In this contest, although the BV Th. is considered a seismogenic potential structure (Barba et al., 2013), no significant seismic events affected Follina and the surrounding areas during the last millennium (Guidoboni et al., 2018, 2019; Rovida et al., 2022) (Fig. 1). To better investigate the seismotectonics of this sector of the eastern Southalpine front, we made a morphotectonic survey along the San Pietro and Soligo valleys (i.e. the Vallata valley) (Fig. 2). Moreover, in correspondence of the main morphotectonic evidence (widespread river anomalies, scarps and elongated warping of the topographic surfaces), a series of Electroresistivity Tomography (ERT) investigations were also conducted in order to constrain the fault trace. Lastly, on the bases of the preliminary results, we dug some paleoseismological trenches across the possible surficial trace of the tectonic structure.

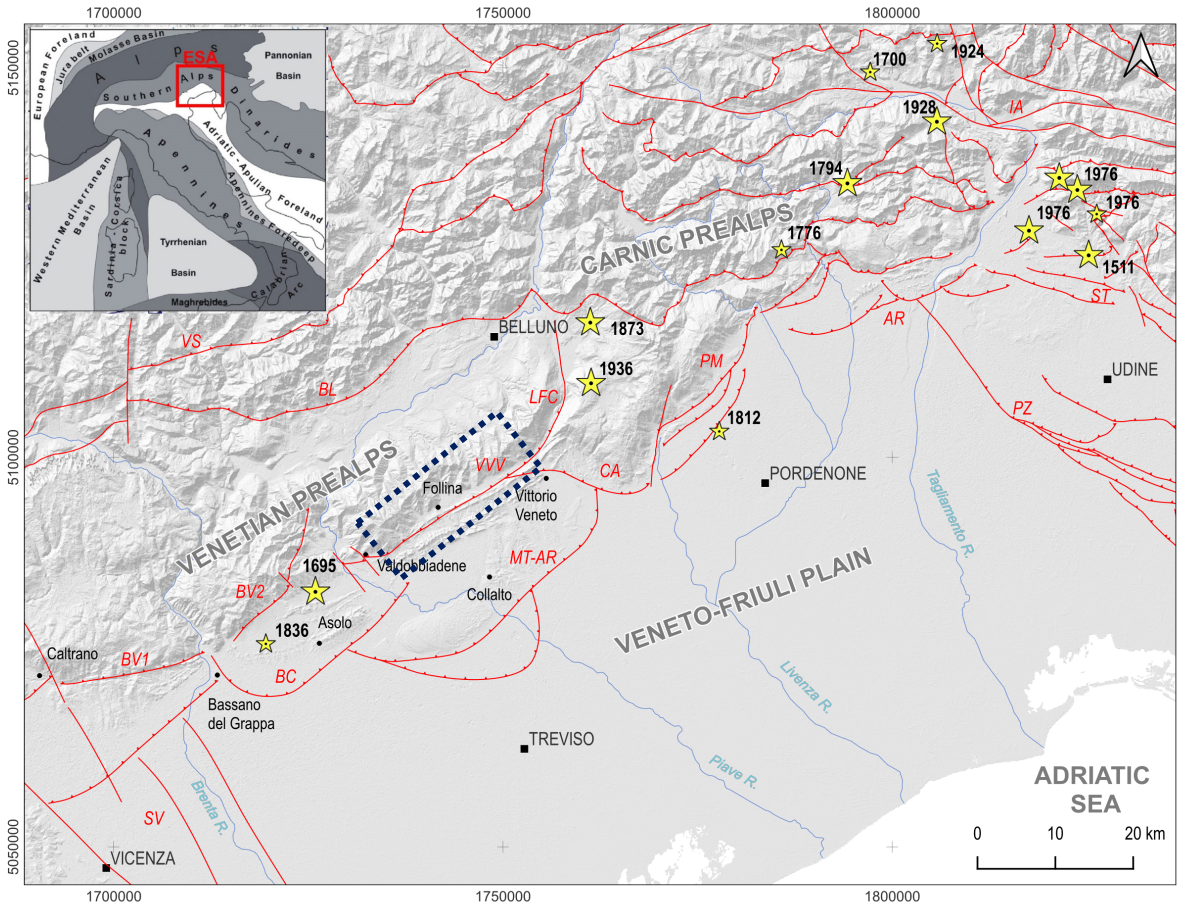

Figure 1 - Structural sketch map of the eastern Southern Alps. Yellow stars indicate the historical and instrumental M≥5.5 earthquakes that hit ESA during the last millennium (Rovida et al., 2022). Legend: AR: Arba-Ragogna Thrust system; BC: Bassano–Cornuda Thrust; BL: Belluno Th; BV1: Caltrano-Bassano del Grappa Th.; BV2: Bassano del Grappa – Alano; VVV: Valdobbiadene- Vittorio-Veneto Th.; CA: Cansiglio Th.; IA: Idrija –Ampezzo line; LCF: Longhere-Fadalto Cadola line; MT-AR: Montello-Arcade Th.; PM: Polcenigo –Montereale Th.; PZ: Pozzuolo Th.; ST: Susans-Tricesimo Th.; SV: Schio-Vicenza Fault-system; VS: Valsugana Th.

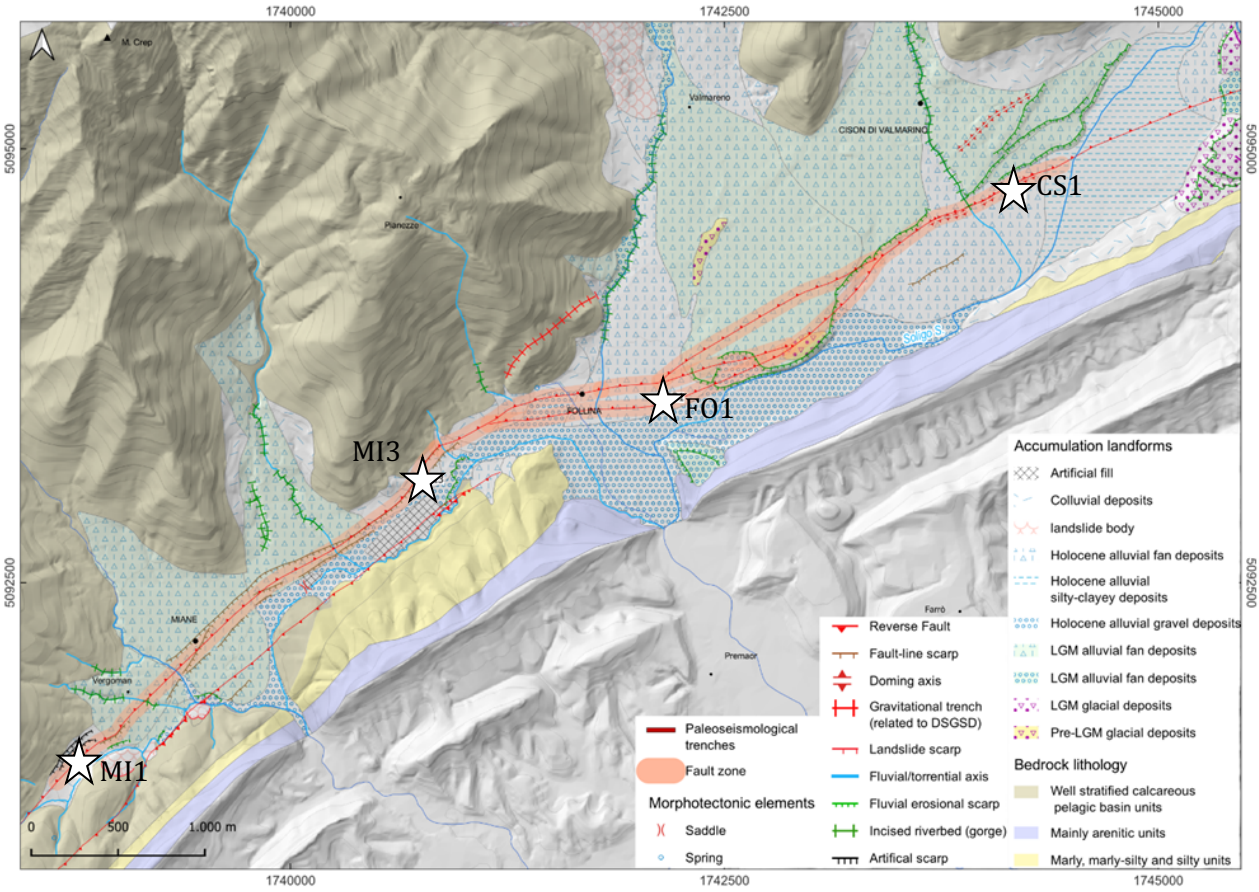

Figure 2 – Morphotectonic map of the Valdobbiadene-Vittorio Veneto thrust between Cison di Valmarino and Miane. Along the Vallata Valley, widespread river anomalies, scarps and elongated warping of the topographic surfaces underline the possible tectonic activity of the VVV Th. Stars are the paleoseismological trenches: Miane 1 (MI1), Miane 3 (MI3), Follina 1 (FO1), Cison 1 (CI1).

The results of our study pinpointed that the easternmost segment of the Bassano-Valdobbiadene Th. (i.e. Valdobbiadene -Vittorio Veneto) is an active fault, capable to generate linear morphogenic earthquakes. Particularly, the paleoseismological analysis highlighted that the last seismic event referable to the investigated structure occurred during the High-Middle Age (XII-XIV century). The observed displacement *per event* ranges from 24 to 35 cm corresponding to a possible earthquake with $6.2<Mw<6.4$ (Wells and Coppersmith, 1994). Moreover, paleoseismological analysis highlighted that the study area was affected by other seismic events, even during the Bronze Age. These data provide new important seismotectonic hints, which have to be considered in order to re-evaluate the seismic hazard of the Venetian Prealpine region, characterized by high population and industrial density.

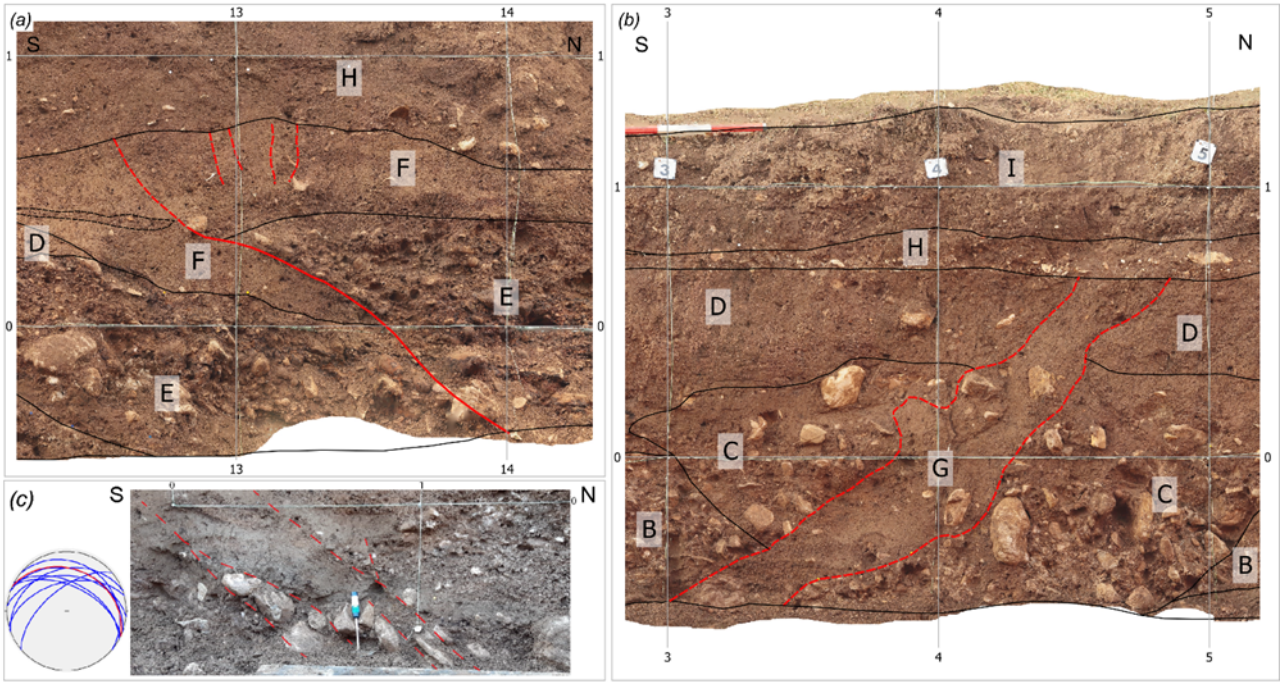

Figure 3 – Particular of Follina 1 trench: (a) S-verging reverse fault plane displacing historical units E, F and D between sections 12-14. Fault is sealed by unit H; (b) paleoliquefaction dike filled by massive sands crossing units B, C and D; (c) aligned clasts marking the S-verging shear zone in the southern portion of the wall. In the left the stereographic plot of the shear planes.

References

Antonelli, R., Barbieri, G., Dal Piaz, G.V., Dal Pra, A., De Zanche, V., Grandesso, P., Mietto, P., Sedea, R. & Zanferrari A. (1990) - Carta geologica del Veneto 1:250.000. Regione Veneto, Segreteria Regionale per il Territorio, Università di Padova, 31 pp.

Barba S., Finocchio D., Sikdar &., Burrato P. (2013) - Modelling the interseismic deformation of a thrust system: seismogenic potential of the Southern Alps. Terra Nova 25, 221–227. http://dx.doi.org/10.1111/ter.12026.Castellarin (1981)

Castellarin A. (a cura di) (1981) – Carta tettonica delle Alpi Meridionali alla scala 1:200.000. CNR Progetto Finalizzato Geodinamica. Pubblicazione n. 441 del Progetto Finalizzato Geodinamica.

Castellarin A. and Cantelli L. (2000) - Neo-Alpine evolution of the Southern Eastern Alps. J. Geodyn., 30, 251-274.

Costa V. & Doglioni C. (1996) – Note illustrative della Carta Geologica d'Italia, alla scala 1:50000. Foglio Belluno. Servizio Geologico d'Italia. Istituto Poligrafico dello Stato, pagg. 4-15.

Gruppo di lavoro MS, 2008. Indirizzi e criteri per la microzonazione sismica. Conferenza delle Regioni e delle Province autonome - Dipartimento della protezione civile, Roma, 3 vol. e Dvd.

Guidoboni E., Ferrari G., Mariotti D., Comastri A., Tarabusi G., Sgattoni G., Valensise G. (2018) - CFTI5Med, Catalogo dei Forti Terremoti in Italia (461 a.C.-1997) e nell'area Mediterranea (760 a.C.-1500). Istituto Nazionale di Geofisica e Vulcanologia (INGV). https://doi.org/10.6092/ingv.it-cfti5

Guidoboni E., Ferrari G., Tarabusi G., Sgattoni G., Comastri A., Mariotti D., Ciuccarelli C., Bianchi M.G., Valensise G. (2019), CFTI5Med, the new release of the catalogue of strong earthquakes in Italy and in the Mediterranean area, Scientific Data 6, Article number: 80 (2019). https://doi.org/10.1038/s41597-019-0091-9

Rovida A., Locati M., Camassi R., Lolli B., Gasperini P., Antonucci A. (2021). Catalogo Parametrico dei Terremoti Italiani (CPTI15), versione 3.0. Istituto Nazionale di Geofisica e Vulcanologia (INGV). https://doi.org/10.13127/CPTI/CPTI15.3

Serpelloni E., Vannucci G., Anderlini L. and Bennett R.A. (2016) - Kinematics, seismotectonics and seismic potential of the eastern sector of the European Alps from GPS and seismic deformation data. Tectonophysics, 688, 157-181.

Wells, D.L., Coppersmith, K.J. (1994) - New empirical relationships among magnitude, rupture length, rupture width, rupture area, and surface displacement. Bull. Seism. Soc. Am., 84, 4, 974-1002.

Corresponding author: eliana.poli@uniud.it

Towards Near Real-Time 1D Nonlinear Ground Response Modeling in NorthEastern Italy

Mehdi R. Foumeshi[1], Elisa Zuccolo[2], Carla Barnaba[2], Fabian Bonilla[3], Srihari Sangaraju[4] , Angelo Carini [1]

[1] DICATAM, Universitá degli Studi di Brescia, Via Branze 43, 25123 Brescia, Italy
[2] National Institute of Oceanography and Applied Geophysics- OGS, Sgonico, Trieste, Italy
[3] Geotechnical Engineering, Environment, Natural Hazards and Earth Sciences Department, Université Gustave Eiffel, Marne-La-Vallée, 77447, France
[4] Earthquake Engineering and Geophysics, Grenoble INP–UGA, Université Grenoble Alpes, Grenoble, France.

The destructive 1976 Friuli earthquake, which produced marked variations in the ground shaking intensity across short distances, underscored the critical influence of local soil and geological conditions on seismic ground motion. Motivated by these observations, this study aims at including one-dimensional nonlinear ground response analyses in the system for near real-time physics-based ground shaking simulations currently under testing in NorthEastern Italy (UrgentShake, Zuccolo et al., 2025). The site response modeling framework incorporates detailed geological and geotechnical information, including sediment stratigraphy, soil stiffness profiles, and shear-wave velocity distributions, which are essential in defining representative subsurface models. A suite of 1D broadband synthetic seismograms associated with sample events that occurred in North-Eastern Italy was computed at the locations of the recording seismic stations. Each station was associated with a representative one-dimensional stratigraphic soil column derived from a subdivision of the regional territory into several polygons. This subdivision was performed to account for spatial variability in geological and geotechnical conditions, including different shear-wave velocity profiles and sediment thicknesses ranging from 0 to approximately 800 m. Each polygon was modeled as an independent one-dimensional soil column implemented within the NOAH code (Bonilla, 2001). The simulated ground motions were compared with the recordings in order to assess the strengths and limitations of the methodology and its suitability for future near–real-time applications.

References

Bonilla L.F.; 2001: NOAH: User's Manual, Institute for Crustal Studies. University of California, Santa Barbara, USA, Institut de Radioprotection et de Sureté Nucléaire, France

Zuccolo, E., Bolzon, G., Pitari, F., Rodríguez Muñoz, L., Scaini, C., Vanini, M., Poggi, V., Salon, S.; 2025: Advancing rapid response to earthquakes with tiered physics-based ground-shaking simulations: The UrgentShake system. Seismological Research Letters, 96(5), 2995–3011. https://doi.org/10.1785/0220240472

Corresponding author: mehdi.ramezanpourfoumeshi@unibs.it

Multi-technique SAR Coseismic Deformation Retrieval and Fault Modeling of the 2025 Mw 7.7 Myanmar Earthquake

Valerio Ruocco[1,2], Silvia Puliero[2], Simone Atzori[2], Cristiano Tolomei[2], Andrea Antonioli[2], Marco Polcari[2], Matteo Albano[2], Marco Moro[2], Salvatore Stramondo[2], Michele Saroli[1,2], Pasquale Striano[3], Fernando Monterroso[3], Manuela Bonano[3], Francesco Casu[3], Claudio De Luca[3], Riccardo Lanari[3].

[1]DICeM - Università degli Studi di Cassino e del Lazio meridionale, Cassino, Italy.
[2]Istituto Nazionale di Geofisica e Vulcanologia, Rome, Italy.
[3]Istituto per il Rilevamento Elettromagnetico dell'Ambiente, Consiglio Nazionale delle Ricerche (IREA-CNR), Naples-Milan, Italy.

Introduction

On 28 March 2025 at 06:20 UTC, a major earthquake of Mw 7.7 occurred in central Myanmar, with its epicenter located along the central segment of the Sagaing Fault, one of the main tectonic structures in Southeast Asia (Bradley & Hubbard, 2025; Vera et al., 2025). The event, characterized by a shallow hypocenter (~10 km), generated intense ground shaking (Modified Mercalli Intensity IX) in densely populated areas, causing significant casualties and widespread infrastructural damage. Effects were felt at distances exceeding 1000 km from the epicentral area, likely related to local seismic amplification controlled by geological conditions (Shahzada et al., 2025). The rupture propagated for approximately 90 s along a ~490 km fault segment, suggesting supershear dynamics, as confirmed by teleseismic data (Vera et al., 2025; Melgar et al., 2025). Twelve minutes after the mainshock, an Mw 6.7 aftershock occurred, likely triggered by static stress changes induced by the main event (USGSa, 2025).

Tectonic Setting

Myanmar is located within a complex tectonic collision zone between the southeastern margin of the Eurasian Plate and the Indian Plate (Mitchell et al., 2012; Tha Zin Htet Tin et al., 2022). The major right-lateral strike-slip Sagaing Fault, extending over 1200 km with a predominantly N–S orientation, accommodates a significant portion of the relative motion between the Burma and Sunda plates, with slip rates estimated at approximately 20 mm/year in the central sections (Vigny et al., 2003; Socquet et al., 2006; Wang et al., 2014; Tha Zin Htet Tin et al., 2022). The area affected by the 2025 earthquake coincides with a known seismic gap identified by previous geological and seismotectonic studies, suggesting long-term elastic strain accumulation and partial rupture of this gap (Hurukawa & Maung Maung, 2011; Bradley & Hubbard, 2025) (Fig.1).

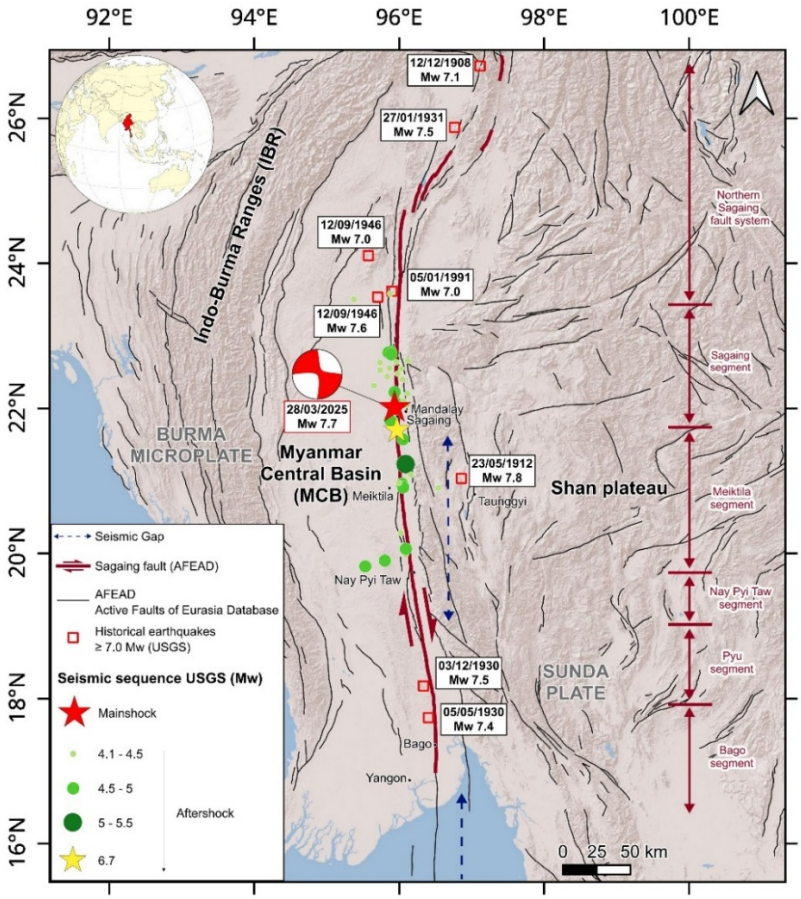

Fig.1 – Overview of the geographical setting and seismicity of the Myanmar area. The focal mechanism of the mainshock is shown together with the aftershocks and the historical earthquakes (USGS, 2025). The active faults are part of the Active Faults of Eurasia Database (AFEAD) (Zelenin et al., 2022). Fault segmentation is based on the classification proposed by Wang et al. (2014). The illustrated seismic gaps refer to the study by Hurukawa and Maung Maung (2011).

Data and Methods

Coseismic deformation associated with the Mw 7.7 event was reconstructed through the integration of SAR Sentinel-1-based techniques: Pixel Offset Tracking (POT) (Gray et al., 1998; Casu et al., 2010, 2011), Multiple Aperture Interferometry (MAI) (Bechor & Zebker, 2006; Jiang et al., 2017), and Interferometric Synthetic Aperture Radar (InSAR) (Massonnet et al., 1993; Massonnet & Feigl, 1998). This integrated approach was crucial to constrain horizontal displacement components, particularly the predominant N–S motion, which is nearly imperceptible with conventional InSAR. Data inversion was conducted in two steps: a nonlinear inversion to estimate the source location, depth, geometry, and rupture mechanism (Okada, 1985; Williams & Wadge, 1998; Atzori et al., 2009), followed by a linear inversion to reconstruct the slip distribution and orientation along the fault (Atzori & Antonioli, 2011; Atzori et al., 2019). A Coulomb Failure Function (ΔCFF) analysis was also performed to assess the interaction between the mainshock and the Mw 6.7 aftershock (Stein et al., 1992; Simpson & Reasemberg, 1994; Harris, 1998).

Results and Discussion

Results show a surface deformation field consistent with right-lateral strike-slip motion along an almost vertical structure, with horizontal displacements reaching ~5 m along the fault trace. Maximum slip occurs in the central segment, corresponding to the seismic gap (Hurukawa &

Maung Maung, 2011). The rupture is confined to the upper 15–20 km of the crust and extends for ~490 km, consistent with supershear propagation (Walker & Shearer, 2009; Petersen et al., 2023; Zeng et al., 2025; Melgar et al., 2025; Vera et al., 2025;) (Fig. 2). Finally, the performed ΔCFF analysis supports the hypothesis that the Mw 6.7 aftershock was triggered by static stress changes (a strong positive static stress transfer, with values up to 1.9 MPa) induced by the mainshock through rupture propagation and stress concentration along the fault system.

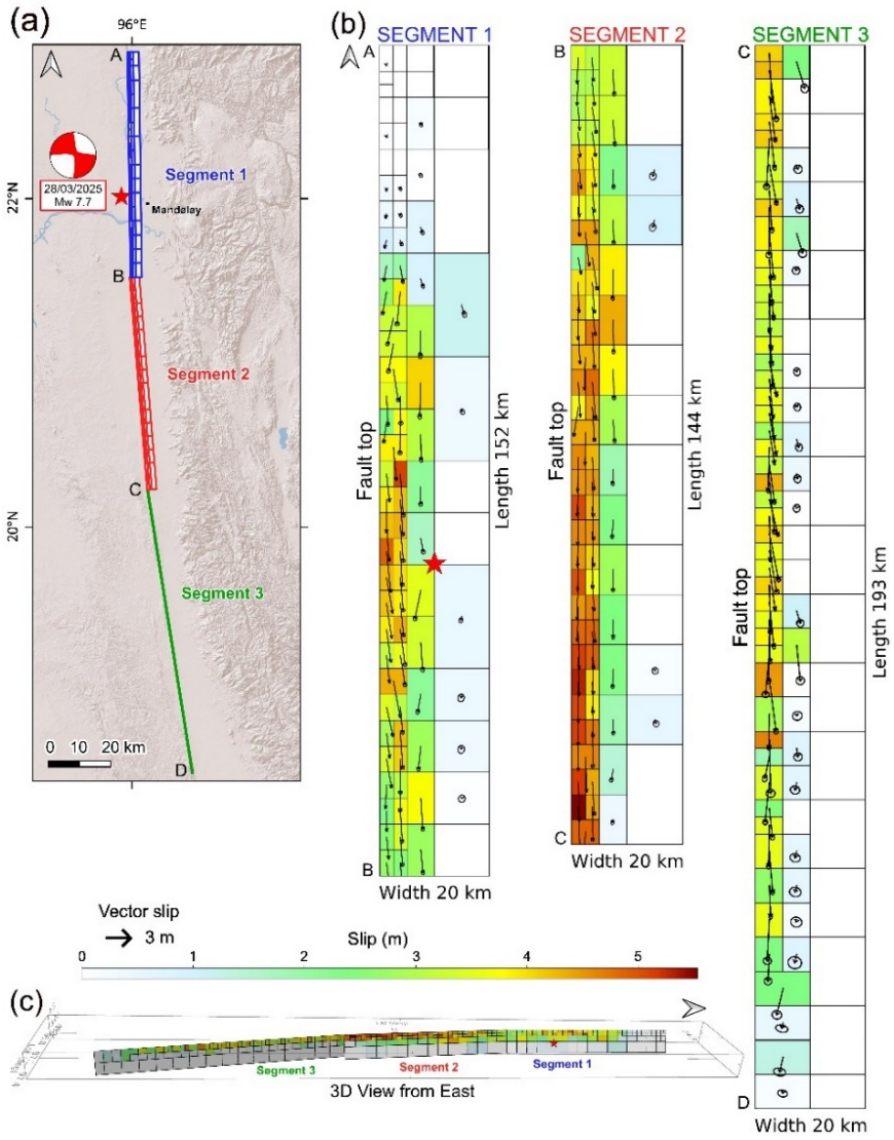

Fig.2 – Modeling of the three segments with the corresponding slip distribution derived from the inversion of InSAR data. (a) The 2D map view; (b) the slip distribution of each segment, in the strike/dip reference system, with associated 1-sigma uncertainties, represented by ellipses for each cell; (c) the 3D view from the east.

Conclusions

The 2025 Mw 7.7 Myanmar earthquake was one of the most significant seismic events in Southeast Asia over the past century. The combined use of different Sentinel-1 datasets enabled full spatial coverage of the rupture extent and a robust characterization of the seismogenic source, including its slip distribution. The results provide new constraints on fault kinematics and

segmentation, as well as insights into stress transfer and aftershock triggering mechanisms, with important implications for seismic hazard assessment in the region.

References

Atzori, S., Hunstad, I., Chini, M., Salvi, S., Tolomei, C., Bignami, C., Stramondo, S., Trasatti, E., Antonioli, A., & Boschi, E. (2009). Finite fault inversion of DInSAR coseismic displacement of the 2009 L'Aquila earthquake (central Italy). *Geophysical Research Letters*, *36*(15). https://doi.org/https://doi.org/10.1029/2009GL039293

Atzori, S., & Antonioli, A. (2011). Optimal fault resolution in geodetic inversion of coseismic data. *Geophysical Journal International*, *185*(1), 529–538. https://doi.org/10.1111/j.1365-246X.2011.04955.x.

Atzori, S., Antonioli, A., Tolomei, C., De Novellis, V., De Luca, C., & Monterroso, F. (2019). InSAR full-resolution analysis of the 2017–2018 M>6 earthquakes in Mexico. *Remote Sensing of Environment*, *234*, 111461. https://doi.org/https://doi.org/10.1016/j.rse.2019.111461.

Bechor, N. B. D., & Zebker, H. A. (2006). Measuring two-dimensional movements using a single InSAR pair. *Geophysical Research Letters*, *33*(16). https://doi.org/https://doi.org/10.1029/2006GL026883.

Bradley, K., & Hubbard, J. A. (2025). Updates on the M7.7 Myanmar earthquake. *Earthquake Insights*. https://doi.org/10.62481/9e49eb4a.

Casu, F., Manconi, A., Pepe, A., Manzo, M., & Lanari, R. (2010). Advances in the generation of deformation time series from SAR data sequences in areas affected by large dynamics. *2010 IEEE International Geoscience and Remote Sensing Symposium*, 2618–2621. https://doi.org/10.1109/IGARSS.2010.5651926.

Casu, F., Manconi, A., Pepe, A., & Lanari, R. (2011). Deformation Time-Series Generation in Areas Characterized by Large Displacement Dynamics: The SAR Amplitude Pixel-Offset SBAS Technique. *IEEE Transactions on Geoscience and Remote Sensing*, *49*(7), 2752–2763. https://doi.org/10.1109/TGRS.2010.2104325.

Gray, A. L., Mattar, K. E., Vachon, P. W., Bindschadler, R., Jezek, K. C., Forster, R., & Crawford, J. P. (1998). InSAR results from the RADARSAT Antarctic Mapping Mission data: estimation of glacier motion using a simple registration procedure. *IGARSS '98. Sensing and Managing the Environment. 1998 IEEE International Geoscience and Remote Sensing. Symposium Proceedings. (Cat. No.98CH36174)*, *3*, 1638–1640 vol.3. https://doi.org/10.1109/IGARSS.1998.691662.

Harris, R. A. (1998). Introduction to Special Section: Stress Triggers, Stress Shadows, and Implications for Seismic Hazard. *Journal of Geophysical Research: Solid Earth*, *103*(B10), 24347–24358. https://doi.org/https://doi.org/10.1029/98JB01576.

Hurukawa, N., & Maung Maung, P. (2011). Two seismic gaps on the Sagaing Fault, Myanmar, derived from relocation of historical earthquakes since 1918. *Geophysical Research Letters*, *38*(1). https://doi.org/https://doi.org/10.1029/2010GL046099.

Jiang, H., Feng, G., Wang, T., & Bürgmann, R. (2017). Toward full exploitation of coherent and incoherent information in Sentinel-1 TOPS data for retrieving surface displacement: Application to the 2016 Kumamoto (Japan) earthquake. *Geophysical Research Letters*, 44(4), 1758–1767. https://doi.org/10.1002/2016gl072253.

Massonnet, D., Rossi, M., Carmona, C., Adragna, F., Peltzer, G., Feigl, K., & Rabaute, T. (1993). The displacement field of the Landers earthquake mapped by radar interferometry. *Nature*, *364*(6433), 138–142. https://doi.org/10.1038/364138a0.

Massonnet, D., & Feigl, K. L. (1998). Radar interferometry and its application to changes in the Earth's surface. *Reviews of Geophysics*, *36*(4), 441–500. https://doi.org/https://doi.org/10.1029/97RG03139.

Melgar, D., Weldon, R., Wang, Y., Bato, M. G., Aung, L. T., Shi, X., Wiwegwing, W., Khaing, S. N., Min, S., Thant, M., Speed, C., Zinke, R., Fielding, E., Meltzner, A., & Dawson, T. (2025). Supershear source model of the 2025 M7.8 Myanmar earthquake and paleoseismology of the Sagaing Fault: regions of significant overlap with past earthquakes. Seismica, 4(2). https://doi.org/10.26443/seismica.v4i2.1771.

Mitchell, A., Chung, S.-L., Oo, T., Lin, T.-H., & Hung, C.-H. (2012). Zircon U–Pb ages in Myanmar: Magmatic–metamorphic events and the closure of a neo-Tethys ocean? *Journal of Asian Earth Sciences*, *56*, 1–23. https://doi.org/https://doi.org/10.1016/j.jseaes.2012.04.019.

Okada, Y. (1985). Surface deformation due to shear and tensile faults in a half-space. *Bulletin of the Seismological Society of America*, *75*(4), 1135–1154. https://doi.org/10.1785/BSSA0750041135.

Petersen, G. M., Büyükakpinar, P., Vera Sanhueza, F. O., Metz, M., Cesca, S., Akbayram, K., Saul, J., & Dahm, T. (2023). The 2023 Southeast Türkiye Seismic Sequence: Rupture of a Complex Fault Network. *The Seismic Record*, 3(2), 134–143. https://doi.org/10.1785/0320230008.

Shahzada, K., Noor, U. A., & Xu, Z.-D. (2025). In the wake of the March 28, 2025 Myanmar earthquake: A detailed examination. *Journal of Dynamic Disasters*, *1*(2), 100017. https://doi.org/https://doi.org/10.1016/j.jdd.2025.100017.

Simpson, R. W., & Reasemberg, P. A. (1994). Earthquake-induced static stress changes on central California faults. *U. S. Geol. Surv. Profess Pap. 1550-F*, *F55–F89*.

Socquet, A., Vigny, C., Chamot-Rooke, N., Simons, W., Rangin, C., & Ambrosius, B. (2006). India and Sunda plates motion and deformation along their boundary in Myanmar determined by GPS. *Journal of Geophysical Research: Solid Earth*, *111*(B5). https://doi.org/https://doi.org/10.1029/2005JB003877.

Stein, R. S., King, G. C. P., & Lin, J. (1992). Change in Failure Stress on the Southern San Andreas Fault System Caused by the 1992 Magnitude = 7.4 Landers Earthquake. *Science*, *258*(5086), 1328–1332. https://doi.org/10.1126/science.258.5086.1328.

Tha Zin Htet Tin, Nishimura, T., Hashimoto, M., Lindsey, E. O., Aung, L. T., Min, S. M., & Thant, M. (2022). Present-day crustal deformation and slip rate along the southern Sagaing fault in Myanmar by GNSS observation. *Journal of Asian Earth Sciences*, *228*, 105125. https://doi.org/https://doi.org/10.1016/j.jseaes.2022.105125.

USGS (2025). *M 7.7 - 2025 Mandalay, Burma (Myanmar) Earthquake*. https://earthquake.usgs.gov/earthquakes/eventpage/us7000pn9s/executive.

Vera, F., Carrillo-Ponce, A., Crosetto, S., Kosari, E., Metzger, S., Motagh, M., Liang, Y., Lyu, S., Petersen, G., Saul, J., Sudhaus, H., Symmes-Lopetegui, B., Than, O., Xiao, H., & Tilmann, F. (2025). *Supershear Rupture Along the Sagaing Fault Superhighway: The 2025 Myanmar Earthquake*. https://doi.org/10.22541/essoar.175034871.19414276/v1.

Vigny, C., Socquet, A., Rangin, C., Chamot-Rooke, N., Pubellier, M., Bouin, M.-N., Bertrand, G., & Becker, M. (2003). Present-day crustal deformation around Sagaing fault, Myanmar. *Journal of*

Geophysical Research: Solid Earth, *108*(B11). https://doi.org/https://doi.org/10.1029/2002JB001999.

Walker, K. T., & Shearer, P. M. (2009). Illuminating the near-sonic rupture velocities of the intracontinental Kokoxili Mw 7.8 and Denali fault Mw 7.9 strike-slip earthquakes with global P wave back projection imaging. *Journal of Geophysical Research: Solid Earth*, *114*(B2). https://doi.org/https://doi.org/10.1029/2008JB005738.

Wang, Y., Sieh, K., Tun, S. T., Lai, K.-Y., & Myint, T. (2014). Active tectonics and earthquake potential of the Myanmar region. *Journal of Geophysical Research: Solid Earth*, *119*(4), 3767–3822. https://doi.org/https://doi.org/10.1002/2013JB010762.

Williams, C. A., & Wadge, G. (1998). The effects of topography on magma chamber deformation models: Application to Mt. Etna and radar interferometry. *Geophysical Research Letters*, *25*(10), 1549–1552. https://doi.org/https://doi.org/10.1029/98GL01136.

Zelenin, E., Bachmanov, D., Garipova, S., Trifonov, V., & Kozhurin, A. (2022). The Active Faults of Eurasia Database (AFEAD): the ontology and design behind the continental-scale dataset. *Earth System Science Data*, *14*(10), 4489–4503. https://doi.org/10.5194/essd-14-4489-2022.

Zeng, H., Ma, Z., Li, C., Yin, X., Jiang, Y., Chen, Y., Rosakis, A., Konca, O., & Wei, S. (2025). Super-Shear and Generalized Rayleigh Rupture of the 2023 Turkey Earthquake Doublet Influenced by Fault Material Contrast. *Journal of Geophysical Research: Solid Earth*, 130(6). https://doi.org/10.1029/2025jb031560.

Corresponding author: valerio.ruocco@studentmail.unicas.it

Reconciling advanced detection techniques on different monitoring scales: from dense monitoring infrastructures to DAS

F. Scotto di Uccio[1], A. Scala[1,2], C. Strumia[1], M. Picozzi[1,3], T. Muzellec[1], G. De Landro[1], G. Beroza[3], G. Festa[1,5]

[1] Dipartimento di Fisica Ettore Pancini, Università degli Studi di Napoli Federico II, Naples, Italy
[2] Istituto Nazionale di Geofisica e Vulcanologia (INGV), Sezione Osservatorio Vesuviano, Napoli, Italy
[3] National Institute of Oceanography and Applied Geophysics, Center for Seismological Research, Udine, Italy
[4]Department of Geophysics, Stanford University, Stanford, USA
[5] Istituto Nazionale di Geofisica e Vulcanologia (INGV), Sezione Osservatorio Nazionale Terremoti, Roma, Italy

Microseismicity continuously occurs along the seismogenic structures that can also host larger, destructive earthquakes. Therefore, its characterization can potentially provide crucial information on the geometry and mechanical state of the underlying faults, before the occurrence of notable events. However, conventional catalogs are limited in size, since many small events are hidden in the noise. Therefore, discovering such events calls for advances in both earthquake detection techniques and monitoring infrastructures. Dense permanent multidisciplinary observatories have been deploying near active seismogenic areas (Near-Fault Observatories, NFO, Chiaraluce et al. 2022) and target the identification and characterization of small-magnitude events, lowering the detection threshold down to $\sim$ Ml 1. Temporary experiments involving stations organized in dense arrays, with aperture of few hundred meters have been proposed to further decrease this threshold. Moreover, the progressive adoption of fiber optic systems for seismological purposes, enables continuous recording of the seismic wavefield with a novel decametric resolution, potentially offering a significantly larger number of observations for earthquake characterization (Strumia et al., 2024, Baillet et al., 2025). To fulfil the continuous growth and complexity of the recorded seismic measurements, advanced machine learning models and similarity-based approaches have been developed to systematically identify low-magnitude earthquakes, reconciling the needing of efficient and reliable strategies.

In this work, we apply innovative strategies for the identification of low-magnitude events occurring within the Irpinia Near-Fault Observatory (Southern Italy, Iannaccone et al. 2010), which

monitors the area struck by the destructive 1980 M6.9 Irpinia earthquake. This monitoring infrastructure collects high-resolution seismic observations, progressively moving from the kilometric scale of the permanent seismic network (ISNet) to the decametric resolution offered by two Distributed Acoustic Sensing (DAS) systems deployed in the area.

We showcase how the integration of machine learning (Zhu & Beroza, 2019; Mousavi et al. 2020) and similarity-based (Chamberlain et al., 2018) detection techniques can increase the content of seismic catalogs both for background seismicity and seismic sequences, up to one order of magnitude as compared to conventional manual catalogs. In this framework, machine learning models provide an enhanced set of events as compared to the standard catalog, which can be used as templates to effectively detect lower magnitude, collocated events, also with a short interevent time. The location of the earthquakes in the enhanced catalog revealed the activated fault patches, while the determination of source properties enabled the definition of evolutive models for the seismic sequences (Scotto di Uccio et al. 2023; 2024). We confirmed the effectiveness of the integrated detection strategy within the framework of the DETECT experiment, consisting in the installation of 200 stations in dense arrays in the area for one year. We demonstrated the possibility to consistently detect small magnitude earthquakes with the use of short-term dense arrays and established machine learning models, whose integration with template matching approaches lowers the magnitude of completeness of seismic catalogs down to M 0. This also results in higher percentage (65%) of accurately relocated hypocenters as compared with conventional networks. The new DETECT catalog enables to downscale the seismicity characteristics to small, decametric-size events, illuminating active seismogenic structures capable to generate events up to M 7.

To exploit the novel resolution offered by DAS systems, we finally explored the exportation of established single-station machine learning models for the identification of P and S waves on native DAS records. We highlight the possibility to apply existing models for the recognition of phase arrival times on DAS records, with reliable arrival times that can be followed with spatial continuity on the fiber. We integrated machine learning models for an automatic characterization of the earthquakes recorded by the DAS systems operating in the Irpinia region, tackling earthquake detection, phase association and local magnitude estimation.

Acknowledgments

We thank Giovanni Camanni, Francesco Carotenuto, Lauro Chiaraluce, Nicola D'Agostino, Luca Elia, Maddalena Michele, Mariano Supino and Aldo Zollo for their contribution to modelling and interpretation of some of the results.

References

Baillet, M., Rivet, D., Trabattoni, A., Cheze, J., Peix, F., Ambrois, D., ... & Barrientos, S. (2025). Automatic earthquake catalogs from a permanent DAS offshore network. Journal of Geophysical Research: Solid Earth, 130(10), e2025JB031565.

Chamberlain, C. J., Hopp, C. J., Boese, C. M., Warren-Smith, E., Chambers, D., Chu, S. X., ... & Townend, J. (2018). EQcorrscan: Repeating and near-repeating earthquake detection and analysis in Python. Seismological Research Letters, 89(1), 173-181.

Chiaraluce, L., Festa, G., Bernard, P., Caracausi, A., Carluccio, I., Clinton, J. F., ... & Sokos, E. (2022). The Near Fault Observatory community in Europe: a new resource for faulting and hazard studies. Annals of Geophysics, 65(3), DM316.

Iannaccone, G., Zollo, A., Elia, L., Convertito, V., Satriano, C., Martino, C., ... & Emolo, A. (2010). A prototype system for earthquake early-warning and alert management in southern Italy. Bulletin of Earthquake Engineering, 8(5), 1105-1129.

Mousavi, S. M., Ellsworth, W. L., Zhu, W., Chuang, L. Y., & Beroza, G. C. (2020). Earthquake transformer—an attentive deep-learning model for simultaneous earthquake detection and phase picking. Nature communications, 11(1), 3952.

Scotto di Uccio, F., Scala, A., Festa, G., Picozzi, M., & Beroza, G. C. (2023). Comparing and integrating artificial intelligence and similarity search detection techniques: application to seismic sequences in Southern Italy. Geophysical Journal International, 233(2), 861-874.

Scotto di Uccio, F., Michele, M., Strumia, C., Supino, M., Beroza, G. C., Chiaraluce, L., ... & Festa, G. (2024). Characterization and evolution of seismic sequences in the normal fault environment of the Southern Apennines. Journal of Geophysical Research: Solid Earth, 129(8), e2023JB028644.

Strumia, C., Trabattoni, A., Supino, M., Baillet, M., Rivet, D., & Festa, G. (2024). Sensing optical fibers for earthquake source characterization using raw DAS records. Journal of Geophysical Research: Solid Earth, 129(1), e2023JB027860.

Zhu, W., & Beroza, G. C. (2019). PhaseNet: a deep-neural-network-based seismic arrival-time picking method. Geophysical Journal International, 216(1), 261-273.

Towards the generalization of the Visibility Graph method in earthquake catalogues

S. Scudero[1], A. D'Alessandro[1]

[1] *Istituto Nazionale di Geofisica e Vulcanologia (INGV), Rome, Italy*

The method called "visibility graph analysis" (VGA) converts a generic time series into a graph. In this representation, values of the time series are described as nodes, and the connections among the various nodes represent their relationships. Therefore, in this method, the relationship which defines the connections among two nodes is given by the reciprocal "visibility" among the series' values. The connectivity degree "*k*" is defined as the number of links that each observation holds with the others. The network resulting from the VGA transformation inherits the properties possessed by the original time series (Lacasa et al., 2008).

The application of VGA to the study of earthquake catalogues gained interest as a reliable method to investigate statistical properties of seismicity. The literature reports numerous examples of VGA applications to natural and synthetic earthquake catalogues, suggesting the occurrence of an universal, linear, relationship linking the so-called *k*-M slope (i.e. the slope of the linear regression between VG connectivity degree (*k*) and earthquake magnitude (M) for a given catalogue) with the *b*-value of the Gutenberg–Richter law (Scudero and D'Alessandro, 2025).

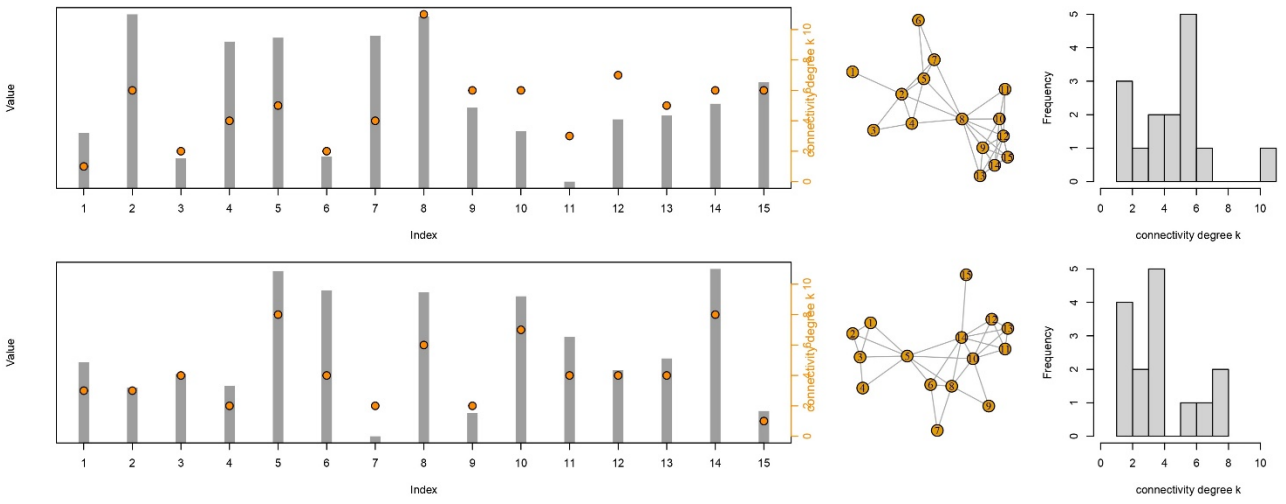

Fig. 1 – Example of Visibility Graph transformation for two series with identical observations and different indexing (left). The resulting graphs (center) and the distribution of the connectivity degree (right) might differ significantly.

However, given a seismic catalogue, changing the sequential order of the observation, the resulting frequency distribution may vary, and in turn, also the *k*-M slope varies (Fig. 1). For this reason, it is worth to explore how the *k*-M slope varies if the observations are randomly shuffled, and how the relationship with the *b*-value is affected, in turn.

To achieve this task, we simulated earthquake catalogues with different characteristics (*b*-value of the G-R law and size), obtaining a set of 42 different combination. Then, each catalogue is shuffled into 200 different random versions, and VGA is applied to all of them to calculated the *k*-M relationship and analyze the frequency distribution of *k*-M slope. Results indicate that the average *k*-M slope (over the 200 permutations) can be considered representative of each catalogue resulting from the combination of size and *b*-value. The resulting linear relationships between the *k*-M slope and the *b*-value are unbiased by the order of the events.

To obtain a full view of these relationships and to take into account all the involved variables, we performed gridded interpolations of obtained values for the mean *k*-M slope in the continuous *b*-N space (Fig. 2). With such representations, it is possible to retrieve the VGA parameters for a generic seismic catalogue with a given *b*-value and N, and compare them with the calculated values. conversely, given information from the VGA, it is possible to indirectly calculate (or verify other methods for) the *b*-value.

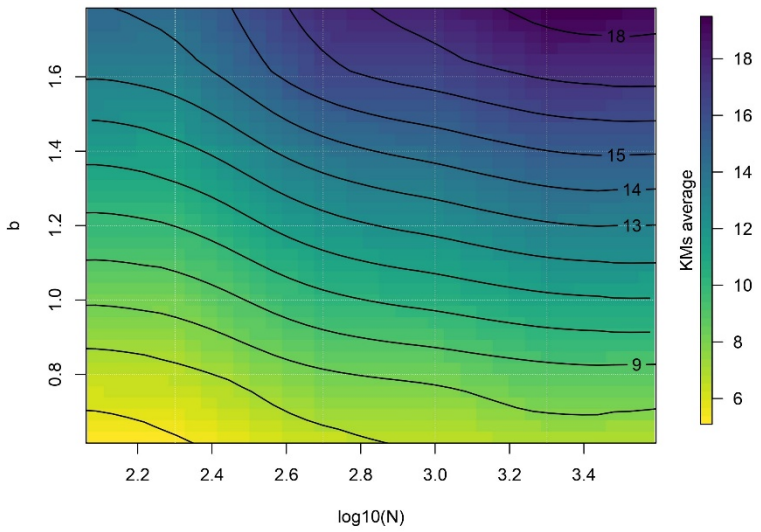

Fig. 2 – Gridded interpolation of the average k-Mslope.

Finally, we explore the application of this method on different real earthquake catalogues, with different number of events and related to different tectonic settings. In particular, we calculated the *b*-value after calculating the *k*-M slope; then we compared these calculated values with those obtained using the classical method (Fig. 3). Values show a general agreement, except for five catalogues. According to the taken assumptions, the over-estimation of the *b*-value can be interpreted as a measure of the departure from the G-R distribution of a given catalogue.

In conclusion, the calculation of the *k*-M slope over a sufficient number of randomly shuffled versions of the same catalogue can provide a statistically robust estimation of the *b*-value, which can be used as verification of other methods. Moreover, deviations from the expected values can be interpreted in terms of peculiar earthquake sequences or deviations from G-R trend.

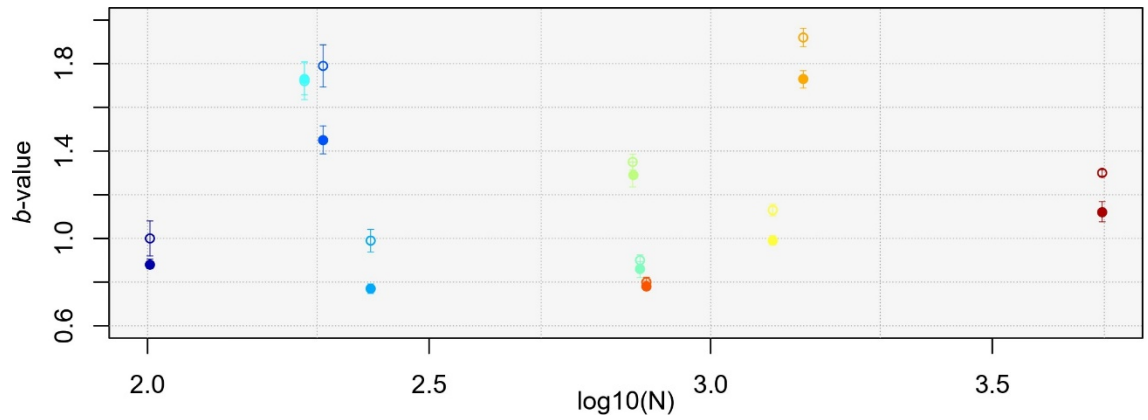

Fig. 3 – *b*-values of ten real earthquake catalogues (full colored dots), and same values calculated from k-Mslope (empty dots).

References

Lacasa, L., Luque, B., Ballesteros, F., Luque, J., Nuno, J.C.: 2008: From time series to complex networks: The visibility graph. Proceedings of the National Academy of Sciences, 105(13), 4972-4975.

Scudero, S., & D'Alessandro, A.: 2025. Investigating the universal character of k–M slope in earthquake catalogs from the Visibility Graph method. Scientific Reports, 15(1), 34264.

Corresponding author: salvatore.scudero@ingv.it

Investigating Seismogenic Processes in the High Agri Valley: Research Activities within the FRACTURES Project

T.A. Stabile[1], F. Accomando[2], R. Castaldo[2], G. De Landro[3], F. Falabella[2], F. Izzi[1], M. Palo[3], S. Panebianco[1], A. Pepe[2], S. Pepe[2], M. Perrini[2,3], A. Perrone[1], V. Serlenga[1], P. Tizzani[2]

[1] Institute of Methodologies for Environmental Analysis (IMAA), National Research Council of Italy (CNR), Tito, Italy
[2] Institute for the Electromagnetic Sensing of the Environment (IREA), National Research Council of Italy (CNR), Naples, Italy
[3] University of Naples Federico II, Department of Physics "Ettore Pancini", Naples, Italy

The High Agri Valley (HAV), located in the axial sector of the Southern Apennines (southern Italy), represents a natural laboratory for investigating the interplay between natural and anthropogenic seismicity. The area is characterized by a high seismogenic potential, as testified by the 1857 Mw 7.0 Basilicata earthquake, and currently hosts two major infrastructures: the Val d'Agri oil production plant, exploiting the largest onshore oil field in Western Europe, and the Pertusillo artificial water reservoir, with a storage capacity of 155 million cubic meters. Both infrastructures are associated with distinct clusters of anthropogenic microseismicity that have been extensively documented over the last decade. Since 2016, the HAV has been continuously monitored by a public, open-access virtual seismic network composed primarily of stations from the permanent High Agri Valley Observatory (HAVO; FDSN code VD), integrated with stations from the Italian National Seismic Network (IV), ISNet (IX), and GEOFON (GE).

Within the framework of the PRIN-MUR 2022 FRACTURES project (grant no. 2022BEKFN2), funded by the European Union – NextGenerationEU, we analysed the seismicity recorded in the study area between 2016 and 2023 by automatically processing continuous seismic data streams using machine learning algorithms and high-performance computing. The adopted automated workflow was implemented on a DGX A100 NVIDIA server equipped with 8 GPUs and 256 CPU cores. Here we present both the computational performance of each processing step and the resulting high-resolution seismic catalogue for the HAV.

The main objective of this project, with specific reference to the HAV case study, was to exploit this extensive seismic dataset to improve our understanding of seismicity triggering and clustering mechanisms and to enhance knowledge of fault structures and seismogenic processes in this complex tectonic and anthropogenic setting. Particular attention was devoted to the identification of seismic sequences, swarms, and repeating earthquakes using clustering techniques.

To further gain insights on the fluid-induced microseismic swarm associated with wastewater injection at the Costa Molina 2 well, we adopted an integrated, non-invasive, physics-based approach to investigate fluid migration and pore-pressure evolution from passive microseismicity. By jointly analysing temporal variations in elastic parameters (Vp/Vs and ΔV/V) inferred from induced microearthquakes, we reconstructed fluid-migration dynamics and assessed their relationship with injection parameters such as pressure and injected volumes.

With the aim to better characterize the reservoir-induced seismicity, we developed a Finite Element Method (FEM)-based numerical model to simulate stress and strain variations resulting from seasonal lake-level fluctuations. In addition, we took into account potential contributions from nearby aquifers, and we incorporated geological information together with in situ and satellite-based geophysical data. The model allowed us to explore different scenarios and improve our understanding of the complex interactions among geology, aquifers, the Pertusillo reservoir, and the network of faults and fractures that may act as hydraulic connections with active seismogenic structures.

Corresponding author: tonyalfredo.stabile@cnr.it

Leveraging fibre optic networks for rapid response: DAS based earthquake early Warning

C. Strumia[1], D. Rivet[2], A. Trabattoni[2], F. Scotto di Uccio[1], L. Elia[3], S. Colombelli[1], G. Festa[1, 4]

[1] Università di Napoli Federico II, Physics Department, Complesso Monte S. Angelo, Napoli, Italy.
[2]Université Côte d'Azur, Observatoire de la Côte d'Azur, CNRS, IRD, Géoazur, Valbonne, France.
[3]Istituto Nazionale di Geofisica e Vulcanologia (INGV), Sezione Osservatorio Vesuviano, Naples, Italy.
[4]Istituto Nazionale di Geofisica e Vulcanologia, Osservatorio Nazionale Terremoti, Roma, Italy.

Distributed Acoustic Sensing (DAS) is a sensing technique that transforms fibre optic cables into dense linear arrays of strainmeters with metre-scale spacing over lengths up to hundreds of kilometres. These systems execute interferometric measurements of backscattered light coming from laser pulses injected into fibre optic cables, used to map the deformation rate along the cable path (Hartog, 2017). The measurements result in single component recordings of the longitudinal component of the deformation following the fibre path.

This instrumentation is a transformative tool for geosciences, delivering extremely dense information over regional distances. Moreover, the possibility of exploiting unlit telecommunication lines allows for monitoring remote and less instrumented areas like volcanic environments (Currenti et al, 2021), geothermal fields (Vera Rodriguez, 2025), and glaciers (Fichtner et al., 2025), where standard instrumentation becomes too expansive or unpractical.

In Seismology the effectiveness of DAS has been proven in several applications. The dense sampling allows wide coverage of seismic rays for tomographic investigations at regional scale (Biondi et al., 2023) but is also key for fine-scale characterization of the shallow layers (Vernet et al., 2025). DAS is also beneficial in seismic monitoring. The dense and coherent travel time information is directly exportable to existing seismological tools. Seismic phase picking can be obtained leveraging established artificial intelligence tools adapted to process space and time continuous data (Zhu et al., 2023), even if the integration into earthquake location approaches can be complex due to the strong dependency on cable geometry (Bozzi et al., 2024). Earthquake source characterization is also feasible, with established approaches for local magnitude estimation (Trabattoni et al., 2023), source parameter estimation (Strumia et al., 2024), and possibly focal mechanism determination (Li et al., 2023; Funabiki and Miyazawa, 2025).

While the potential in offline seismic characterization is becoming clear, a fundamental field of application for the exploitation of this new sensing paradigm is real time monitoring for Earthquake

Early Warning. The integration of DAS data into operative EEW system is an ongoing effort explored in few studies (Gou et al., 2025; Ben-Zeev and Lior, 2025), that requires novel strategies to combine dense spatial information and DAS-specific characteristics, like the unique azimuthal sensitivity and the saturation of strain rate due to unwrapping of the backscattered light (Van den Ende et al., 2025).

In this work we explore the exportability of operational EEW systems to DAS data. To conduct this study, we focus on earthquakes recorded by three DAS systems along an offshore fibre network of 450km in central Chile and running parallel to the subduction trench. This infrastructure composes the ABYSS network (Baillet et al., 2025). This area offers a perfect testbed, where the exceptionally high rate of seismicity is characterized by moderate to large events that are fundamental in assessing the potential of this technique for EEW. Moreover, the potential for large and devastating earthquakes in the study area requires operational systems for rapid alerts, and DAS could be a key asset allowing for improvement in the time of response in the order of tens of seconds (Lior et al., 2023).

First, we defined a strategy for real time magnitude estimation, overcoming the limitations of offshore environments where direct P waves are often poorly recorded by DAS and followed by more energetic secondary phases. We integrate DAS-specific magnitude laws into the PRESTo algorithm (Satriano et al., 2011), whose performances are tested on earthquakes recorded by the ABYSS network, proposing a prototypal system for DAS based EEW in Chile.

This approach could also improve the performances of EEWS in existing seismic networks. Here the key aspect is the integration between seismic stations and fibre data, which requires the definition of common strategies for digesting these different data paradigms. Leveraging a continuous monitoring infrastructure built within the Irpinia Near Fault Observatory (INFO, Chiaraluce et al., 2022) we export the prototypal system to the tectonic environment of the Southern Apennines, exploring the performance on small magnitude event records in an area capable of generating devastating events like the 1980 M6.9 Irpinia Earthquake (Bernard and Zollo, 1984).

References

Hartog, H.A.; 2017: An introduction to distributed optical fibre sensors (A. H. Hartog, Ed.). CRC Press.

Currenti, G., Jousset, P., Napoli, R., Krawczyk, C., & Weber, M.; 2021: On the comparison of strain measurements from fibre optics with a dense seismometer array at Etna volcano (Italy). Solid Earth, 12(4), 993–1003. hps://doi.org/10.5194/se-12-993-2021

Vera Rodriguez, I., Podrasky, D., Coleman, T., Maldaner, C., Ma, Y., & Ajo-Franklin, J. (2025). DAS Moment Magnitude Calculation in the Time Domain for General Dislocations: Application at Utah FORGE. *Bulletin of the Seismological Society of America*, *115*(6), 2592-2607.

Fichtner, A., Hofstede, C., Kennett, B. L., Svensson, A., Westhoff, J., Walter, F., ... & Eisen, O. (2025). Hidden cascades of seismic ice stream deformation. *Science*, *387*(6736), 858-864.Biondi, E., Zhu, W., Li, J., Williams, E. F., & Zhan, Z. (2023). An upper-crust lid over the Long Valley magma chamber. *Science Advances*, *9*(42), eadi9878.

Vernet, C., Trabattoni, A., Baillet, M., van den Ende, M., & Rivet, D. (2025). Imaging the sediment cover offshore central Chile with surface-wave dispersion and P-Wave conversion using distributed acoustic sensing. *Journal of Geophysical Research: Solid Earth*, *130*(7), e2024JB030507.

Zhu, W., Biondi, E., Li, J., Yin, J., Ross, Z. E., & Zhan, Z. (2023). Seismic arrival-time picking on distributed acoustic sensing data using semi-supervised learning. *Nature Communications*, *14*(1), 8192.

Bozzi, E., Agostinetti, N. P., Fichtner, A., Klaasen, S., Ugalde, A., Biondi, B., ... & Saccorotti, G. (2024). Modelling uncertainty in P-wave arrival-times retrieved from DAS data: case-studies from 15 fibre optic cables. *Geophysical Journal International*, *239*(3), 1928-1942.

Trabattoni, A., Biagioli, F., Strumia, C., van den Ende, M., Scotto di Uccio, F., Festa, G., ... & Stutzmann, É. (2023). From strain to displacement: using deformation to enhance distributed acoustic sensing applications. *Geophysical Journal International*, *235*(3), 2372-2384.

Strumia, C., Trabattoni, A., Supino, M., Baillet, M., Rivet, D., & Festa, G. (2024). Sensing optical fibres for earthquake source characterization using raw DAS records. *Journal of Geophysical Research: Solid Earth*, *129*(1), e2023JB027860.

Li, J., Zhu, W., Biondi, E., & Zhan, Z. (2023). Earthquake focal mechanisms with distributed acoustic sensing. Nature Communications, 14(1), 4181.

Funabiki, Y., & Miyazawa, M. (2025). Estimating focal mechanism of small earthquakes using S/P amplitude ratios of distributed acoustic sensing records. *Geophysical Research Letters*, *52*(9), e2024GL113963.

Gou, Y., Nof, R. N., Pardini, B., & Allen, R. M. (2025). Integrating fibre-optic seismic arrays into earthquake early warning systems with the dEPIC framework. *Scientific Reports*.

Ben-Zeev, S., & Lior, I. (2025). Physics-based earthquake early warning using distributed acoustic sensing. *Scientific Reports*.

van den Ende, M., Trabattoni, A., Baillet, M., & Rivet, D. (2025). An analysis of the dynamic range of Distributed Acoustic Sensing for Earthquake Early Warning. *Seismica*, *4*(1). https://doi.org/10.26443/seismica.v4i1.1371

Baillet, Marie, Diane Rivet, Alister Trabattoni, Jérôme Cheze, Fabrice Peix, David Ambrois, Martijn van den Ende et al. "Automatic earthquake catalogs from a permanent DAS offshore network." *Journal of Geophysical Research: Solid Earth* 130, no. 10 (2025): e2025JB031565.

Lior, I., Rivet, D., Ampuero, J. P., Sladen, A., Barrientos, S., Sánchez-Olavarría, R., ... & Bustamante Prado, J. A. (2023). Magnitude estimation and ground motion prediction to harness fibre optic distributed acoustic sensing for earthquake early warning. *Scientific Reports*, *13*(1), 424.

Satriano, Claudio, Luca Elia, Claudio Martino, Maria Lancieri, Aldo Zollo, and Giovanni Iannaccone. "PRESTo, the earthquake early warning system for southern Italy: Concepts, capabilities and future perspectives." *Soil Dynamics and Earthquake Engineering* 31, no. 2 (2011): 137-153.

Chiaraluce, L., Festa, G., Bernard, P., Caracausi, A., Carluccio, I., Clinton, J. F., ... & Sokos, E. (2022). The Near Fault Observatory community in Europe: a new resource for faulting and hazard studies. *Annals of Geophysics*, *65*(3), DM316.

Bernard, P., & Zollo, A. (1989). The Irpinia (Italy) 1980 earthquake: detailed analysis of a complex normal faulting. *Journal of Geophysical Research: Solid Earth*, *94*(B2), 1631-1647.

Corresponding author: claudio.strumia@unina.it

INTEGRATED MORPHOTECTONIC, SEISMIC, AND NEAR-SURFACE GEOPHYSICAL INVESTIGATION OF THE VIGONOVO THRUST (EASTERN SOUTHERN ALPS, NE ITALY)

L. Suranna[1], G. M. Caielli[1,2], F. L. Bonali[1,3], R. De Franco[1,2], E. Rizzo[5], A. Tibaldi[1], M.E. Poli[3,4], G. Patricelli[3,4,5], A. Villa[1]

[1] Department of Earth and Environmental Sciences, University of Milan-Bicocca, Milan, Italy;
[2] Istituto di Geologia Ambientale e Geoingegneria (IGAG) – CNR, Milan, Italy;
[3] CRUST-Interuniversity Center for 3D Seismotectonics with Territorial Applications, Chieti Scalo, Italy;
[4] University of Udine, Department. of AgriFood, Environmental and Animal Sciences, Udine, Italy;
[5] University of Ferrara, Department. of Physics and Earth Sciences, Ferrara, Italy

The recognition and characterization of shallow active and capable faults at the front of compressional orogenic belts is a critical issue for both tectonic interpretation and seismic hazard assessment. In the eastern Southern Alps (NE Italy), the Polcenigo-Montereale Thrust-System represents a major active structure accommodating ongoing shortening at the transition between the Pliocene-Quaternary Southalpine front and its foreland here represented by the piedmont Last Glacial Maximum (LGM) Friulian plain (Castellarin and Cantelli, 2000; Carulli et al., 2006;Fontana et al., 2019 Fig. 1). Within this framework, a series of minor splays (Budoia-Aviano and Vigonovo thrusts respectively) give rise to prominent morphotectonic features, interpreted as the surface expression of recent fault-related deformation affecting Late Quaternary deposits (Poli et al., 2014; Poli et al., 2025).

This study focuses on a near-surface active seismic profile coupled with Electroresistivity Tomography (ERT) and Ground Penetrating Radar (GPR) acquired across the Aviano scarp (Fig. 2). The location of the seismic line, and the subsequent ERT and GPR surveys, was guided by detailed geological, structural, and morphotectonic analyses, with the aim of investigating the existence, shallow geometry, and continuity of the fault responsible for the observed surface deformation. In particular, the geological and structural framework of the area indicates that the scarp is spatially consistent with the expected trace of the Vigonovo Thrust, representing the outermost front of the Eastern Southern Alps in the western Carnic Prealps (Poli et al., 2014; Fig. 1). Morphotectonic analysis highlights a clear and laterally continuous slope break, associated with measurable vertical offsets of Upper Pleistocene LGM alluvial deposits (Fontana et al., 2019), which provided the primary constraint for positioning the geophysical profiles.

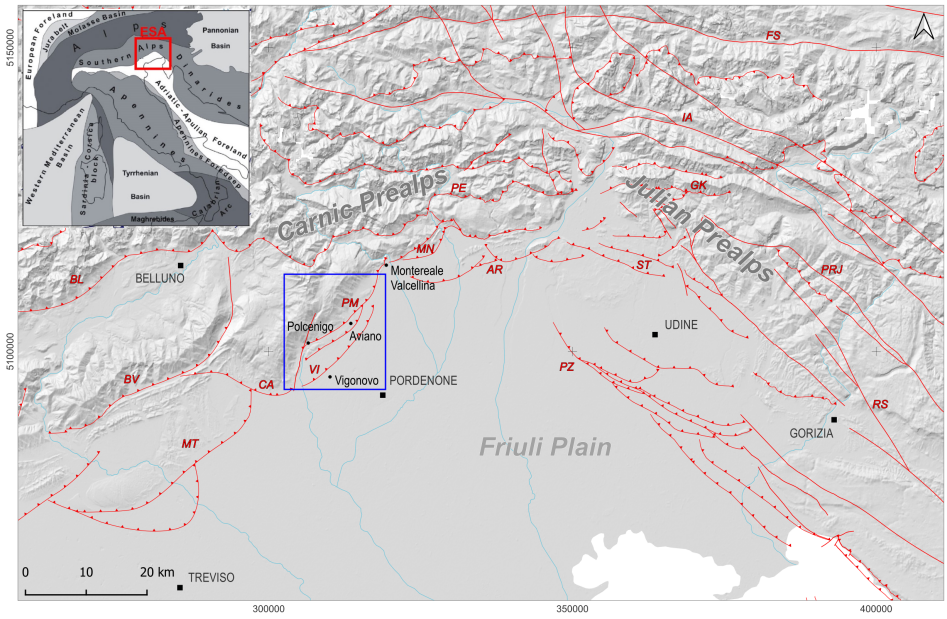

Fig. 1 – Structural sketch map of the eastern Southern Alps in Friuli (from Poli et al., 2025). The blue box indicates the study area of Fig. 2. Faults acronyms: AR: Arba-Ragogna ts., BL: Belluno th., BV: Bassano-Valdobbiadene th., CA: Cansiglio th., FS: Fella-Sava fs., GK: Gemona-Kobarid th., IA: Idrija-Ampezzo fs., MN: Maniago th., MT: Montello th., PE: Periadriatic th., PM: Polcenigo-Montereale th., PRJ: Predjama f., PZ: Pozzuolo ts., RS: Rasa f., ST: Susans-Tricesimo th., VI: Vigonovo th. RS: EPSG 3004.

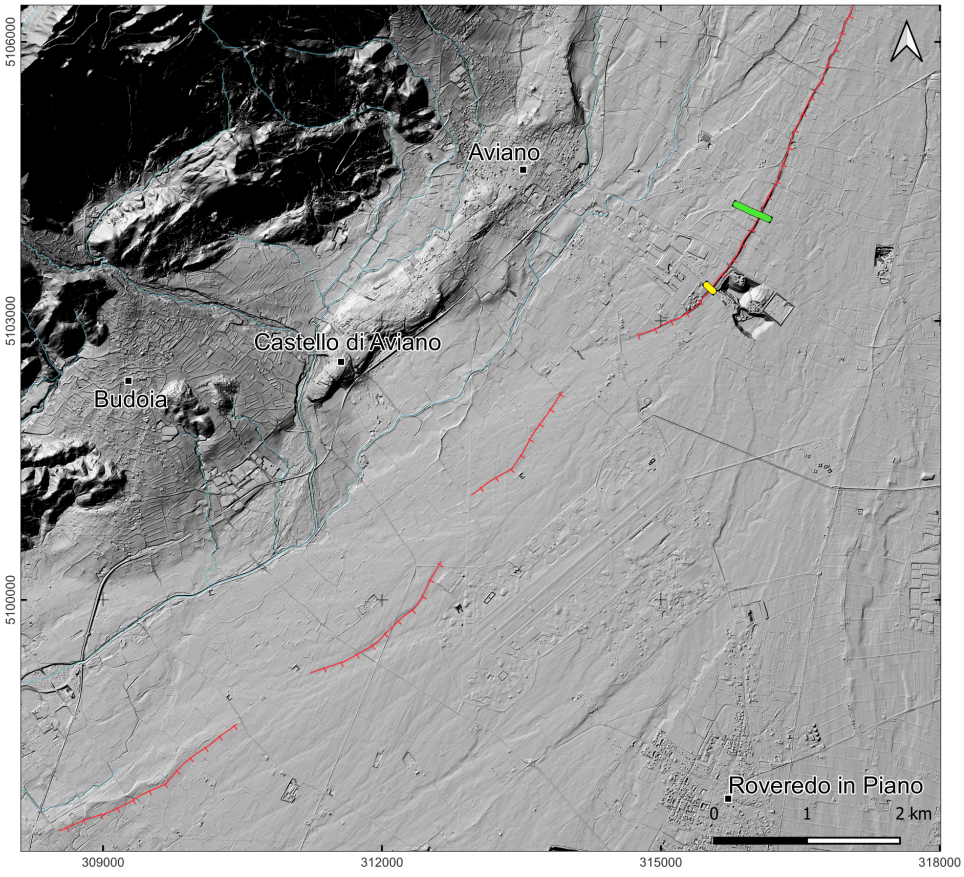

Fig. 2 – The Holocene tectonic activity of Vigonovo Thrust gave rise to an ENE-WSW trending morphotectonic scarp developed in the piedmont Friuli Plain near Aviano locality. Red lines indicate morphological scarps, green and yellow lines represent the trace of seismic and ERT investigation, respectively.

On the basis of these geological and geomorphological constraints, an active-source seismic survey (Fig. 3) was carried out along a line oriented orthogonally to the scarp and positioned across its central sector, where the morphotectonic expression is most evident and unambiguous and where logistical conditions allowed efficient deployment of the seismic instrumentation, with the primary aim of imaging the shallow subsurface architecture beneath the scarp. The seismic acquisition was designed to maximize resolution in the upper tens of meters, where fault-related deformation is expected to affect both unconsolidated Upper Pleistocene alluvial deposits and the underlying consolidated units. Field acquisition was conducted under controlled conditions, allowing for reliable imaging of lateral variations in seismic response across the scarp.

Results

A near-surface active seismic profile was acquired using a linear array of 48 geophones with a natural frequency of 4.5 Hz, spaced at 5 m intervals, for a total profile length of 235 m. This acquisition geometry allowed the generation of both seismic refraction and reflection profiles. The refraction analysis imaged the subsurface down to depths of approximately 40 m, providing a velocity model of the shallow subsurface beneath the morphotectonic scarp. The reflection data show laterally continuous and well-defined reflectors down to depths of approximately 150 m, allowing the identification of deeper structural discontinuities.

The seismic data reveal significant lateral changes in wave propagation characteristics and inferred subsurface structure beneath the Aviano scarp. These variations are spatially correlated with the surface morphotectonic expression and are interpreted as the seismic signature of a shallow fault zone and its associated damage zone (Fig. 3). The geometry of the imaged discontinuity suggests a low-angle thrust gently dipping toward the ONO, when analysed along a section oriented orthogonally to the morphotectonic scarp, with an overall ESE-directed vergence toward the Friulian plain, consistent with the regional tectonic framework of the eastern Southern Alps. The observed seismic features therefore provide depth continuity to the surface geomorphic evidence, strengthening the interpretation of the Aviano scarp as the surface expression of an active fault within the Vigonovo thrust as suggested by Poli et al.(2014) and Fontana et al. (2019).

In addition to seismic data, two near-surface geophysical surveys were carried out. A shallow Electrical Resistivity Tomography (ERT) profile was acquired using 48 electrodes with an electrode spacing of 2 m, resulting in a total profile length of 94 m and providing an investigation depth of approximately 20 m. A second dataset was acquired using Ground-Penetrating Radar (GPR) with a Pulsekko system operating at 100 MHz along an 80 m long profile. Both geophysical datasets indicate shallow subsurface deformation consistent with the presence of the observed morphological scarp.

This work demonstrates that starting from detailed morphotectonic and structural analyses to guide the design of active seismic imaging represents a robust and effective approach for detecting and characterizing shallow active faults in low strain-rate compressional settings. The integration of seismic data with near-surface geophysical investigations, including ERT and GPR, allows a coherent interpretation of deformation from depth to the surface.

Results obtained along the Aviano scarp provide new constraints on the shallow geometry and activity of the Vigonovo Thrust, contributing to an improved understanding of deformation processes at the eastern Southalpine front. These findings have direct implications for fault capability assessment and for the evaluation of local seismic hazard in the Friulian piedmont.

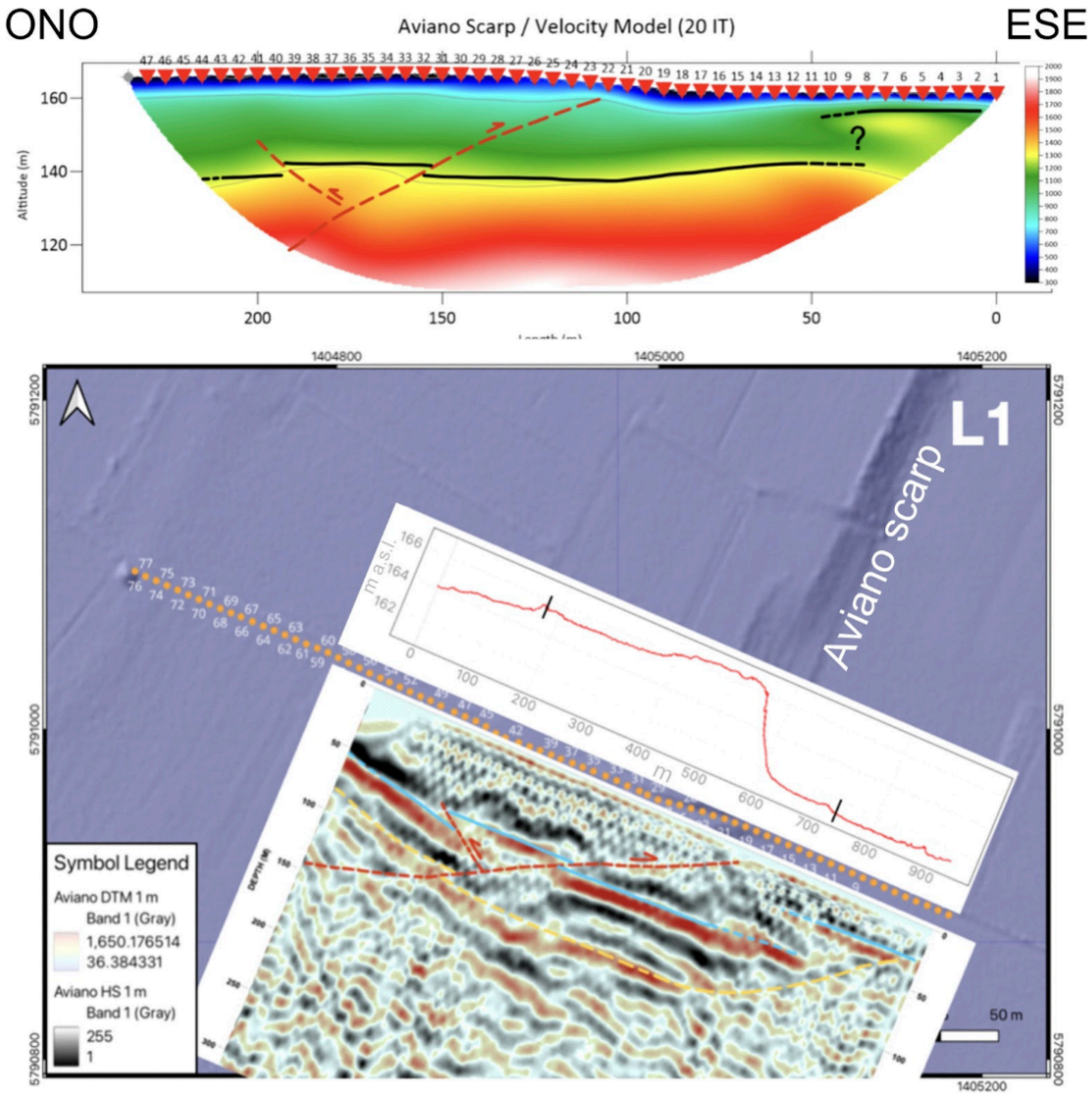

Fig. 3 (A) Active seismic velocity model across the Vigonovo (Aviano) morphotectonic scarp, showing lateral velocity contrasts and localized disruptions interpreted as a shallow fault zone beneath the scarp. Geophone numbers are reported. (B) Seismic reflection section across the Vigonovo (Aviano) morphotectonic scarp, overlain on the morphotectonic and structural framework of the study area, including a hillshaded DTM and a topographic profile showing the surface scarp and the location of the seismic line.

References

Carulli G.B. (a cura di) (2006) – Carta geologica del Friuli Venezia Giulia alla scala 1:150000 e Note Illustrative. Regione Autonoma FVG. Servizio Geologico.

Castellarin, A., & Cantelli, L. (2000). Neo-Alpine evolution of the Southern Eastern Alps. Journal of Geodynamics, 30, 251–274.

Fontana A., Monegato G., Rossato S., Poli M. E., Furlani S., Stefani C. (2019) – Carta delle unità geologiche della pianura del Friuli Venezia Giulia alla scala 1:150000 e Note Illustrative. Regione Autonoma FVG. Servizio geologico. Trieste. 80 pag.

Marchesini A., Poli M.E., Bonini L., Busetti M., Piano C., Dal Cin M., Paiero G., Areggi G., Civile D., Ponton M., Patricelli G., Tamaro A. e gruppo di lavoro Faglie Attive FVg (2023) – Linee guida per l'utilizzo della banca dati georiferita delle faglie attive della Regione FVG. Servizio geologico. 64 pag.

Poli M.E., Monegato G., Zanferrari A., Falcucci E., Marchesini A., Grimaz S., Malisan P., Del Pin E. (2015). Seismotectonic characterization of the western Carnic pre-alpine area between Caneva and Meduno (Ne Italy, Friuli). DPC-INGV-S1 Project "Base-knowledge improvement for assessing the seismogenic potential of Italy" (D6/a2.1).

Poli M.E., Patricelli G., Falcucci E., Gori S., Rizzo E., Paiero G., Marchesini A., Franceschet A., Russo D., Boldrin P., Sobbe A., and Riccardo Caputo (2025) -Recent tectonic activity of the Budoia-Aviano Thrust: the example of the LatePleistocene-Holocene Artugna alluvial fan (eastern Southern Alps, NE Italy) Miscellanea INGV 2025/102 ISSN 2039-6651

Corresponding author: Lorenzo Suranna lorenzo.suranna@unimib.it – lsura24@gmail.com

Artificial Intelligence (AI) and Machine Learning (ML) on Big Data seismology

Ken Tanaka Hernández[1, 2], Jannes Münchmeyer[3], Andrea Magrin[1], Serafina Di Gioia[4], Alejandro Rodriguez Garcia[2], Monica Sugan[1]

[1] Istituto Nazionale di Oceanografia e di Geofisica Sperimentale – OGS, Centro di Ricerche Sismologiche, Italy
[2] Università Degli Studi di Trieste, Italy
[3] Deutsches GeoForschungsZentrum GFZ, Potsdam, Germany
[4] International Center for Theoretical Physics – ICTP, Italy

A rapid increase in continuous seismic data volumes demands automated solutions that can operate efficiently at regional scales. This work evaluates an end-to-end, scalable machine-learning (ML) pipeline for earthquake detection and characterization, designed for deployment in a high-performance computing (HPC) environment. The pipeline integrates publicly available models from the seismological community (Woollam et al., 2022) and addresses the challenges of large-scale seismic processing by combining advanced computational techniques with state-of-the-art ML methods. It is configured to process seismic data collected by the Northeast Italy Monitoring System (SMINO; Bragato et al., 2021), managed by the Istituto Nazionale di Oceanografia e di Geofisica Sperimentale - OGS, as well as data from other Italian and international seismic networks in neighboring region and countries. This enables a comprehensive regional analysis of seismic activity in northeastern Italy allowing OGS to support civil protection by issuing alerts when earthquakes occur and providing rapid event solutions along with preliminary estimates of ground shaking.

The workflow includes specialized modules for phase picking (PhaseNet, Zhu and Beroza, 2019; EQTransformer, Mousavi et al., 2020), event association (GaMMA, Zhu et al., 2022; PyOcto, Münchmeyer, 2024), hypocenter localization (NonLinLoc, Lomax et al., 2000), and magnitude estimation. Deep-learning phase pickers for NE Italy are extensively evaluated using diverse training datasets, including INSTANCE (Michelini et al., 2021), STEAD (Mousavi et al., 2019), SCEDC (Southern California Earthquake Center, 2013), and the original PhaseNet training dataset, to determine the most effective combinations and ensure robust detection across the region. To rigorously validate the pipeline, a physically informed evaluation framework is introduced, based on a domain-specific confusion matrix that defines “matched,” “missed,” and “proposed” detections using strict criteria, including temporal tolerances of 0.5 s for picks and 1.5 s for events, and spatial constraints of 3 km for event locations. A bipartite optimization scheme based on weighted similarity scores is used to resolve ambiguities and ensure accurate one-to-one matching with the OGS reference catalogs (e.g. Snidarcig et al., 2021, 2022; Brondi et al., 2024; 2025). Performance is quantified through recall, complemented by detailed analyses of timing, spatial,

and magnitude residuals to characterize systematic biases and uncertainties. Supported by a HPC infrastructure, this methodology establishes a robust, transparent, and reproducible standard for benchmarking automated seismic monitoring systems in modern, data-intensive seismology.

Results show that the pipeline achieves high fidelity in detecting P- and S-wave arrivals and in associating events, substantially outperforming traditional CPU-only implementations in both speed and scalability. The HPC architecture provides enhanced operational flexibility, enabling rapid near-real-time analysis as well as large-scale historical reprocessing on the same platform. Overall, the proposed framework offers a practical blueprint for next-generation regional earthquake monitoring in environments characterized by continuously growing data volumes.

Acknowledgments

This work has been partially supported by the National Recovery and Resilience Plan project TeRABIT (Terabit network for Research and Academic Big data in Italy - IR0000022 - PNRR Missione 4, Componente 2, Investimento 3.1 CUP I53C21000370006) in the frame of the European Union - NextGenerationEU funding.

References

Bragato, P.L., Comelli, P., Saraò, A., Zuliani, D., Moratto, L. et al.; 2021: The OGS–Northeastern Italy seismic and deformation network: current status and outlook, Seismological Research Letters, 92(3): 1704–1716, https://doi.org/10.1785/0220200372

Brondi, P., Snidarcig, A., Bernardi, P., Bragato, P.L., Di Bartolomeo, P.; 2024: Bollettino della Rete Sismometrica dell'Italia Nord Orientale (RSINO), Anno 2022 [Data set]. Istituto Nazionale di Oceanografia e di Geofisica Sperimentale - OGS, https://doi.org/10.13120/w1vp-b578

Brondi, P., Snidarcig A., Di Bartolomeo, P., Magrin, A., Barnaba, C., Poggi, V., Pettenati, F., Romanelli, M., Rebez, A., Moratto, L., Sandron, D., Plasencia, M., Pesaresi, D., Compagno, A., Del Negro, E., Comelli, P., Magrin, E., Zuliani, D., Bertoni, M., Fabris, P., Bernardi, P.; 2025: Bollettino della Rete Sismometrica dell'Italia Nord Orientale (RSINO), Anno 2023 [Data set]. Istituto Nazionale di Oceanografia e di Geofisica Sperimentale - OGS, https://doi.org/10.13120/m4pk-nd81

Lomax, A., Virieux, J., Volant, P., Berge-Thierry, C.; 2000: Probabilistic Earthquake Location in 3D and Layered Models. In: Thurber, C.H., Rabinowitz, N. (eds) Advances in Seismic Event Location. Modern Approaches in Geophysics, vol 18. Springer, Dordrecht, https://doi.org/10.1007/978-94-015-9536-0_5

Michelini, A., Cianetti, S., Gaviano, S., Giunchi, C., Jozinović, D., Lauciani, V.; 2021: INSTANCE – the Italian seismic dataset for machine learning, Earth Syst. Sci. Data, 13, 5509–5544, https://doi.org/10.5194/essd-13-5509-2021

Mousavi, S. M., Sheng, Y., Zhu, W., Beroza, G. C.; 2019: STanford EArthquake Dataset (STEAD): A Global Data Set of Seismic Signals for AI, in IEEE Access, vol. 7, pp. 179464-179476, https://doi.org/10.1109/ACCESS.2019.2947848

Mousavi, S. M.; Ellsworth, W. L.; Zhu, W.; Chuang, L. Y.; Beroza, G. C.; 2020: Earthquake transformer — an attentive deep-learning model for simultaneous earthquake detection and phase picking. Nature Communications, 1, 3952, https://doi.org/10.1038/s41467-020-17591-w

Münchmeyer, J.; 2024: PyOcto: A high-throughput seismic phase associator, Seismica, 3(1), https://doi.org/10.26443/seismica.v3i1.1130

Snidarcig, A., Bernardi, P., Bragato, P.L., Di Bartolomeo, P., Garbin, M., Urban, S.; 2021: Bollettino della Rete Sismometrica dell'Italia Nord Orientale (RSINO), Anno 2020 [Data set]. Istituto Nazionale di Oceanografia e di Geofisica Sperimentale – OGS, https://doi.org/10.13120/108b8d94-361a-45f3-8195-fc4e8f73d264

Snidarcig, A., Bernardi, P., Bragato, P.L., Di Bartolomeo, P., Garbin, M., Urban, S.; 2022: Bollettino della Rete Sismometrica dell'Italia Nord Orientale (RSINO), Anno 2021 [Data set]. Istituto Nazionale di Oceanografia e di Geofisica Sperimentale - OGS, https://doi.org/10.13120/8b252b09-314f-456f-812a-b05268ecd001

Southern California Earthquake Center; 2013: SCEDC, https://doi.org/10.7909/C3WD3xH1

Woollam, J., Münchmeyer, J., Tilmann, F., Rietbrock, A., Lange, D., Bornstein, T., Diehl, T., Giunchi, C., Haslinger, F., Jozinović, D., Michelini, A., Saul, J., Soto, H.; 2022: SeisBench — A Toolbox for Machine Learning in Seismology, Seismological Research Letters, 93(3), 1695–1709, https://doi.org/10.1785/0220210324

Zhu, W., Beroza, G. C.; 2019: PhaseNet: a deep-neural-network-based seismic arrival-time picking method. Geophysical Journal International, Volume 216, Issue 1, January 2019, Pages 261–273, https://doi.org/10.1093/gji/ggy423

Zhu, W., McBrearty, I. W., Mousavi, S. M., Ellsworth, W. L., Beroza, G. C.; 2022: Earthquake phase association using a Bayesian Gaussian Mixture Model. Journal of Geophysical Research: Solid Earth, Vol. 127, n. 5, e2021JB023249, https://doi.org/10.1029/2021JB023249

Corresponding author: ktanaka@ogs.it

REVISION OF THE MACROSEISMIC DATASET OF THE MAY 5, 1990 EARTHQUAKE, IN THE POTENZA AREA.

Subtitle: better late than never

A. Tertulliani[1], A. Antonucci[1], C. Castellano[1], L. Cucci[1]

[1] *Istituto Nazionale di Geofisica e Vulcanologia INGV*

Macroseismic intensity is a key parameter for seismic hazard assessments and for many seismological approaches that analyse the impact of an earthquake on a given area.

However, several Italian earthquakes, quoted in the catalogues, still present highly incoherent and inconsistent macroseismic datasets that require in-depth investigation to prevent inaccuracies in future seismological analysis. For this reason, revisions are necessary to re- examine the event's basic data, eliminate sources of uncertainty and misunderstanding, recover new and reliable information, and assign new intensity values based on consistent criteria (Tertulliani et al., 2025).

One such case is the earthquake that occurred on May 5, 1990, in Basilicata (Southern Italy), with Mw 5.77 (CPTI15, Rovida et al. 2020; 2022).

The May 5, 1990, Potenza earthquake (Mw 5.77) was a significant event for southern Italy, despite its moderate magnitude and limited damage, and was one of the strongest earthquakes in a region with relatively low seismicity. Previous macroseismic studies of this earthquake (Gasparini et al., 1991; Tertulliani et al., 1992) contained inconsistent and often exaggerated intensity values, particularly in areas far from the epicentre.

In this work, we present a comprehensive analysis of the macroseismic dataset of the 5 May 1990 earthquake, in order to reappraise the origin of the numerous uncertainties and reconstruct a more probable picture of the earthquake impact.

To achieve this goal, we considered all available sources and analysed the pre-existing datasets. Our analysis reveals that some overestimated intensities were caused by the overlapping damage patterns from previous earthquakes (especially the 23 November 1980, Irpinia earthquake), due to the tendency to emphasize pre-existing or unrepaired damage, or attribute them to the most recent earthquake. In this respect, we re-evaluate all available data from original sources and compile a new and robust dataset comprising 1393 intensity values, assessed using both MCS and EMS-98 scales. This updated dataset shows a general decrease in higher intensity values compared to previous assessments, especially within 150 km of the epicentre. We also identify new data

sources and remove unreliable entries. Recalculated macroseismic epicentres agree with the instrumental estimate (i.e., 7.3 km using MCS data), while macroseismic magnitudes (Mw 5.05–5.19) are lower than the instrumental one.

This work significantly improves the knowledge of the seismic effects related to the May 1990 earthquake in southern Italy. The resulting dataset can be integrated into future versions of the Italian Macroseismic Database – DBMI (Locati et al. 2022). Furthermore, this dataset can now be used for a wide range of seismological purposes, including calibrating methodologies to derive earthquake parameters, developing accurate intensity prediction equations and ground-motion-to-intensity conversion equations, and assessing seismic hazard using a site-specific approach.

References

Gasparini, C., Tertulliani, A., Riguzzi, F., Anzidei, M., Maramai, A., Murru, M., De Rubeis, V., Vecchi, M., Del Mese, S., Vannucci, C., Conte, S., Massucci, A., and Saraceni, A. M.; 1991: Bollettino macrosismico 1990, Istituto Nazionale di Geofisica, Roma, 285 pp..

Locati, M., Camassi, R., Rovida, A., Ercolani, E., Bernardini, F., Castelli, V., Caracciolo, C. H., Tertulliani, A., Rossi, A., Azzaro, R., D'Amico, S., and Antonucci, A.; 2022: Database Macrosismico Italiano (DBMI15), versione 4.0, Istituto Nazionale di Geofisica e Vulcanologia (INGV), doi: 10.13127/DBMI/DBMI15.4.

Rovida, A., Locati, M., Camassi, R., Lolli, B., and Gasperini, P.; 2020: The Italian earthquake Catalogue CPTI15, Bull. Earthq. Eng., 18, 2953–2984, doi: 10.1007/s10518-020-00818-y.

Rovida, A., Locati, M., Camassi, R., Lolli, B., Gasperini, P., and Antonucci, A.; 2022: Italian Parametric Earthquake Catalogue (CPTI15), version 4.0, Istituto Nazionale di Geofisica e Vulcanologia (INGV), doi: 10.13127/cpti/cpti15.4.

Tertulliani, A., Anzidei, M., Maramai, A., Murru, M., and Riguzzi, F.; 1992: Macroseismic study of the Potenza (Southern Italy) earthquake of May 5, 1990, Nat. Hazards, 6, 25–38.

Tertulliani, A., Antonucci, A., Bernardini, F., Castelli, V., Ercolani, E., Graziani, L., Maramai, A., Orlando, M., Rossi, A., and Tuvè, T.; 2025: A comprehensive integrated macroseismic dataset from multiple earthquake studies, Earth Syst. Sci. Data, 17, 4063–4077, doi: 10.5194/essd-17-4063-2025.

Corresponding author: andrea.tertulliani@ingv.it

Can We Quickly Calculate Reliable Earthquake Parameters from Citizen Testimonies?

G. Vannucci[1], R. Bossu[2,3], M. Landès[2], P. Gasperini[4,1]

[1] *Istituto Nazionale di Geofisica e Vulcanologia, Bologna, Italy*

[2] *Euro-Mediterranean Seismological Centre, Arpajon Cedex, France*

[3] *CEA, DAM, DIF, F-91297 Arpajon, France*

[4] *Dipartimento di Fisica e Astronomia, Università di Bologna, Italy*

Introduction

The crowdsourcing science, based on near real-time information provided directly by citizens, has grown significantly In recent years. Agencies like the European-Mediterranean Seismological Centre (EMSC) collect this data through systems such as the LastQuake smartphone application (Bossu et al. 2015, 2017, 2018). The intensity assessed by each individual user is referred to as an Individual Data Point (IDP).

Vannucci et al. (2024) previously verified the feasibility of deriving reliable earthquake parameters (location and size) from IDPs using the BOXER code (Gasperini et al. 2010). However, IDPs cannot be treated as classical macroseismic intensities; they must be grouped into spatial clusters, requiring a minimum of three IDPs per cluster (Vannucci et al. 2024). This clustering procedure generates Macroseismic Data Points (MDPs), i.e. intensities, which are comparable to classical ones. The study concluded that the DBSCAN (DB) clustering method (Ester et al. 1996) with a 2 km radius (DB2) and a 20% trimmed mean (mn20) as central tendency estimator for distance and 10% trimmed mean (mn10) for magnitude, is the optimal combination for minimising deviations from instrumental data (Vannucci et al. 2024).

Subsequently, Vannucci et al. (2025) focused on a critical question: whether the IDPs/MDPs available within a few minutes of an event are sufficient to reliably locate and size earthquakes (location and magnitude). This analysis assesses the time-dependent reliability of location and magnitude estimates using the BOXER code for potential future real-time applications and early warning estimates.

Method

A retrospective analysis was performed on global-scale earthquakes from 2012 to 31 May 2024. The IDPs distributed by EMSC include a time delay in seconds from the earthquake origin time (T0), at which users sent their reports. The available IDPs were subdivided into predefined, successive time intervals relative to T0 (e.g., every 30 seconds up to 10 min).

MDPs were obtained by requiring a minimum of three IDPs per cluster for each time interval. The DB2-mn20 combination was systematically applied to compute both macroseismic epicentre and magnitude, as it is the most effective and fast method. The analysed dataset consisted of 17243 earthquakes with sufficient IDPs to generate at least one MDP.

The BOXER code (Gasperini et al. 1999, 2010) was used to locate earthquakes using two methods: 0 and 1 (BOXER-0 and BOXER-1, respectively). BOXER-0 computes the barycentre of the localities with the most severe effects and requires a minimum of only one MDP. Method 1 (BOXER-1): Computes the centre of the entire intensity distribution by minimising the squared residuals of the intensity prediction equation (IPE) (Gasperini et al. 1999; Pasolini et al. 2008). This method requires a minimum of five MDPs. Magnitude estimation requires a minimum of four MDPs. Consequently, BOXER-0 provides the earliest epicentre estimate, followed by magnitude, and finally the BOXER-1 epicentre.

Results and Discussions

Macroseismic and Instrumental Epicentres

The number of earthquakes increases over time: within 4 minutes from T0, BOXER-0 located 6186 earthquakes i.e. the 45% of events localised at 1 day, a time used only as a final reference for data collection for the event analysed (Fig. 1). We observed that, using BOXER-0, the agreement between macroseismic and instrumental epicentres is noteworthy, with high percentages within 10 km and 20 km. The relative percentage of events consistent with instrumental data stabilises at approximately 25% within 10 km and approximately 50% within 20 km after the first 4 minutes (Fig. 1). The average distance tends to stabilise around values of 30-40 km for the median and trimmed means after the 4-minute interval.

BOXER-1 locates a lower number of earthquakes than BOXER-0 due to the minimum threshold of five MDPs. However, the method shows a slightly better agreement with instrumental data, particularly for time intervals less than 5 minutes (Fig. 1). Although the total number of located events is lower, the percentage of successfully located events is higher in BOXER-1, making it the preferable location method.

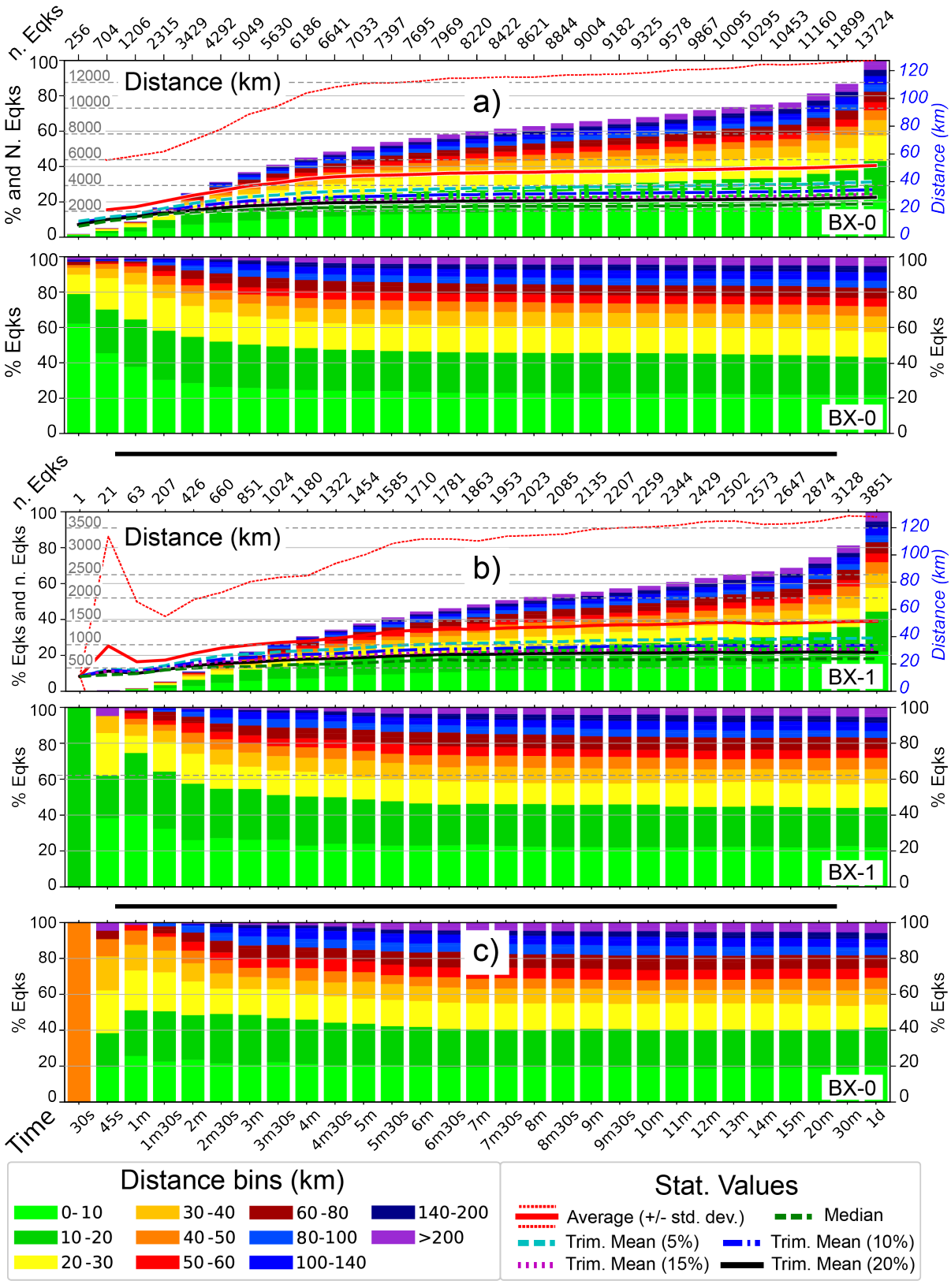

Fig 1- Distribution of the distance (in km) between macroseismic and instrumental epicentres at the global scale, calculated using both BOXER methods (BX-0, and BX-1) on MDPs derived from DB2-mn20 approach (see text for details). Distance ranges of earthquakes are colour-coded (see legend). The group of panels representing the elaborations BX-0 and BX-1, are indicated with a) and b), respectively. For both group of panels, the top X-axis indicates the number of earthquakes (n. Eqks) for each time interval, while the bottom X-axis shows the different time intervals relative to the event origin time T0 (s=seconds, m=minutes, d=day). For a) and b) groups, the top panel shows the

cumulative histogram showing, over time (X-axis), the percentage (left Y-axis) and number (grey labels with dashed lines, on left Y-axis) of earthquakes on a global scale. The percentage of earthquakes is related to the total number of events (13724) at 1 day. Coloured lines on the graph indicate central tendency estimators: mean, median, and trimmed means (with 5%, 10%, 15% and 20% of tail trimming) of the earthquakes in each time interval (right Y-axis, in italic blue colour). For a) and b) groups the bottom panel represent the percentage distribution of earthquakes per distance bins (in km), relative to the number of events in each time interval. Numerical values in Tables S1-S9 of the Supplementary material. The panel c) shows the relative percentages for the same dataset of earthquakes of BOXER-1 computed by BOXER-0.

Macroseismic and Instrumental Magnitudes

The difference between macroseismic and instrumental magnitudes exhibits a remarkable symmetry between positive (overestimation) and negative (underestimation) values over time (Fig.2). On average, the difference is close to zero, in the order of 0.01-0.03 magnitude unit (m.u.). About 50% of earthquakes fall within an absolute difference of 0.5 m.u. for both BOXER methods at most time intervals (except the first 30 s). In detail, the macroseismic magnitudes tend to be slightly overestimated at lower instrumental values and slightly underestimated at higher values, by using General Orthogonal Regression (GOR) method (Fuller 1987; Castellaro et al. 2006; Gasperini et al. 2012; Lolli et al. 2014, 2020) for each time interval. As the number of MDPs increases, the agreement improves, with the GOR regression slope approaching 1:1.

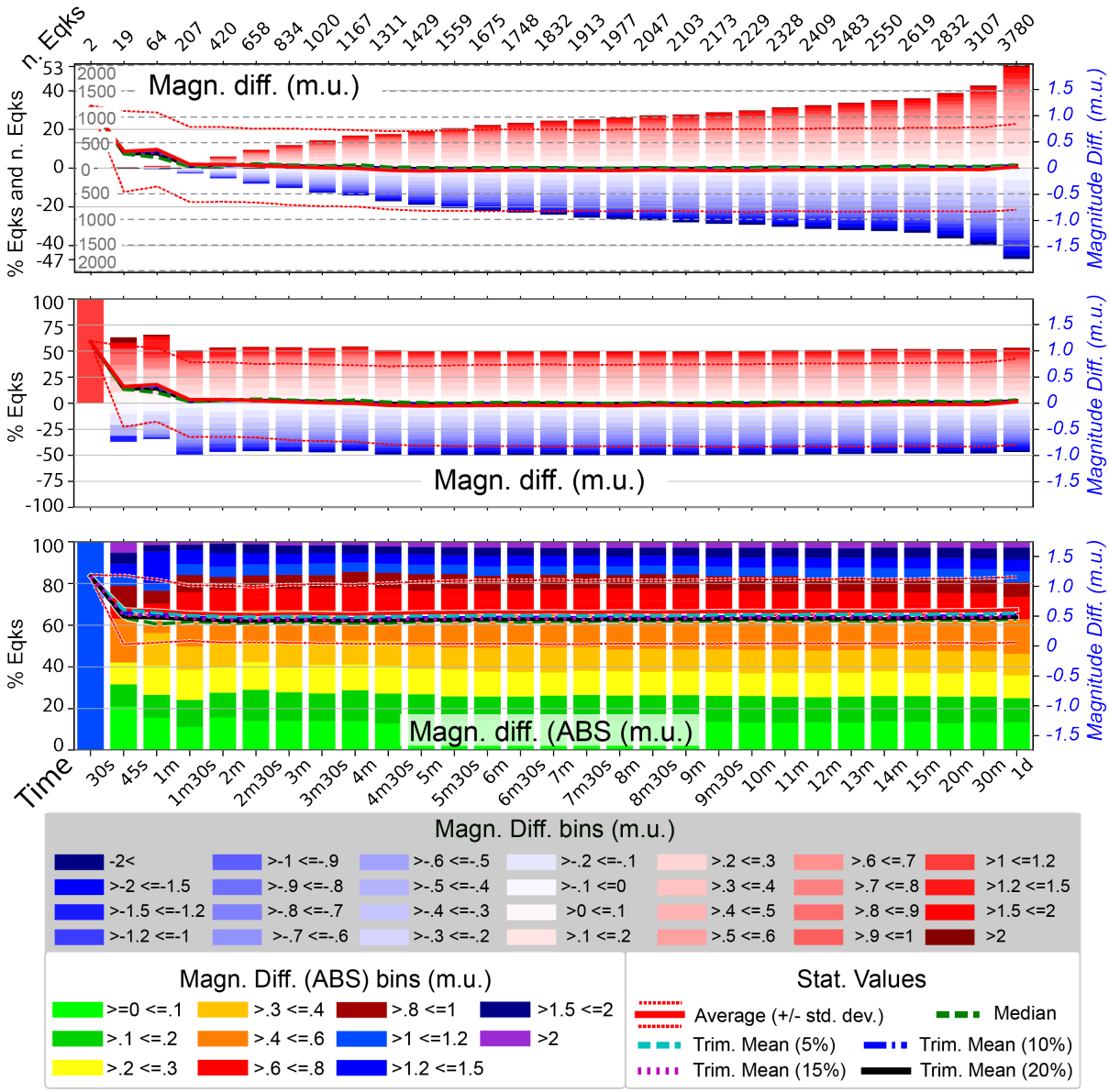

Fig 2- Difference (in m.u.) between macroseismic and instrumental magnitudes for BX-0. Cumulative values (top panel), percentages for negative and positive differences (middle panel) and absolute (ABS) value (bottom panel).

Timeliness of Macroseismic Parameter Availability

The macroseismic procedure allows for a rapid estimation of location and size, often preceding the availability of corresponding instrumental data. This comparison uses records since 2016. Using BOXER-0, 7532 macroseismic epicentres (64% of the total sample) are located before the corresponding instrumental ones. Within the first 4 minutes from T0, 5145 epicentres (approximately 44% of the total) were available earlier than the instrumental data (Fig. 3). Similarly, 1000 magnitudes (approximately 27% of the total) were assessed within the first 4 minutes from T0 before the corresponding instrumental ones.

These earlier locations are likely related to low-magnitude earthquakes and influenced by population density and the LastQuake system's data collection.

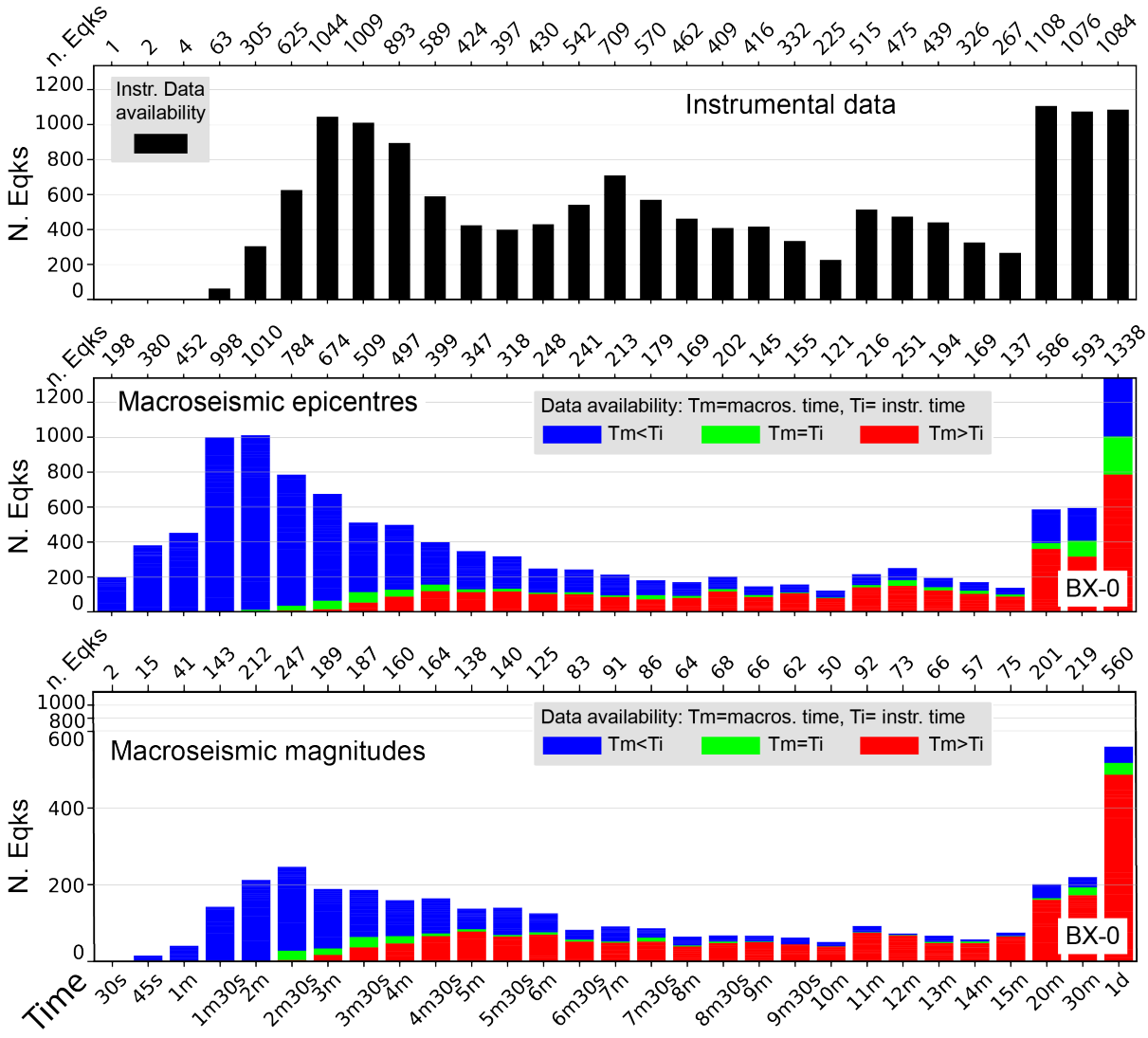

Fig 3- Number of earthquakes (N. Eqks) over time for which the first instrumental (top panel, in black) or macroseismic epicentre and magnitude (middle and bottom panels, respectively) are available. Macroseismic epicentre and magnitude, computed using BOXER-0, indicate whether they precede (blue), follow (red), or are contemporaneous (green) with the instrumental ones. Please note that the plots refer to the data since 2016, therefore, n. Eqks on the upper X-axis for macroseismic data are lower than the corresponding Figs 1-2.

Effect of IDP Grouping Radius (DB2, DB1, DB0.5)

The variability of calculated parameters may depend on the dimensional scale of IDP cluster method. Testing smaller radii (DB1, DB0.5) showed: Smaller radii (1 and 0.5 km) reduce the total number of located events but yield slightly higher percentages of accurate locations, especially within short intervals from T0. The percentage of earthquakes within 20 km of the instrumental epicentre consistently exceeds 60% with DB0.5. BOXER-1 showed slightly higher percentages of agreement (lower distance) with instrumental epicentres when combined with the smaller radii DB1 and DB0.5.

For densely populated areas, DB1 and DB0.5 are better at pinpointing the epicentre in shorter time intervals, while DB2 allows for parameter estimation for more events.

Conclusions

The study confirms the reliability of the macroseismic location and magnitude calculated using citizen-reported IDPs grouped into MDPs and processed with the BOXER code.

Within the first four minutes, a significant percentage of earthquakes are located at relatively short distances (10-20 km), and these data often predate the instrumental data availability. The average absolute difference in magnitude remains relatively constant over time, at about 0.5 m.u. For shorter time intervals (less than 5 minutes), BOXER-1 shows better agreement in distance compared to BOXER-0. Since BOXER-1 is less sensitive to near-field effects, it constrains the epicentre more effectively.

For real-time applications, adopting smaller DB radii (e.g., 1 km or 0.5 km) is suggested for better location accuracy in densely populated areas and near T0. The reliability of computed parameters increases with a high number of MDPs and a low azimuthal gap between them.

The procedure reliability over predefined time intervals emphasises its potential for application in near real-time to provide information to users and stakeholders, including civil protection agencies.

References

Bossu R., Laurin M., Mazet-Roux G., Roussel F. and Steed R.; 2015: The importance of smartphones as public earthquake-information tools and tools for the rapid engagement with eyewitnesses: A case study of the 2015 Nepal earthquake sequence, Seismol. Res. Lett. 86, 6, 1587–1592

Bossu R., Landès M., Roussel F., Steed R., Mazet-Roux G., Martin S. S. and Hough S.; 2017: Thumbnail-based questionnaires for the rapid and efficient collection of macroseismic data from global earthquakes, Seismol. Res. Lett. 88, 1, 72-81.

Bossu R., Roussel F., Fallou L., Landès M., Steed R., Mazet-Roux G., Dupont A., Frobert L. and Petersen L.; 2018: LastQuake: From rapid information to global seismic risk reduction, Int. J. Disast. Risk Reduc. 28, 32-42.

Castellaro S., Mulargia F. and Kagan Y. Y.; 2006: Regression problems for magnitudes, Geophys. J. Int. 165, 913-930, doi: 10.1111/j.1365-246X.2006.02955.x.

Ester M., Kriegel H.P., Sander J. and Xiaowei X.; 1996: A Density-Based Algorithm for Discovering Clusters in Large Spatial Databases with Noise. KDD'96: Proceedings of the Second International Conference on Knowledge Discovery and Data Mining, 226-231

Fuller W. A.; 1987: Measurement Error Models, John Wiley, New York, 440 pp, doi: 10.1002/ jae.3950030407.

Gasperini P., Bernardini F. , Valensise G. and Boschi E.; 1999: Defining seismogenic sources from historical earthquake felt reports. Bull. Seismol. Soc. Am. 89, 94-110.

Gasperini P., Vannucci G., Tripone D. and Boschi E.; 2010: The location and sizing of historical earthquakes using the attenuation of macroseismic intensity with distance. Bull. Seismol. Soc. Am. 100, 2035-2066, doi: /10.1785/0120090330.

Gasperini P., Lolli B., Vannucci G. and Boschi E.; 2012: A comparison of moment magnitude estimates for the European-Mediterranean and Italian regions, Geophys. J. Int., 190, 3, 1733-1745, doi:10.1111/j.1365-246X.2012.05575.x

Lolli B., Gasperini P. and Vannucci G.; 2014: Empirical conversion between teleseismic magnitudes (mb and Ms) and moment magnitude (Mw) at the Global, Euro-Mediterranean and Italian scale, Geophys. J. Int., 199, 805-828, doi: 10.1093/gji/ggu264

Lolli B., Randazzo D., Vannucci G. and Gasperini P.; 2020: The Homogenized Instrumental Seismic Catalog (HORUS) of Italy from 1960 to Present, Seismol. Res. Lett. 91, 3208–3222, doi: 10.1785/0220200148.

Pasolini C., Albarello D., Gasperini P., D'Amico V. and Lolli B.; 2008: The attenuation of seismic intensity in Italy part II: modeling and validation. Bull. Seismol. Soc. Am. 98, 692-708. doi.org/ 10.1785/0120070021.

Vannucci G., Gasperini P., Gulia L. and Lolli B.; 2024: Earthquakes Parameters from Citizen Testimonies: A Retrospective Analysis of EMSC Database, Seismol. Res. Lett. 95, 969–996, doi: 10.1785/0220230245.

Vannucci G., Bossu R., Landès M. and Gasperini P.; 2025: Can we quickly calculate reliable earthquake parameters from citizen testimonies? Bull Earthquake Eng. https://doi.org/10.1007/ s10518-025-02299-3

Corresponding author: gianfranco.vannucci@ingv.it

I-HADES: A seismic event locator combining deep learning with distance geometry methods

Guglielmo Vullo[1], Francesco Grigoli[1]

[1] *University of Pisa*

Accurate earthquake location of seismicity is a longstanding challenge in seismology, particularly when analyzing clusters of seismicity recorded by sparse (i.e., one or two stations only) and/or asymmetric seismic networks. In such conditions, traditional location methods often struggle to correctly locate seismic events, producing large uncertainties that may lead to wrong interpretations of the results.

Relative location techniques have improved precision by exploiting the similarity between close events. Among them, the **HADES** algorithm (eartHquake locAtion via Distance gEometry Solvers) marked a major step forward, reformulating the problem through distance geometry to reconstruct earthquake clusters even with very sparse seismic networks. However, its effectiveness depends on inter-event distances derived from P- and S-wave arrival-time estimates, which are sensitive to noise and inaccuracies in the velocity model.

Meanwhile, the rise of artificial intelligence (AI) is reshaping how science faces complex problems. By learning from data, AI handles noisy signals, reduces model bias, and finds patterns that traditional methods often miss. Seismology, with its data richness and natural uncertainties, is an ideal field to benefit from this new approach.

This work introduces **I-HADES**, an AI-powered extension of HADES that integrates machine learning into the earthquake relocation process of seismicity clusters using distance geometry approaches. A fully connected neural network (FC-ANN) was trained on synthetic datasets, where true event separations are known, to directly predict inter-event distances from observed data. Two configurations were tested using two and four stations to evaluate the impact of network density.

The results are clear: AI enhances distance prediction, mitigates the effects of noise and model errors, and makes the I-HADES framework more robust and reliable. By merging distance-geometry methods with the power of AI, this work demonstrates how artificial intelligence can unlock a new level of precision in earthquake location, opening the way for applications from sparse monitoring environments to complex seismic networks.

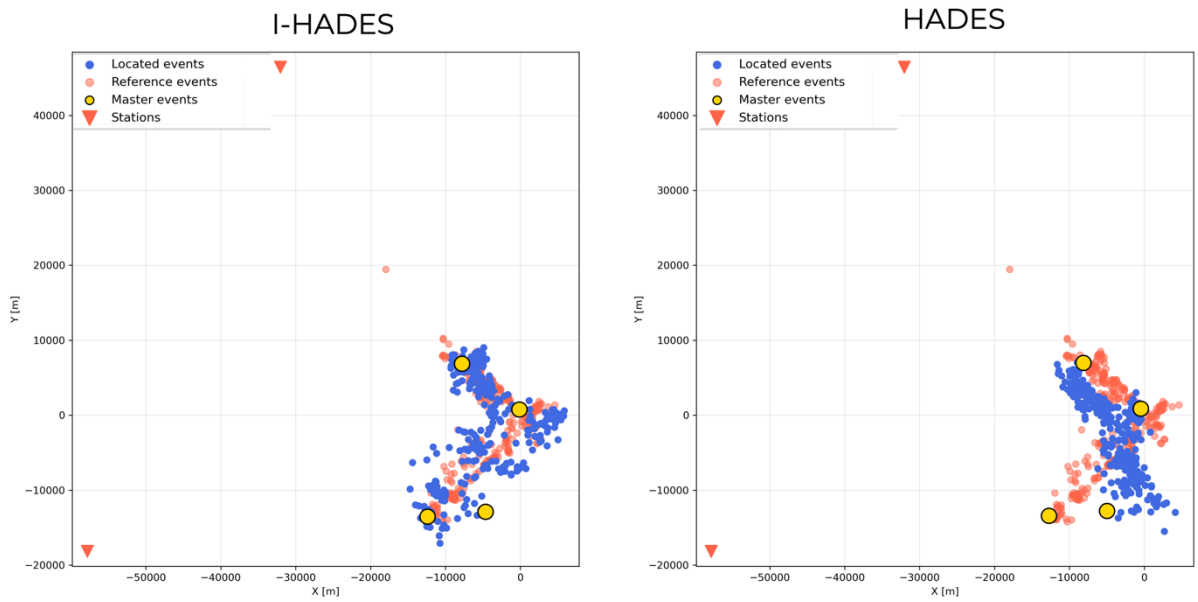

Figure 1. Comparison of I-HADES and HADES with 4 master events for Ridgecrest seismic sequence localization (2019)

References

Grigoli, F., Ellsworth, W.L., Zhang, M., Mousavi, M., Cesca, S., Satriano, C., Beroza, G.C. and Wiemer, S., 2021. Relative earthquake location procedure for clustered seismicity with a single station. *Geophysical Journal International*, *225*(1), pp.608-626.

Testing a Robust Approach for Laboratory Acoustic Emissions Source Mechanism

Wen Zhou [1], Sergio Carmelo Vinciguerra [1], Guido Maria Adinolfi [1]

[1] *Università degli Studi di Torino*

Source mechanism describes the geometry and kinematics of earthquake source, and it is related to fault mechanics, and stress evolution during rupture. Reliable focal mechanism solutions are therefore essential for understanding multiscale rupture processes for both laboratory scale earthquakes, i.e. Acoustic Emissions (AE) and natural earthquakes, given their well-established seismic analogy. However, conventional focal mechanism inversions become particularly critical for small-magnitude and high-frequency events due to their low signal-to-noise ratio (SNR).

Here, we developed an automated focal mechanism inversion workflow for AE based on P-wave first-motion, integrating polarity and amplitude measurements. The workflow includes automatic P-wave first-motion polarity picking and amplitude determination, combined with existing inversion techniques to automatically obtain focal mechanism solutions. Input data quality is systematically evaluated, and solution uncertainties are quantified and used to classify the resulting focal mechanisms according to their robustness. The proposed workflow is designed to achieve stable and reliable results while maintaining computational efficiency, making it suitable for large datasets.

The workflow is validated on AE datasets obtained during rock deformation laboratory experiments under controlled conditions to systematically assess inversion performance. AE data originates from compressional triaxial rock deformation experiments carried out at the Rock Mechanics Laboratory, University of Portsmouth (UK), where cylindrical marble samples (100 × 40 mm) from the Lorgino Quarry in Crevoladossola (NW Italy) were loaded in to failure at a constant effective pressure of 20 MPa while an array of 16 piezoelectric transducers recorded the ongoing Acoustic Emissions (AE). The time and spatial distribution of AE reveal the nucleation and growth of patches led by limited occurrence of low energy AE events and the coalescence of microfractures into cm-scale macroscopic ruptures planes leading to AE clustering and stress drop and a peak in number of events and energy (Fig. 1). Preliminary source mechanism analysis suggest that the inverted focal mechanisms are stable and broadly consistent with the imposed stress conditions, highlighting the potential of the workflow to improve source mechanism quality by identifying and excluding unreliable solutions.

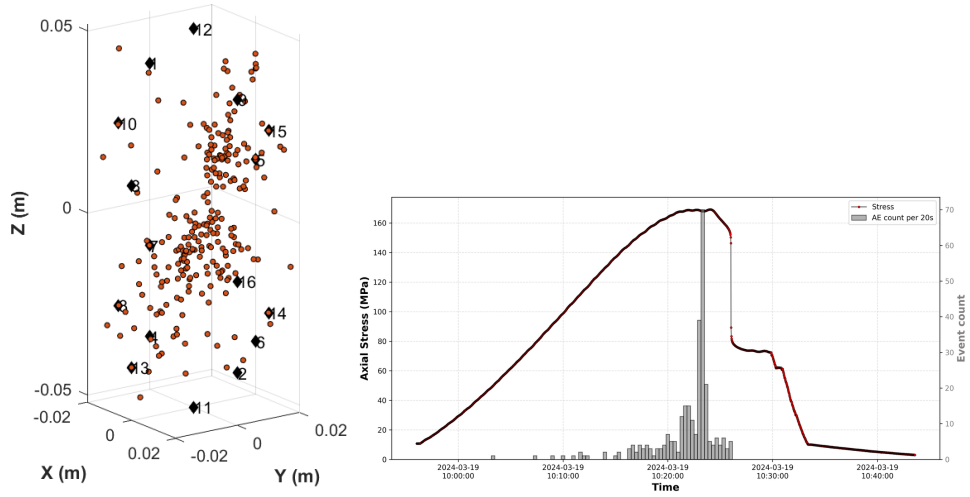

Fig. 1 – Left - spatial distribution of AE events. Right – AE time occurrence vs. Axial Stress

Corresponding author: wen.zhou@unito.it

Contribution of the local seismic network 'Fiumenet' to study microseismicity in the Provenzana-Pernicana fault system (Mt. Etna, Italy) during 2016-2017

S. Zingales[1], S. Alparone[2], A. Cannata[1,2], F. Panzera[1] , S. Rapisarda[2] , A. Ursino[2]

[1] Dipartimento di Scienze Biologiche, Geologiche e Ambientali, Università di Catania, Italy
[2] Istituto Nazionale di Geofisica e Vulcanologia, Sezione Osservatorio Etneo, Catania, Italy

The Provenzana–Pernicana Fault system (P-PF), which accommodates the seaward sliding of the eastern flank of Mt. Etna, is characterized by shallow microseismicity that is difficult to locate accurately. Previous studies (Neri et al., 2004; Alparone et al., 2013) describe a markedly heterogeneous seismic behaviour along the structure: the western and central segments, up to the vicinity of the village of Vena, show high microseismicity activity, whereas the eastern segment is aseismic, probably due to fault creep. To improve the monitoring capability of the Permanent Seismic Network (P.S.N.) managed by Istituto Nazionale di Geofisica e Vulcanologia – Osservatorio Etneo (INGV-OE) and to investigate in detail the microseismicity of the P-PF, a temporary seismic network named “Fiumenet” (Alparone et al., 2017) was deployed between August 2015 and December 2018. It consisted of six seismic stations equipped with three-component broadband sensors, located near the easternmost portion of the structure under study.

This work aims to assess the influence of the P.S.N. geometry on event locations while simultaneously quantifying the contribution of Fiumenet temporary network to improve hypocentral parameter quality. For each catalogued event, the location obtained using only the P.S.N. was compared with that obtained by adding Fiumenet seismic station pickings.

The integration of the Fiumenet mobile network allowed the relocation of two events that occurred in 2016, increasing the number of pickings, reducing the azimuthal gap, and improving epicentral accuracy. The first occurred on 4 July and the second on 6 July; in both cases, the new solutions showed a shift of the epicenters towards the P-PF trace and the cluster of events recorded by the P.S.N. during the same period, which thereby strengthening the spatial coherence of the dataset.

The analysis of the considered time intervals highlights several issues related to the geometric coverage of the P.S.N. . In particular, several events recorded by the permanent stations were catalogued as “imploc”, as they were detected by an insufficient number of stations to allow reliable location: 11 earthquakes during the July 2016 sequence and 8 during the January 2017 sequence, corresponding to more than 46% of the total seismic events detected in the Etna area during those

periods. The integration of the temporary network made possible the location of 11 “imploc” events (Table 1): 7 in 2016 and 4 in 2017, reducing the percentage of non-located events to less than 20% of the earthquakes listed in the INGV-OE catalog. In the two analyzed windows, the Fiumenet network also recorded and located four additional events not reported in the P.S.N. catalog nor classified as “imploc”: three events on 04/07/2016 and one on 18/01/2017. In other words, approximately 9% of the events recorded by the P.S.N. in the Mt. Etna area would have remained undetected without the contribution of the Fiumenet network.

Type	Origin time	Toponym	Ml
F	04/07-19:35	2.1 km E from Vena (CT)	1.0 (±0.4)
F	04/07-20:19	2.2 km E from Vena (CT)	1.3 (±0.5)
F	04/07-20:22	0.7 km E from Vena (CT)	0.9 (±0.6)
I	04/07-20:51	2.7 km E from Vena (CT)	0.5 (±0.5)
I	04/07-20:54	1.7 km E from Vena (CT)	0.8 (±0.6)
I	05/07-03:13	1.8 km E from Piedimonte Etneo	0.1 (±0.1)
I	05/07-18:56	3.3 km NE from Piano Pernicana	0.4 (±0.3)
I	06/07-01:52	2.3 km E from Linguaglossa (CT)	0.0 (±1.1)
I	06/07-03:39	2.0 km E from Vena (CT)	0.4 (±0.2)
I	06/07-03:50	0.8 km NE from Vena (CT)	0.4 (±0.8)
F	18/01-15:56	3.1 km E from Vena (CT)	0.8 (±0.3)
I	19/01-08:42	2.7 km E from Vena (CT)	1.0 (±0.0)
I	19/01-09:12	3.2 km E from Pietrafucile (CT)	1.1 (±0.3)
I	19/01-10:25	1.5 km E from Pietrafucile (CT)	0.8 (±0.3)
I	19/01-17:41	1.7 km S from i Due Monti (CT)	0.9 (±0.2)

Table 1 - Catalog of events located in this work: ‘Imploc’ (I), present in the P.S.N. catalog but initially not located, and ‘Fiumenet’ (F), absent from the P.S.N. catalog, during the analyzed time intervals of 4-7 July 2017 and 17-19 January 2017.

The quality of the obtained locations considering both “imploc” events and those recorded solely by Fiumenet yet absent in the P.S.N. catalog ranges overall from good to acceptable, despite some limitations caused by occasionally high GAP values and difficulties in constraining hypocentral depth due to the poor readability of S-phases, typical of shallow microseismicity. During July 2016, epicenters tend to concentrate in the central portion of the P-PF, near the village of Vena (~700 m a.s.l.), consistent with the relocations obtained by integrating the temporary network for the two July 2016 events, with the seismicity distribution observed by the P.S.N. during the same period, and with previous studies (Alparone et al., 2013; Cannata et al., 2021). However, unlike the three 2016 Fiumenet events (absent from the P.S.N. catalog), which show a tendency to cluster, the “imploc” events appear more dispersed. This pattern is consistent with the high variability of arrival times but may also reflect uncertainties in the location process. For January 2017, the five located events (four “imploc” and one detected by Fiumenet but absent from the P.S.N. catalog) also fall

along the P-PF area, though slightly shifted westward compared to those of July 2016.
Considering all the events located in this study, from both 2016 and 2017, a classification was proposed to assign epicenters to specific categories based on spatial distribution (Fig. 1). The analysis allowed the distinction of four main groups, each with peculiar characteristics. Although useful from an interpretative standpoint and providing a more complete representation of the microseismicity along the P-PF, this classification must be considered in light of the previously discussed limitations related to location quality.
The spatial distribution of events was also analyzed as a function of local magnitude and time for July 2016 and January 2017. Regarding magnitude, most earthquakes fall within the 0.8-1.5 range, with a clear peak at Ml 1.0. This trend, typical of microseismicity, reflects the detectability threshold of monitoring networks: events with magnitude <1.0 are difficult to locate. In this framework, the integration of "imploc" and Fiumenet events did not change the magnitude range but increased dataset completeness. From a temporal perspective, activity in both sequences is concentrated over a few days; however, while the July 2016 sequence appears more extended and complex, the January 2017 sequence is shorter and more compact, likely reflecting a less extensive dynamic.

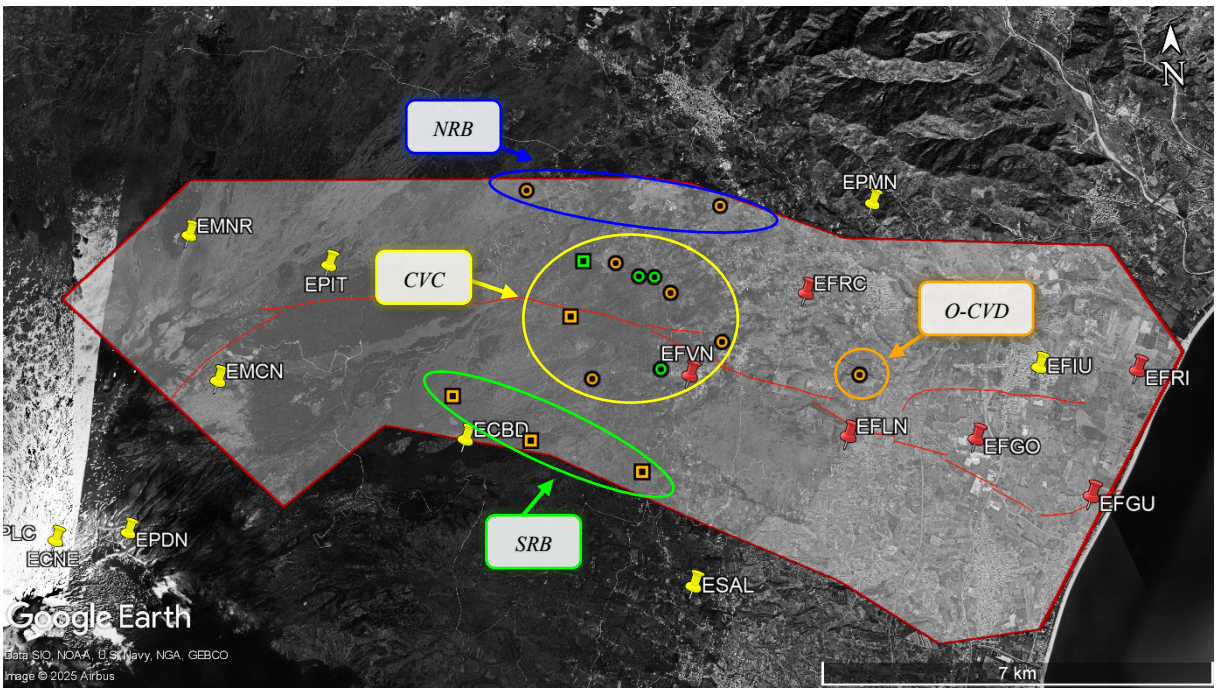

Fig. 1 - Distribution of the P.S.N. stations (yellow) in the P-PF area and of the six mobile Fiumenet stations (red) with red lines indicating the P-PF trace and the light gray area showing a reference polygon obtained by applying a 3 km buffer to the P-PF trace. This figure also shows the locations obtained for "imploc" events (orange, present in the P.S.N. catalog but initially not located) and for Fiumenet events (green, absent from the P.S.N. catalog), belonging to the July 2016 (circles) and January 2017 (squares) sequences. The events, as indicated in the figure, were divided into four main groups based on their spatial distribution: CVC - Central Vena Cluster; NRB - Northern Rim Belt; SRB - Southern Rim Belt; O-CVD - Outlier Central Vena District. Image from Google Earth, © Google.

The results indicate that, although the P.S.N. provides good location capabilities, it is unable to capture the entire microseismicity of the P-PF, particularly in its central sector. Based on these findings, the installation of new stations in the central eastern portion of the P-PF is recommended. A denser and structurally coherent network would improve the detection of microseismicity along the P-PF and enhance the understanding of the processes governing its activity. Finally, the methodological approach adopted in this study can be applied to future seismic sequences, contributing to a broader understanding of the shallow seismicity associated with the P-PF and other active tectonic structures of Mt. Etna.

Acknowledgements

This study benefited from access to seismic data and internal tools made available through the institutional facilities of INGV–Osservatorio Etneo and was carried out in the frame of a Master thesis project in Geophysics at the University of Catania.

References

Alparone S., Cocina O., Gambino S., Mostaccio A., Spampinato S., Tuvè T., Ursino A.; 2013: Seismological features of the Pernicana–Provenzana Fault System (Mt. Etna, Italy) and implications for the dynamics of northeastern flank of the volcano. Journal of Volcanology and Geothermal Research, 251, 16–26. DOI: 10.1016/j.jvolgeores.2012.03.010

Alparone S., Caruso S., Contrafatto D., Ferrari F., Ferro A., Gambino S., Larocca G., Messina A. A., Rapisarda S. C., Reitano D., Sassano M., Scuderi L., Torrisi O., Ursino A., Zuccarello L.; 2017: Analisi preliminare dei dati acquisiti dalla rete sismica mobile Fiumenet installata nel settore orientale della faglia della Pernicana-Provenzana (Mt. Etna, Italia). Rapporto INGV n. 385, Istituto Nazionale di Geofisica e Vulcanologia. URL: https://doi.org/10.13127/rpt/385

Cannata A., Iozzia A., Alparone S., Bonforte A., Cannavò F., Cesca S., Gresta S., Rivalta E., Ursino A.; 2021: Repeating Earthquakes and Ground Deformation Reveal the Structure and Triggering Mechanisms of the Pernicana Fault, Mt. Etna. Communications Earth & Environment, 2(1), 116. DOI: 10.1038/s43247-021-00188-6

Neri M., Acocella V., Behncke B.; 2004: The Role of the Pernicana Fault System in the Spreading of Mt. Etna (Italy) during the 2002–2003 Eruption. Bulletin of Volcanology, 66(5), 417–430. DOI: 10.1007/s00445-003-0322-x

Corresponding author: zingalessalvo98@gmail.com